MIXED SURFACTANT LAMELLAR PHASES: STUDIES UNDER SHEAR

A thesis submitted to The University of Manchester for the degree of Doctor of Philosophy in the Faculty of Engineering and Physical Sciences

2010

ANTRI THEODOROU

SCHOOL OF CHEMICAL ENGINEERING AND ANALYTICAL SCIENCE

Table of Contents

The final word count is 51.726

List of Tables

List of Figures

Chapter Five

Chapter Six

The University of Manchester
Faculty of Engineering and Physical Sciences

ABSTRACT OF THESIS submitted by Antri Theodorou for the degree of Doctor of Philosophy and entitled **Mixed Surfactant Lamellar Phases: Studies under Shear.**
Date of Submission: 17/09/2010

'Structured liquid' detergent products have received much attention as a means of providing liquid detergent compositions with special rheological and other properties. These include the ability to suspend particles and storage stability at ambient temperatures. The challenge is to prevent separation of the product into two or more layers (which requires a high viscosity) while controlling the rheology to allow a sufficient ease of pouring acceptable to the consumer. Liquid laundry detergent compositions are generally formulated with a variety of active ingredients, typically one or more anionic surfactants, often in combination with a nonionic surfactant and detergent builder materials such as electrolytes. The microstructure of these "liquids" (determined by the product formulation, process conditions and procedures) strongly influences the macroscopic properties such as rheology.

In this work, the microstructure, rheology and aging of a range of model structured liquid have been studied. The model systems are complex aqueous mixtures of sodium alkyl benzene sulphate (LAS), sodium alkyl ether sulphate (SLES) and primary alcohol ethoxylate (NEODOL 25-7). The dependence of the phase microstructure on sample composition was investigated by added different amount of electrolyte (tri-sodium citrate, TSC) in the model system. The physical appearance of these systems varied from transparent to milky depending on the concentration of the electrolyte. All were viscous "gels". Optical microscopy and SAXS have been used to elucidate the basic microstructure, its variation with electrolyte concentration and temperature on the angstrom to micrometer length scale. Deuterium nuclear magnetic resonance (^{2}H NMR) spectroscopy on ^{2}H$_2$O-enriched samples has been used to provide information about the phase behaviour of the liquid crystalline systems. Changes in spectral line shape and water quadrupole splittings are presented and discussed as a function of sample composition, temperature and aging process.

The shear-alignment process of the lamellar microstructure has been examined including Linkam optical shear cell, AR 2000 rheometer and ^{2}H Rheo-NMR. A variety of rheological patterns including simple stress sweeps and oscillatory rheology have been investigated and provided information about the effect of shear, shear time and nature of deformation of the model structured liquids. In this context, the relaxation kinetics of the shear-induced structures has been investigated using ^{2}H Rheo-NMR spectroscopy.

Declaration

No portion of the work referred to in the thesis has been submitted in support of an application for another degree or qualification of this or any other University or other Institute of learning.

Copyright Statement

i.   The author of this thesis (including any appendices and/or schedules to this thesis) owns certain copyright or related rights in it (the "Copyright") and she has given The University of Manchester certain rights to use such Copyright, including for administrative purposes.

ii.   Copies of this thesis, either in full or in extracts and whether in hard or electronic copy, may be made only in accordance with the Copyright, Designs and Patents Act 1988 (as amended) and regulations issued under it or, where appropriate, in accordance with licensing agreements which the University has from time to time. This page must form part of any such copies made.

iii.   The ownership of certain Copyright, patents, designs, trade marks and other intellectual property (the "Intellectual Property") and any reproductions of copyright works in the thesis, for example graphs and tables ("Reproductions"), which may be described in this thesis, may not be owned by the author and may be owned by third parties. Such Intellectual Property and Reproductions cannot and must not be made available for use without the prior written permission of the owner(s) of the relevant Intellectual Property and/or Reproductions.

iv.   Further information on the conditions under which disclosure, publication and commercialisation of this thesis, the Copyright and any Intellectual Property and/or Reproductions described in it may take place is available in the University IP policy (see http://www.campus.manchester.ac.uk/medialibrary/policies/intellectual-property.pdf), in any relevant Thesis restriction declarations deposited in the University Library, The University Library's regulations (see http://www.manchester.ac.uk/library/aboutus/regulations) and in The University's policy presentation of Theses.

The journey is the prize....

Acknowledgements

I would like to thank several people for all the help and support I have received during my PhD and while writing this thesis. First and foremost, I would like to thank my supervisor, Dr. Alec E. James who sadly never saw the end of this project. I would also like to thank my co-supervisor Professor Gordon J. T. Tiddy for his fantastic help and guidance throughout the whole of my time in his group. Secondly, I would like to thank my 'Unilever' supervisor Dr. Mike Baker for his help and advice as well as Mr. Geraint Roberts, also from Unilever for helping me with the rheology experiments carried out at Unilever, Research and Development, Port Sunlight. I would also like to thank everyone in C80 (now D39) (Marina, Andy, Soumi, Abdul, Helen and John) for laughs, friendship and cups of coffee. Thanks must go to my family and friends especially Loulou and Vakis, for their love, patient and support.

This thesis is dedicated to my Mum and Dad who were and will continue to be
a constant source of inspiration to me…

The Author

Antri Theodorou graduated with a BSc in Chemistry from University of Cyprus, in 2005. She received her MSc in Polymer and Material Science (School of Material) from The University of Manchester, United Kingdom in 2006. From September 2006 until September 2009 research was carried out at The University of Manchester under the supervision of Dr. Alec E. James. The work involved studying the microstructure of mixed surfactant lamellar phases under shear. The research work was funded by Unilever and was carried out in close collaboration with Dr. Mike Baker, Unilever Research and Development, Port Sunlight, United Kingdom. From October 2009 up to date the author is working as R&D manager in ZX Fami Ltd, Cyprus. ZX Fami Ltd is a company that manufactures and delivers cosmetics, household and cleaning products in Cyprus and East Europe.

Chapter 1

Introduction

This project is collaboration between the University of Manchester and Unilever. The research is concerned with enabling the company to improve its understanding of its liquid laundry detergent systems based on pure lamellar liquid crystals.

Laundry liquids have been marked as both isotropic solutions and lamellar droplets dispersions. Currently there is an interest in using pure lamellar liquid crystal as this would provide an interesting set of consumer properties. Based on previous work carried out at Unilever Research and Development, Port Sunlight, two routes have been explored to convert an isotropic surfactant solution into a lamellar liquid crystal: (i) the addition of a polar hydrophobe (ca. 3-15% added) or (ii) the addition of electrolytes such as tri-sodium citrate and/or sodium chloride. In this project the use of electrolytes is preferred.

The main aim of this project is to develop an underlying understanding between the microstructure and the rheology of the system in question. Important questions addressed in this thesis are (i) which are the factors governing the lamellar microstructure and the physical stability of these phases and (ii) what is the relation between the microstructure and the rheology of these systems as a function of composition, age and shear.

In order to build up this understanding there are three main objectives:

(i)   Characterisation of the structure at several length scales. A range of experimental techniques, namely optical microscopy, small-angle X-ray scattering (SAXS) and deuterium nuclear magnetic resonance (^{2}H NMR) spectroscopy will be used to elucidate several features of the microstructure across the length scales. Optical microscopy (μm level) and SAXS (Å-nm level) will provide information on the number and nature of liquid crystalline phases, while SAXS also provides the dimensions periodic arrangement of the lamellar bilayers. ^{2}H NMR spectroscopy provides information on the molecular structure and the phase behaviour. Bringing all the structural information together will lead to an understanding of the organisation of the microstructure.

(ii)   Relate the phase microstructure to the system composition and age. This enables the system composition to be manipulated to control the optical and rheological properties of the system. In this context, experimental studies will carried out on samples with different salt level and ages.

(iii)   Rheological characterisation to enable a better understanding of the effect of shear, time and nature of deformation of the lamellar structure. These studies investigate the effect of shear and the possible deformations that lamellar structures undergo at a microstructural level. An understanding of the shear effect will lead to a degree of control of the morphology changes under shear and enable industry to deliver products with desired consumer properties.

The systems chosen for this project are commercial surfactants for good fabric cleaning properties (see Chapter 4). These systems are of particular interest of Unilever Research in their aim to produce a double concentrated liquid laundry detergent containing little or no builders and less water volume.

This Chapter introduces to the reader the subject starting with a Section on surfactant structure and functionality, followed by a Section on liquid crystals and finally laundry detergents are discussed. At the end of this Chapter an outline of the thesis can be found.

1.1 Surfactants – a brief introduction

Surfactants or *surf*ace-*act*ive *agents* are species of chemical compounds that adsorb onto surfaces or interfaces and alter certain thermodynamic characteristics of those surfaces. Surfactants are used in many chemical industries such as pharmaceutical, agrochemicals, consumer and specialty industries[1]. They are used in pharmaceuticals, where drugs are not sufficiently soluble in water or ethanol to deliver the required dose, may be solubilised in a biological compatible surfactant system, and injected[2]. Another important application of surfactants is in detergents[3], where the surfactant acts to modify the properties of the interfaces between the substrate, dirt and the wash liquid, thus changing the energy of the interactions between the dirt and the substrate.

The history of surfactant manufacture goes back around 2800 B.C. when the first man-made surfactant was found. It was a soap-like material in clay artifacts excavated from archeological digs in ancient Babylon[4]. In fact, this was firstly concerned as the use of

surfactants in laundry detergents, as it was though that in those times, people used the soap to wash fibres. Despite their continual existence over the years and throughout a wide range of applications, surfactant manufacture and applications have seen the most rapid development in the last century. The production of fatty acid soaps was first present in the early 1940's and was followed, in 1950's, by the production of synthetic detergents of alkylbenzene sulfonate that were displaced soaps for washing machine and other domestic uses. In 1960's the building block of non-ionic surfactant, ethylene oxide, was first introduced from steam cracking[4].

Surfactant manufacture is one of the largest chemical process industries, with worldwide usage of synthetic surfactants in a variety of formulated products[5]. The great demand of today's society combines not only high performance and low cost products, but also products with high biodegradability and with the least environmental impact. To do this, the knowledge of surfactant behaviour and their flow properties are important tools. It is also important to understand how different parts of manufacture process affect the behaviour of the surfactant in order to deliver the most favourable product to the market, to correspond with consumer and market needs.

During manufacture processes, changes in rheology are believed to be as a result of morphology changes[1]. Thus, viscosity plays an important role in product formulation. For example, in hair conditioners, the viscosity is enabling the conditioner to pour from the bottle and spread easily over the hair. In addition, the design of processes such as mixing, pumping and separation can be improved and optimised by the knowledge of the flow properties of surfactants.

Phase diagrams are another tool that helps in finding the correct compositions to use. The properties and uses of phase diagrams of a specific surfactant system depend on the transitions that take place between these phases[6].

1.2 Surfactant Structure and Functionality

Surfactants are known as amphiphilic compounds since they are semi-soluble in both organic and aqueous solvents[7]. For this reason they accumulate at the interface of two

liquids and modify the property of the surface[8]. Their amphiphilic nature determines their functionality and their classification[6]. Amphiphilic compounds are characterised by possessing in the same molecule two groups which differ greatly in their solubility. The basic structure consists of a polar 'head' group (hydrophilic) and a non-polar hydrocarbon tail (hydrophobic).

Unusual properties arise because of the structure of surfactants leading to both widespread and highly specialised applications. A polar head group (hydrophilic group), conveys water solubility or adsorption. The hydrophilic head group is a structural group that has a strong attraction for the solvent (water). This molecular property leads to the microscopic properties of wetting, foaming, detergency and emulsion formation.

The non-polar group (hydrophobic tail) is a structural group which offers neither repulsion nor attraction towards the solvent. However as there are strong interactions among the paraffin chains when placed in a water environment the hydrophobic tail drives the formation of self assembled aggregate structures like micelles, bilayers and liquid crystals[7, 9].

Surfactants can be classified on the basis of the charge (or lack of charge) on their polar 'head' group. The common classes consist of anionic, cationic, nonionic, amphoteric and zwitterionic[10]. The choice of the counter-ion plays an important role in the physico-chemical properties of ionic surfactants. For instance, anionic surfactants have a negatively charged head group and a positive counter-ion. In addition, those that dissociate in water as an amphiphilic anion and a small cation are called anionic surfactants and those that give amphiphilic cations and small anions are called cationic surfactants. Moreover, as is indicated from the name, those that do not ionise in water are termed non-ionic surfactants.

Surfactant has the tendency to reduce the surface tension. Due to their amphiphilic nature can migrate to interfaces where the polar head group dissolves in the polar medium and the non-polar head group dissolves in the hydrophobic medium. By doing this, the two kinds of molecules (the polar medium and the non-polar medium), are hold together minimising the work that has to be done to keep them at the interface. As a result, the surface tension is reduced. The adsorption depends on the degree of hydrophobic and hydrophilic nature.

Another fundamental property of surfactants is the tendency to form aggregates in solution[11]. The first to be formed are called micelles. The importance of micellisation lies in the very different behaviour of surfactant molecules when they are present in micelles compared to when they are free monomers in solution. Due to this importance micelle formation has been fully investigated[12-14]. Surfactant aggregation behaviour is discussed in more detail in Chapter 2. Under suitable conditions of concentration, temperature and pressure surfactant molecules can form other aggregates in solution, such as liquid crystalline phases. The knowledge of the types and the structures of liquid crystalline phases formed in surfactant solutions can provide useful information for manufactures when considering applications for surfactants in industry.

1.3 Liquid Crystals

Liquid crystals, also referred to as mesophases, are intermediary states of matter which have a degree of molecular order intermediate to that found in solid crystals, where there is a perfect long-range positional and orientational order, and that found in isotropic liquids and gasses where there is a long-range disorder. Molecules that can form liquid crystal phases under suitable conditions of temperature, pressure and concentration are called mesogens.

Liquid crystals fall under two categories: thermotropic and lyotropic. In thermotropic liquid crystals the phase transitions depend on temperature, while in lyotropic liquid crystals depend on both temperature and concentration of the solute. The thermotropic liquid crystals are widely used in a variety of applications, such as display devices *e.g.* computer screens and flat screen televisions.

The lyotropic liquid crystals can be based on surfactants, chromonic and polymeric compounds. The surfactant liquid crystals are of great relevance in detergent formulations thus are important to this project and will be described in more detail in Chapter 2.

1.4 Laundry Detergents

Years of research have enabled us to formulate laundry detergents that are incorporating surfactants into complex products. These products come in different forms such as powders, liquids, tablets and even in 'liquid-tabs' but they all made to clean our clothes. Studies on the surfactant mesophases formed during product processing and manufacture as well as when mixed with water have been done by many groups. Chen *et al*[15] investigations indicated that the viscosity of mesophases formed can affect the mixing behaviour during manufacture and the final product in a detrimental way.

There are many components in a laundry detergent that are used to clean clothes. These consist of bleaches, surfactants and enzymes. It is the surfactant choice that is more important because the surfactant mixture is charged with the removal of soil and also the performance and the structure of the product. The most commonly used surfactants in detergents are anionic because of their excellent cleaning properties. Non-ionic surfactants are also used commonly in laundry detergents, at least in Europe.

Surfactants can work to clean clothes in several ways and one of an importance is the soil removal by laundry detergents. That works by reducing the surface tension of the water and allow the water to wet a substrate/soil more thoroughly. In addition, as well as removing dirt, laundry detergents have to be able to prevent dirt re-deposition on the fabric.

There are many forms of laundry detergents in market as mentioned earlier. However, for this project, the surfactant systems investigated are integrated into a laundry liquid. Laundry liquids are rapidly growing and are expected to be the dominant format at least in Europe. Liquids are so successful because of the low risk of dissolution problems and also because of the benefits that consumers enjoy. Laundry liquids can be multipurpose product because cover different situations such as woollens, blacks and whites and also can be used in hand wash.

It has already been launched in EU market the first double concentrated liquid laundry detergent from Unilever called 'small and mighty'. The whole concept is based on a concentrated and low-volume product that consumers can enjoy better results, while using

less volume of product. In addition, the packing has been reduced so is easier for consumers to carry and store the product. Moreover, because the amount of detergent in waste water is reduced, less waste packing and less carbon emissions are the benefits for our environment. Based on that project Unilever aims to develop a liquid laundry detergent which is consisted solely or mostly of surfactants, in effect, a concentrated product that is not affected by the additives. The most important factor to be considered is the product structure as it is clearly very important to consumers.

1.5 Thesis Outline

Chapter 1 has served as a brief introduction to the work contained within this thesis. Important aspects of the surfactant structure and functionality, including liquid crystals are discussed. Chapter 2 reviews the literature to date on important aspects of surfactant self-assembly process, including micellisation, type of liquid crystal formed and factors affecting the formation and transitions in surfactant liquid crystalline phases. Finally, surfactants relevance to laundry detergents is discussed.

Complex structured liquids based on lamellar systems, which are the focus of this work, are discussed in Chapter 3. Initially, the concept of microstructure is introduced and then the relation between microstructure and rheology is briefly discussed. The lamellar phase morphologies and the main factors that influence the lamellar microstructure are discussed in detail. The concept of rheology with relevance to structured liquids is then discussed. Finally, the composition dependence of lamellar phase microstructure is briefly introduced.

In Chapter 4 the materials and methods used in this research are discussed. Details are given concerning the major raw materials used and the exact procedures undertaken. In addition the experimental techniques used are presented, with their underlying theory and a short explanation of data analysis.

Chapter 5 discusses the experimental results in a static environment related to the microstructure of the main system. This Chapter discusses the effect of added salt, aging and temperature on the microstructure. Chapter 6 presents the experimental results under shear. The effects of composition and aging on the shear-induced structures are discussed. This Chapter focuses on the relation between the microstructure and the rheology.

In the final Chapter, the main conclusions are presented. In addition suggested future work is discussed.

1.6 References

1.   Tiddy, G. J. T., Khan, A., Formulation Science and Technology - Surfactants Needed! *Current Opinion in Colloid & Interface Science* **1999,** 4, (6), 379-380.
2.   Florence, A. T., Drug solubilisation in surfactant systems. In *Techniques of solubilisation of drugs*, Yalkowsky, S. H., Ed. New York, 1981.
3.   Durham, K., *Surface activity and detergency*. MacMillan & Co Ltd: London, 1961.
4.   http://www.cleaninginstitute.org, The Association of Soaps and Detergents, History of Soap **2005**.
5.   Mccoy, M., Below the surface. Coming off a bad year, surfactant producers are looking for signs of recovery In 2004; Vol. 82, pp 29-30.
6.   Tiddy, G. J. T., Surfactant Liquid Crystals. In *Handbook of Applied Surface and Colloid Chemistry*, Holmberg, K., Ed. John Wiley and Sons: New York, 2002; pp 465-468.
7.   Jonsson, B., Lindman, B., Kronberg, B., Holmberg, K., In *Surfactants and Polymers in Aqueous Solution*, Second Ed.; Jonsson, B., Ed. John Wiley & Sons Ltd: Chichester, 2003; pp 1-217.
8.   Atkins, P. W., In *The Element of Physical Chemistry*, Oxford University Press: London, 1993; pp 317-461.
9.   Gharibi, H., Takisawa, N., Brown, P., Thomason, M. A., Painter, D. M., Bloor, D. M., Hall, D. G., Wyn-Jones, E., Analysis of the fast relaxation times for micelle kinetics taking into account new EMF data. *Journal of Chemical Society Faraday Transaction 1* **1991,** 87, 707-710.
10.   Rosen, M. J., *Surfactants and Interfacial Phenomena*. John Wiley & Sons Ltd: New York, 1978.
11.   Israelachvili, J. N., *Intermolecular and Surface Forces*. First Ed.; Academic Press: London, 1985.
12.   Lindman, B., Wennerström, H., Amphiphile aggregation in aqueous solution. *Topics in Current Chemistry* **1980,** 87, 1-83.
13.   Gunnarsson, G., Joensson, B., Wennerstrom, H., Surfactant association into micelles. An electrostatic approach. *Journal of Physical Chemistry* **1980,** 84, (23), 3114–3121.
14.   Israelachvili, J. N., Mitchell, D. J., Ninham, B. W., Theory of self-assembly of hydrocarbon amphiphiles into micelles and bilayers. *Journal of Chemical Society Faraday Transaction 2* **1976,** 72, 1525-1568.
15.   Chen, B. H., Miller, C. A., Walsh, J. M., Warren, P. B., Ruddock, J. N., Garrett, P. R., Argoul, F., Leger, C., Dissolution Rates of Pure Non-ionic Surfactants. *Langmuir* **2000,** 16, 5276–5283.

Chapter 2

Introduction to surfactant aggregation behaviour, the liquid crystalline phases and their relevance to liquid laundry detergents

A brief summary is given in this Chapter, of the literature available to date on the surfactant behaviour in solution beginning with the formation of micelles. This is followed by a review on liquid crystalline phases concentrating on the factors affecting the formation and the transitions in lyotropic liquid crystalline phases. The phase behaviour of some of the surfactant systems present in this work is also discussed. This is followed by a review of the liquid crystalline phases present in daily used products and a brief discussion on the liquid laundry detergents and their relation to the surfactant aggregation.

2.1 Micellisation

Amphiphiles like surfactants and lipids can associate into a variety of structures in aqueous solutions. Different aggregate shapes are shown in Figure 2.1.
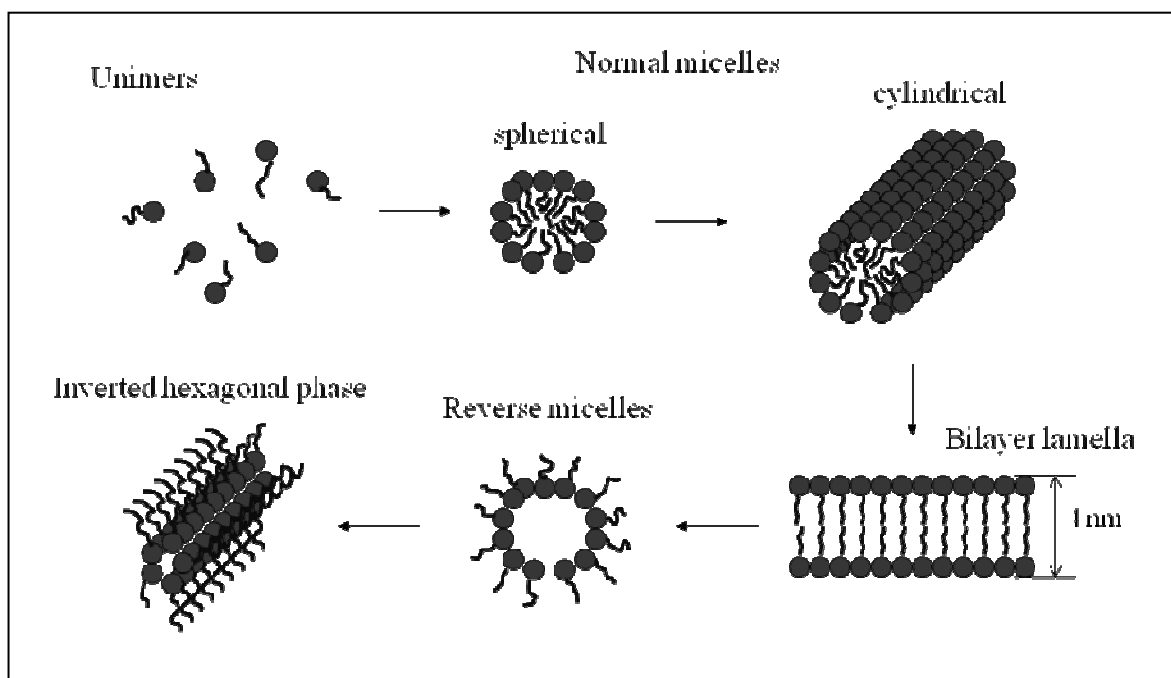
Figure 2.1: Schematic of various types of micellar structures due to self assembly of surfactant monomers[1].

The transformation from one structure to the other is controlled by the system composition, the concentration of the amphiphilic molecules, the temperature and the pH of the solution. The structures depend on the thermodynamics of self assembly and the forces between the aggregates. The number of molecules in an aggregate is known as the aggregation number and depends on the surfactant type.

2.1.1 Critical Micelle Concentration and Krafft Temperature

When surfactants dissolve in water at low concentrations, they exist as monomers. However, the amphiphilic nature of surfactant molecules leads to their self assembly in solution into a variety of structures as the concentration is increased. This idea was first introduced by McBain[2] over ninety years ago. He worked on the conductivity and osmostic properties of soap solutions and he observed changes in conductivity measurements, while slowly increasing soap concentration in an aqueous solution. By comparing these values he led to the understanding that the changes result from the aggregation behaviour of the surfactant molecules and he called the aggregates 'micelles'[3]. According to McBain[3]

micelles are locally disordered aggregates with almost free molecular mobility and a lifetime of the order of 10^{-5}-10s.

Micelle formation occurs over a very narrow region of concentrations known as the 'critical micelle concentration' (CMC)[4]. This region is very small to define and therefore for the purpose of practicality, this region is represented as a single value: the CMC. For pure single surfactants below the CMC, all the surfactant molecules are monomers in solution. However, above the CMC self-aggregation occurs and micelles form. With surfactant mixtures the micelle formation is more complex due to the different individual CMCs of the components[1].

Experimentally the determination of the CMC can be obtained by the measurement of some key physical properties of the solution which it affects, such as the turbidity, the surface tension, the conductivity and the light scattering intensity. A representation of the effects of CMC is given below in Figure 2.2[5]. Unfortunately these methods of detection can not detect the whole range of CMC values apart from those surfactants with high CMC values (those with short chain lengths). Factors that affect the critical micelle concentration are described later in this Chapter.
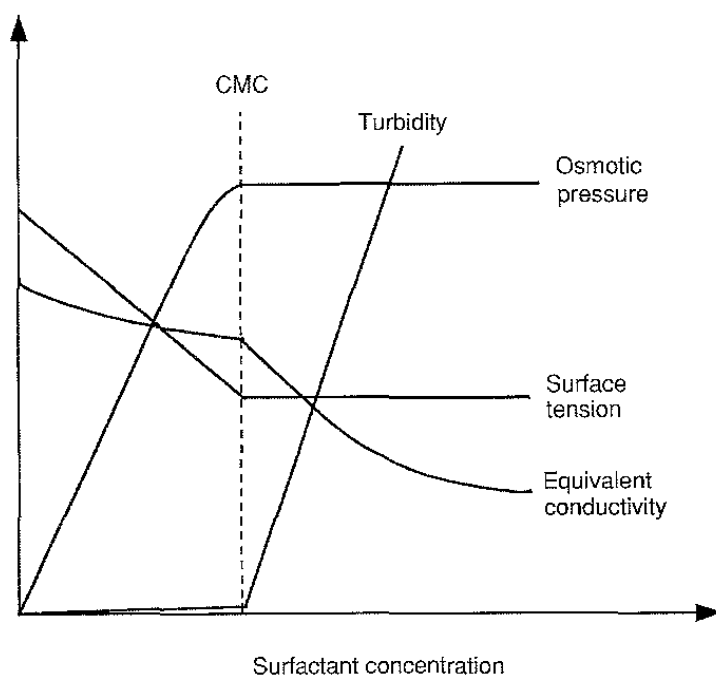
Figure 2.2: Schematic representation of the concentration dependence of some physical properties for solutions of a micelle-forming surfactant (reproduced from reference[5]).

The changes in the physical properties of the solutions are occurred at a particular concentration (or narrow range of concentrations), with a change from a state where the surfactant exists as monomers in solution, to where the surfactant begins to form an aggregate or self-assembled structures-micelles. However, at CMC many unusual changes of key physical properties can be observed. For instance at CMC, turbidity rapidly increases while the surface tension takes an approximately constant value.

We have so far established that micelles can only form when the surfactant solubility is equal to or greater than the CMC. Additionally micelles only form above a particular temperature known as the Krafft temperature or 'Krafft point'[6-8]. The Krafft temperature (T_K) corresponds to the temperature at which the surfactant solubility equals the CMC.

Below the Krafft temperature the surfactant solubility increases slowly with increasing temperature because the surfactant dissolves as monomers. At Krafft temperature surfactant dissolves as micelles therefore the dramatic increase in solubility with increasing temperature. The Krafft point is strongly dependent on the alkyl chain length of the surfactants and on the head group structure, hence the packing efficiency in the solid crystalline state. Different chain lengths lead to differences in packing of the molecules which alternates with the number of carbons in the hydrophobic tail. In the same way, strong head group interactions stabilise the crystal therefore strongly increasing the Krafft temperature. This temperature dependence is displayed in Figure 2.3.
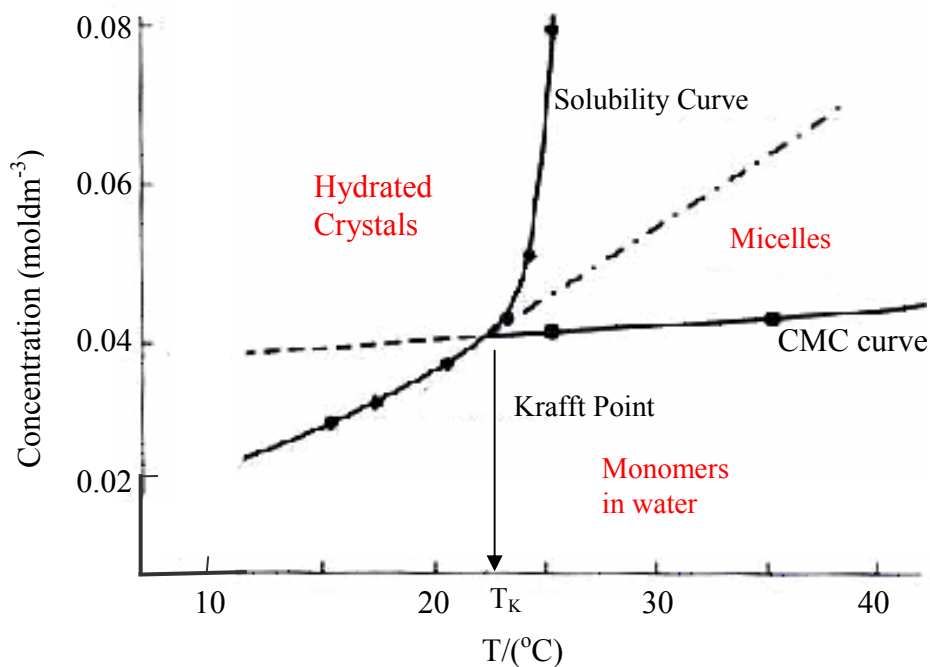
Figure 2.3: Temperature dependence of surfactant solubility in the region of the Krafft temperature (reproduced from references[8, 9]).

The development of surfactants with lower Krafft point but still being efficient at decreasing surface tension is usually accomplished by introducing branched chains and multiple bonds in the alkyl chain or bulkier hydrophilic groups. For ionic surfactant the Krafft point is also found to vary with counter-ion[10].

2.1.2 Hydrophobic Effect

The hydrophilic nature of the surfactant molecules is the major factor behind the mechanism of micelle formation with micellisation attributed to the hydrophobic effect[7, 11-13]. This is the term used to describe how non-polar molecules or non-polar parts of molecules are spontaneously removed from water. It was originally thought that this phenomenon arises by the 'like to like interaction' between the hydrocarbon chains. However, the interaction between hydrocarbon chains has a minor contribution to this effect.

Actually, the hydrophobic effect arises from the strong attractive forces occurring between water molecules by the introduction of a non-polar molecule into water. If the solute is strongly polar or ionic, strong bonds can be formed with the water molecules. However, if the solute is non-polar its dissolution in water is resisted[7].

It is well known that hydrocarbons have a limited degree of solubility in water, with the solubility decreasing rapidly with increasing solute size[7]. From a thermodynamic point of view the introduction of a hydrocarbon into water is always associated with a decrease of entropy in the system, and an enthalpy of about zero, resulting in large and positive free energy[12, 14].

Micelle formation is therefore entropy driven and the entropy change was originally attributed to structuring of water molecules around the hydrocarbon chain[15]. However, the 'water-structuring' theory has not been upheld with frequent attempts to measure the 'structure' next to the alkyl chains failing, with evidence supporting only one layer of water around the solute that differs from bulk water[16]. A more likely explanation to support the water-structuring concept is that the water molecules next to the alkyl groups have reduced configurational freedom, therefore entropy loss.

Kronberg and co-workers[12, 14] have been discussed this problem in a series of papers. These authors view the hydrophobic effect as a result of two contributions. The first contribution arises from the 'ordering' of water molecules around the solute and the second from the energy required making a cavity in the water large enough to accommodate the non-polar solute.

The first contribution is related to a negative entropy associated with the water molecules next to the non-polar solute which have fewer conformations available than the 'free' water resulting in an entropy decrease. Negative entropy is also due to the stronger hydrogen bonds formed by water molecules close to solute. The combination of these effects gives a small negative Gibbs free energy.

The second and opposite contribution arises from the large amount of energy required to make a cavity in the water to accommodate the non-polar solute. This is large due to the high cohesion in water arising from strong hydrogen-bonding density, and the small size of

water molecules compared to hydrocarbons (*e.g.* alkanes). An important conclusion from this mechanism is that the magnitude of the hydrophobic effect is proportional to the surface area of the cavity created in the solvent by the hydrophobic solute. The CMC value for many surfactant systems can therefore be predicted by using this concept.

2.1.3 Factors affecting the CMC

Many factors are known to strongly affect the CMC. Of major effect is the hydrophobic nature of the surfactant molecules. Also important, however to a lesser extent, are parameters such as counter-ion nature, presence of additives and the temperature.

<u>The hydrophobic chain</u>

As mentioned above, the hydrophobic effect provides the major determinant of the CMC with its contribution to be proportional to the area of the non-polar chain removed from exposure to water when micelles are formed[12, 13]. As a result a logarithmic relationship between the alkyl chain length of the surfactant with linear hydrocarbon chain and the CMC is established as shown in Equation 2.1

$$Log\ (CMC) = An + B \hspace{3cm} \textbf{Equation 2.1}$$

where *A* and *B* are constants and *n* is the alkyl chain number.

An increase in hydrocarbon chain length generally reduces the CMC in aqueous solutions, *e.g.* for aqueous solutions of ionic surfactants, the CMC decreases by a factor of 4 with the addition of two $-CH_2$ groups, while the CMC decreases by a factor of 10 with the addition of two $-CH_2$ groups to non-ionics. Ionic surfactants in water generally have larger CMCs than that of non-ionics with similar chain length, because the electrostatic repulsion between the head groups hinders micellisation in a charged micelle.

The counter ion valences have a huge effect on the CMC as solutions with multivalent having considerably lower CMC than those of monovalents. Branching, unsaturation and the presence of other polar groups in the alkyl chain produce noticeable changes in the CMC all resulting in a somewhat higher value.

The magnitude of the head group charge (*s*) also plays an effect in the relationship stated in Equation 2.1. Constant *A* is dependent on the value of *s* and so it takes certain values. The charge on the counter-ion in ionic surfactants is also significant and it influences the value of *B*. In ionic surfactants micelle formation is related to the interactions between the solvent and the ionic head group. Since electrostatic repulsions between ionic groups are greatest for complete ionisation, changing the counter-ion to multivalent (thus an increase in the degree of ion binding) tends to decrease the CMC because fewer ions are required close to the micelle surface to partially balance the high surface charge density.

The hydrophilic group

For surfactants with the same alkyl chain, the head group nature (*i.e.* from non-ionic to ionic) has an important effect on the CMC values. CMC values for non-ionic surfactants are much lower than for ionic surfactants. However, the exact nature of the ionic head group has no dramatic effect on the CMC values, since the mechanism for micelle formation is entropy driven.

Effect of temperature

The effect of temperature on micellisation is quite complex. Studies[17-19] on some ionic surfactants show that the CMC passes through a minimum as the temperature increases from 0 to 70°C. However, for non-ionic surfactants the CMC decreases with increasing temperature but the effect is small[8]. As already mentioned (Section 2.1.1) the major effect of temperature on the mechanism of micelle formation is the Krafft temperature.

Effect of added salt

The effect of additives on the CMC has been investigated by many groups[17, 20]. Electrolytes have a dramatic effect on the CMC when added to a surfactant solution. For ionic surfactants, the situation is simple. Take for instance the changes in the CMC of different sodium alkyl sulfate surfactant solutions in the presence of added sodium chloride, an electrolyte with a common counter-ion. In this case the added electrolyte dramatically lowers the CMC[21]. This is because the electrolyte effectively reduces the electrostatic repulsions present between the head groups, enabling the micelles to form at lower concentrations.

The effect of added electrolyte is small for non-ionic surfactants. Electrolytes that are known as 'salting-out' electrolytes reduce the CMC of non-ionic surfactants. Other electrolytes are capable of 'salting-in' non-ionic surfactants. The 'salting-in' behaviour is probably due to adsorption of anions to the micelles surface.

In most surfactant applications mixed surfactants systems are used. With mixed surfactants, the CMC of the mixed micelles varies according to the CMCs of the individual components, and their composition in the mixture. In such a mixed system the CMC values depend on whether there are specific interactions between head groups which lead to non-ideal mixing in the micelle. This behaviour is been described in detail by Lindman *et al*[8].

The factors affecting the CMC are usually affecting the Krafft temperature. For example when introducing a *cis* double bond into an alkyl chain lowers the stability of the surfactant crystals as compared to an all *trans* configuration. Hence, the chains pack less efficiently, thus the Krafft temperature is lowered.

2.1.4 Structure of micelles and molecular packing

As described previously, the major forces control the self association process are the hydrophobic attraction at the hydrocarbon-water interface, which causes the molecules to associate, and the hydrophilic, ionic or steric repulsion of the head groups which work in the opposite sense. The basic idea was reviewed and quantified by Mitchell and Ninham[22] and Israelachvili[23], resulting in the concept that surfactants aggregation is controlled by a balanced molecular geometry.

In the micellisation process, molecular geometry thus, the micelle shape and size, plays an important role and hence an understanding of the packing constraint concepts related with micelle formation is vital[11, 22, 23].
Packing constraint concepts offer a simple description of the relationship between surfactant molecular shape and micelle shape and consequently liquid crystalline phase structure[9, 11, 22] (Section 2.2). For these considerations the micelles assume to be smooth with only the hydrophobic volume in the micelle interior. The geometrical consideration of the micelles depends upon the volume of the hydrophobic tail (*v*), the minimum area

occupied by the head group at the micelle surface (α) and the maximum micelle radius, taken as the all-trans length of the surfactant, (l_t) as indicated in Figure 2.4.
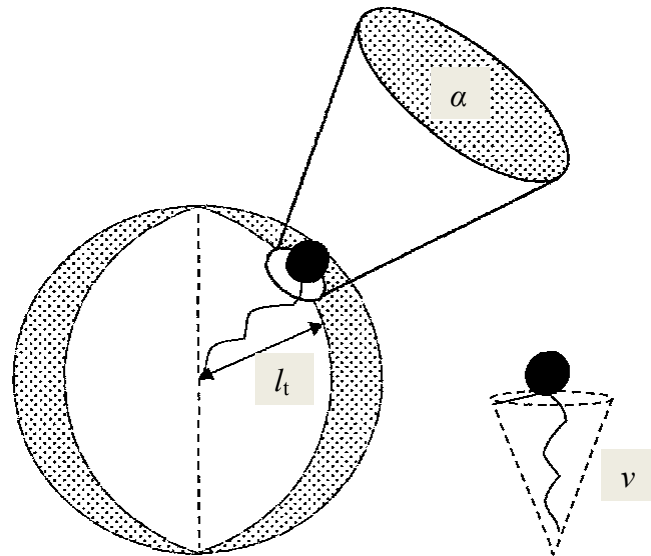
Figure 2.4: Schematic of surfactant molecule indicating parameters important for packing[24].

The contribution coming from these parameters has been combined into a dimensionless function called the critical packing parameter (P) $v/\alpha l_t$. For instance, for a spherical micelle having a hydrophobic volume (V), radius (r), total surface area (A) and aggregation number (q) we have the following relationships:

$$A = q\alpha = 4\pi r^2 \qquad \qquad \textbf{Equation 2.2}$$

$$V = qv = 4/3\pi r^3 \qquad \qquad \textbf{Equation 2.3}$$

Thus:

$$\alpha = 3v/r \geq 3v/l_t \qquad \qquad \textbf{Equation 2.4}$$

Ignoring end effects or edge effects for rod and disc shapes the resulting relationship for a rod micelle (radius r) is:

$$\alpha = 2v/r \geq 2v/l_t \qquad \qquad \textbf{Equation 2.5}$$

And for a bilayer/disc (thickness *2r*) is:

$$\alpha = v/r \geq v/l_t \qquad \textbf{Equation 2.6}$$

The value of *r* can not be larger than l_t therefore there are limitations on the lowest value of α for a given shape.

$$\alpha \geq 3v/l_t \text{ (sphere); } \alpha \geq 2v/l_t \text{ (rod); } \alpha \geq v/l_t \text{ (disc)} \qquad \textbf{Equation 2.7}$$

The main structures of micelle encountered are sphere, rod and disc and Table 2.1 summarises the packing constraints required for the micelle to pack in this way.

Class	Micelle size and aggregation (q) number	Limitations on size of the head group (a)
Sphere	Largest head group, smallest alkyl chain length. Low aggregation number, $q < 60$	$P \leq \dfrac{1}{3}$ $a \geq 3 \dfrac{v}{l_t}$
Rod	Small head group, large alkyl chain length. Large aggregation number, $q > 60$	$\dfrac{1}{3} \leq P \leq \dfrac{1}{2}$ $a \geq 2 \dfrac{v}{l_t}$
Disc	Smallest head group, largest alkyl chain length. Low aggregation number, $q < 300$	$\dfrac{1}{2} \leq P \leq 1$ $a \geq \dfrac{v}{l_t}$

Table 2.1: Summary of the major micelle shape classification with packing constraints.

Once these parameters have been calculated it is possible to determine the size and the shape of the liquid crystal structure into which the surfactant can pack. This is demonstrated in Figure 2.5.
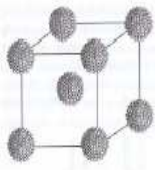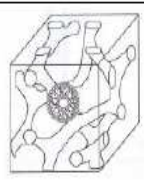
Micelle Shape	Liquid Crystal	Packing Constraints	LC and Surfactant		Notation
Spherical	Cubic	$a \leq \dfrac{3\upsilon}{l_t}$			I_1
Rod	Hexagonal	$a \leq \dfrac{2\upsilon}{l_t}$			H_1
-	Cubic	-		-	V_1
Disc	Lamellar	$a \leq \dfrac{\upsilon}{l_t}$			L_α
Curved Continuous Bilayer	Cubic	-			V_2
Where a is the head group cross sectional surface area, υ is the volume of the hydrophobic group and l_t the all trans length of the alkyl chain.					

Figure 2.5: Packing constraints and liquid crystal structure (adapted from reference[25]).

It is clear that a surfactant can pack into spheres, rods or discs, according to the size of the head group, with all these three shapes being possible for the largest α values and only the disc micelles for small α values. Entropy favours the formation of the smallest possible aggregate at the CMC thus spheres over rods and rods over discs.

Micelle size (aggregation number) varies according to the shape of the micelle and the alkyl chain length. For spherical micelle the micelle radius is limited by the all-*trans* alkyl chain length and hence the surface area is limited. Thus, spherical micelles always have low aggregation numbers limit and therefore the 'end' effects will not significantly affect the size of the micelle. For rod and disc micelles, the number of edge or end molecules

plays a significant part in micelle size. A fundamental thermodynamic approach to self association in solution has been described by Israelachvili *et al*[23, 26] which takes into account the fraction of edge or end molecules present in disc or rod micelles.

2.2 Lyotropic Liquid Crystalline Phases

When the concentration of surfactant in a micellar solution is increased, typically above the threshold of about 40%, a series of lyotropic liquid crystalline phases (mesophases) is encountered. This is because initially the surfactant molecules aggregate to form micelles and at higher concentrations these aggregate to form larger 'ordered' solutions[27, 28].

In 'ordered' solutions the size of the head group, number of alkyl chains and polarity of the solvent are important and packing constraints must therefore be considered[24]. Interactions between micellar surfaces are repulsive (from electrostatic or hydration forces), so that as the number of aggregates increases the micelles get closer to one another, the only way to maximise separation is to change the aggregate shape and size.

The addition of more surfactant in a micellar solution will mean movement to a shape with a higher packing limit and therefore lower aggregate curvature. It should be noted that as the polar head group increases the curvature also increases so liquid crystal formation depends on the type of micelle at the lowest concentration[7].

There are many different liquid crystal structures formed, although there are considered to be six main classes with well characterised structures. These are lamellar, hexagonal, cubic, gel, nematic and intermediate phases. Each structure can exist in oil continuous or water continuous media in either a 'normal' or 'reverse' configuration often denoted by subscripts 1 and 2 respectively[28-31].

The most important technique to identify the mesophase type is polarising optical microscopy. All the phases are birefringent and display a unique texture when viewed under crossed polarisers, while cubic phases have none. The cubic phases are isotropic and therefore appear black under crossed polarisers however, are very viscous. This technique is explained in Chapter 4.

2.2.1 Lamellar Phase (L_α)

The most common surfactant mesophase is the lamellar phase (L_α), also known as the 'neat phase'[7, 31-33]. Within this phase, the surfactant molecules are arranged into stacks of ordered bilayers extending over large distances (a micron or more), which are separated by water layers[32]. Figure 2.6 contains a schematic illustration of a lamellar liquid crystalline phase.

The L_α phase is easily recognisable from both its rheological and optical properties. Within the L_α phase the layers are flat and the alkyl chains are in a liquid-like state so each parallel layer can slide over each other with ease during shear which accounts for the low viscosity of the system. It can usually easily be shaken into a container and at high water concentrations is even pourable. When viewed under crossed polarisers on a polarising optical microscope, the L_α phase exhibits characteristic optical textures. If the sample is non-oriented a mosaic texture with many defects and birefrigence colours results. Shear orientation of the lamellar bilayers parallel to the surface of the microscope slide produces pseudo-isotropic textures such as oily streaks and Maltese crosses[34, 35]. Air bubbles are spherical (if present) due to low viscosity medium they reside in.

The hydrophobic chains within the bilayers can have varying degrees of randomness and mobility. X-ray diffraction studies provide two instantly recognisable features that are characteristic of the L_α phase. The first is the 'fluid like' character of the alkyl chains that is shown by a diffuse wide-angle X-ray diffraction peak corresponding to a Bragg reflection of 4.5Å[33]. The second, is the repeat bilayer spacing d (where d is equal to the sum of the water and alkyl chain layer dimensions) that follows the Bragg's Law and displays sharp reflections in the ratio *d : d/2 : d/3* …etc[3, 36]. The thickness of the bilayer can vary from 1.0 to 1.9 times the all-*trans* chain length (l_t) of the surfactant. In contrast, the water layer thickness varies over a much larger range from 0 to 500Å.

Lamellar phases can also fold into vesicles, which can either be multi-lamellar (MLV) (consisting of multiple bilayers) or uni-lamellar (ULV) with just a single layer as the outer shell. The different variants of the lamellar phase are described in detail in Chapter 3.
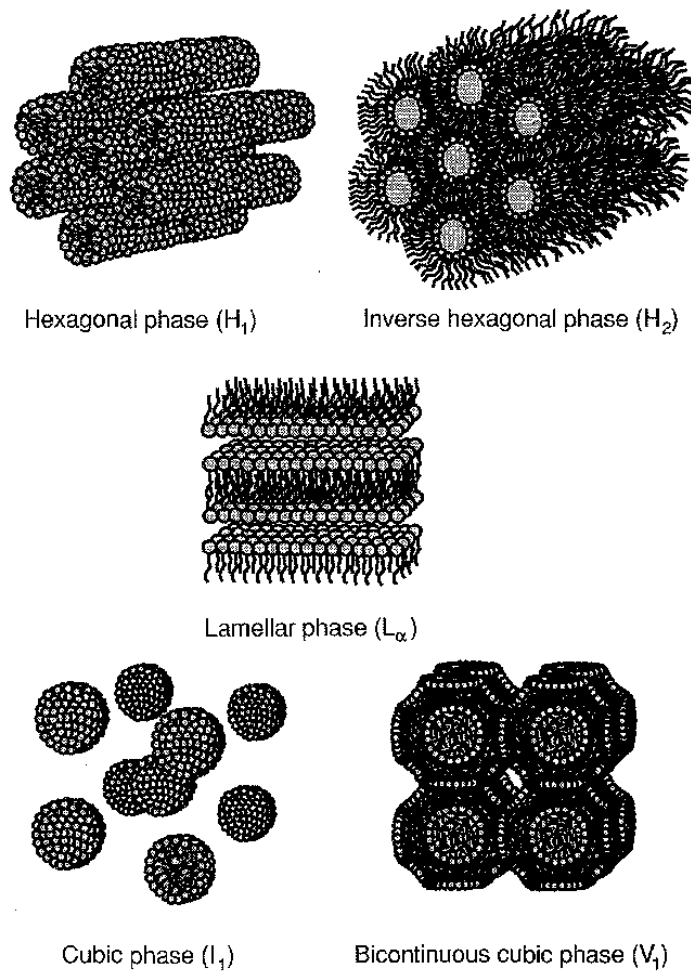
Figure 2.6: Common surfactant liquid crystalline phases[1].

2.2.2 Gel Phase (L_β)

The gel phase, like the L_α phase, consists of surfactant bilayers, although here the alkyl chains have restricted movement about the long axis only (perpendicular to the plane of the lamellar). The chains are packed in a two-dimensional hexagonal lattice, with rotational disorder[37]. These restrictions lead to a structure with a high viscosity which is only pourable at very low concentrations and limited industrial applications such as in hair and fabric conditioners and in the processing of low fat frozen deserts.

It has been reported[7, 38] that the cooling of a lamellar, L_α, phase can lead to the formation of a gel, L_β, phase, with three possible states which are dependent on the size of the hydrated head-group. In the normal gel phase (L_β), the bilayer is normal to the liquid crystal axis with vertical chains. The area of the polar head group matches that of the chain. The alkyl

layer thickness is found to be twice the all-*trans* alkyl chain length of the surfactant. These structures are mostly found in dialkyl lipid systems and are slightly more ordered than the other types[39]. The tilted gel phase is formed in systems where the polar head group area is larger than that of the alkyl chain, such as in monoglyceride systems. The interdigitated form is observed with long chain monoalkyl systems, for example, in potassium stearate system[40].

The stability of the gel phase (L_β) formed depends on the packing of the alkyl chains and the size of the hydrated head-group which determine which of the three structures (normal, tilted or interdigitated) will be formed (see Figure 2.7)[41]. The hydration of head-groups in the gel phase is lower than that of the lamellar phase and so L_β does not swell to the same extent as L_α[7].
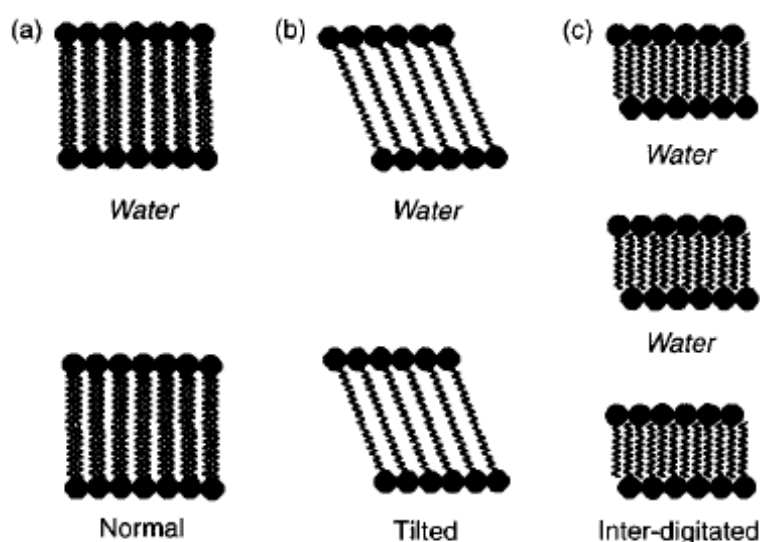
Figure 2.7: Schematic representation of gel phases: (a) normal, (b) tilted and (c) interdigitated[41].

2.2.3 Hexagonal Phase (H_1, H_2)

Hexagonal phase is the second common mesophase also known as the middle phase[7, 42]. This mesophase possess a high viscosity somewhere between that of the lamellar phase and the extremely viscous cubic phases that are described later. There are two types of hexagonal phase, which are the 'normal hexagonal' (H_1) phase, also known as the middle

phase from soap industry, and the 'reversed hexagonal' (H_2) phase. H_1 is water continuous forming if the surfactant is added to a polar liquid such as water. At low water concentrations, reversed hexagonal phase H_2 can occur. H_2 is alkyl-chain-continuous forming if the surfactant is added to a non-polar liquid such as oil. Both structures are described schematically in Figure 2.6.

Hexagonal phase is identifiable by unique optical textures observed under polarised light including 'fan like' and so called non-geometric textures. The optical textures are similar for both types of hexagonal phase.

The micelle diameter in normal structures is usually between 1.3-2.0 times the all-*trans* alkyl chain length (l_t) with the inter-micellar separation being in the region of 10-50Å. The micelle diameter in reversed structures is of order (1-1.5l_t) in thickness, and the inter-micellar separation is in the same region as for the normal but values above 30Å are rare. X-ray studies again show a diffuse reflection at 4.5Å corresponding to 'fluid like' alkyl chain region as well as reflections in the ratio $d : d/\sqrt{3} : d/\sqrt{4} : d/\sqrt{7} \ldots$ etc.

2.2.4 Cubic Phase (I_1, I_2, V_1, V_2)

There are two distinct aggregate structures that are classes as cubic phases, also known as viscous, isotropic phases[7, 43]. One of these consists of small micelles (normal or reversed) and the other one is based on three-dimensional bicontinuous aggregates (see Figure 2.6). In some cases, as the micelle concentration is increased, the micelles arrange into loose lattice patterns which are similar to crystal structures in terms of the arrangement. The first set of structures (small micelles) is labelled *I*, again with 1 or 2 to distinguish between normal and reverse micelles respectively. As their name suggests the structures are based around one of several cubic lattices, namely, normal cubic lattice, face-centred cubic lattice and body-centred cubic lattice. The bicontinuous classes are labelled V_1 and V_2 again corresponding to normal and reversed structures.

The cubic phases are isotropic and therefore appear black under crossed polarisers. They posses extremely high viscosity and they are distinguished by their position in the phase

diagram. The *I* phases occur at compositions between micellar solutions and hexagonal phases whereas the *V* phases between the hexagonal and lamellar phases.

2.2.5 Factors affecting the formation and transition in surfactant liquid crystalline phases

As discussed above surfactant molecules aggregate to form micelles and at higher concentrations these aggregate to form liquid crystalline phases. The factors that govern the formation and type of surfactant mesophase, and its transition from one form to another can be described simply in terms of micelle shape at the CMC and the 'effective' volume fraction of micelles[32]. The 'effective' volume fraction which governs what happens to the micelle packing at high concentration includes the actual volume occupied by tails, head groups and bound water. It also includes the effects of intra-aggregate and inter-aggregate interactions. The intra-aggregate interactions are those that are involved in determining the shape of the aggregates such as the head group interactions and the alkyl chain packing constraints (Section 2.1.4). The contributions to the inter-aggregate interactions include all the factors similar to the intra-aggregate interactions and in addition, the hydration of the head groups, the electrostatic and steric repulsions between the head groups[32]. Differences in the chemical structure of the surfactant have an effect on the concentration ranges of the mesophases formed but not on their sequences. However this is only true for the normal mesophases. For reversed mesophases the sequence varies with head group structure.

It has previously been discussed how the micelle shape can be predicted from surfactant structures and packing constraints. When the surfactant concentration increases, the aggregate concentration increases and the aggregates would be forced to come closer. There is a critical volume fraction above which random (disordered) solutions cannot occur. The inter-aggregation repulsions cause a transition to more ordered phases. For instance, spherical micelles form a cubic phase, cylindrical micelles form hexagonal phase and disc micelles/ bilayers form a lamellar phase. The diagram in Figure 2.8 describes this schematically.
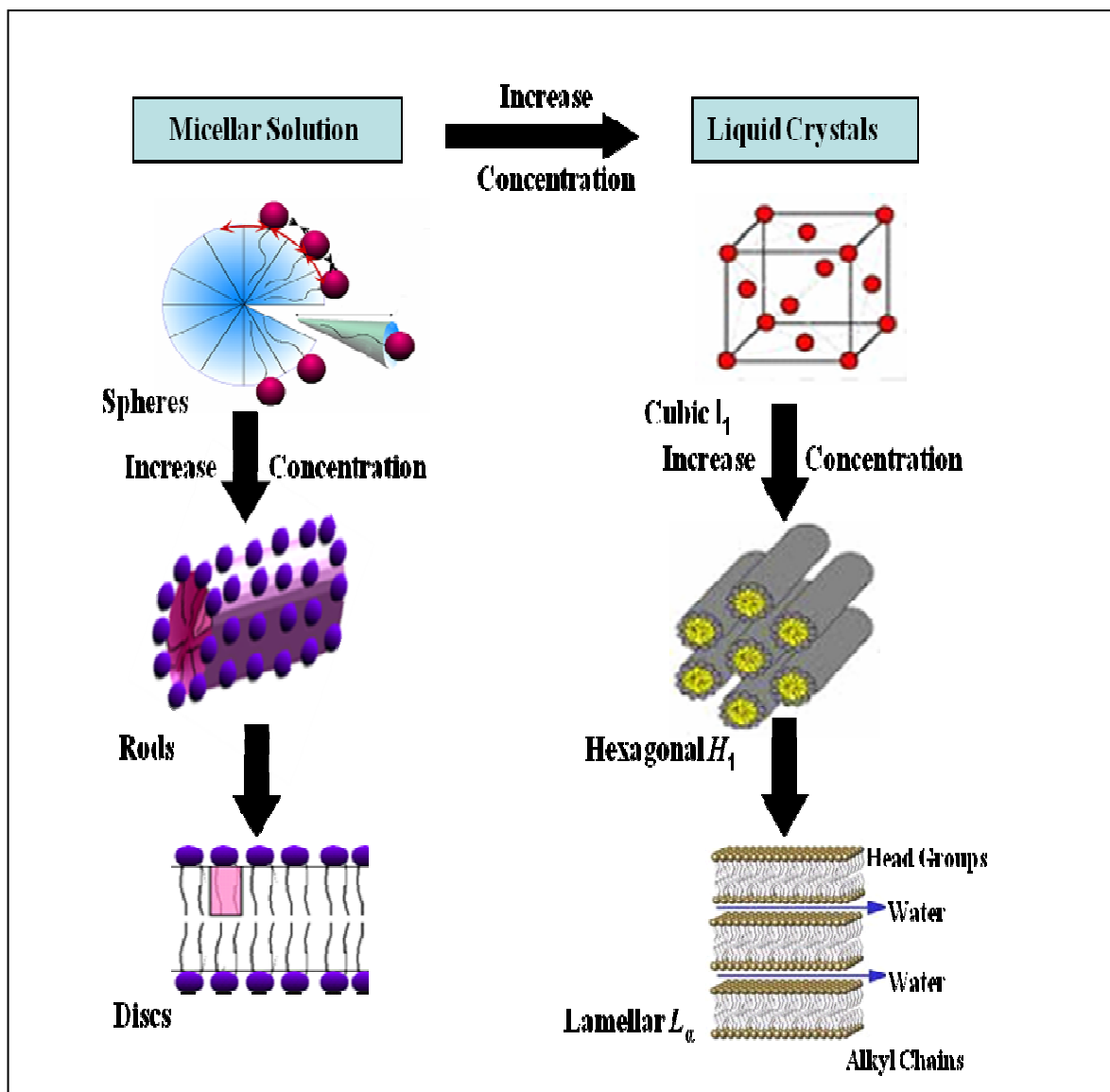
Figure 2.8: Schematic representation of the effect of increasing surfactant concentration on the formation and transitions in liquid crystalline phases.

At even higher concentrations within the mesophase, more surfactant can only dissolve with a reduction of interface curvature to a shape with a higher packing limit. Hence, a phase transition occurs to one of a smaller aggregate head group area. A summary of the relationship between head group size and micelle shape and liquid crystal transitions is shown in Table 2.2.

Head Group Area	Micelle shape	Liquid Crystal shape				
Small	Disc	Lamellar				
Medium	Rod	Hexagonal	Intermediate (V_1)	Lamellar		
Large	Spherical	Cubic	Hexagonal	Intermediate (V_1)	Lamellar	

Increasing surfactant concentration →

Table 2.2: The relationship between head group size, micelle shape and liquid crystal transitions.

The general order sequence of the phases would be expected to form is determined by the mean curvature of the polar/non-polar interface, and this sequence is shown in Figure 2.9[28]. The intermediate and bicontinuous cubic phases have unusual micellar aggregate curvatures, in-between that of hexagonal and lamellar phases so their packing behaviour is not easily visualised. Nevertheless, in the sequence they would be expected to form between hexagonal and lamellar phases[7].

The L_1 (normal) and L_2 (reversed) isotropic micellar solutions form at high and low concentrations of water respectively. These micellar solutions are not unstructured although the structural elements within are randomly arrayed and have molecular dimensions[3].
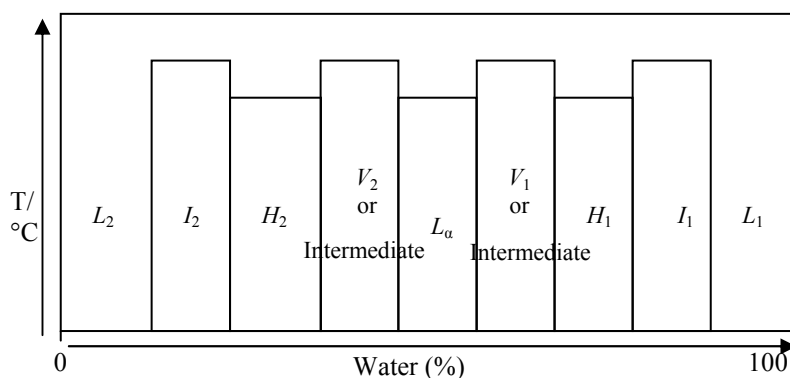
Figure 2.9: Schematic illustration of the mesophase sequence with increasing concentration as a function of temperature (redrawn from[28]).

46

Figure 2.9 summarises the sequence of mesophases formation as a function of increasing water concentration. This diagram used by Seddon[28], also takes into account the reversed phases although in terms of packing, their sequence is not fully understood. However, although this diagram is useful, it does not include clearly the role of the head group size in normal and reversed phases[7].

2.2.6 The Phase Rule and Phase Diagrams

A phase diagram is a graphical representation of all the equilibrium phases present at a particular composition, temperature and pressure. Phase diagrams are a useful tool for determining how many phases are formed, the type of phases formed and the compositions and temperatures that the phases form at. A typical phase diagram represents the formation of phases with respect to temperature changes against concentration.

The liquid crystalline phases are governed also by the same rules governing the solid, liquid or gas phases at equilibrium. Phase equilibrium exists when the chemical potential of a substrate in one phase is equal to that in other phases. The Gibbs phase rule is a useful equation to present the relationship between the various phases, mainly the transitions between them and the number of phases that can co-exist at equilibrium. The Gibbs Rule states that:

$$P + F = C + 2 \hspace{4cm} \textbf{Equation 2.8}$$

where P is the number of phases, F is the number of degrees of freedom and C, the number of components. The phase rule proves to be an important tool for the studies of lyotropic mesophases as well as the investigations of many multi-component systems.

2.3 Phase Behaviour

2.3.1 Anionic Surfactants

Anionic surfactants are used in greater volume in laundry detergents than the other surfactant class. It has been proposed that in detergent formulations the C_{12}-C_{18} chain lengths anionic surfactants give the best detergency properties. The most commonly used

anionic surfactants are the alkyl sulfates and sulfonates including linear alkyl benzene sulfonate (LAS) and sodium dodecyl sulphate (SDS), which are discussed below.

Linear Alkyl Benzene Sulfonate (LAS)

Commercial LAS is a multi-component mixture of different alkyl chain lengths (usually C_9-C_{14}) and isomers with 2,3,4,5 and higher isomers present. The 1-isomer is never present and therefore all components are actually branched and not linear as indicated by the name 'linear' alkyl benzene sulfonate. LAS (sodium LAS) is formed by the neutralisation of LAS acid (HLAS). This is performed, in commercial systems, using sodium hydroxide (NaOH) or sodium carbonate (Na_2CO_3)[25]. The chemical structures of the positional isomers of sodium dodecylbenzene sulfonate are illustrated in Figure 2.10.
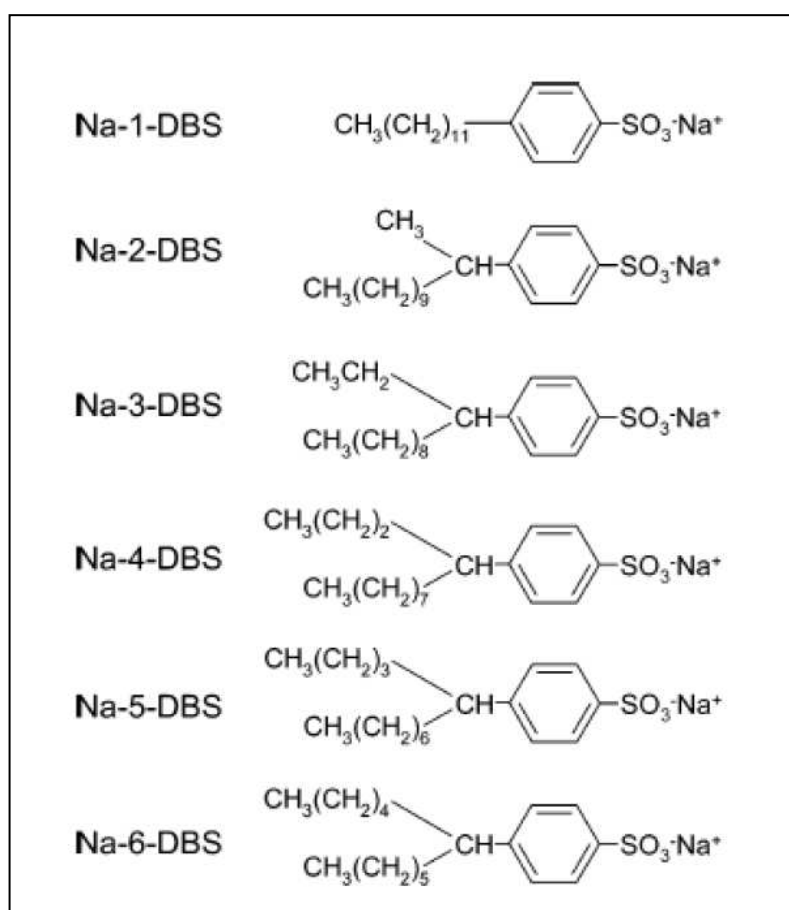
Figure 2.10: Positional isomers of Sodium Dodecylbenzene Sulfonate[44].

From a commercial point of view, LAS is the world's most extensive used synthetic surfactant[45]. Nevertheless the phase behaviour of commercial LAS is complicated and this

is because each commercial sample is a mixture of components of different alkyl chain-lengths and position of substitution of the benzene ring on the alkyl chain.

Commercial LAS systems are known to form a broad two-phase region of lamellar/micellar co-existence. All phase diagrams show an unusually wide two phase L_α/L_1 region appearing at room temperature. The wide region observed during phase behaviour studies of commercial LAS has been reported as the region where two lamellar phases co-exist at equilibrium for the 5-C_{12} isomer[46]. Shown in Figure 2.11 is the phase diagram for a mixed (commercial) surfactant system and multiple lamellar phases are observed.
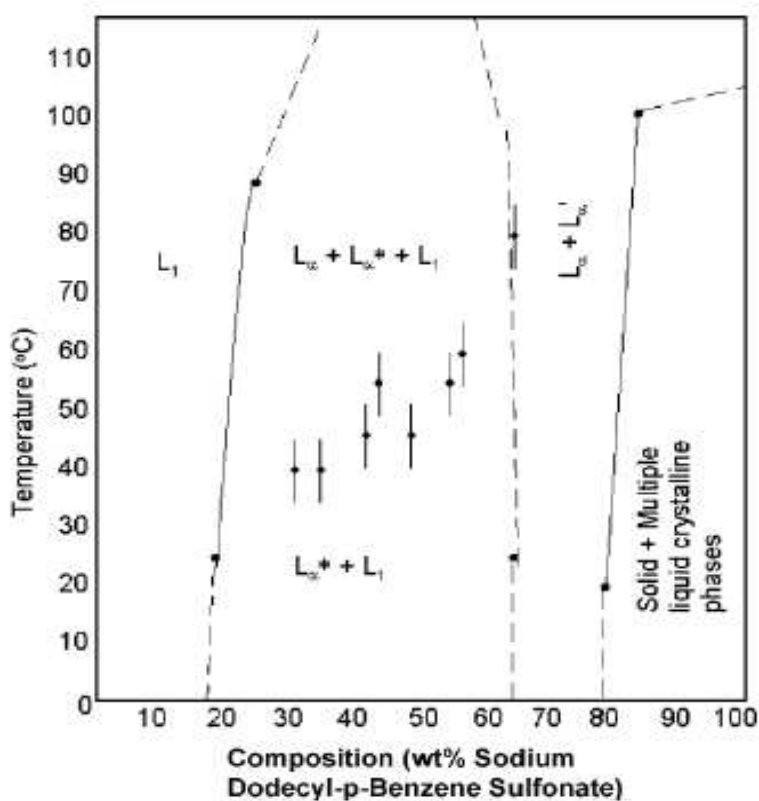
Figure 2.11: Phase diagram of commercial LAS/H_2O. L_α^* and L_α' are additional lamellar phases[47].

Studies on the pure LAS system have been done by Timimi *et al*[48] in 1992. Previous attempts to determine the phase diagram of the binary system have been in a good agreement with the phase diagram proposed by Timimi *et al*[48]. The pure isomers show different independent phase behaviour as shown in Figure 2.12.
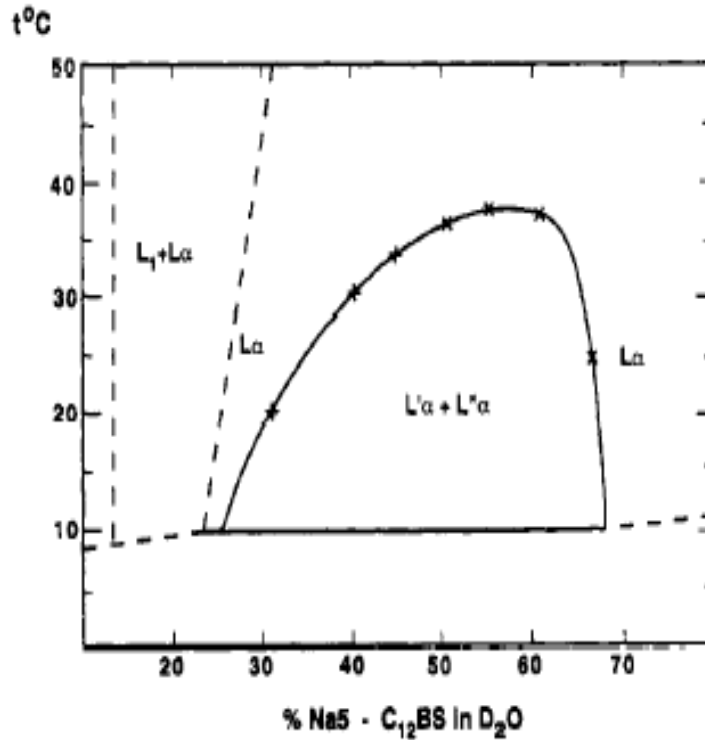
Figure 2.12: Phase diagram of pure 5-C_{12} LAS[46].

Tiddy *et al*[46] reports on the 5-C_{12} commercial LAS suggested the lamellar-lamellar co-existence. Different groups attempt to explain the reason for the co-existence of two lamellar phases. The discussion is based on a mean field potential using a long-range repulsion and a short-range attraction[49]. The long-range repulsion comes from the electrostatic forces as well as hydration repulsion when the fraction of free water is small. The short-range attractive forces have been investigated by Tiddy *et al*[46] who suggested that these forces arise from a specific counter-ion/head group association. This will increase the counter-ions concentration at the head group surface as the concentration of the surfactant increases. That may explain the appearance of multiple phases on the phase diagram of commercial LAS, since so many pure isomers exhibit these regions of partial miscibility.

Sodium dodecyl sulfate (SDS)

Sodium dodecyl sulfate or SDS is widely used commercially. Its full phase diagram was reported by Kekicheff[50, 51] in 1989 and is shown in Figure 2.13. It can be seen from the diagram that besides the lamellar (L_α) and hexagonal (H_1) phases (hexagonal is denoted as H_α) there are several intermediate phases that exist over a narrow range of concentration.
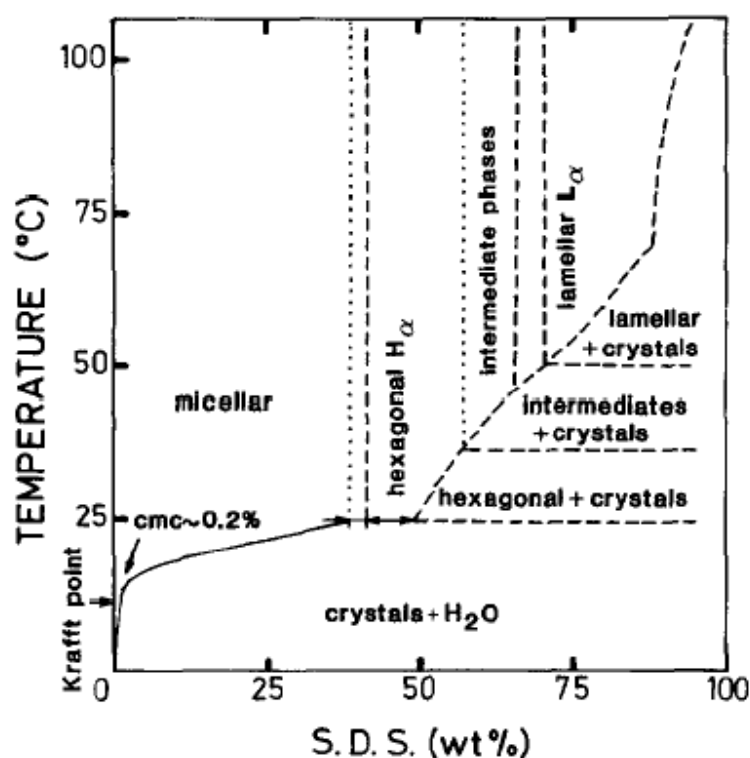
Figure 2.13: Schematic SDS/H_2O phase diagram (adapted from reference[51]).

Hexagonal appears at 37% in co-existence with a micellar solution and then at 40% as a single phase. A lamellar phase is the major phase between 69 and 86% surfactant and appears even at higher temperatures. Between hexagonal and lamellar phases a number of intermediate phases exist. Above 87% surfactant the lamellar phase co-exists with a crystal phase. The phase behaviour of ionic surfactants has been studied for a long time starting in 1943 with studies on soap by McBain[52, 53]. Due to the complicate electrostatic interactions present in ionic surfactant systems, there is still a lot of work to be done in order to fully understand their phase behaviour.

It has been reported that with increasing chain length, long rod-micelles form and a rod nematic phase can occur at the L_1/H_1 boundary. At higher concentrations with increasing alkyl chain-length, the $H_1/V_1/L_\alpha$ sequence changes to H_1/Intermediate/L_α or a combination of both. In this region because of the long-lived metastable phases difficulties can present when attempting to determine the equilibrium boundaries.

2.3.2 Nonionic Surfactants

Alcohol and ethoxylate based surfactants are widely used in detergents formulation. They are generally indicated as C_mE_n where C_m corresponds to the number of carbon atoms in the hydrocarbon tail and E_n represents the number of ethoxylate groups in the polar head group (sometimes denoted as EO_n). The structure of $C_{12}E_6$ is displayed in Figure 2.14 as an example.

$O(CH_2CH_2)_6OH$
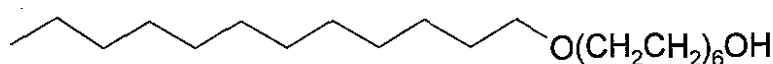
Figure 2.14: Chemical structure of $C_{12}EO_6$ (polyoxyethylene-6-dodecyl ether).

The equilibrium phase behaviour of these series of surfactants is well known and many phase diagrams are reported in the literature[54, 55]. Many studies have been focused on the lower consolute temperature termed cloudy point that is a characteristic temperature for nonionic surfactants[40]. Due to the absence of the long-range inter- micellar interactions present in ionic surfactants the association of non-ionic surfactants in water to form aggregates is simpler to understand. In non-ionic surfactants the intra and inter-micellar interactions exist over a much shorter range than in ionic surfactants. The effect of head group size on mesophase structure has been illustrated and has been reported that surfactants with large head groups form cubic (I_1) and hexagonal (H_1) phases. However, with increasing temperature the head group dehydrates and reduces in effective size, often until the interfacial curvature becomes zero or even negative.

As a result, the lamellar phase can be formed and a further temperature increase can lead to the formation of reversed phases. Additional studies on the effect of varying the head group size on phase behaviour have been done with reference to the $C_{12}E_n$ where n= 2-6, 8, 12[54]. Investigations on increasing further the head group size even further to E_{12} suggest that the clouding region shifts to higher temperature as the head group size increases. However, increasing the head group size results in the formation of tiny micelles with very small aggregation numbers which will not form mesophases. Furthermore, studies on the influence of alkyl chain length on the phase behaviour for C_mE_6 surfactant series have also been carried out. These studies suggest that on increasing the chain length to C_{16} the V_1

phase begins to be replaced by many intermediate phases including a random-mesh lamellar phase and also other metastable intermediate phases.

Overall, from the studies carried out so far, it can be said that an increasing alkyl chain length has little effect on the composition ranges of phases with positive curvature. The main consequence of increasing alkyl chain length is that the upper temperature limit of the micelles is increased. In addition, it has been reported that for very short chain length surfactants (C_n, n<8) no mesophases are formed at all.

Figure 2.15 below shows the phase diagrams of various polyoxyethylene surfactants in water.
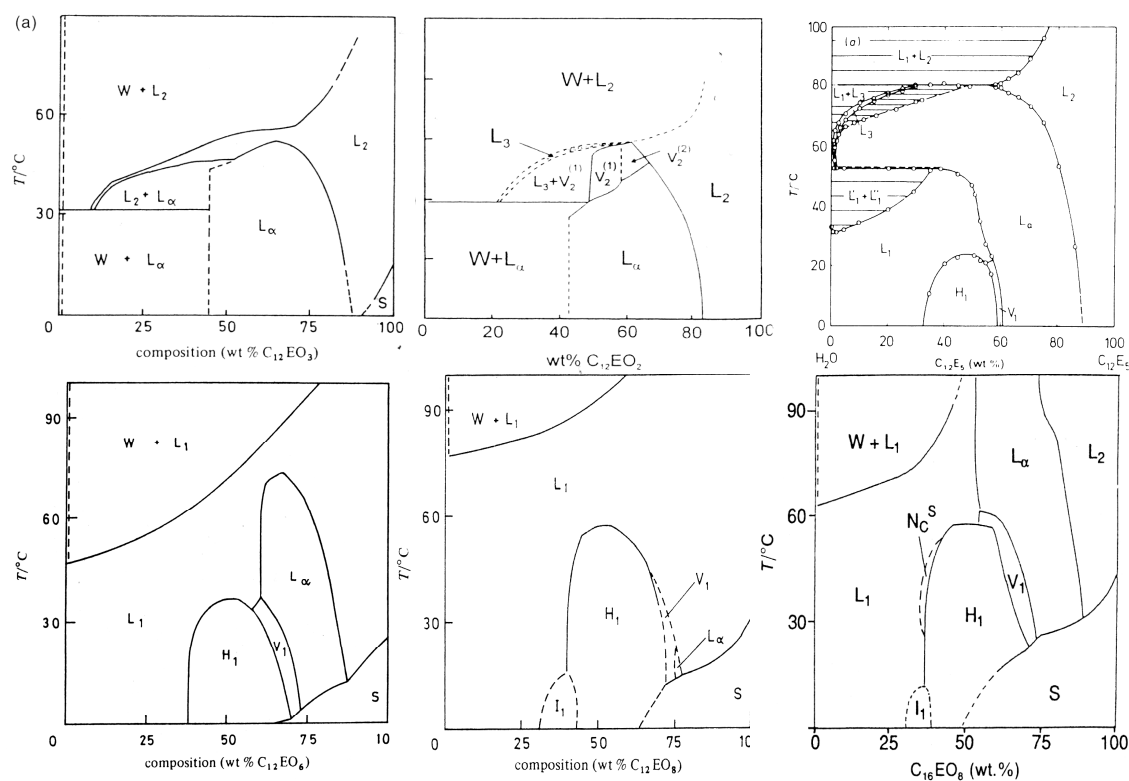
Figure 2.15: Phase diagrams of C_nEO_x/water. Note that most of phase regions are small and not shown. Phases L_1, L_2, H_1, L_α, I_1, and V_1 have all previously been derived. W is a very dilute surfactant solution and S indicates the presence of solid surfactant. In $C_{12}EO_5$ phase diagram $L_1{'}$ and $L_2{''}$ are surfactant solutions[31, 56, 57].

2.3.3 Surfactant Mixture

By the addition of third component such as electrolytes, hydrotropes, and co-surfactants into the surfactant/water system the phase behaviour can be very complex. The simplest way to study the changes in mesophase behaviour when third component is introduced to a system is through a ternary phase diagram. The important factors to consider are firstly the phase behaviour as a function of surfactant/additive ratio and secondly, the volume fraction of surfactant plus amphiphile for mesophase formation.

In order to gain a simplified picture is vital to consider firstly that surfactants do not generally form mixed crystals and secondly, all the concepts described in the preceding sections (micelle formation, packing constraints, volume fractions and inter-micellar interactions).

2.4 Liquid crystalline phases in everyday life

Liquid crystalline phases are important in a number of different areas of science and technology. Life on Earth begins with the self-organization of molecules *i.e.* the self-assembly of lipids into bilayers within the cell membrane. Numerous biological supramolecular structures, *e.g.* the spontaneous formation of the double helix of nucleic acids, collagen, *etc.*, result from self-assembly of organic molecules[58, 59].

From a technological point of view thermotropic liquid crystals may be found in optical devices, as sound wave and pressure detectors, and in the well-known electro-optical display devices. Lyotropic liquid crystals may be found in most household-care and personal-care products like shampoos, hair conditioners, hair creams, toothpastes, fabric and dish washing liquids, food items (*i.e.* mayonnaise, ice creams, spreads and sauces), paints, ink and coatings .

In this work we will focus on the lamellar phases. Lamellar phases even at high surfactant concentrations can flow easily as their layer slide past one another even under low shears. In addition the physical stability and viscoelastic properties of food emulsions have been attributed to the presence of a layer of lamellar phase around the oil droplets[60, 61]. There are several products, where lamellar phases find applications such as liquid detergent products,

personal care products, food items, paints and coatings. Furthermore, dispersed lamellar phases, *e.g.* vesicles, are also important in science and technology. Due to their structural properties multi lamellar vesicles (MLV) can be used in the pharmaceutical and cosmetic industries as encapsulates for drug delivery[62].

Most of the daily used products today are complex formulation involving two or more surfactant molecules. The 'attractiveness' of the product is a combination of many factors, including its multifunctional performance profile, aesthetic factors such as viscosity and clarity, product physical stability and processing. All of the ingredients in the formulation but especially the surfactants interact with each other to affect several of these criteria. It is important to know how the mixing phenomena are related to the product formulation in order to control and enhance the better performance of the product. For instance, in products like liquid detergents which are concentrated mixed surfactant solutions the question need to be addressed is how to use the fundamental principles to more effectively apply surfactant mixtures in order to address each of these topics in turn surface activity, mixing phenomena and liquid crystal phase behaviour.

Lamellar phases due to their wide range of applications have been a research subject of great interest. A great deal of knowledge of the basic principle of self-assembly of lamellar phases exists however research revolving around their structure across the length scales has not been fully understood. Questions arise on the liquid crystal phase behaviour of mixed surfactant systems and how that is related to the physical characteristic of the final product need to be considered. In turn, the microstructure of lamellar phases influences their microscopic properties such as rheology, optical texture and physical appearance. Therefore it would be of great importance to carry out research in this direction.

2.5 References

1.   Clint, J. H., *Surfactant Aggregation*. Blackie: Glasgow, 1990.

2.   McBain, J. W., Burnett, A. J., The effect of an electrolyte on solutions of pure soap. Phase-rule equilibria in the system sodium laurate-sodium chloride-water *Journal of the Chemical Society, Transactions* **1922,** 121, 1320-1333

3.   Figueiredo, N., Antonio, M., Salinas, S. R. A., *The physics of lyotropic liquid crystals*. Oxford University Press: New York, 2005.

4.   Hartley, G. S., *Aqueous solutions of Paraffin Chain Salts*. Hermann and Cie: Paris, 1936.

5.   Lindman, B., Wennertsrom, H., Amphiphile aggregation in aqueous solution *Topics in current chemistry* **1980,** 87, 1-83.

6.   Krafft, F., Berichte, D. B. G., *Physical Chemistry Chemical Physics* **1899,** 32, 1596.

7.   Tiddy, G. J. T., Hassan, S., Rowe, W., Surfactant Liquid Crystals and Surfactant Chemical Structure In *Handbook of Applied Surface and Colloid Chemistry*, Holmberg, K., Ed. John Wiley and Sons Ltd: Chichester, 2001; Vol. 1, p 465.

8.   Jonsson, B., Lindman, B., Holmberg, K., Kronberg, B., *Surfactants and Polymers in Aqueous Solutions* John Wiley and Sons: Chichester, 1998.

9.   Ottewill, R. H., Introduction. In *Surfactants*, Tadros, T. F., Ed. Academic Press: London, 1984.

10.   Masakatsu H., Masao, T., Yoshio, S., Colloidal properties of aqueous bivalent metal dodecylpoly (oxyethylene) sulfates and hexadecylpoly (oxyethylene) sulfates (I). *Journal of Colloid and Interface Science* **1979,** 72, (3), 458-464.

11.   Tanford, C., *The Hydrophobic effet: Formation of micelles and biological membranes*. Wiley-Interscience: New York, 1980.

12.   Costas, M., Kronberg, B., Silveston, R., General thermodynamic analysis of the dissolution of non-polar molecules into water. Origin of hydrophobicity. *Journal of the Chemical Society, Faraday Transactions* **1994,** 90, 1513 - 1522.

13.   Kronberg, B., Castas. M., Silvestonti, R., Understanding the Hydrophobic Effect. *Journal of Dispersion Science and Technology* **1994,** 15, (3), 333-351.

14.   Kronberg, B., Thermodynamics of adsorption of nonionic surfactants on latexes. *Journal of Colloid and Interface Science* **1983,** 96, (1), 55-68.

15.   Glew, D. N., Aqueous Solubility and The Gas-Hydrates. The Methane-Water system. *The Journal of Physical Chemistry* **1962,** 66, (4), 605–609.

16.   Eriksson, P. O., Lindblom, G., Burnell, E. E., Tiddy, G. J. T., Influence of organic solutes on the self-diffusion of water as studied by nuclear magnetic resonance spectroscopy. *Journal of the Chemical Society, Faraday Transactions 1: Physical Chemistry in Condensed Phases* **1988,** 84, 3129 - 3139.

17.   Akhter, M. S., Al-Alawi, S. M., Influence of alcohols on the critical micelle concentration of non-aqueous micellar solutions *Colloids and Surfaces A:Physicochemical and Engineering Aspects* **2000,** 164, (2-3), 247-255.

18.   Flockhart, B. D., The effect of temperature on the critical micelle concentration of some paraffin-chain salts *Journal of Colloid Science* **1961,** 16, 484-492.

19.   Stead, J. A., Taylor, H., Some solution properties of certain surface-active N-alkylpyridinium halides : I. Effect of temperature on the critical micelle concentrations. *Journal of Colloid and Interface Science* **1969,** 30, (4), 482-488.

20.   Hayase, K., Hayano, S., Effect of alcohols on the critical micelle concentration decrease in the aqueous sodium dodecyl sulfate solution. *Journal of Colloid and Interface Science* **1978,** 63, (3), 446-451.

21.   Gunnarsson, G., Joensson, B., Wennerstroem, H., Surfactant association into micelles. An electrostatic approach. *The Journal of Physical Chemistry* **1980,** 83, (23), 3114–3121.

22.   Israelachvili, J. N., Mitchella, D. J., Ninham, B. W., Theory of self-assembly of lipid bilayers and vesicles *Biochimica et Biophysica Acta* **1977,** 470, 185-201.

23.   Israelachvili, J. N., *Intermolecular and Surface Forces*. Academic Press: London, 1985.

24.   Israelachvili, J. N., *Surfactants in Solution*. Plenum Press: New York, 1984; Vol. 4.

25.   Ramaraju, S. M., Carroll, B. J., Chambers, J. G., Tiddy, G. J. T., The liquid crystalline phases formed by linear-dodecylbenzene sulphonic acid during neutralisation with sodium carbonate. *Journal of Colloids Surfaces A* **2006,** 288, 77-85.

26.   Israelachvili, J. N., Mitchell, D. J., Ninham, B. W., Theory of self-assembly of lipid bilayers and vesicles *Biochimica et Biophysica Acta* **1977,** 470, 185-201.

27.   Eastoe, J., Surfactant Aggregation and Adsorption at Interfaces. In *Colloid Science: Principles, Methods and Applications*, Cosgrove, T., Ed. Blackwell Publishing: 2005.

28.   Seddon, J. M., Structure of the Inverted Hexagonal (H2) Phase, and Non-Lamellar phase transitions of lipids. *Biochimica et Biophysica Acta* **1990,** 1031, (1), 1-69.

29.   Seddon, J. M., Templer, R. H., In *Structure and Dynamic of Membranes: from cells to vesicles*, Lipowsky, R., Sackmann, E., Ed. Elsevier Science: Amsterdam, 1995.

30.   Leigh, I. D., McDonald, M. P., Wood, R. M., Tiddy, G. J. T., Trevethan, M. A, Structure of liquid-crystalline phases formed by sodium dodecyl sulphate and water as determined by optical microscopy, X-ray diffraction and nuclear magnetic resonance spectroscopy. *Journal of the Chemical Society, Faraday Transactions 1: Physical Chemistry in Condensed Phases* **1981,** 77, (12), 2867 - 2876.

31.   Rendall, K., Tiddy, G. J. T., Trevethan, M. A., Optical microscopy and nuclear magnetic resonance studies of mesophases formed at compositions between hexagonal and lamellar phases in sodium n-alkanoate + water mixtures and related surfactant systems. *Journal of the Chemical Society, Faraday Transactions 1: Physical Chemistry in Condensed Phases* **1983,** 79, 637 - 649.

32.   Mitchell, D. J., Tiddy, G. J. T., Waring, L., Bostock, T., McDonald, M. P., Phase behaviour of polyoxyethylene surfactants with water. Mesophase structures and partial miscibility (cloud points). *Journal of the Chemical Society, Faraday Transactions 1: Physical Chemistry in Condensed Phases* **1983,** 79, 975 - 1000.

33.   Luzzati, V., *Biological Membranes, Physical Fact and function*. Academic Press: New York, 1968.

34.   Rosevear, F. B., The Microscopy of the liquid crystalline Neat and Middle Phases of Soaps and Synthetic Detergents. *Journal of American Oil Chemists Society* **1954,** 31, 628.

35.   Friberg, S. E., El-Nokaly, M. A., Marcel Dekker: New York, 1985; Vol. 16.

36.   Kumar, S., Structure: X-Ray Diffraction Studies of Liquid Crystals. In *Liquid Crystals, Experimental Study of Physical Properties and Phase Transitions*, Kumar, S., Cambridge University Press, Ed. 2001.

37.   Figueiredo-Neto, A. M., Salinas, S. R. A., *The physics of lyotropic liquid crystals* Oxford University Press: New York, 2005.

38.   Sadtler, V. M., Guely, M., Marchal, P., Choplin, L., Shear-induced phase transitions in sucrose ester surfactant. *Journal of Colloid and Interface Science* **2004,** 270, (2), 270-275.

39.   Chapman, D., Williams, R. M., Ladbrooke, B. D., Physical studies of phospholipids. VI. Thermotropic and lyotropic mesomorphism of some 1,2-diacylphosphatidylcholines (lecithins). *Chemistry and Physics of Lipids* **1967,** 1, (5), 445-475.

40.   Vincent, J. M., Skoulios, A., `Gel' et `coagel'. I. Indentification. Localisation dans un diagramme de phases et détermination de la structure du `gel' dans le cas du stéarate de potassium. *Acta Crystallographica* **1966,** 20, 432-440.

41.   Small, D. M., *The handbook of lipid research-The physical chemistry of lipids*. Plenum Press: New York, 1988.

42.   Ekwall, P., *Advances in Liquid Crystals*. Academic Press: New York, 1975.

43.   Luzzati, V., Vargas, R., Mariani, P., Gulik, A., Delacroix, H., Cubic Phases of Lipid-containing Systems: Elements of a Theory and Biological Connotations. *Journal of molecular biology* **1993,** 229, (2), 540.

44.   Ma, J.-G., Boyd, B. J., Drummond, C. J., Positional Isomers of Linear Sodium Dodecyl Benzene Sulphonate: Solubility, Self-Assembly, and Air/Water Interfacial Activity *Langmuir* **2006** 22, 8646-8654.

45.   HERA-Initiative, Human and environmental risk assesment on ingredients of household cleaning products: LAS linear alkylbenzene sulphonate, 2007.

46.   Tiddy, G. J. T., Timimi, B. A., Narayan, K. S. Ockelford, J. *Unilever Research Internal Report*; Port Sunlight Laboratory, 1991.

47.   Richards, C., Tiddy, G. J. T., Casey, S., Lateral Phase Separation Gives Multiple Lamellar Phases in a "Binary" Surfactant/Water System: The Phase Behaviour of Sodium Alkyl Benzene Sulfonate/Water Mixtures. *Langmuir* **2006**, 23, (2), 467-474.

48.   Ockelford, J., Timimi, B. A., Narayan, K. S., Tiddy, G. J. T., An upper critical point in a lamellar liquid crystalline phase. *The Journal of Physical Chemistry* **1993,** 97, (26), 6767-6769.

49.   Israelachvili, J. N., Wennerstroem, H., Hydration or steric forces between amphiphilic surfaces? *Langmuir* **1990,** 6, (4), 873-876.

50.   Kékicheff, P., Phase diagram of sodium dodecyl sulfate-water system: 2. Complementary isoplethal and isothermal phase studies. *Journal of Colloid and Interface Science* **1989,** 131, (1), 133-152.

51.   Kékicheff, P., Madelmont, C. G., Ollivon, M., Phase diagram of sodium dodecyl sulfate-water system: 1. A calorimetric study *Journal of Colloid and Interface Science* **1989,** 131, (1), 112-132.

52.   McBain, J. W., Vold, R. D., Jameson, W.T., A Phase Rule Study of the Mixed Soap System Sodium Palmitate-Sodium Laurate-Sodium Chloride-Water at 90°. *Journal of American Chemical Society* **1939,** 61, (1), 30-37.

53.   McBain, J. W., Vold, R. D., Frick, M., A Phase Rule Study of the System Sodium Stearate–Water. *The Journal of Physical Chemistry* **1940,** 44, (9), 1013–1024.

54.   Goggin, P. L., Kemeny, G., Mink, J., Infrared, Raman and force field studies of methyl- and perdeuteriomethyl-mercury(II) halides. *Journal of the Chemical Society, Faraday Transactions 2: Molecular and Chemical Physics* **1976,** 72, 1025 - 1035.

55.   Tanford, C., Nozaki, Y., Rohde, M. F., Size and shape of globular micelles formed in aqueous solution by n-alkyl polyoxyethylene ethers. *Journal of Physical Chemistry* **1977,** 81, (16), 1555-1560.

56.   Funari, S. S., Rapp. G., X-ray Studies on the C12EO2/Water System. *Journal of the physical chemistry* **1997,** 101, (5), 732-739.

57.   Corcoran, J., Fuller, S., Rahman, A., Shinde, N., Tiddy, G. J. T., Attard, G. S., Amphitropic liquid crystals. Part 1. Effect of a thermotropic mesogen on lyotropic

mesomorphism, and of a surfactant on thermotropic mesomorphism. The C16EO8–5-CB–water system. *Journal of Materials Chemistry* **1992,** 2, (7), 695-702.

58.   Whitesides, G. M., Grzybowski, B., Self-Assembly at All Scales *Science* **2002,** 295, 2418-2421.

59.   Kato, T., Self-Assembly of Phase-Segregated Liquid Crystal Structures *Science* **2002,** 295, 2414-2418.

60.   Pilpel, N., Rabbani, M. E., Formation of liquid crystals in sunflower oil in water emulsions. *Journal of Colloid and Interface Science* **1987,** 119, (2), 550-558.

61.   Friberg, S., Mandell, L., Larsson, M., Mesomorphous phases, a factor of importance for the properties of emulsions. *Journal of Colloid and Interface Science* **1969,** 29, (1), 155-156.

62.   Diat, O., Roux, D., Preparation of monodisperse multilayer vesicles of controlled size and high encapsulation ratio. *Journal de Physique II* **1993,** 3, (1), 9-14.

Chapter 3

Structured liquids based on lamellar phases

Surfactant molecules in solution form a wide range of self-assembled structures, which have motivated many theoretical and experimental developments[1, 2]. Packing constraints have previously been considered (Table 2.1), and the influence that these have on the microstructure discussed in Chapter 2.

One way to obtain structured liquid products is to make formulations containing lamellar (liquid crystalline) phases. The lamellar phases are the most widespread of all surfactant phases due to their wide range of applications and flow behaviours[2-4]. Structured liquids based on lamellar phases have attractive flow properties, which are very different from the Newtonian behaviour of normal liquids (Section 3.2). They are therefore described as non-Newtonian or complex liquids[5]. Examples include daily used products such as hard surface cleaners (Cif/Jif), liquid detergents, creams and body lotions[6].

Knowledge of the rheological behaviour of lamellar liquid crystalline systems is of decisive importance, especially when considering their functionality and performance when in use by the consumer. Factors such as flow from the bottle, physical stability upon storage, cosmetic appeal and many such crucial issues are all dependent on the microstructure-rheology relationship[7]. The various macroscale properties such as rheology (which governs the sensory properties such as mouth feel and texture), appearance (governed by the formulation process) and stability, all depend on the microstructure. The microstructure of structured liquids is in turn determined by product formulation, process conditions and procedures.

The relationship between rheology and microstructure is of both fundamental and practical importance[7, 8]. The rheological response during processing is directly related to the microstructural changes taking place. A better understanding of the changes in microstructure under shear could provide significant opportunities for the development of novel processes and the improvement of existing process routes[5].

A large amount of work has focused on understanding the changes in microstructural conformation taking place in the lamellar phase during shear[9-12]. The complicated rheological behaviour exhibited by such structured liquids depends on the re-arrangement and the re-orientations of the structure during flow[13-15]. Recent techniques have been involved combining rheological experiments with *in situ* observations such as small angle light scattering and nuclear magnetic resonance spectroscopy[8, 15-19]. These techniques have helped to elucidate the microstructural transitions or re-arrangements that occur in the lamellar phase of a wide range of surfactant systems.

In this Chapter, the introduction is followed by a discussion of the different morphologies of the lamellar phases (Section 3.1) and the main factors that influence the lamellar microstructure, namely formulation and process factors. The concept of rheology with relevance to structured liquids is described in more detail in Section 3.2. This is followed by Section 3.3 which introduces the shear-induced transitions in lamellar phases. In Section 3.4, we focus on the composition dependence of the lamellar phase rheology and describe work done in probing the key microstructural transitions that have been found to take place for a wide range of lamellar systems including both anionic and non-ionic surfactants.

3.1 Lamellar morphology

In aqueous media, surfactant molecules self-assemble to form aggregates of different microstructures and shapes depending on the composition, the temperature and the type of surfactant as discussed in Chapter 2. Studies on the microstructures of structured liquids can generally give information about the self-assembly or organization of the amphiphilic molecules on the micron level. The typical microstructures that are already well known in structured liquids are cubic, hexagonal and lamellar which are introduced in Chapter 2. Any structured liquid system might be formed of one or a combination of these microstructures at a certain temperature and concentration.

In detergency two commonly encountered aggregates are the lamellar and micellar arrays. The microstructure that is of importance of this work is the lamellar phase. In general, lamellar phases are known to consist of a stack of ordered bilayers aggregate separated by aqueous layers. In an excess of aqueous phase, the lamellar phases may exist in a dispersed

form. This dispersed form is normally spherical or oval structures, where one or several bilayers entrap water in its interior[20]. These vesicles can be further classified in uni-lamellar vesicles (ULV) and multi lamellar vesicles (MLV). The term "liposomes" is often used and referred to vesicle-like structures as well as the term droplets, spherulites and onions[21]. The lamellar morphologies are described in more detail in the following Sections.

3.1.1 Planar Lamellar phase, (L_α)

The Lamellar phase (L_α) is the most common type of surfactant mesophase with extensive applications in industry[22]. Because of the low viscosity of the structure and its pourability at high water concentrations one of the main applications is in laundry detergency (with optimum detergency achieved with the number of hydrocarbon groups in the range C_{12}–C_{20})[23]. Within this phase, the surfactant molecules are arranged into bilayers extending over large distances of at least a micron, which are separated by water layers. Here the layers are flat and the paraffinic chains are in a liquid-like state so each parallel layer can slide over each other with ease during shear which accounts for the low viscosity of the system. The thickness of the water layers, depending on surfactant, can be over the wide range of 0-50nm. The lamellar phase, relative to the other phases, is a low viscosity phase and it can easily be shaken into a container or, at high concentrations, can be poured[24].

Polarising microscopy and X-ray diffraction both assist in the identification of the lamellar phase (Section 4.1 and 4.3). Birefringence (Section 4.1) is observed when viewed under crossed polarisers on a polarising microscope displaying the easily distinguishable optical textures used to identify lamellar phases. If the sample is non-oriented a mosaic texture with many defects results. Orienting the lamellar parallel to the surface of the microscope slide produces pseudo-isotropic textures such as oily streaks and Maltese crosses[25-27]. In addition wide-angle X-ray diffraction gives a diffuse 4.5Å peak which corresponds to the fluid-like alkyl chains in the bilayer. For L_α phases small-angle X-ray scattering yield sharp Bragg reflections in the ratio of *d: d/2: d/3: etc* …, due to the organised supermolecular aggregates forming repeat layers. Here *d* is the sum of the water and alkyl chain dimensions[28, 29].
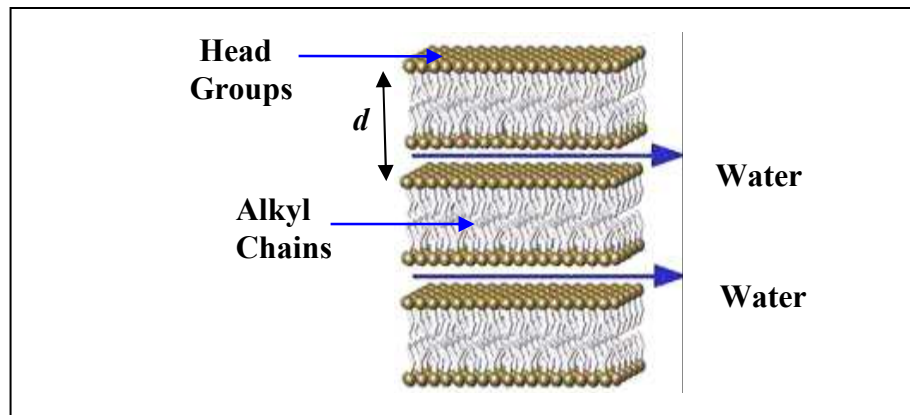
Figure 3.1: Schematic representation of bilayer structure exhibited in Lamellar phases (L_α).

3.1.2 Uni- and Multi-Lamellar Vesicles

Lamellar phases can also fold into vesicles, which are spherical or oval structures built from lipid or surfactant bilayers[20]. They are normally formed in an excess of dispersed aqueous phase. The vesicles formed when a single bilayer entraps a portion of aqueous phase are called uni-lamellar vesicles (ULVs). Alternatively, when several concentric bilayers entrap portions of aqueous phase, they are denoted as multi-lamellar vesicles (MLVs). MLVs usually referred to as onions simply due to the arrangement of bilayers into a concentric vesicle.

Vesicles have potential applications in pharmaceutical industry as encapsulates and carriers for drugs[30]. Vesicles could be used in the case of liquid detergents as carriers for enzymes and perfume[31, 32]. For all these applications vesicles can promote the structuring properties of lamellar phases, either by using the bilayer as an accessible surface or by using the entrapped aqueous region as a controlled reaction environment[33].

It seems that in most of the research on MLVs shear is assumed to convert a planar array to a vesicular one[13, 34]. The shear induced structural changes in the planar lamellar phases is a complicated subject and is covered separately here.

The use of packing parameters is a useful tool to predict what phase is likely to form, however does not give any information on the morphology of the expected microstructure. A detailed understanding of the microstructure of lamellar phases has been the main object

of several studies by using a wide range of experimental techniques such as optical microscopy, X-ray scattering and nuclear magnetic resonance spectroscopy. The relationship between their structure at several length scales and their physical properties is still unclear[35]. The knowledge of the structure, at different levels such as the molecular, micro, meso and macroscopic level, is a fundamental issue in order to understand the properties and the functionality of structured liquid products.

The key factors affecting the microstructure are the product formulation routes and the process conditions. The product formulation is the composition of its ingredients and their relative proportions by weight. The basic formulation of structured liquids includes surfactants in concentrated electrolyte solutions[1]. An important feature of the electrolyte is that it induces a transition from isotropic micellar solution into a lamellar phase. An additional feature of the salt is that by dissolving large amounts of specific salts (up to 20% by weight) in low pourability lamellar phases, better pourable phases can be obtained. The salt-induced changes in lamellar microstructure are discussed below.

Other additional ingredients can range from polymers, silicones, fragrances, preservatives and perfumes. When mixed, a single or a combination of phases can be formed depending on the concentration and temperature. These phases form the microstructure of the product and are responsible for the final properties of the product and therefore its performance when in use by the consumer.

The physicochemical stability of the product is another important factor to consider in designing the product formulation. The product must be easily applicable and also be able to incorporate all the mentioned additional ingredients. Another important consideration in process design is the order of addition of ingredients. A change in the order of ingredients added into the process can often result in products with different functionalities. The challenge is to identify the effect of processing on the microstructure of structured liquids and to use this understanding to manufacture products with improved performance[36]. Macroscopic measurements such as the viscometer flow curves and any other rheological patterns provide a first step towards understanding the effect of process on product microstructure and, as a consequence, on the product's properties.

3.1.3 Salt-induced transition from a planar to a vesicular array

Typically on adding a surfactant to water, as concentration is increased, micelles are expected to form. As already discussed in Chapter 2 further increase of the surfactant concentration leads to the formation of a number of mesophases. However the addition of some salts can lead to changes in the microstructure of mesophases formed. The present project is concerned with salt-induced changes in lamellar morphology and its underlying salting-out behaviour. Important aspects of the influence of salt on the microstructure include salting-out behaviour and screening of electrostatic repulsions between head groups, between bilayers and between aggregates.

The actual mechanism by which salting-out occurs is not clear. However it seems likely that initially adding salt increases the aggregation number in the micelles thus it lowers the CMC and changes the aggregate morphology [2, 37]. These changes are caused by breaking-down the hydration layer of the surfactant, decreased electrostatic repulsions, and an increased counter-ion binding[38].

Studies on the microstructure dependence on the electrolyte added into the system showed that the addition of salt has significant effects on the packing parameters for micellisation and therefore on the properties of the liquid crystalline phases. Versluis *et al*[13] reported a stable dispersed onion phase formed with sufficient salt concentration. Bergenholtz and Wagner[39] studied the rheology of the lamellar phases formed in samples with different salinities. They reported that the onions are observed at very low salt concentration, whereas a sheet-like lamellar phase observed above 0.9% salt concentration.

Sein *et al*[40] reported the salt-induced formation of a lamellar phase in a mixture of anionic surfactant, sodium dodecyl benzenesulfonate, and a non-ionic poly(ethylene oxide) alkyl monoether. They reported that at low surfactant concentration and high salt concentration (>15% by weight) a regular lamellar phase is formed. At intermediate salt concentration (6-12% by weight) they reported that very large spherical aggregates are formed consist of one or several bilayers.

3.2 Rheology

Professor Bingham of Lafayette College, Easton, PA, invented the term 'Rheology'. It means the study of flow and deformation of matter[5, 41, 42]. The practical and the theoretical interest in the properties and behaviour of widely used materials under shear have increased over the past few decades. Nowadays, significant advances have been made and the scope of rheology is even wider. There has been a significant appreciation of the importance of rheology in many areas such as biochemistry, polymer science and in chemical processing industries.

The theory of rheology has its beginnings in 1678 when Robert Hooke developed his theory of elasticity. A few years after, in 1687, Isaac Newton published his hypothesis associated with steady shearing flow. He stated that "the resistance which arises from the lack of slipperiness of the parts of the liquid, other things being equal is proportional to the velocity with which the parts of the liquid are separated from one another". The lack of slipperiness refers to what we now call 'viscosity'. Viscosity is a measure of 'resistance to flow'.

As mentioned above the concept of viscosity was introduced by Newton as the 'lack of slipperiness' when a material is subjected to a shear stress. Newton's Law state that the shear stress σ, acting on an element of material is proportional to the velocity gradient, or shear rate of deformation, through the follow equations:

$$\sigma = F/A \qquad \text{(Pa)} \qquad\qquad \textbf{Equation 3.1}$$

$$(\dot{\gamma}) = \frac{\text{Change in velocity in x direction } (\partial v_x)}{\text{Change in distance in y direction } (\partial y)} = \frac{\sigma}{t}(\text{s}^{-1}) \qquad\qquad \textbf{Equation 3.2}$$

$$\eta = \frac{\sigma}{\dot{\gamma}} \qquad \text{(Pa s)} \qquad\qquad \textbf{Equation 3.3}$$

When dealing with rheology fluids are classified into two classes, these with the simplest rheological behaviour, called Newtonian fluids and those which depart from this type behaviour the non-Newtonian fluids[43]. For Newtonian fluids η sometimes is called the coefficient of viscosity but it is more commonly referred as the viscosity.

For Newtonian fluids the shear stress, σ, is proportional to the shear rate, $\dot{\gamma}$ and the viscosity remains constant. However, in Non-Newtonian systems the relationship between shear stress and viscosity is no longer linear (Figure 3.2).
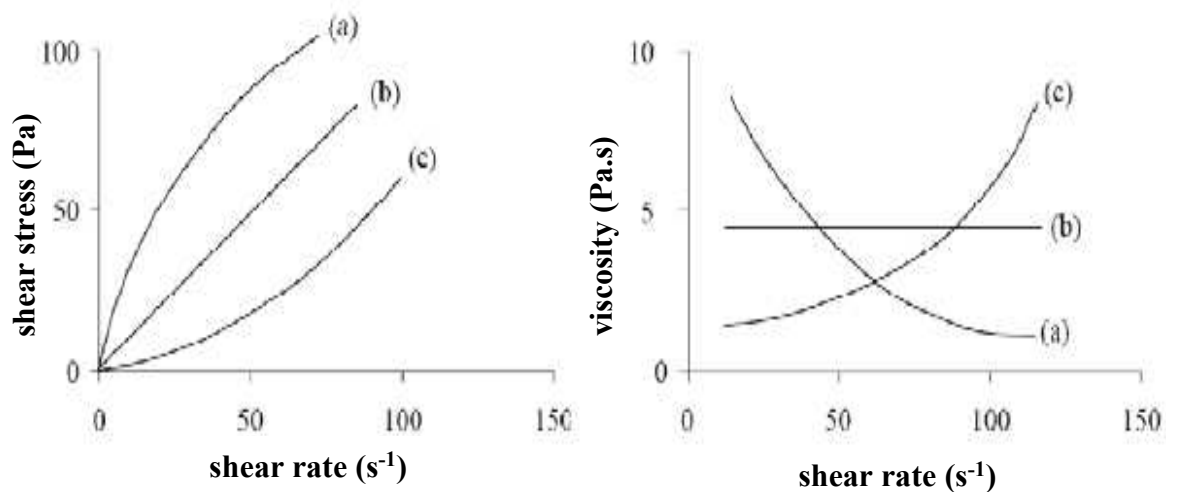
Figure 3.2: Shear profiles as a function of shear rate where (a) is shear thinning, (b) is Newtonian and (c) shear thickening[44].

Structured liquids exhibit non-Newtonian rheological behaviour[5]. The viscosity of these complex fluids is dependent on the applied stress, the strain rate and the strain history. In addition, the viscosity of structured liquids depends on the concentration of the overall ingredients in the system, the microstructure of the phases formed by the ingredients, pressure, temperature, time of shearing, shear history, age and the shear rate applied. For example, the viscosity of a structured liquid decreases with an increase in shear rate like in shampoo, conditioner and other consumer products. Such behaviour is called shear thinning behaviour. For shear thinning liquids, the general shape of the steady state flow curve representing the variation of viscosity with shear stress is shown in Figure 3.3.
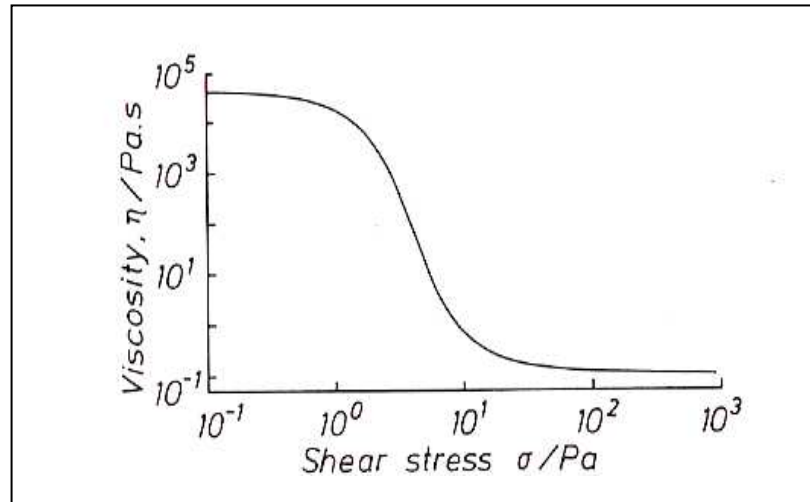
Figure 3.3: Typical behaviour of a shear-thinning non-Newtonian liquid[5]. In this case the system is at steady state and $\eta = \dfrac{\sigma}{\dot{\gamma}}$.

From the curve shown in Figure 3.3 three regions characteristic for a shear thinning liquid are observed. In the limit of very low shear stresses the viscosity is constant and that is known as the first Newtonian plateau. The term 'zero-shear viscosity' has been used to describe the high constant value of viscosity observed in the first Newtonian plateau. The second Newtonian plateau is observed in the limit of high shear stresses, where the viscosity is again constant but at lower level. In the first Newtonian plateau, the stress applied is too small to cause changes in viscosity. The low magnitude applied shear stress is stored in the elastic components. After application of sufficient magnitude of stress, changes in viscosity are observed and this happens at the end of the first Newtonian plateau. At this point the elastic components break. In the shear thinning regime, the microstructure of the structured liquid deforms and reorganise itself in such a way to accommodate the applied stress. The viscosity decreases until to reach a constant value. The second Newtonian plateau exists only for some structured liquids at higher shear stresses. In this regime, the deformation of the microstructure of the structured liquid will be much less and so the viscosity will be almost constant.

An instrument designed to measure viscosity is called 'viscometer'. A viscometer is a special type of rheometer which is limited to the measurement of viscosity. A rheometer measures the rheological properties of a complex liquid, such as the viscosity, as a function of the rate or frequency of deformation. For complex liquids, the simplest devices impose a

shearing flow on the sample and measure the resulting stresses, or alternatively, impose a shearing stress and measure the resulting shearing rate.

The rheometer can be used in either controlled stress mode (used for freely flowing samples, η = ca. <100mPas) or controlled rate mode (used if the sample will not flow freely η = ca. >100mPas). If controlled stress mode is employed the instrument applies a torque (force) and measures the resultant displacement (movement). These values are converted into viscosity after calculating the corresponding shear-rate values and using measuring system constants. If controlled rate mode is employed the instrument works in the opposite manner measuring the force as the movement is set. Again viscosity is calculated after firstly evaluating the corresponding shear-stress values. The cone and plate geometry has been chosen for all the rheology experiments throughout this study (Figure 3.4).
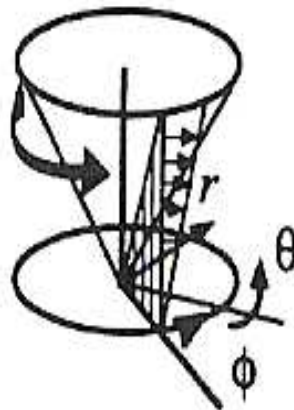
Figure 3.4: Schematic representation of the cone and plate geometry for producing shearing flows[5].

The non-Newtonian behaviour can be described by a number of models. One of the most common is the Power Law model (Equation 3.4).

$$\sigma = K \dot{\gamma}^{\eta}$$

Equation 3.4

where K is the consistency index and η is the power law exponent where for shear thinning liquids $\eta<1$.

Rheology as stated above can be about the effect of shear or it can be about the factors influencing the rheological behaviour and properties. This means that it is possible through rheology to study the viscoelastic properties of a substance. The word 'viscoelastic' means the existence of viscous and elastic properties in a material.

Structured liquids are usually viscoelastic[5, 45]. Their rheological behaviour needs to be examined bearing in mind their viscous and elastic properties. Therefore, steady-shear viscometry can not fully characterise structured liquids. Viscometry (shearing flow deformations) can be used to measure viscosity and oscillatory rheology (oscillatory deformations) to obtain dynamic parameters such as the complex modulus (G^*), elastic modulus (G'), viscous modulus (G'') and complex dynamic viscosity ($|\eta^*|$).

Oscillation testing is a dynamic test which oscillates the sample with very small oscillatory stresses without significantly deforming the microstructures. In oscillatory measurements, the response in stress of a viscoelastic material is monitored as a function of strain amplitude and frequency. Firstly, a strain sweep step is performed, where the frequency is fixed and the amplitude varied. The viscoelastic response of the material is a linear function of the applied strain until the critical strain is reached (γ_c). When the critical strain value is reached, a break down of the structure is achieved. The next step, if there is no need to disturb the structure, is the frequency sweep step. This step is carried out below γ_c. Herein, the viscoelastic properties of the material known as the storage modulus, G', and the loss modulus, G'', are obtained. G' and G'' can be obtained from the response of the material to the applied strain of variable frequency (ω).

The relationship between the loss and elastic modulus is given by Equation 3.5

$$\tan \delta = \frac{G''}{G'}$$
                                                                            Equation 3.5

The value of δ can describe the nature of the fluid. For an ideal elastic solid (G' dominates) and δ has a value of 0° and if δ has a value of 90° there is a completely viscous flow and an ideal viscous material (G'' is dominant).

In an oscillatory experiment, any number of instantaneous values of the stress and strain yields the complex modulus $G*$. $G*$ represents the overall resistace to deformation. The complex modulus is obtained from the ratio of stress amplitude to the strain amplitude. This modulus is the sum of the elastic modulus G' and the viscous modulus G''. Thus,

$$G^*(\omega) = G'(\omega) + iG''(\omega)$$ **Equation 3.6**

Since $G*$ is fundamentally stress/strain, G' and G'' have units of Pa (Nm^{-2}). The complex viscosity ($|\eta*|$) is the ratio of the complex modulus and frequency ($G*/\omega$).In a typical rheological experiment, we seek to measure $G'(\omega)$ and $G''(\omega)$. The measurements are obtained as a function of frequency (ω) because soft material's behaviour is solid-like or liquid-like depending on the time scale at which it is deformed.

These moduli are measures of particle-particle or domain-domain interactions, and although these are macroscopic rheological measurements they are dependent on microscopic considerations, and thus can yield information on microstructure. In some cases these moduli can be used to observe changes caused by changing the composition of the system.

3.3 The effect of shear on L_α phases

When lyotropic liquid crystals are subjected to shear, they present complicated rheological behaviour dependent on the rearrangement and reorganisation of structures during the flow[9, 10, 46-48]. A short review of the influence of shear on lamellar systems is given here as this is central to this project.

The effect of shear on lamellar phases has been investigated by a variety of experimental techniques such as optical microscopy and rheo-optics (birefringence), small-angle neutron scattering (SANS), small-angle light scattering (SALS) and deuterium nuclear magnetic resonance (^{2}H NMR) spectroscopy.

A significant fraction of recent studies have focused on lamellar phases, both the planar sheets and systems where the bilayers fold to form closed structures, such as uni- or multi-layered lamellar vesicles. According to many authors[49-51] the lamellar phase becomes

spatially ordered by the shear flow. They suggested that the orientation in the resting sample is essentially determined by the interdomain interactions. However, when an external force (shear) is applied on such a system, the formerly disordered internal structure becomes more ordered. The studies on the structural changes in shear flow, especially with materials of a well-characterised lamellar structure, have suggested a rich variety of shear-induced orientation states and these states are characterised according to the direction of the layer normal. In all cases, a shear-induced alignment of the lamellar was found, which can be characterised by comparing the orientation of the layer normal with the direction of flow, the direction of the velocity gradient and the vorticity direction respectively[17].

Shear thinning lamellar phases have been studied in order to investigate the relation between microstructure and shear-induced orientation. In this direction, works by Roux and co-workers[34, 52] using a combination of techniques including microscopy, SALS, SANS, birefringence and rheology, have been very informative. Their work was based on the quaternary mixture water/SDS/pentanol/dodecane. They investigated the effects of shear on a defective lamellar phase. They detected three different microstructure regimes for their system as shown in Figure 3.5.
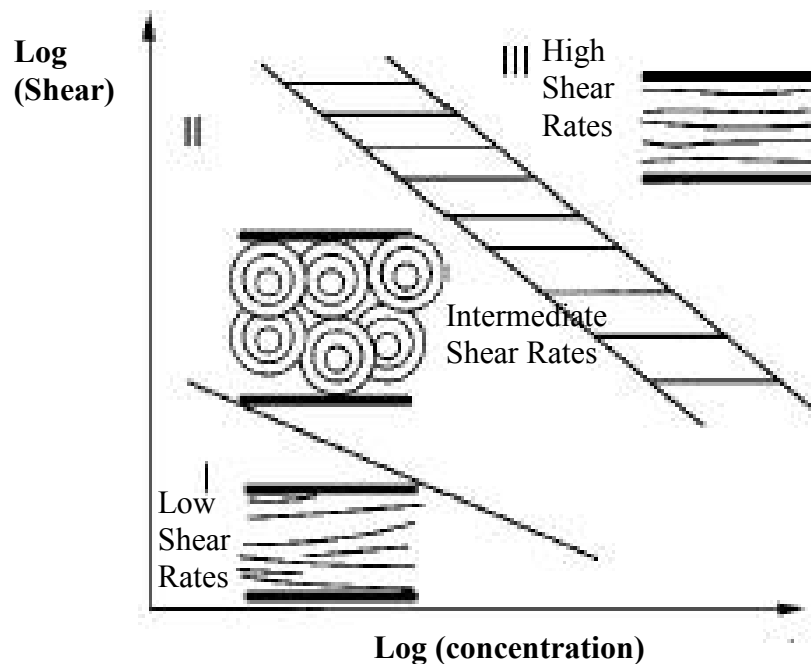
Figure 3.5: Schematic representation of the effect of shear on a defective lamellar phase as reported by Roux and co-workers[34, 52].

Regime I corresponds to a state in which the lamellar phase is aligned parallel to the flow direction, however defects remain in the velocity direction as well as in the vorticity direction. In regime II, the layers are broken into pieces by the flow and rearrange themselves into an isotropic state of monodisperse multi-lamellar vesicles (onions). Regime III corresponds to the same orientated structure as regime I, however fewer defects are present in the flow direction. Thus, regime III represents a highly ordered or uniform lamellar phase. The intermediate regime called II+III represents the coexistence of regime II and III.

In different systems, however, do not always exhibit the same scenario. There can be considerable variations. SDS/octanol/water, for example shows a hexagonal packing of onions and a transition from small to large onions[16]. For other systems, such as the $C_{16}E_6$/water system, a transition from the parallel to the perpendicular orientation has been observed without the transition to vesicles[49].

In addition to shear aligned lamellar, a shear induced formation of multi-lamellar vesicles in aqueous solutions has been reported for ionic and nonionic surfactants by Diat *et al*[53]. According to Diat, Roux and co-workers[34, 52, 53], the formation of MLV (onion phase) is dependent on the nature of the system, its concentration, composition and the shear rates applied.

In lamellar system many studies show that shear will lead to a transition from a planar array into MLVs[54-58]. In early 1992, Jonstromer and Strey[59] found that stirring an aqueous system of non-ionic surfactant in the lamellar phase produced an opalescent solution. Scattering experiments have proven that this phase is a vesicle phase[16]. In 1993 Roux and co-workers presented the orientation rheogram described earlier and report the formation of vesicles at intermediate shear rates (Figure 3.5). Similar behaviour, as seen in the complex system of water/SDS/pentanol/dodecane, has also been reported for a non-ionic system studied by Le and co-workers[60].

In addition, shear induced vesicle formation has been studied by many groups investigating the role of factors such as shear rate, stress, strain and frequency. Vesicles are believed to form because as the shear rate increases the sample is forced to deform more rapidly and

the bilayer oscillations can no longer accommodate the flow, leading to undulation instability and ultimately the formation of vesicles[61, 62].

The undulation stability of lamellar phases has been investigated theoretically by many groups[62, 63]. The mechanism proposed is that a layered system under shear leads to alignment of the layers parallel to the plates but with tilt that causes the layers to have a tendency to reduce their thickness and, above a critical shear rate, develop undulations[63]. Zilman et al[62] proposed a mechanism for vesicle formation based on the undulation instability. They suggested that the formation of vesicles is observed above a critical shear rate. Below that critical shear rate the shear stress induced in the structure is balanced by the elastic restoring forces of the lamellar phase. Above the critical shear rate, the lamellar folds into a curved shape characterised by stability limit, which is the limit of where the lamellar breaks up into the MLV phase.

Studies on the effects of surfactant concentration on the rheology of the lamellar phase have motivated a great deal of specific work into the changing lamellar conformation from planar lamellar to the multi-lamellar vesicles. The changes as well as the properties of the multi-lamellar vesicles have been studied extensively by Diat and co-workers[53]. It has been reported that at high surfactant concentrations the formation of onions is shifted to higher shear rates[52].

The size of the vesicles formed by shearing a planar lamellar phase has been investigated by Courbin et al[64]. The resulting size of the vesicles can be controlled by the shear rate[65]. Diat et al[34] reported that the vesicle size varies as the inverse of the square root of shear rate. The MLVs structure can be disappeared when the shear is stopped, and the relaxation back to planar lamellar phase is very slow (time depends on the system composition)[65]. The size of the vesicles depends on the applied shear rate, decreasing from a few microns to a tenth of a micron, as the applied shear rate increases. Although many groups attempted to investigate the effect of shear rate on the size of the vesicles, the actual mechanisms leading to vesicle formation are still not fully understood as a result of a lack in understanding of the relation between flow and structure in structured liquids[34, 64].

Studies on the planar lamellar to vesicle transition suggested that MLVs only form from the planar lamellar structure under shear conditions[13, 34]. Some other groups reported that

the formation of MLVs with increased shear rate gives a significant increase in viscosity thus resulting to a shear thickening behaviour[66, 67]. Other authors proposed that shear induced transformations are also dependent on the density of structural defects, like dislocations, in the lamellar phases[34, 68, 69]. It is difficult to achieve a perfect lamellar structure in any system. The lamellar phase usually contains many defects in the form of dislocation loops or thermodynamically stable defects where the lamellar bilayer is highly curved[47]. Defects in the form of dislocation loops were extensively investigated by Allain[70]. Zipfel *et al*[17, 49] studied the effect of shear induced structures on a defective and defect free lamellar phase, formed in SDS/decanol/water system. The parallel to perpendicular transition was observed in the defect free lamellar phase, while for the defective lamellar phase a transition to vesicles was reported.

Different processes have been reported for shear induced vesicle formation. In addition, vesicles have been found in the lamellar phase of several structured liquids, even when no mechanical shear was applied to the system. In some cases, the vesicles were formed simultaneously during simple mixing of the sample[13]. In these cases the vesicles are usually polydisperse, while the vesicles produced by controlled shear rate have a narrow size distribution.

The rheology of lamellar phases is a subject of considerable importance from both fundamental and applied points of view. The rheological response during flow conditions is directly related to the microstructural changes as has already been discussed. However, there are many other factors controlling the details of the general flow of lamellar phases which need to be considered. These factors are the volume fraction of the lamellar phase, the forces acting on particles during flow and the chemical composition of the system under investigation.

As mentioned above, one way to obtain information about the rheological behaviour of L_α phases is to measure their viscosity during flow conditions. The rheology measured macroscopically is strongly dependent on the microstructure of the phase formed. As mentioned in Section 3.1 the microstructure of structured liquids depends on the product formulation that means the composition of its ingredients and their relative proportions by weight. Therefore, the chemical composition of the system and thus the ingredients and

their concentration also affects the rheological behaviour of the lamellar phases and will be discussed in detail in the following Section.

3.4 Effect of chemical composition on the rheology of the lamellar phase

In this Section, we focus on the chemical composition dependence of the lamellar phase rheology and describe work done in probing the key microstructural transitions that have been found to take place for a wide range of lamellar systems including anionic and non-ionic surfactants.

Matsumoto *et al*[10] were the first to study the rheology of lamellar phases in the late 1980s. They focused on the effect of surfactant concentration on the rheological properties of systems of aqueous colloids. Their findings suggested that the structure of the lamellar phases is strongly dependent on the concentration of water in the system.

Diat *et al*[34, 69] studies on the influence of shear on the lamellar phase of anionic surfactant system reported the shear-induced formation of MLVs from a planar lamellar phase. The anionic systems studied were sodium dodecyl-sulphate (SDS) and sodium di(2-ethylhexyl)sulphosuccinate (AOT). Zipfel *et al*[71] investigated SDS/decanol in water. They showed that the orientation of layers in lamellar phases is strongly influenced by shear flow-a result in agreement with earlier studies by Diat *et al*[34, 53]. In addition, they reported that the nature of defects in the defective lamellar phase formed in SDS/decanol/water system is strongly dependent on the decanol molar content.

Hirsch *et al*[72] studied the rheological behaviour of a lamellar phase formed in a quaternary anionic surfactant/alcohol/hydrocarbon/water system under flow conditions. They reported shear thinning flow properties and the viscosity dependence on the surfactant concentration.

In addition to the work done on the shear-induced transitions in anionic surfactant systems, investigations have been performed on lamellar phases formed in non-ionic surfactant systems. Many groups studied the effect of the ethylene oxide (EO) chain length on the microstructure and the rheology of the system[13].

Robles-Vasques *et al*[73] have studied the viscoelasticity of some non-ionic surfactant/water systems. They proposed that a weak gel-like lamellar phase is formed in the system. Muller *et al*'s studies[16] on the shear-induced orientation of the $C_{12}EO_4$/water systems reported a parallel orientation at low shear rates followed by the onion phase. Nettesheim *et al*[74] and Oliviero *et al*[75] investigated $C_{10}EO_3$ and $C_{12}EO_4$ in ^2H_2O with similar results. Panizza *et al*[76] have studied the viscolestic properties of the onion phase both experimentally and theoretically. Penfold and co-workers[49, 54] investigated $C_{16}EO_6$ system under both constant and oscillatory shear. They identified two distinct orientations of the lamellar phase the perpendicular orientation at low shear rates and the parallel orientation at higher shear rates. They reported that if the shear flow is continued the lamellar phase transforms to a highly ordered solution of monodisperse MLVs [49].

There is a dearth of experimental work of this nature on highly complex structured liquids form lamellar structures. The missing link between macroscopic viscosity and the underlying microscopic structure is certainly a challenge aimed to be addressed in this work. The use of deuterium Rheo-NMR to study the changes in microstructure subsequent to the application of shear is a promising technique for lamellar systems. This is due to the fact that most lamellar systems of commercial interest are shear thinning and often met problems such as wall slip, during flow.

3.5 References

1.   Tiddy, G. J. T., Surfactant-water liquid crystal phases. *Physics Reports* **1980,** 57, (1), 1-46.
2.   Laughlin, R. G., *The aqueous phase behavior of surfactants* Academic Press: London, 1994; Vol. 6.
3.   Berni, M. G., Lawrence, C. J., Machin, D., A review of the rheology of the lamellar phase in surfactant systems. *Advances in Colloid and Interface Science* **2002,** 98, (2), 217-243.
4.   Ekwall, P., In *Advances in liquid crystals*, Halstead, G., Ed. Academic Press: New York, 1975; Vol. 1, pp 1-142.
5.   Barnes, H. A., Hutton, J. F., Walters, K., *An introduction to rheology*. Oxford: Elsevier: Amsterdam, 1989; Vol. 3.
6.   Dobraszczyk, B. J., Chemistry and Technology. In *Cereals and cereal products : chemistry and technology*, Dendy, D. A. V., Ed. Gaithersburg: Aspen: Maryland, 2001.
7.   Panine, P., Gradzielski, M., Narayanan, T., Combined rheometry and small-angle x-ray scattering. *Review of Scientific Instruments* **2003,** 74, (4), 2451-2455.
8.   Villadsen, J., Review article number 51. Putting structure into chemical engineering. *Proceedings of an industry/university conference* **1997,** 52, (17), 2857-2864.
9.   Franco, J. M., Munoz, J., Gallegos, C., Transient and Steady Flow of a Lamellar Liquid-Crystalline Surfactant/Water System. *Langmuir* **1995,** 11, (2), 669-673.
10.   Matsumoto, T., Heiuchi, T., Horie, K., Morphology and viscoelasticity of bilayer aqueous colloids of low-molecular and macromolecular amphiphiles. *Colloid and Polymer Science* **1989,** 267, (1), 71-79
11.   Soltero, J. F. A., Robles-Vasquez, O., Puig, J. E., Manero, O., Thixotropic-antithixotropic behavior of surfactant-based lamellar liquid crystals under shear flows. *Journal of Rheology (New York)* **1995,** 39, (1), 235-240
12.   Basappa, G., Kumaran, V., Nott, P. R., Ramaswamy, S., Naik, V. M., Rout, D., Structure and rheology of the defect-gel states of pure and particle-dispersed lyotropic lamellar phases. *European Physical Journal B: Condensed Matter Physics* **1999,** 12, (2), 269-276.
13.   Versluis, P., Van de Pas, J. C., Mellema, J., Microstructure and Rheology of Lamellar Liquid Crystalline Phases. *Langmuir* **1997,** 13, (21), 5732-5738
14.   Szymanski, J., Wilk, A., Holyst, R., Roberts, G., Sinclair, K., Kowalski, A., Micro- and macro-shear viscosity in dispersed lamellar phases. *Journal of Non-Newtonian Fluid Mechanics* **2008,** 148, 134-140.
15.   Filippelli, L., Mendronho, B., Rossi, C. O., Miguel, M. G., Olsson, U., Metastability of Multi-Lamellar Vesicles in a Nonionic System. *Molecular Crystals and Liquid Crystals* **2009,** 500, 166-181
16.   Mueller, S., Boerschig, C., Gronski, W., Schmidt, C., Roux, D., Shear-Induced States of Orientation of the Lamellar Phase of C12E4/Water. *Langmuir* **1999,** 15, (22), 7558-7564
17.   Berghausen, J., Zipfel, J., Lindner, P., Richtering, W., Shear-induced orientations in a lyotropic defective lamellar phase. *Europhysics Letters* **1998,** 43, (6), 683-689.
18.   Imai, M., Nakaya, K., Kato, T., Shear-induced ordering of lamellar and gyroid structures observed in a nonionic surfactant/water system. *European Physical Journal E: Soft Matter* **2001,** 5, (4), 391-402.
19.   Atkin, J. M., Cormier, R. J., Callaghan, P. T., Time-dependence of nuclear magnetic resonance quadrupole interactions for polymers under shear. *Journal of Magnetic Resonance* **2005,** 172, (1), 91-97.

20.   Lasic, D. D., The mechanism of vesicle formation. *Biochemical Journal* **1988,** 256, (1), 1-11.

21.   Van de Pas, J. C. A study of the physical properties of lamellar liquid crystalline dispersions. University of Groningen, Groningen, The Netherlands, 1993.

22.   Wilson, C. *The history of Unilever: a study in economic growth and social change*; London, 1954.

23.   Eastoe, J., Surfactant Aggregation and Adsorption at Interfaces. In *Colloid Science: Principles, Methods and Applications*, Cosgrove, T., Ed. Blackwell Publishing: 2005.

24.   Hyde, S. T., Identification of lyotropic liquid crystalline mesophases. In *Handbook of applied surface and colloid chemistry*, Holmberg, K., Ed. John Wiley and Sons, Ltd: Australian National University, Camberra, 2001.

25.   Friberg, S. E., El-Nokaly, M. A., In *Surfactant Science Series*, Rieger, M. M., Ed. Marcel Dekker: New York, 1985; Vol. 16.

26.   Rosevear, F. B., Liquid crystals: the mesomorphic phases of surfactant compositions. *Journal of the Society of Cosmetic Chemists* **1968,** 19, 581-594.

27.   Rosevear, F. B., The microscopy of the liquid crystalline neat and middle phases of soaps and synthetic detergents. *Journal of the American Oil Chemists' Society* **1954,** 31, 628-639.

28.   Figueiredo-Neto, A. M., Salinas, S. R. A., *The physics of lyotropic liquid crystals* Oxford University Press: New York, 2005.

29.   Kumar, S., Structure: X-Ray Diffraction Studies of liquid crystals. In *Liquid Crystals-Experimental study of physical properties and phase transitions*, Kumar, S., Cambridge University Press, Ed. 2001.

30.   Jung, M., Casteren, V. I., Monteiro, J. M., Herk, A., German, A., Pulsed-Laser Polymerization in Compartmentalized Liquids. 1. Polymerization in Vesicles. *Macromolecules* **2000,** 33, (10), 3620-3629.

31.   Murtagh, J., Thomas, J. K., Mobility and reactivity in colloidal aggregates with motion restricted by polymerization. *Faraday Discussions of the Chemical Society* **1986,** 81, (1), 127-136.

32.   Hotz, J., Meier, W., Vesicle-Templated Polymer Hollow Spheres. *Langmuir* **1998,** 14, (5), 1031-1036

33.   Bernheim-Grosswasser, A., Ugazio, S., Gauffre, F., Viratelle, O., Mahy, P., Roux, D., Spherulites: A new vesicular system with promising applications. An example: Enzyme microencapsulation. *Journal of Chemical Physics* **2000,** 112, (7), 3424-3430

34.   Diat, O., Roux, D., Nallet, F., Effect of shear on a lyotropic lamellar phase. *Journal de Physique II* **1993,** 3, (9), 1427-1452.

35.   Horanyi, T., Halasz, L., Palinkas, J., Nemeth, Z., Relationship between Optical and Rheological Properties of Polymer-Added Lamellar Liquid-Crystalline Systems. *Langmuir* **2004,** 20, (5), 1639-1646.

36.   Stokes, J. R., Telford, J. H., Measuring the yield behavior of structured fluids. *Journal of Non-Newtonian Fluid Mechanics* **2004,** 124, (1-3), 137-146.

37.   Ooshika, Y., Ikeda, Y., A Theory of the Salt Effects on the Critical Micelle Concentration. *Colloid and Polymer Science* **1956,** 145, 3-7.

38.   Tanford, C., *The Hydrophobic effect*. Willey: New York, 1980.

39.   Bergenholtz, J., Wagner, N. J., Formation of AOT/Brine multilamellar vesicles. *Langmuir* **1996,** 12, (13), 3122-3126.

40.   Sein, A., Engberts, J. B. F. N., Salt-induced transition from a micellar to a lamellar liquid crystalline phase in dilute mixtures of anionic and nonionc surfactants in aqueous solution. *Langmuir* **1993,** 9, 1714-1720.

41.   Tanner, I. R., *Engineering Rheology*. Second Ed.; Oxford University Press: Oxford New York, 2000.

42.   Balzer, D., Varwig, S., Weihrauch, M., Viscoelasticity of personal care products. *Colloids and Surfaces, A: Physicochemical and Engineering Aspects* **1995,** 99, 233-246.

43.   Holland, F. A., Bragg, R., *Fluid Flow for Chemical Engineers*. Second Ed.; Elsevier: London, 1995.

44.   Kim, S. A Study of Non-Newtonian Viscosity and Yield Stress of Blood in a Scanning Capillary-Tube Rheometer. Drexel 2002.

45.   Larson, R. G., *The structure and rheology of complex fluids*. Oxford : Oxford University Press: New York, 1999.

46.   Singh, M., Agarwal, V., De Kee, D., McPherson, G., John, V., Bose, A., Shear-Induced Orientation of a Rigid Surfactant Mesophase. *Langmuir* **2004,** 20, (14), 5693-5702.

47.   Oswald, P., Allain, M., Rheology and structural defects in a lyotropic lamellar phase. *Journal of Colloid and Interface Science* **1988,** 126, (1), 45-53.

48.   McKeown, S. A., Mackley, M. R., Moggridge, G. D., Shear-induced structural changes in a commercial surfactant-based system. *Chemical Engineering Research and Design* **2003,** 81, 649-664.

49.   Penfold, J., Staples, E., Khan, L., Tucker, I., Tiddy, G. J. T., Shear-Induced Transformations in the Lamellar Phase of Hexaethylene Glycol Monohexadecyl Ether. *Journal of Physical Chemistry B* **1997,** 101, (1), 66-72.

50.   Alcantara, M. R., Vanin, J. A., Rheological properties of lyotropic liquid crystals. *Colloids and Surfaces, A: Physicochemical and Engineering Aspects* **1995,** 97, (2), 151-156.

51.   Valiente, M., Influence of a cationic surfactant on the phase behavior of C12E4 /hexanol /water system at low surfactant concentration. *Colloids and Surfaces, A: Physicochemical and Engineering Aspects* **1995,** 105, 265-275.

52.   Roux, D., Nallet, F., Diat, O., Relation between rheology and microstructure of lyotropic lamellar phases. *A.C.S Symposium Series (Part 78)* **1994,** 5, 300-305.

53.   Diat, O., Roux, D., Nallet, F., "Layering" effect in a sheared lyotropic lamellar phase. *Physical Review E: Statistical Physics, Plasmas, Fluids, and Related Interdisciplinary Topics* **1995,** 51, 3296-3299.

54.   Penfold, J., Staples, E., Tucker, I., Tiddy, G. J. T., Lodi, K. A., Shear-Induced Structures in Concentrated Surfactant Micellar Phases. *Journal of Applied Crystallography* **1997,** 30, 744-749.

55.   Lauger, J., Weigel, R., Berger, K., Hiltrop, K., Richtering, W., Rheo-small-angle-Light-Scattering Investigation of Shear-Induced Structural Changes in a Lyotropic Lamellar Phase. *Journal of Colloid and Interface Science* **1996,** 181, 521-529.

56.   Dreher, K. D., Gogarty, W. B., Sydansk, R. D., Rheological Properties of Fluids Composed of an Alkylbenzene Sulfonate, Decane, Cyclohexanol, and Water. *Journal of Colloid and Interface Science* **1976,** 57, 379-387.

57.   Wunenburger, A. S., Colin, A., Colin, T., Roux, D., Undulation instability under shear: A model to explain the different orientations of a lamellar phase under shear? *European Physical Journal E* **2007,** 2, 277-283.

58.   Sierro, P., Roux, D., Structure of a Lyotropic Lamellar Phase under Shear. *Physical Review Letters* **1997,** 78, 1496-1499.

59.   Jonstromer, M., Strey, R., Non-ionic bilayers in dilute solutions-effect of additives. *Journal of Physical Chemistry* **1992,** 96, (14), 5993-6000.

60.   Le, T. D., Olsson, U., Mortensen, K., Zipfel, J., Richtering, W., Non-ionic amphiphilic bilayer structures under shear. *Langmuir* **1992,** 17, (4), 999-1008.

61.   Laughlin, R. G., Equilibrium vesicles: fact or friction? *Colloids and Surfaces, A: Physicochemical and Engineering Aspects* **1997,** 128, (1-3), 5993-6000.

62.   Zilman, A. G., Granek, R., Undulation instability of lamellar phases under shear: A mechanism for onion formation? *European Physical Journal B: Condensed Matter Physics* **1999,** 11, (4), 593-608.

63.   Auernhammer, G. K., Brand, H. R., Pleiner, H., The undulation instability in layered systems under shear flow-a simple model. *Rheologica Acta* **2000,** 39, (3), 215-222.

64.   Rubinstein, M., In *Theoretical challenges in the dynamic of complex fluids*, McLeish, T. C. B., Ed. Kluwer Academic: Dordrecht, 1997.

65.   Mcleish, T. C., *Theoretical challenges in the dynamic of complex fluids*. Kluwer Academic: Dordrecht, London, 1997.

66.   Fritz, G., Wagner, N. J., Lee, Y. C., Lin, S. Y., Formation of multi-lammelar vesicles by oscillatory shear. *Langmuir* **2003,** 19, (21), 8709-8714.

67.   Panizza, P., Archambault, P., Roux, D., Effects of shear on the smectic A-phase of thermotropic liquid-crystals. *Journal de Physique II* **1995,** 5, (2), 303-311.

68.   Dhez, O., Nallet, F., Diat, O., Influence of screw dislocations on the orientation of a sheared lamellar phase. *Europhysics Letters* **2001,** 55, 821-826.

69.   Diat, O., Roux, D., Nallet, F., Lamellar phase under shear-SANS measurements. *Journal de Physique II* **1993,** 3, 193-204.

70.   Allain, M., Possible defect-mediated phase transition in a lyotropic liquid crystal.Electron microscopy observations. *Europhysics Letters* **1986,** 2, 597-602.

71.   Zipfel, J., Berghausen, J., Lindner, P., Richtering, W., Influence of Shear on Lyotropic Lamellar Phases with Different Membrane Defects. *Journal of Physical Chemistry B* **1999,** 103, (15), 2841-1849.

72.   Hirsch, E., Wittmann, J. C., Candau, F., Structure and viscometric behaviour of gel phases in quaternary systems containing anionic surfactants. *Journal of Dispersion Science and Technology* **1982,** 3, (4), 351-372.

73.   Robles-Vasquez, O., Corona-Galvan, S., Soltero, F. A., Puig, J. E., Tripodi, S. B., Valles, E., Manero, O. Rheology of lyotropic liquid crystals of aerosol OT. II. High concentration regime. *Journal of Colloid and Interface Science* **1993,** 160, (1), 65-71.

74.   Nettesheim, F., Zipfel, J., Olsson, U., Renth, F., Lindner, P., Richtering, W., Pathway of the Shear-Induced Transition between Planar Lamellae and Multilamellar Vesicles as Studied by Time-Resolved Scattering Techniques. *Langmuir* **2003,** 19, (9), 351-372.

75.   Oliviero, C., Coppola, L., Gianferri, R., Nicotera, I., Olsson, U., Dynamic phase diagram and onion formation in the system C10E3/D2O. *Colloids and Surfaces A: Physicochemical and Engineering Aspects* **2003,** 228, (1-3), 85-90.

76.   Panizza, P., Roux, D., Vuillaume, V., Lu, C.-Y. D., Cates, M. E., Viscoelasticity of the Onion Phase. *Langmuir* **1996,** 12, (2), 248-252.

Chapter 4

Materials and Methods

4.1 Materials

The surfactant systems in most commercial laundry detergents are often mixtures for many reasons. One reason, of relevance to this project, is that using mixtures of surfactants can improve the flow properties of the final product. The system in question is a mixture of commercial anionic/anionic/non-ionic surfactants.

This Section presents the origin of the raw materials and the preparation of the samples investigated in this project.

4.1.1 Raw materials

Linear alkylbenzene sulfonic acid (HLAS)

The linear alkylbenzene sulfonic acid (HLAS) used in this project was a commercial material obtained from Unilever. The HLAS is manufactured via Hydrogen Fluoride (HF) route in Unilever-Port Sunlight. The HF process is more favourable as it gives a more homogeneous distribution of phenyl isomers. Unilever buys the Alkylbenzene raw material (LAB) and sulfonates it. The chain length distribution is shown in Table 4.1.1 and the 2-phenyl isomer content has been determined by mass spectroscopy as 25.2% (Unilever confidential report).

Isomer	Alkyl chain distribution (% of sample)			
	C_{10}	C_{11}	C_{12}	C_{13}
2-Phenyl	10.9	28.1	26.6	21.0

Table 4.1.1: Chain length distribution of the commercial LAS system as obtained at Unilever-Port Sunlight Laboratory by mass spectroscopy.

Specific details on the HLAS used are presented in Table 4.1.2.

	Value (Specifications)
Appearance	Slightly viscous, brown liquid
Active matter (wt%)	96.91
Sulphuric Acid	1.14
Moisture	0.15

Table 4.1.2: The raw material specification for HLAS.

The HLAS was neutralised with laboratory grade sodium hydroxide. The neutralisation is described in Section 4.1.2.

Sodium Alkyl (C_{12}-C_{13}) Ether Sulphate (3EO)

Sodium Alkyl Ether Sulphate is an anionic surfactant with an alkyl chain of 12-13 carbon backbone and three ether groups before the sulphonate head group. This system was again a commercial raw material provided by Unilever. Throughout this thesis Sodium Alkyl Ether Sulphate will be referred to as Sodium Lauryl Ether Sulphate (SLES). Specific details on the SLES used are displayed in Table 4.1.3.

	Value (Specifications)
Appearance	Yellowish opaque, mobile fluid
Active matter (wt%)	70.35
Free Alkalinity as Na$_2$O	0.26
Sodium sulphate	0.8
1-4 Dioxane(mg/kg of AD)	8

Table 4.1.3: The raw material specification for SLES.

NEODOL 25-7 (C$_{12-15}$ EO$_7$) Primary Alcohol Ethoxylate

NEODOL 25-7 is based on Shell Chemicals high purity C$_{12-15}$ NEODOL alcohol with an average of approximately 7 moles of ethylene oxide per mole of alcohol. Throughout this thesis C$_{12-15}$ EO$_7$ will be referred to as non-ionic (NI). The distribution of alkyl chain length (see Table 4.1.4) and the distribution of EO groups (see Table 4.1.5) are shown below.

Property	Unit	Value
C$_{11}$ and lower alcohols	%m/m	<1
C$_{12}$ alcohol	%m/m	21
C$_{13}$ alcohol	%m/m	29
C$_{14}$ alcohol	%m/m	25
C$_{15}$ alcohol	%m/m	25
C$_{16}$ alcohol	%m/m	<1

Table 4.1.4: Distribution of the alkyl chain length of C$_{12-15}$ EO$_7$.

Typical Distribution of Ethoxylate Adducts Weight percentage of $RO(CH_2CH_2O)_nH$, n=7			
n		n	
0	3	10	8
1	2	11	7
2	4	12	6
3	5	13	5
4	6	14	4
5	7	15	3
6	7	16	2
7	8	17	2
8	8	18	1
9	8	Higher	4

Table 4.1.5: Distribution of the EO head groups of $C_{12-15}EO_7$.

One of the objectives of this project is to investigate the extent that system composition and the added salt affect the lamellar microstructure. The salt used was tri-sodium citrate dihydrate (purity 99.0% from BDH). Throughout the Chapters 5 to 7, Appendix and Abstract, tri-sodium citrate will be referred to as TSC.

The other constituent of the studied systems is water. Heavy water (^2H_2O) was used as the results are being directly comparable to ^2H NMR and ^2H Rheo-NMR studies (see Section 5.3 and 6.3 respectively). ^2H_2O was purchased from Sigma-Aldrich and was 99.9% ^2H. All materials were used without further purification.

4.1.2 Sample preparation

Neutralisation of HLAS carried out based on previous work done by Unilever-Port Sunlight. The required mass of sodium hydroxide to neutralise a given mass of HLAS is calculated on a stoichiometric basis (adjust the pH at 8.0-8.5) (see Table 4.1.6). The sodium hydroxide requirement was determined via titration against known $NaOH_{(aq)}$ concentrations. Previous experience suggests that 0.5g NaOH-47 will increase the pH from 6.2 to 8.3.

Ingredient	Raw Material (AD)	Formula	wt% as received
HLAS	97	40.00	41.24
NaOH	47	5.04	10.72
H_2O	100	54.96	48.04
Total	-	100.00	100.00

Table 4.1.6: Neutralisation of HLAS to prepare LAS with Active Detergent, AD 40 and pH=8.2.

The HLAS neutralisation carried out in a 3kg batch. Initially, the 80% by weight of the total feed water was introduced into the batch. Then, the HLAS was added slowly and mix well by using a high shear mixer. This was subsequently followed by the addition of the required amount of NaOH-47. The sample was then mixed for ca. 10mins and then the remaining 20% by weight of the feed water was added in the batch. The sample was left to cool at room temperature and store in a sealed vessel to minimise water loss. To ensure that LAS is well mixed and homogeneous before any mixing process it was centrifuged at 6000rpm for 15mins.

The surfactant concentration (active detergent, AD) in the samples in question was 53% by weight, with a LAS/SLES/NI weight ratio of 2/1/1. All concentrations of the samples are given in weight percentage, denoted wt% throughout this thesis. For ^{2}H NMR studies the 47 and 50 wt% surfactant to water samples with a LAS/SLES/NI weight ratio of 2/1/1 were also prepared (see Table 4.1.7).

		53 wt% surfactant/water		50 wt% surfactant/water		47 wt% surfactant/water	
Ingredients	AD	Formula	% as received	Formula	% as received	Formula	% as received
LAS	40	26.5	66.25	25.0	62.5	23.5	58.75
Sodium Alkyl Ether Sulphate	70	13.25	18.93	12.5	17.85	11.75	16.78
$C_{12-15}EO_7$	100	13.25	13.25	12.5	12.5	11.75	11.75
^2H_2O		47	1.57	50	7.14	53	12.71

Table 4.1.7: Compositional details of the electrolyte free systems manufactured in this work (where AD is the active detergent of the raw material).

A range of samples was prepared by mixing the aforementioned surfactants in specific compositions of heavy water and tri-sodium citrate (TSC), and the details are given in Table 4.1.8. Samples were prepared by weighing the required amount of surfactant, heavy water and salt into a glass vial using a calibrated balance accurate to ±0.0001g. The samples were manufactured according to the following procedure (also see Table 4.1.8). Initially, the total feed heavy water was introduced into the vial. Then, LAS was added and mixed well with water. This was subsequently followed by the addition and mixing of SLES. The non-ionic C_{12-15} EO_7 was melted at ca. 40°C before it was added into the vial. The sample was then mixed by using a spatula and TSC was then added whenever required (see Table 4.1.8). To ensure the samples are well mixed they were heated to 50°C for ca. 24hrs. Samples were then stored at ambient conditions in a laboratory. The age of the sample is noted for experiments. Prior any experimental studies the samples were shaken by hand several times. All sample weights were noted after preparation and prior to any experimental studies to prevent water loss.

Ingredients	0 wt% TSC	1 wt% TSC	2 wt% TSC	3 wt% TSC	4 wt% TSC	5 wt% TSC
LAS	66.25	66.25	66.25	66.25	66.25	66.25
Sodium Alkyl Ether Sulphate	18.93	18.93	18.93	18.93	18.93	18.93
$C_{12-15}EO_7$	13.25	13.25	13.25	13.25	13.25	13.25
TSC	-	0.04	0.07	0.1	0.13	0.16
^2H_2O	1.57	1.53	1.50	1.47	1.43	1.40

Table 4.1.8: Compositional details (mass fraction) of the samples studied in this project.

4.2 Methods

The principal aim of this work is to investigate to what extent the lamellar phase microstructure is affected by the composition of the mixed surfactant system and how this affects the optical and rheological behaviour of the system. A number of techniques were employed in order to do this, including polarising optical microscopy, optical shear cell microscopy, rheology, small-angle X-rays scattering (SAXS) and deuterium NMR (^2H NMR) spectroscopy.

This Section describes the techniques used and their capability for study of the liquid crystalline systems. At the end of each Section, data analysis is discussed followed by an experimental Section, providing details about the specific equipment and various experimental parameters used in these studies. Specific information such as sample preparation is discussed in Section 4.1.2.

4.2.1 Polarising Optical Microscopy

Optical microscopy is an extremely powerful tool when a study on the microstructure of liquid crystal mesophases is initiated. Polarised optical microscopy exploits optical properties of anisotropy and offers a wealth of information, which is simply not available with any other optical technique[1]. The idea is to identify the mesophases formed by the liquid crystals since most of the mesophases display unique optical textures[1-5] as shown in

Figure 4.2.1. These textures are caused by the ability of an anisotropic substance to rotate plane polarised light.
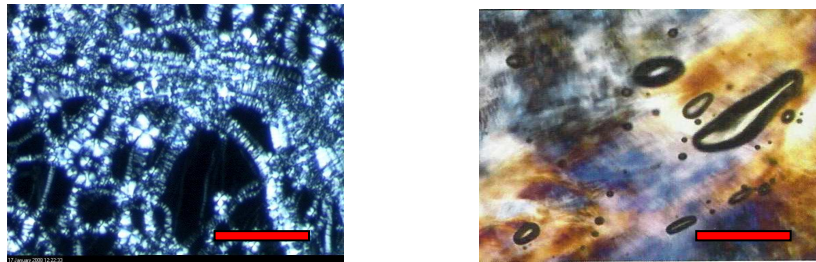
<div align="center">(a)   (b)</div>

Figure 4.2.1: Optical micrographs displaying (a) typical lamellar texture and (b) a non-geometric hexagonal texture. The scale bar represents 100μm. These textures were viewed through crossed polars.

Polarised Light

Normal light is an electromagnetic radiation composed of electric (E) and magnetic (B) components vibrating perpendicular to each other and to the direction of propagation. In a microscope, normal un-polarised light from radiant halogen bulb passes through the polariser to transform it to plane polarised light. There are two polarising filters in a polarising microscope called polariser and analyser (see Figure 4.2.2).
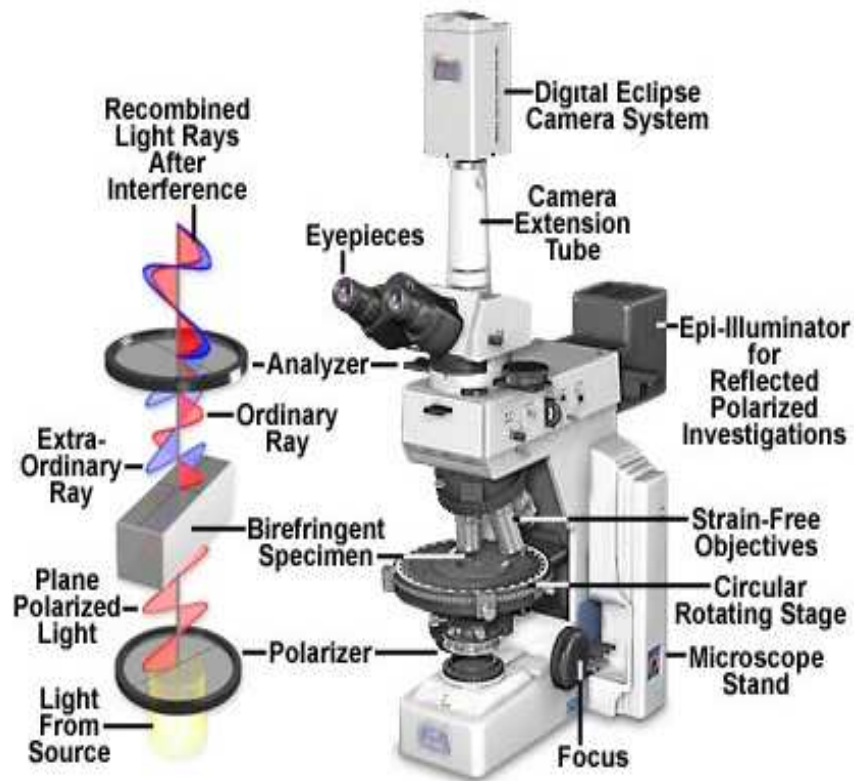
Figure 4.2.2: The polarising microscope[6].

The polariser is sited below the specimen stage and the analyser is situated above the objectives and can be moved in and out of the light path as required. When both the analyser and polariser are in the optical path, their permitted vibration directions are positioned at right angles to each other. In this configuration, the polariser and analyser are crossed, with no light passing through the system under investigation and a dark texture present in the eyepieces[7]. When an anisotropic substance is placed between crossed polarisers, the plane of polarised light is rotate in such a way that some light passes through the analyser and the object appears bright.

Birefringence

Liquid crystals are classified as anisotropic or isotropic. Anisotropic material contains a molecular density which depends on the directions. As a result, light travels with different velocities along different directions in the material leading to different refractive indices. The refractive index is given by

$$n = \frac{c}{v}$$

<div align="right">**Equation 4.2.1**</div>

where c is the velocity of the light in vacuum and v is the velocity of the light in that media.

When polarised light passes through an anisotropic phase, it is split into two parallel rays named 'ordinary' and 'extra-ordinary' rays associated with ordinary refractive index (n_0) and extra-ordinary refractive index (n_e). This phenomenon is known as double or bi-refraction. The birefringence is given by

$$\Delta n = n_e - n_0$$

<div align="right">**Equation 4.2.2**</div>

Birefringence can be of two types, positive birefringence and negative birefringence. If the characteristic index along the optic axis (n_e) is greater than the characteristic index normal to this axis (n_0) the material is said to be 'optically positive'. In the reverse situation the birefringence is said to be negative.

As the refractive index (n) defines the speed of light in the material, the wavelength (λ) and velocity of the light (v) will be slowed down by (n), the degree of which is dependent on the polarisation. The change in (λ) means changes in the colours observed and that is related to the sample thickness.

On the other hand, isotropic substances have only one refractive index and no restriction on the vibration direction of light passing through them. The isotropic phases under crossed polarisers appear dark (black).

Experimental

All optical microscopy experiments were carried out using a Zeiss Jenaval polarising optical microscope and photographs were taken using a camera and analysed using image analysis software attached to the microscope. For some scans the Olympus BX41 polarised optical microscope was also used and photographs were taken using a JVC KY-F55BE camera. A Linkam hot-stage was attached on both microscopes to obtain temperature control with an accuracy of ±0.5ºC. Cooling rates were controlled using a stream of

nitrogen gas which passes though a reservoir of liquid nitrogen thus allowing rapid cooling rates to be obtained.

A drop of the sample is added on the slide and a cover slip placed over the sample. Thin, well-defined samples offer high contrast and thereby enable the structures to be studied in detail. The textures obtained are determined by the alignment of the molecules in relation to the slide. The alignment of the molecules is affected by the structure of the molecules and the surfaces of the slide and cover-slip used[2].

4.2.2 Linkam CSS-450 Optical Shear Cell

The Linkam Cambridge Shearing System (CSS450) has been developed in collaboration with the Department of Chemical Engineering at Cambridge University. The system used in this work is a high temperature (ca. 25–450°C) parallel-plate shearing stage designed for use in *in-situ* optical microscopy experiments (see Figure 4.2.3)[8, 9].

The sample is placed between two windows that are in close thermal contact with silver heaters. The bottom window, located within the lower section of the shearing cell, contains a 5mm diameter disc on its underside to allow light to enter the cell and a 40mm diameter quartz disc, which is attached to a metal carrier that can rotate under the control of a stepper motor. The top window is fixed to the upper section of the cell contains a 30mm diameter, bevelled-edge quartz disc (with a 3mm aperture hole) which remains stationary throughout experimental runs.

The bottom window is controlled by a stepper motor. This motor is a micro-stepped motor enabling a resolution of 25600 steps per revolution. The motor can drive the system in three ways: steady velocity, step movement at constant velocity and an oscillatory motion with constant frequency and amplitude. The steady velocity mode has been used for studies undertaken in this research.

The gap between the windows can be set from 5 to 2500μm and is controlled by a second stepper motor and gap mechanism. In this work the gap was set at 200μm. The speed at which the lid moves up and down may also be set. Sensors in the body and lid determine the upper and lower limits.
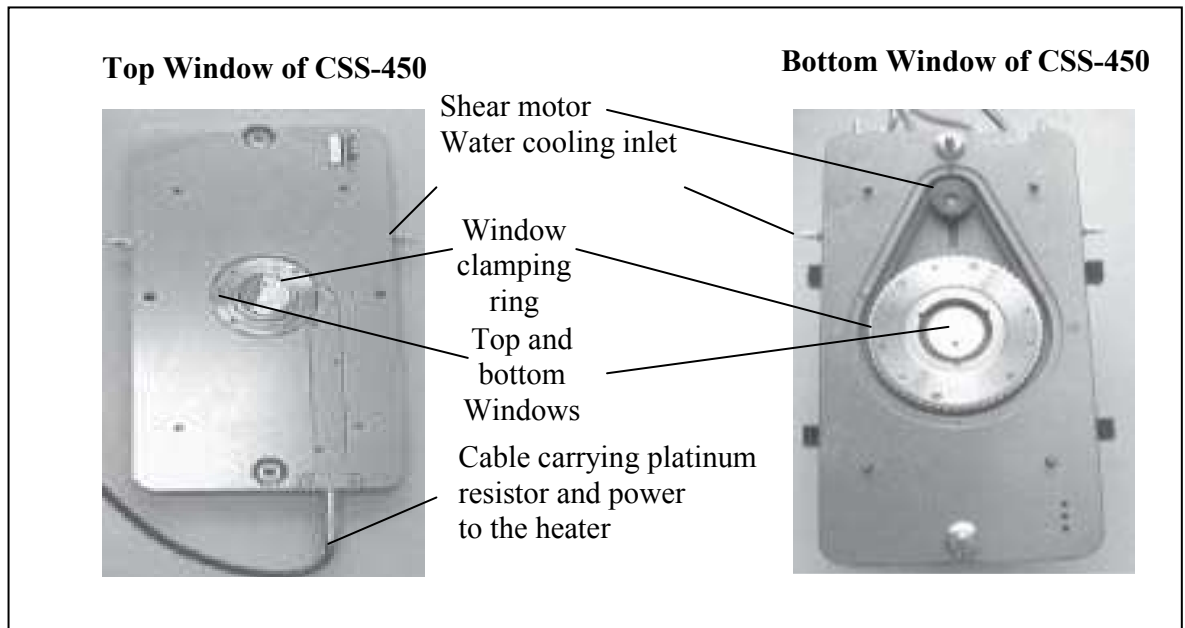
Figure 4.2.3: A complete CSS-450 shearing cell consisting of an upper section (the lid) and a lower section (the base). (The Figure adapted from the manual of the instrument).

As the sample must fill the gap this was kept small to minimise air entering the sample and to ensure close contact of the sample with the two parallel discs and hence the thermal silver heating block. The shear cell was mounted to an Olympus BH2-UMA polarising microscope and the sample sheared by rotating the bottom plate at an angular velocity, ω (corresponding to the desired shear rate, $\dot{\gamma} = {r\omega}/{d}$ where r is the observation radius (7500μm) and d is the gap size (or sample thickness).

Through out this work the shear cell rotates clockwise. However it should be noted that as this is a parallel-plate arrangement there are varying shear rates across between the plates (maximum shear at the edge, minimum at the centre).

Images were recorded using a JVC-TK 1280E CCD (charged coupled device) camera (shutter speed 15-25 frames/s) and analysis was performed using Linksys Version 2.41 software. Operating specifications (adapted from the manual of the instrument) are displayed in Table 4.2.1.

Quantity	Range	Resolution
Angular Velocity (rad/s)	0.001 – 10	0.001
Amplitude (rad)	0.001 – 1.6	0.001
Frequency (Hz)	0.01 – 9.9	0.1
Gap Setting (μm)	10 – 2500	1
Limit Temperature (^{o}C)	Ambient – 450	1
Heating Range (^{o}C/min)	1 – 30	1

Table 4.2.1: Operating Specifications for the Linkam CSS450 optical shear cell. A liquid nitrogen pump was attached on the optical shear cell to obtain temperature control with an accuracy of ±0.5°C.

4.2.3 X-Ray Diffraction (XRD)

X-Ray Diffraction (XRD) is one of the most reliable techniques for studying liquid crystalline phase structures. Because the wavelength of X-rays (λ) is comparable to atomic size they can be used to provide information about a structure's molecular arrangement. The energetic X-rays can penetrate into the material and by interpreting the scattering pattern of the transmitted X-rays, provide information about the structure. The scattering originates in electron density fluctuations of the substance. Thus, when the X-rays hit the sample, they will be scattered at an angle 2θ. If the ability to scatter X-rays depends on the number of electrons in an atom, and since atoms in a crystal are lined in planes, each plane can diffract X-rays[10].

Bragg's Law

Bragg and his son Lawrence report that X-rays were diffracted at certain angles that depended on the wavelength of the radiation (of the X-rays) and the spacing of the lined planes (interplanar spacings of the crystal structure). Their explanation for this phenomenon is shown in Figure 4.2.4 where several atomic planes of the liquid crystal are shown.

Incoming X-rays in the crystal are at angle θ and of wavelength λ. The incident X-rays are reflected by the crystal planes in the same way as light is reflected by mirror, incident angle equals the reflecting angles $\theta_{in}=\theta_{out}$. At each atomic plane a small portion of the beam consider to be reflected from the surface atoms such as point A. If the reflected beams are not absorbed on their way through a crystal exit from the crystal in such a way

that they are in-phase and they do not cancel each other by interference, a diffracted beam is observed. The law describes the conditions where the reflected beams positively interfere to give a strong diffracted beam. Constructive interference occurs only if the difference in distances travelled by the two beams is an integral number of wavelengths. Otherwise no diffraction will be observed[11]. Using the diagram below the expression for Bragg's Law derive by applying trigonometry.
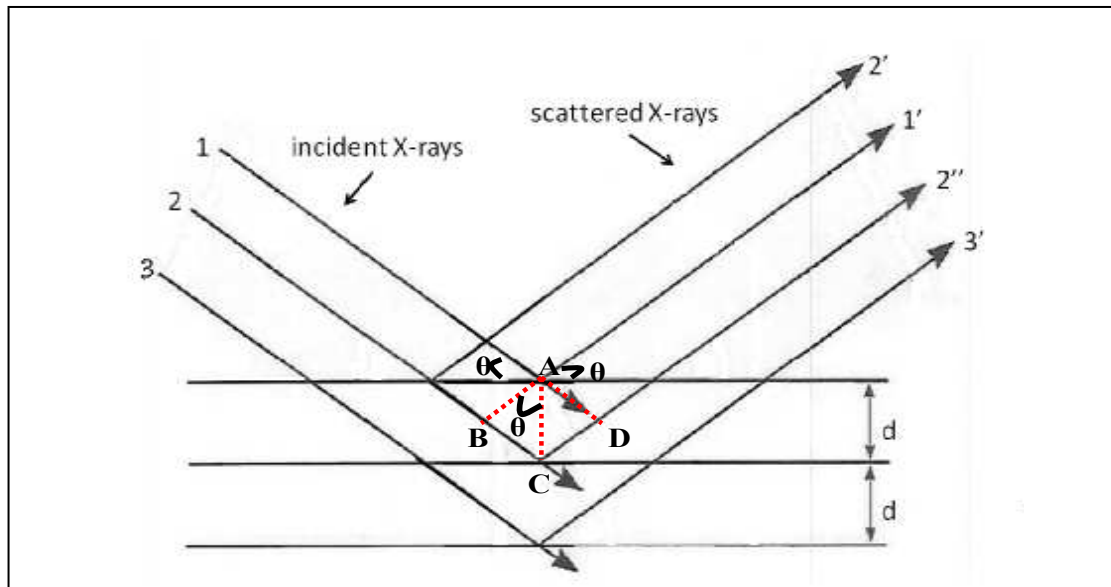
Figure 4.2.4: Schematic diagram outlining the principles of Bragg's Law (adapted from reference[10]).

It is evident that the second ray travels an extra distance *BC+CD* with respect to the first ray. In summary, the necessary condition for constructive interference of the reflected rays is that the distance *BC+CD* should be equal to a whole number of wavelengths,

$$BC+CD=n\lambda \qquad\qquad \textbf{Equation 4.2.3}$$

where λ is the wavelength of the incident light. But *BC=CD*, therefore

$$2BC= n\lambda \qquad\qquad \textbf{Equation 4.2.4}$$

Now, in order to relate the inter-planar spacing between atomic planes, *d*, with the wavelength, λ, trigonometry should be applied on the triangle ABC.

$$sin\theta = BC/d \qquad\qquad \textbf{Equation 4.2.5}$$

and by combining Equations 4.2.4 and 4.2.5,

$$2sin\theta = n\lambda/d \qquad\qquad \textbf{Equation 4.2.6}$$

Hence,

$$n\lambda = 2dsin\theta \text{ (Bragg's Law)} \qquad\qquad \textbf{Equation 4.2.7}$$

Equation 4.2.7 is known as Bragg's equation where λ is the wavelength used, d is the inter-planar spacing between identical crystal planes and n is the order of reflection that takes an integer value.

At other angles than θ there is a little or no diffraction because of negative interference. Maximum diffraction of the beam depends on the angle of incidence θ. As θ increases, a series of maxima is obtained corresponding to n=1, 2, 3, etc. Thus, the successive maxima in an X-ray diffraction pattern are called the first-order, second-order, etc., reflections, depending on the value of n[10].

It has been stated in previous Chapter that the most important property of amphiphilic liquid crystal phases is the periodicity of the structure. This property is used in an X-ray diffraction experiment where the state of organisation of the hydrocarbon alkyl chains can be determined thus providing information about the structure of the sample. The technique used for this examination is the 'powder' method[12].

The 'powder' method was originally developed by Debye and Scherrer but the whole idea came from Laue's work[13]. The idea behind Laue's work was that the crystals within a particular structure will not be oriented (unless subject to external forces), but randomly arranged in space. Thus, X-rays will scatter at all angles in space, and the scattered beam will produce a cone of diffraction. Indeed, due to the nature of the set of lattice planes, each set of planes gives its own cone of radiation thus concentric cones are formed. These cones create the arcs of rings, known as Debye-Scherrer rings, which are recorded during data collection.

Synchrotron Radiation: Daresbury Laboratory

Synchrotron radiation is the electromagnetic radiation produced when charged particles travel in curved paths. The X-rays emitted by synchrotron radiation sources are very intense and are used for a number of different types of X-ray diffraction experiments such as the small-angle and wide-angle X-ray scattering (SAXS and WAXS) which are related to the length scale of interest.

SAXS determines any long-range order or structuring present in a liquid crystal corresponding to unit cell dimensions of the order 10-1000Å. SAXS patterns contain data concerning correlations on an inter-molecular level and higher orders, such as systems with macromolecular or aggregate self-assembly. In contrast, WAXS determines the short-range order (<10Å) and their patterns contain information relating to correlations on an inter-molecular and intra-molecular or atomic level. The main difference between the two arrangements is the incident angle of the X-ray beam. The output from both techniques is the same (usually a 2-D spectrum), but the length scale is quite different, with SAXS generally resolving in the 10-1000Å, whereas WAXS can detect structures as small as 2Å. In this study, SAXS is used and the data obtained are used to calculate unit cell size, repeat distances and the dimensions of separate water and surfactant regions.

Mesophase Identification Using X-ray Diffraction

The main lyotropic liquid crystal phases can be distinguished by their characteristic diffraction patterns. Due to their periodicity liquid crystalline structures show higher order Bragg peaks.

The lamellar phases, which they have one-dimensional periodicity they usually show sharp reflections in the low-angle region correspond to d-values ('d-spacing') in the ratio of
1: 1/2: 1/3: 1/4 etc. The intensity of the reflections decreases for the higher orders, and often with aqueous system only the first reflection is observable[1]. For lamellar phase, the first-order reflection, d_0, corresponds to the unit cell dimension, the lamellar spacing which is equal to the sum of the water layer thickness (d_W) plus the thickness of the surfactant bilayer (d_H)[14, 15].

The hexagonal phases are considered to be composed of parallel rod-shaped aggregates arranged in two-dimensional lattice. The X-ray pattern for hexagonal phases has reflections

in the ratio of 1: $1/\sqrt{3}$: $1/\sqrt{4}$:$1/\sqrt{7}$:$1/\sqrt{9}$:$1/\sqrt{12}$ etc. In contrast to the lamellar phase, the measured d_0-value corresponds to the separation of adjacent rows of rod micelles. Cubic phases have a three dimension order resulting in complex diffraction patterns.

Experimental Work

SAXS experiments were carried out on Station 2.1 at the Synchrotron Radiation Source (SRS), Daresbury Laboratories. The experimental Station operates with a fixed wavelength of 1.54Å. The detector distance used on this Station was approximately 1m. Samples were loaded in Lindemann tubes which are invisible to X-rays on this length scale. The tubes were then flame sealed to prevent water loss. Heating and cooling cycles were carried out using a Linkam hot-stage made to fit capillaries. Temperatures were obtained with an accuracy of ±0.5ºC.

The SAXS beamlines in Station 2.1 were calibrated against wet rat-tail collagen, which has specific orders of reflection and corresponding d-spacings. The orders of reflection which are strong and therefore used in calibration are: 3rd order (223Å), 5th order (134Å), 9th order (74Å) and the 12th order (56Å) (see Figure 4.2.5).
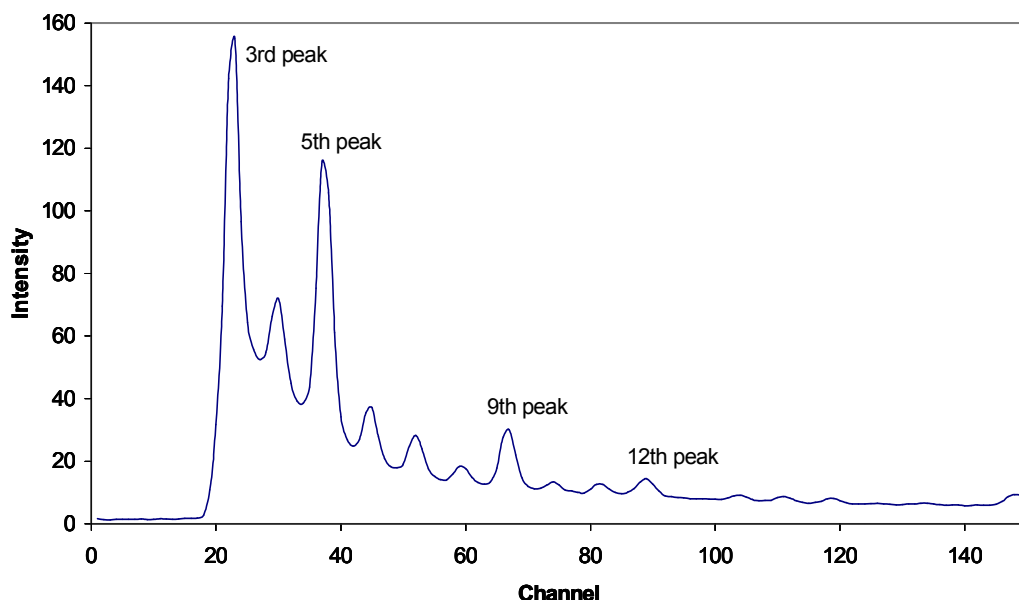
Figure 4.2.5: X-ray diffraction (SAXS) of the wet rat-tail collagen calibration at 25°C at Station 2.1 at Daresbury Laboratories showing the distinct peaks.

Data from all the experiments carried out at Station 2.1 were collected on a 2-D CCD detector. In order to obtain *d*-spacing from these data a software package named FIT2D

was used. This software converts the 'raw' 2-D patterns into 1-D format providing a plot of intensity versus channel number. The channel numbers are then converted into the scattering vector Q which is a measure of reciprocal space (Å^{-1}). Q can then be converted into d-spacings as described in Equation 4.2.8

$$Q=2\pi/d \qquad \textbf{Equation 4.2.8}$$

Calculating dimensions from d-spacings

The area per molecule and the water layer can be calculating using the X-ray d-spacings. The basic equations shown below are for a lamellar system as this will be determined during analysis of results.

The moles of surfactant, m_s, in 1g can be determined using the equation 4.2.9

$$m_s = \frac{Z}{100*S} \qquad \textbf{Equation 4.2.9}$$

where Z is the wt% of surfactant of molar mass, S in the sample. The head groups have a molar mass G and the non-polar parts have a molar mass H, and so it can be said $H+G=S$.

Z_W and Z_H are the weight fractions of the aqueous region and the non-polar region respectively and can be determined using the Equation 4.2.10 and 4.2.11.

$$Z_H = \frac{H}{S}\frac{Z}{100} \qquad \textbf{Equation 4.2.10}$$

$$Z_W = 1 - Z_H \qquad \textbf{Equation 4.2.11}$$

The volume fractions of the non-polar region, φ_H and the polar region, φ_W are

$$\varphi_H = \frac{Z_H/\rho_H}{Z_H/\rho_H + (1-Z_H)/\rho_W} \qquad \textbf{Equation 4.2.12}$$

$$\varphi_W = 1 - \varphi_H \qquad \textbf{Equation 4.2.13}$$

where ρ_W and ρ_H are the density of water and for L_α phase respectively and assuming ρ_W=1.0kg/m^3 and ρ_H=0.8kg/m^3.

For the L_α phase the thickness of the non-polar and polar region, d_H and d_W respectively are

$$d_H = \varphi_H d_0 \qquad \textbf{Equation 4.2.14}$$

$$d_W = \varphi_W d_0 = (1 - \varphi_H)d_0 \qquad \textbf{Equation 4.2.15}$$

For the area per surfactant molecule, α_0, assuming bilayer structure is given by Equation 4.2.16

$$\alpha_0 = \frac{2}{d_0}\left(\frac{Z_W}{\rho_W} + \frac{Z_H}{\rho_H}\right)\frac{10^{24}}{m_S N} \qquad \textbf{Equation 4.2.16}$$

where N=6.0221415*10^{23}.

4.2.4 Rheology

Rheology by definition is the science of the deformation and flow of matter[16, 17]. It is an important tool in chemical engineering because the knowledge of the rheological properties of a material will improve the manufacture and the design of the product with the desirable fluidic properties[18, 19]. Since rheology has already been discussed in Chapter 3, in this Section will briefly describe the different shear patterns that are generally used to investigate the rheological behaviour of structured liquids[17].

Experimental

Both viscometry and oscillation measurements have been performed to investigate if a sample exhibits shear thickening or shear thinning rheology. The rate of relaxation can also be measured and it is known that this is much slower than the rate of alignment. A TA (thermal analysis) instrument, advanced rheometer AR 2000, was used for rheological

measurements of the surfactant systems. The rheometer is a cone and plate system with 40mm plate and 53μm gap to replicate the gap in the optical shear cell.

Geometry moves down to the set gap distance and the sample is in close contact with the two parallel discs, which are in turn in close thermal contact with the cell.
Compressed air allows rotation of the disk.
The sample is placed on cell from where the temperature is controlled.
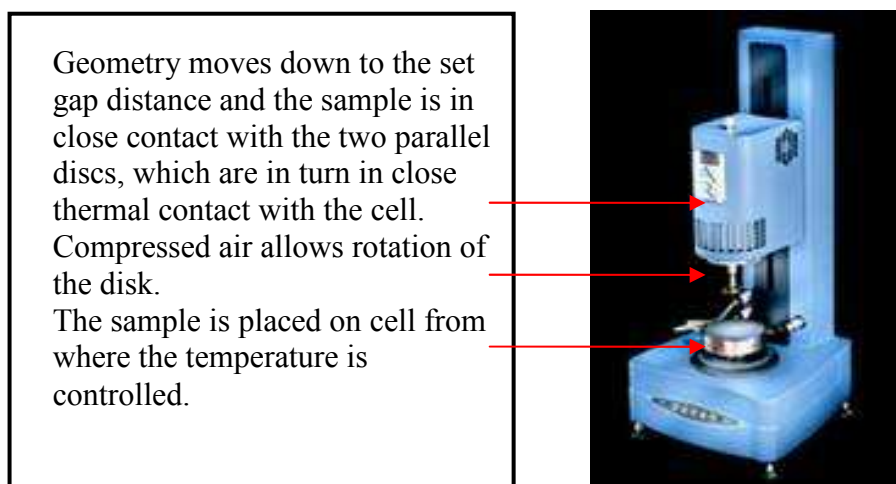
Figure 4.2.6: AR 2000 Rheometer.

The sample was transferred with a spatula to the lower plate with care to minimise structure disturbances. The top plate was then lowered into position. A solvent trap is used throughout experiments to minimise evaporation of solvent in sample. The sample is added to the cell using a spatula to limit the amount of shear induced. Note that any air bubbles appeared in the sample should be removed before starting the experiment.

The rheometer can be used in either controlled stress mode or controlled rate mode. If controlled stress mode is employed the instrument applies a torque (force) and measures the resultant displacement (movement). These values are converted into viscosity (a rheological format) after calculating the corresponding shear-rate values and using measuring system constants.

If controlled rate mode is employed the instrument works in the opposite manner measuring the force as the movement is set. Again viscosity is calculated after firstly evaluating the corresponding shear-stress values. If the viscosity reading is high the sample is thick hence giving more resistance to flow and limiting the movement (slow shear rate).

The cone and plate system gives a constant shear rate across the gap and therefore measurements will be taken in later research to allow comparisons to be made and to create

a further understanding of the rheology of the liquid crystalline material. Also the viscometry mode can be used to produce results of the viscosity as a function of increasing shear rate (shear profile), and as a function of time for a constant shear rate.

Viscometry tests are simple rotational shear experiments and are destructive tests as the sample must flow. They are also referred to as sweep tests. The flow behaviour can be described using shear profile which measures instantaneous viscosity as a function of shear stress, temperature and time.

Oscillation testing is a dynamic test which oscillates the sample though fixed stress/strain to determine the viscoelasticity (material is characterised by both viscous and elastic properties). Oscillation testing experiments include the amplitude sweep step and the frequency sweep step. The amplitude sweep identifies the linear viscoelastic region which is an indication of how tough the material is (long LVR enables the sample to 'absorb' a broader range of deformations before the structure breaks down).

Frequency sweep measures the phase angle, δ, complex modulus, G^*, storage (elastic) modulus, G', loss (viscous) modulus G'' and the dynamic complex viscosity, $|\eta^*|$, based on a fixed amplitude. These properties can be measured as a function of time, frequency and/or amplitude of shear and temperature.

Test parameters will be given when results are discussed in Chapter 6 alongside the type of test performed. Note for all experiments the work was repeated and checked for validity. Any results which involved 'strange' results were checked. All data discussed are therefore believed to be portrayed accurately with all changes being noted as 'real' effects of the sample behaviour before, during and after shear flow.

4.2.5 Deuterium Nuclear Magnetic Resonance (^{2}H NMR) Spectroscopy

Nuclear magnetic resonance (NMR) is a spectroscopic method that uses the weak interaction of the nuclear spins with their molecular environment to provide information about molecular structure and dynamics[20-32]. NMR is the phenomenon that occurs when

the nuclei of certain atoms, are immersed in a static magnetic field then exposed to a second oscillating magnetic field and hit with radio waves[33-37].

NMR technique is based on the fact that certain nuclei possess a characteristic property called spin[33, 37, 38]. Spin is a property of protons, neutrons and electrons in atomic nuclei and is described by the spin quantum number I. I is used to describe the magnetic properties of nuclei[39, 40] and is expressed in multiples of ½. An important property of spinning nuclei is the magnetic moment vectors which are described using the magnetic quantum number m having values from I to $-I$. Thus the series used is $m= I$, (I-1), (I-2)…,-I.

Nuclei with $I >$ ½ such as ^{2}H, ^{14}N, ^{23}Na and ^{35}Cl spin as a non-spherical body and an electric field gradient, eq, is created when a probing charge approaches as this will experience different electrostatic fields in different approaching directions. All nuclei with a spin $>$ ½ are therefore termed electric quadrupoles. Deuterium (^{2}H) therefore has a quadrupole moment, Q, which is $0.0028*10^{-28}m^{2}$.

Deuterium (^{2}H) has a spin quantum number I=1, thus in a magnetic field each spin can align in one of three possible orientations as shown in Figure 4.2.6[39, 40]. However, interaction between the nuclear quadrupoles and electric field gradient leads to rapid changes of the spin states of the nuclei, which further leads to an additional splitting of the energy level when m=0. The energy levels are shown in Figure 4.2.7 where e_{Q} is the angular term relating the different angles between the principal coupling tensor, V, and the applied magnetic field[29, 41].
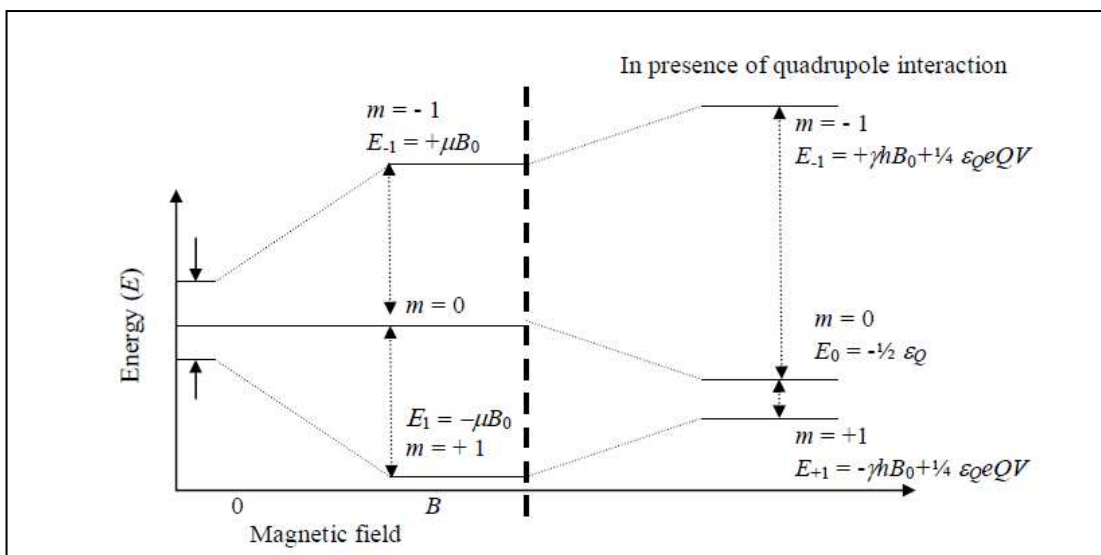
Figure 4.2.7: Alignment of spins in a magnetic field where I=1, with and without the influence of the quadrupole interaction, obtained from[39, 40].

Thus the resultant NMR spectrum will be either broadened or consist of a doublet separated by a splitting Δ, whose magnitude is given by

$$\Delta = \frac{3}{2}\frac{eQV}{h} = \frac{3}{2}\frac{e^2qQ}{h}\frac{1}{2}\left(3\cos^2\Theta_0 - 1\right)$$
                                                                            Equation 4.2.17

where Θ is the angle between the axis of rotational symmetry and the magnetic field and e^2qQ/h is the quadrupole coupling constant, E_Q.

When viewing lyotropic mesophases, the electric field gradients are apparent in the head group region near the alkyl chain/ water boundary. This is because the ^2H_2O molecules are oriented at interface, so it has anisotropic and restricted motion. Thus, when discussing liquid crystals the quadrupole splitting, Δ, will be directly related to the orientation order.

^2H NMR spectroscopy provides valuable information about the phase behaviour of lyotropic liquid crystalline systems. ^2H NMR easily detects anisotropic motions. For a rapid isotropic motion the ^2H NMR spectrum of deuteron consists of one single line, while for an anisotropic motion each deuteron contributes a doublet due to the quadrupole moment of the deuteron nucleus. The doublet splitting Δ depends on degree of anisotropy and on the orientation of the deuteron with respect to the molecular symmetry axis. In

oriented samples the quadrupole splitting depends further on the angle between the magnetic field and the liquid crystal director-axis as shown in Equation 4.2.17. The value of the quadrupole splitting can be used to differentiate between such liquid crystalline phases.

^{2}H NMR can easily be used to identify both single phase and multiphase samples. A single anisotropic liquid crystalline phase exhibits a characteristic NMR line shape which depends on the anisotropy, geometry, and domain size of the liquid crystalline aggregates and on the motion of ^{2}H$_2$O molecules. For multiphase samples, the spectrum is composed of the sum of the individual spectra for each phase.

Samples may be aligned by various method such as shear or an exposure to an electric or magnetic field, prior to being run. This causes the alignment of the director to be either parallel or perpendicular to the magnetic field (B_0). In the case of perfectly random distribution of orientations all possible spectra will be superimposed to yield a powder pattern, where well-defined tuning points exist at frequencies corresponding to angles 0° and 90° between the principal axis of the quadrupolar splitting tensor and the applied magnetic field[39]. This is known as a 'Pake' doublet[42] where the peaks correspond to angles 90° thus for the parallel alignment of the liquid crystal director with respect to the magnetic field. The shoulders correspond to angles 0° and thus for perpendicular alignment of the liquid crystal director with respect to the magnetic field.
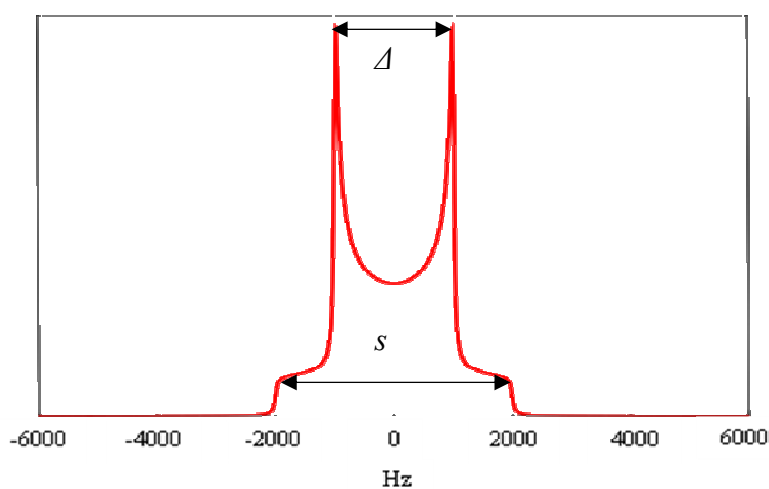
Figure 4.2.8: Schematic representation of a typical 3-D powder spectrum, displaying 'Pake' doublet as produced by ^{2}H-NMR redrawn from reference[42].

<u>Experimental</u>

All experimental work was completed using a bench-top Maran Ultra NMR Spectrometer which can be fitted with either a proton or deuterium probe (each probe is 10mm diameter). The spectrometer frequencies, for the 0.54T magnet, are measured at 23.3MHz and 3.66MHz for ^{1}H and ^{2}H probes respectively. All samples were loaded into 10mm diameter, 7inches height, high-precision NMR tubes from Wilmad Glass. From previous studies[43] the optimum sample depth for NMR experiments has been determined to be 8mm.

The number of scans run for each sweep was 2048, the number of data points acquired during a pulse is 16384 and the spectra width is 200000Hz. The dead-time of the spectrometer must be accounted for to ensure key NMR signal is not lost. These are defined as Dead 1 and Dead 2 parameters. Dead 1 is the wait time between the application of the radio frequency (rf) pulse and the collection of data whereas Dead 2 is wait time to allow the filter to stabilise (applied to smooth the NMR signal). Note any baseline distortions are corrected prior to manipulation using the data analysis software, RINMR.

The simplest NMR experiment is called an FID (Free Induction Decay) experiment. A single radio frequency (rf) pulse (normally a 90 degree pulse) is applied to the sample and the response is measured as a function of time after the rf excitation. A Fourier algorithm translates the NMR signal from time domain data to frequency domain data (spectrum).

4.2.6 Rheological Deuterium NMR (Rheo-NMR) Spectroscopy

It has already been stated that rheology involves mechanical measurement of flow properties of complex fluids concerning the molecular basis of these properties. Under flow, competition arises between the molecular organization dynamics and the imposed deformation[44]. However, in order to understand the rheology of complex fluids, it is important to link the macroscopic mechanical properties to the molecular level properties[45, 46].

NMR has proven to be an excellent technique for gaining knowledge of the behaviour of molecules in a magnetic field. It provides structural, orientational, and dynamic information on the molecular level and tying the information back to the macroscopic

mechanical properties being investigated. However, it is also possible to perform NMR spectroscopy under conditions of flow. The combination of NMR and Rheology is known as Rheological-NMR (Rheo-NMR)[47-49].

Rheo-NMR is capable of investigating molecular order and alignment though nuclear quadrupole interactions. Rheo-NMR applies a stress to a sample and allows the study of shear orientation of aggregates through utilising inter-nuclear dipole interactions[47-49]. The term 'Rheo-NMR', now widely used, was introduced by Nakatani *et al*[50] in 1990 for their proton NMR studies of polydimethylsiloxane melt under shear. There have been an increasing number of investigations with Rheo-NMR over the years using different flow geometries including cone-and-plate cells and cylindrical couette cells[48, 51].

Experimental

The Rheo-NMR geometry used for this work is the couette cell geometry and has been used within the bench-top Maran NMR spectrometer. The couette cell is shown in Figure 4.2.9 where it has a rotating inner tube and a static outer tube. As indicated in Figure 4.2.9 different sizes of inner tube can be used and consequently both shear rate and the gap width (r_i/r_0) are variable.

Rotating inner tube
(r_i = 3mm, 4mm, 5mm, 7.5mm or 8mm)

Static outer diameter (10mm) Wall thickness = 1mm.
r_0= 9mm

Variable gap width

$r_i/r_0 = 3/9 = 0.33$
$r_i/r_0 = 4/9 = 0.44$
$r_i/r_0 = 5/9 = 0.55$
$r_i/r_0 = 7.5/9 = 0.83$
$r_i/r_0 = 8/9 = 0.88$
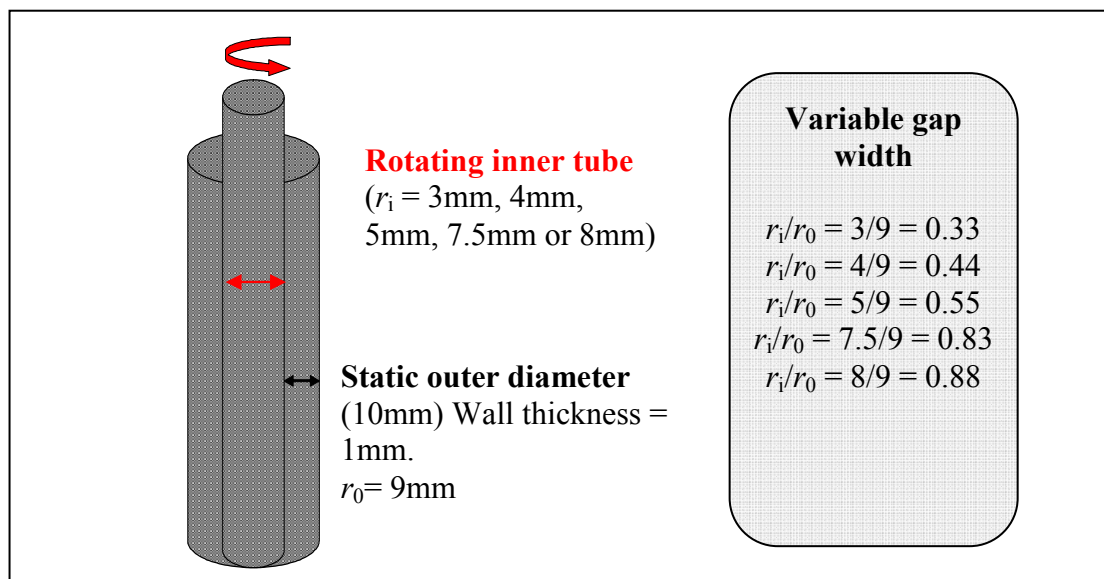
Figure 4.2.9: Schematic representation of the couette cell (obtained from reference[43]).

The amount of shear applied into the samples is a vital parameter for this work. Therefore for quantifying discussions in term of low, moderate and high shear rates the shear rate of the inner tube needs to be determined. The power-law model[16, 52] given below is used as the gap is wide ($r_i/r_o < 0.97$)

$$\dot{\gamma} = \frac{2\Omega}{n\left[1-\left(\dfrac{r_i}{r_o}\right)^{2/n}\right]}$$
Equation 4.2.18

where Ω is the angular velocity (rad/s), r_i is the outer radius of the inner tube, r_o is the inner radius of the outer tube and n is the power law index.

In order to determine the shear rate of the rotating inner tube, a 12V stepper-motor was attached to the inner tube. The motor was powered by a power supply operating up to 30V. The volts (V) settings are transformed to radial velocity using the data from previous work[43] done with the same experimental set-up, where the radial velocity (rad/s) of the rotating tube was determined using a tachometer (outputted reading in rev/min).

The power law index (n) can be determined using the AR 2000 rheometer from the slope of a plot of the natural log of apparent viscosity versus the natural log of shear rate. This relation is based on the power law equation indicated below

$$\sigma = -\kappa\left(\frac{\partial u}{\partial x}\right)^n = -\mu_{app}\left(\frac{\partial u}{\partial x}\right)$$

$$\therefore \mu_{app} = \kappa\left(\frac{\partial u}{\partial x}\right)^{n-1}$$
Equation 4.2.19

$$\log\mu_{app} = \log\kappa + (n-1)\log\left(\frac{\partial u}{\partial x}\right)$$

where σ is the shear stress (Pa), κ is a constant, (du/dx) is the shear rate, μ_{app} is the apparent viscosity and n is the power law index[52].

4.3 References

1.   Hartshorne, N. H., Optical Properties of Liquid Crystals. In *Liquid Crystals and Plastic Crystals* Winsor, G. W., Winsor, P. A., Ed. John Wiley and Sons: London, 1974; Vol. 1.

2.   Neubert, M. E., Characterisation of mesophase types and transitions. In *Experimental Study of Physical Properties and Phase Transitions*, Kumar, S., Ed. Cambridge University Press: New York, 2001.

3.   Gleeson, H. In *The Physics of Liquid Crystals*, British Liquid Crystal Society, Hull, 2003; Hull, 2003.

4.   Hartshorne, N. H., The Microscopy of Liquid Crystals. In London: Microscope Publications Ltd 1974.

5.   Lydon, J. E. In *Polarised Light Microscopy*, British Liquid Crystal Society, Hull, 2003; Hull, 2003.

6.   Davidson, M. W., Abramowitz, M., Optical Microscopy. In 2000.

7.   Sackmann, H., *Advances in Liquid Crystals*. London: Academic Press: 1974; p 1-107.

8.   Madbouly, S. A., Wolf, B. A., Shear-induced crystallization and shear-induced dissolution of poly(ethylene oxide) in mixtures with tetrahydronaphthalene and oligo(dimethyl siloxane-b-ethylene oxide). *Macromolecular Chemistry and Physics* **2003,** 204, (3), 417-424.

9.   Madbouly, S. A., Chiba, T., Ougizawa, T., Inoue, T., Shear effect on the phase behaviour and morphology in oligomer blend of polystyrene/poly(methyl methacrylate). *Polymer* **2001,** 42, (4), 1743-1750.

10.   Laidler, K. J., Meiser, J. H., *Physical Chemistry*. The Benjamin/Cummings Publishing Company, California: 1982.

11.   Bragg, W. L., Diffraction of Short Electromagnetic Waves by a Crystal. *Proceedings of the Cambridge Philosophical Society* **1913,** 17, 43-57.

12.   Fontell, K., In *Liquid Crystals and Plastic Crystals* Brown, G. H., Windsor, P. A., Ed. Ellis Harwood: Chichester 1974; Vol. 2, p 80.

13.   Atkins, P. W., *Physical Chemistry*. Oxford University Press: 1994.

14.   Fontell, K., X-Ray Diffraction. In *Liquid Crystals and Plastic Crystals*, Brown, G. H., Windsor, P. A., Ed. Ellis Horwood: Chichester, 1974; p 71.

15.   Luzzati, V., In *Biological Membranes*, Chapman, D., Ed. Academic Press: London and New York, 1968; p 71.

16.   Barnes, H. A., *A Handbook of Elementary Rheology*. Instiute of Non-Newtonian Fluid Mechanics, University of Wales: Aberystwyth, 2000.

17.   Barnes, H., Hutton, J. F., Walters, K., *An Introduction to Rheology*. Elsevier: New York, 1989.

18.   Hughes, R., Practical Rheology,. In *Colloid Science - Principles, Methods and Applications*, Cosgrove, T., Ed. Blackwell Publishing: 2005.

19.   Kevelam, J., Hoffmann, A. C., Engberts, J. B. F.N., Blokzijl, W., Van de Pas, J., Versluis, P. Rheology of concentrated dispersions of sterically stabilized polydisperse lamellar droplets. *Langmuir* **1999,** 15, (15), 5002-5013.

20.   Eriksson, P. O., Lindblom, G., Burnell, E. E., Tiddy, G. J. T. , Influence of Organic Solutes on the Self-Diffusion of Water as Studied by Nuclear Magnetic-Resonance Spectroscopy. *Journal of the Chemical Society-Faraday Transactions I* **1988,** 84, 3129-3139.

21.   Adam, C. D., Durrant, J. A., Lowry, M.R., Tiddy, G. J .T. , Gel and Liquid-Crystal Phase Structures of the Trioxyethylene Glycol Monohexadecyl Ether Water-System. *Journal of the Chemical Society-Faraday Transactions I* **1984,** 80, 789-801.

22.   Smith, I. C. P., Deuterium NMR In *Liquid Crystals and Plastic Crystals*, Gray, G. W., Ed. John Wiley and Sons London 2001.

23.   Emsley, J. W., Lindon, J. C., *NMR Spectroscopy using Liquid Crystal Solvents*. New York: Pergamon Press: 1975.

24.   Eriksson, P. O., Lindblom, G., Burnell, E. E., Tiddy, G. J. T. , Influence of Organic Solutes on the Self-Diffusion of Water as Studied by Nuclear Magnetic-Resonance Spectroscopy. *Journal of the Chemical Society-Faraday Transactions I* **1988,** 84, 3129-3139.

25.   Johansson, A., Lindman, B., Nuclear Magnetic Resonance Spectroscopy of Liquid Crystals - Amphiphilic Systems, in Liquid Crystals and Plastic Crystals In *Liquid Crystals and Plastic Crystals*, Gray, G. W., Winsor, P. A., Ed. John Wiley and Sons: London 1974.

26.   Rendall, K., Tiddy, G. J. T., Interaction of Water and Oxyethylene Groups in Lyotropic Liquid-Crystalline Phases of Poly(Oxyethylene) N-Dodecyl Ether Surfactants Studied by H-2 Nuclear Magnetic-Resonance Spectroscopy. *Journal of the Chemical Society-Faraday Transactions I* **1984,** 80, 3339-3357

27.   Rendall, K., Tiddy, G. J. T., Trevethan, M. A., Journal of the Chemical Society-Faraday Transactions I. *Optical Microscopy and Nuclear Magnetic-Resonance Studies of Mesophases Formed at Compositions between Hexagonal and Lamellar Phases in Sodium N-Alkanoate+Water Mixtures and Related Surfactant Systems.* **1983,** 79, 637.

28.   Staples, E. J., Tiddy, G. J. T., Nuclear Magnetic-Resonance Technique to Distinguish between Micelle Size Changes and Secondary Aggregation in Anionic and Non-Ionic Surfactant Solutions. *Journal of the Chemical Society-Faraday Transactions I* **1978**, 2530-2541.

29.   Ukleja, P., Finotello, D. NMR Studies of Orientational Order. In *Liquid Crystals: Experimental Study of Physcial Properties and Phase Transitions*, Kumar, S., Ed. Cambridge University Press: New York, 2001.

30.   Various., In *Magnetic Resonance in Colloid and Interface Science*, Fraissard, J. P., Resing, H. A. , Ed. Dordrecht: D. Riedel.: 1979.

31.   Wennerstrom, H., Lindman, B., Engstrom, S., Soderman, O., Lindblom, G., Tiddy, G. J. T., Magnetic Resonance. In *Colloid and Interface Science*, Fraissard, J. P., Resing, H. A., Ed. Reidel, D.: Dordrecht, 1980.

32.   Furo, I., NMR spectroscopy of micelles and related systems. *Journal of Molecular Liquids* 117, (1-3), 117-137.

33.   Bloch, F., Hansen, W. W., Packard, M. E., Nuclear Induction. *Physical Review* **1946,** 69, (3-4), 127.

34.   Hornak, J. P., The Basics of NMR., ed http://www.cis.rit.edu/htbooks/nmr/inside.htm. 1997. Chapter 1.

35.   Purcell, E. M., Torrey, H. C., Pound, R. V., Resonance Absorption by Nuclear Magnetic Moments in a Solid. . *Physical Review* **1946,** 69, (1-2), 37-38.

36.   Abragam, A., *The Principles of Nuclear Magnetism*. Clarendon Press: London, 1961.

37.   Carrington, A., McLachlan, A.D., *Introduction to Magnetic Resonance with Applications to Chemistry and Chemical Physics.* Harper and Row: New York, 1967.

38.   Lawson, K. D., Flautt, T. J., Magnetically oriented lyotropic liquid crystalline phases. *Journal of American Chemical Society* **1967,** 89, (21), 5489-5491.

39.   Szymanski, J., Wilk, A., Holyst, R., Roberts, G., Sinclair, K., Kowalski, A., Micro- and macro-shear viscosity in dispersed lamellar phases. *Journal of Non-Newtonian Fluid Mechanics* **2008,** 148, 134-140.

40.   Bovey, F. A., *Nuclear Magnetic Resonance Spectra*. Second Ed.; Academic Press: London, 1988.

41.   Doane, J. W., NMR of liquid crystals. In *Magnetic Resonance of phase transitions*, Owen, F. J., Ed. Academic Press, New York: 1979.

42.   Pake, G. E., Nuclear Resonance Absorption in Hydrated Crystals - Fine Structure of the Proton Line. *Journal of Chemical Physics* **1948,** 16, (4), 327-226.

43.   Dutton, H. M. The behaviour of surfactant lamellar and gel phases under flow. The University of Manchester, Manchester, 2007.

44.   Graham, A., Rheo-NMR. In *Modern Magnetic Resonance*, Springer Netherlands: 2006; pp 383-388.

45.   Graham, A., Rheo-NMR Spectroscopy. In *Modern Magnetic Resonance* Springer Netherlands: 2006; pp 1515-1521.

46.   Bee, L. C., Linseisen, F. M., Shear-Induced Orientational Order in a Polystyrene/Benzene-d6 Solution As Observed by 2H NMR. *Macromolecules* **1998,** 31, 4986-4989.

47.   Grabowski, D. A., Schmidt, C., Simultaneous Measurement of Shear Viscosity and Director Orientation of a Side-Chain Liquid-Crystalline Polymer by Rheo-NMR. *Macromolecules* **1994,** 27, 2632-2634.

48.   Lukaschek, M., Grabowski, D. A., Schmidt, C., Shear-Induced Alignment of a Hexagonal Lyotropic Liquid Crystal as Studied by Rheo-NMR. *Langmuir* **1995,** 11, 3590-3594.

49.   Callaghan, P., Rheo-NMR: A New Window on the Rheology of Complex Fluids. In Grand, D. M., Harris, R. K., Ed. John Wiley and Sons: Chichester, 2002.

50.   Hartmut, S., Grabowski, D. A., Schmidt, C., Rheo-NMR study of a non-flow-aligning side-chain liquid crystal polymer in nematic solution *Rheologica Acta* **1997,** 36, 618-627.

51.   Callaghan, P., Rheo-NMR: nuclear magnetic resonance and the rheology of complex fluids. *Reports on progress in physics* **1999,** 62, 599-670.

52.   Smith, J., Non-Newtonian Technology. In *Coulson and Richardson's Chemical Engineering* Richardson, J. F., Ed. Butterworth-Heinemann: 1999; Vol. 3.

Chapter 5

Characterisation of the mixed surfactant system before the application of shear

In this study we have employed optical microscopy, small angle X-ray scattering (SAXS) and ^{2}H NMR spectroscopy in an effort to characterise the mesophase structure of the systems in question. It is important to first investigate the microstructure of the electrolyte free system and the effect of the added salt on the mesophase structure prior the application of shear. The effect of aging, extensional flow and temperature on the lamellar liquid crystalline phases have been studied as this work is of particular relevance for industrial processes where the age of the products, the amount of extensional flow and the temperature are important factors to be considered if changes in microstructure observed.

5.1 Polarising Optical Microscopy

5.1.1 Introduction

The basis of this technique is that each non-cubic liquid crystalline phase exhibits distinct optical textures when observed between crossed polars[1, 2]. This experiment relies on differences in the alignment of the layers between the surfaces of the used microscope slide and the cover slip. In preparing a sample for the microscope the material is squashed between the used glass slide and cover slip to obtain a thin layer. According to literature[3] the lamellar phase tends to align with the uni-axis parallel to the glass surfaces and thus a homeotropic alignment. The patches of material with homeotropic alignment are separated by streaks having a characteristic appearance (oily streaks). Additional evidence of phase structure is given by the apparent viscosity, since the viscosity order cubic > hexagonal > lamellar is usually observed. Hexagonal phases have more complex behaviour, but also exhibit district textures the most common of which is termed 'non-geometric'.

Surprisingly a phenomenal amount of information can be gained from polarised light optical microscopy of liquid crystals including mesophase alignment, structural orientation and the homogeneity of the sample.

5.1.2 Experimental Details

Observation of the samples by light microscope was performed for all sample compositions range from 0 to 5 wt% TSC in ^{2}H$_2$O at room temperature. ^{2}H$_2$O is used as the results will be directly comparable to the ^{2}H NMR studies in Section 5.3. Samples were prepared as described in Chapter 4. Before any observation, all samples were kept undisturbed for 1 week because the complete build-up of the liquid crystalline structure is a time-consuming process[4, 5].

All optical microscopy experiments were carried out using a Zeiss Jenaval polarising optical microscope and photographs were taken using a CCD camera and analysed using image analysis software attached to the microscope. A Linkam hot stage was attached on the microscope to obtain temperature control with an accuracy of ±0.5ºC. A stream of nitrogen gas was used which passes though a reservoir of liquid nitrogen thus allowing rapid cooling to be obtained. All images displayed throughout Section 5.1.3 were viewed through crossed polars.

A drop of the sample is placed on a microscope slide, quickly covered with a cover glass while care was taken not to press the upper cover glass. The sample flows to fill the gap between the slide and the cover glass. Thin samples offer a better definition of contrast and thereby enable the structures to be studied in detail because the light scattering is reduced. The textures obtained are determined by the alignment of the layers in relation to the microscope slide. The alignment of the layers is affected by the domain-domain interactions and the surfaces of the microscope slide and cover glass used[2].

5.1.3 Results

The physical stability and appearance of all compositions were assessed by visual inspection (see Table 5.1.1). Samples were characterised as physically stable when there was no visible phase separation after the period of observation. The appearance is

classified as translucent, opaque and milky white based on observations of a few cubic centimetres for each system.

Sample	Appearance	Dominant phase formed
0 wt% TSC	Translucent	L_α
1 wt% TSC	Opaque	L_α
2 wt% TSC	Opaque	L_α
3 wt% TSC	Opaque	L_α
4 wt% TSC	milky white	L_α
5 wt% TSC	milky white	L_α

Table 5.1.1: Appearance and visual identification of the mesophase structure for the 0 to 5 wt% TSC samples after 1 week stored at room temperature.

Changing the electrolyte level has an influence on the observed macroscopic properties of the system. Such a change has previously been associated with a change from a planar lamellar arrangement to liposomes and can be induced by shear or electrolytes. Here it has been observed that the electrolyte free system appears to be translucent. Increasing the electrolyte level the system becomes opaque. In the presence of 4 and 5 wt% TSC the system appears to be milky white. This change might be due to light scattering within the samples. In addition, observation assessed by visual inspection for the 5 wt% TSC sample after 3 months revealed a visible phase separation. A higher volume white phase and a thin colourless layer on top were observed indicate that phase separation has occurred in the sample.

By increasing the electrolyte level in the system, a number of changes in the optical micrographs were highlighted. The origin of these differences lies in the alignment of the layers between the surfaces of the microscope slide and the cover glass. Selected optical micrographs can be seen in Figure 5.1.1 for all sample compositions range from 0 to 5 wt% TSC.

Sample	Optical micrographs	Sample	Optical micrographs
0 wt%		3 wt%	
1 wt%		4 wt%	
2 wt%		5 wt%	
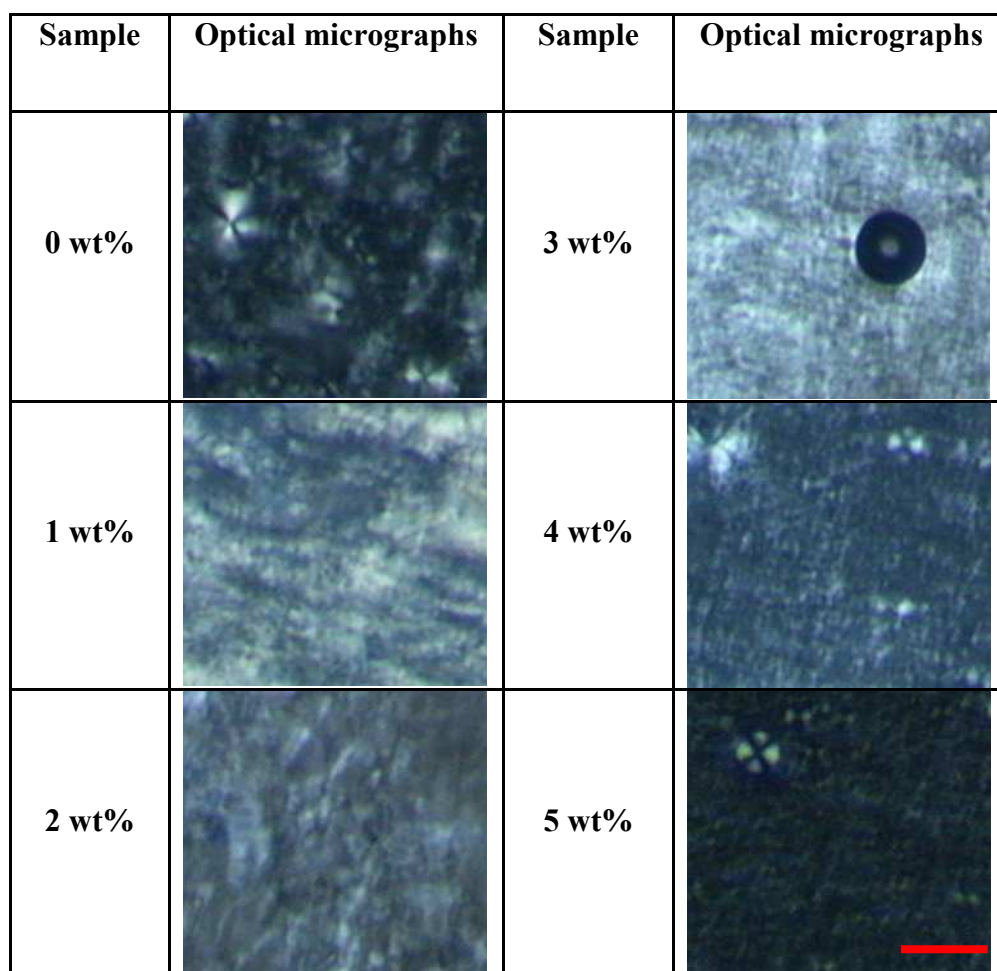
Figure 5.1.1: Optical micrographs viewed through crossed polars for the 0 to 5 wt% TSC samples (1week aged), at 25°C. The scale bar represents 100µm. (Dark spherical regions are air bubbles).

Using polarised light, at first many Maltese crosses can be seen for the electrolyte free system (see Figure 5.1.1). The appearance of the Maltese crosses is characteristic of the existence of lamellar structure and reveals the general disorder of the domains.

The optical micrograph for the 1 wt% TSC sample, illustrated in Figure 5.1.1, shows a strong birefringent bands through crossed polars and bears a mosaic texture similar to the texture observed for the 0 wt% TSC sample. However, the domain sizes of the main areas of birefringence are larger than those observed for the 0 wt% TSC sample. A slightly darker texture is observed for the 2 wt% TSC sample. Darker bands may be caused by the alignment of the layers with their optic axis perpendicular to the glass surfaces.

Spherical air bubbles with birefringent edges are shown in the field of view displayed in Figure 5.1.1. Air bubbles preferably forms a spherical shape, as this has the smallest surface area for a particular amount of air trapped inside. Direct visualisation of the air bubbles was proposed as an easy method for a rapid differentiation between lamellar and hexagonal structures[6].

Birefringence was also detected in the texture observed for the 3 wt% TSC sample. Spherical air bubbles are observed thus a clear indication that the packing of the molecules within the lamellar phase has no significant changes. When further increasing the electrolyte level up to 4 and 5 wt% TSC a grainy texture is observed. The optical micrograph observed for the 4 and 5 wt% TSC samples show Maltese crosses embedded in the background birefringent grainy texture.

The optical micrograph viewed for the 5 wt% TSC sample is darker than the optical micrograph viewed for the 4 wt% TSC sample. It seems likely that the 4 and 5 wt% TSC samples can be a two-phase systems *i.e.* lamellar dispersion of vesicles in an aquatic electrolyte solution. The vesicles are, when their size is large enough, easily detected on the basis of Maltese crosses when view under polarised light. Maltese crosses indicate that curved domains with radial symmetry are present in the system.

To follow the aging process, optical micrographs of the samples were taken over a period of 5 months. Illustrated in Figures 5.1.2a and 5.1.2b are the optical micrographs obtained for all the samples 1 week, 3 and 5 months after the sample preparation. It is important to note that all the samples were stored under the same conditions at room temperature and also all samples were approximately of the same thickness. Although the formation of the lamellar phase established almost immediately, as the samples age changes in the microstructure of the phase were observed.

Polarised light microscopy studies reveal that sample microstructure is changed over the 5 months. More compact texture with high birefringence appears for the 0 and 3 wt% TSC samples. Maltese crosses are observed throughout the concentration range shown in Figure 5.1.2a.

Sample/ Age	0 wt% TSC	1 wt% TSC	2 wt% TSC
1 week			
3 months			
5 months			
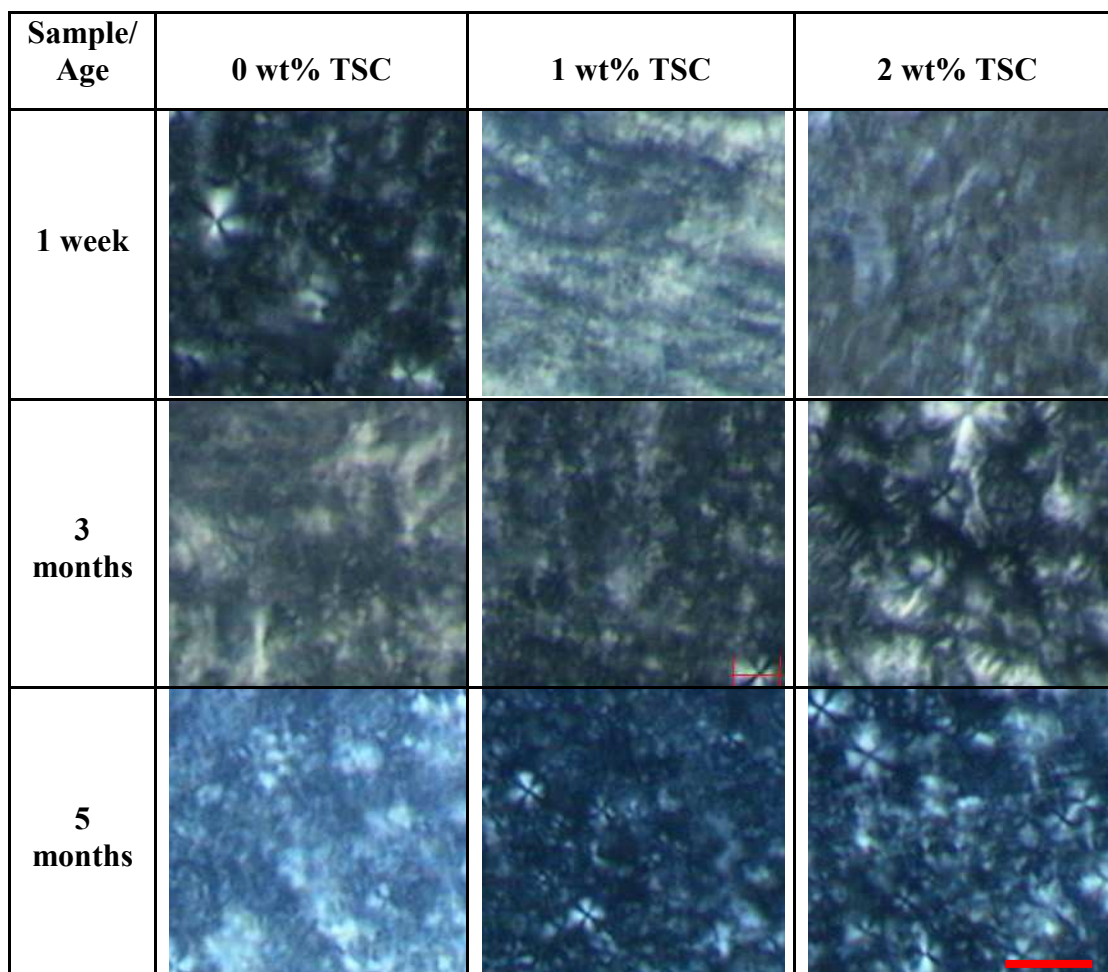
Figure 5.1.2a: Optical micrographs viewed through crossed polars for the 0, 1 and 2 wt% TSC samples at 25°C showing the development of the liquid crystalline phase over time. The scale bar represents 100μm.

Shown in Figure 5.1.2b are the optical micrographs obtained for the 3, 4 and 5 wt% TSC samples. A number of changes in the texture of the samples are observed after the first 3 months. When the alignment of the layers within the sample is changed changes in the brightness of the optical micrographs can be observed. An important observation is the extinction of Maltese crosses for the 4 and 5 wt% TSC samples. The textures seem more compact after 5 months thus better developed structures.

Sample/ Age	3 wt% TSC	4 wt% TSC	5 wt% TSC
1 week			
3 months			
5 months			
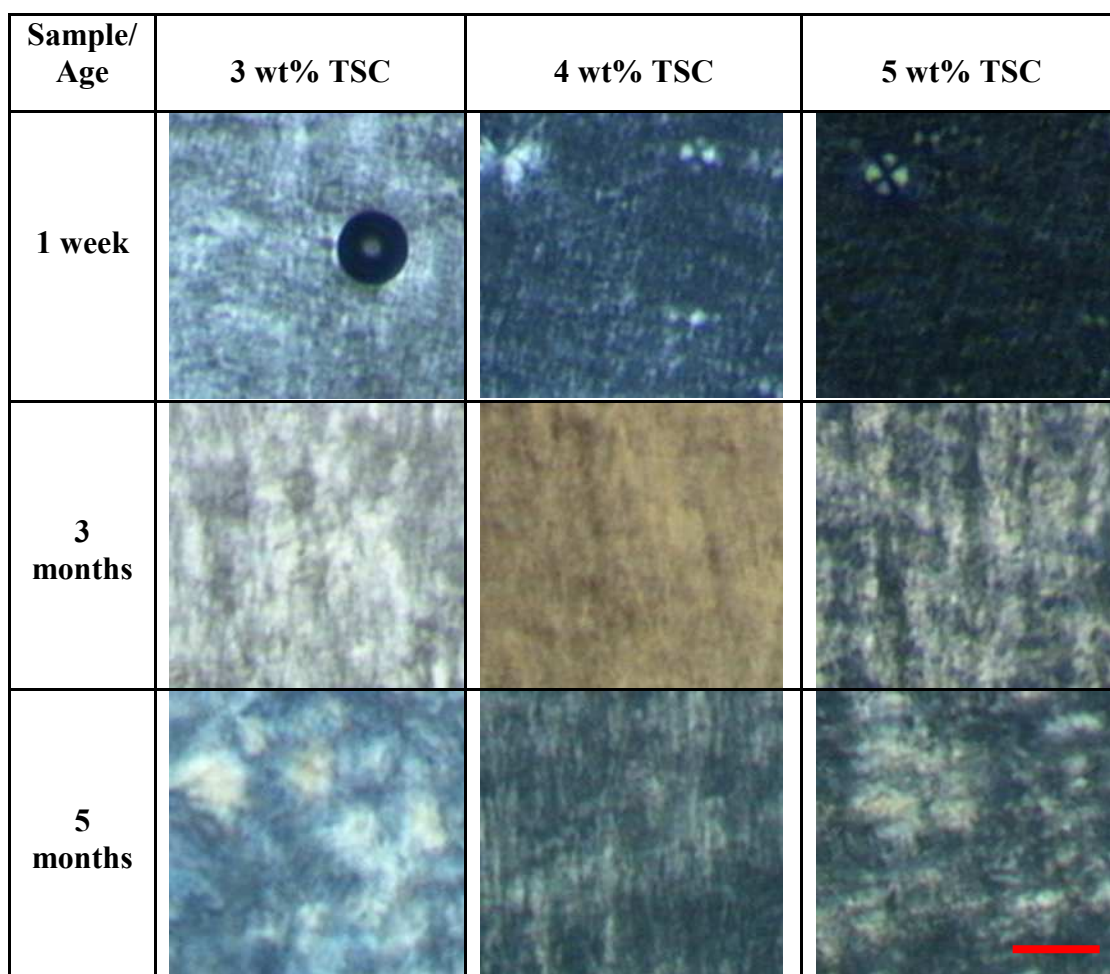
Figure 5.1.2b: Optical micrographs viewed through crossed polars for the 3, 4 and 5 wt% TSC samples at 25°C showing the development of the liquid crystalline phase over time. The scale bar represents 100μm.

One of the main objectives of this work is to study the effect of extensional flow on the microstructure of the lamellar liquid crystalline phase. It was shown by many other groups[7-10] that forcing the lamellar phases to flow can cause changes in the alignment of the layers. Flow birefringence investigations have been completed for the 0, 3 and 5 wt% TSC samples (5 months aged) to see the effect of extensional flow under crossed polars. Pressure has been applied onto the sample by gently pressing the upper cover slip.
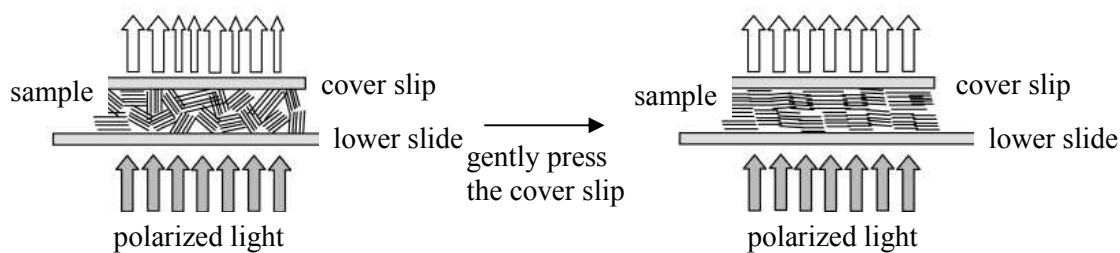
Figure 5.1.3: Schematic picture of the structural orientation caused when pressure was applied to the cover slip (redrawn from reference[11]).

As shown in Figure 5.1.3 after the shear application onto the lamellar phase the layers always tend to align parallel to the plane of shear in order to minimise their mechanical resistance.

When pressure was applied to the cover slip the lamellar phases under investigation undergo structural deformation. Illustrated in Figure 5.1.4 are the optical micrographs obtained before pressure was applied to the cover slip (t_0), immediately after pressing the cover slip (t_1) and 15mins after pressing the cover slip (t_2).

Observations on the optical micrographs for the electrolyte free system reveal that pressing the cover slip induces a slight darkening of the texture which is representative of changes in the alignment of a layered structure. Thus the density of the structural defects is minimized. Another observation to support that is the Maltese crosses extinction when pressure was applied to the cover slip.

A more define texture is observed for the 3 wt% TSC sample immediately after pressing the cover slip. Mosaic domains are observed with black areas between them. The black areas might be homeotropic regions where the optic axis of the molecules is perpendicular to the glass surface. Less bright optical micrographs are obtained after pressing the cover slip compared to that taken before. This suggests that changes in the orientation of the layers do happen indeed but defects are still present as indicated from the large birefringent particles.

Birefringence is observed as a result of the flow process for the 5 wt% TSC sample. Large areas of plate like domains are oriented parallel to the wall of the cover slip with darker pockets embedded in the texture.

Time/ Sample	t_0	t_1	t_2
0 wt% TSC			
3 wt% TSC			
5 wt% TSC			
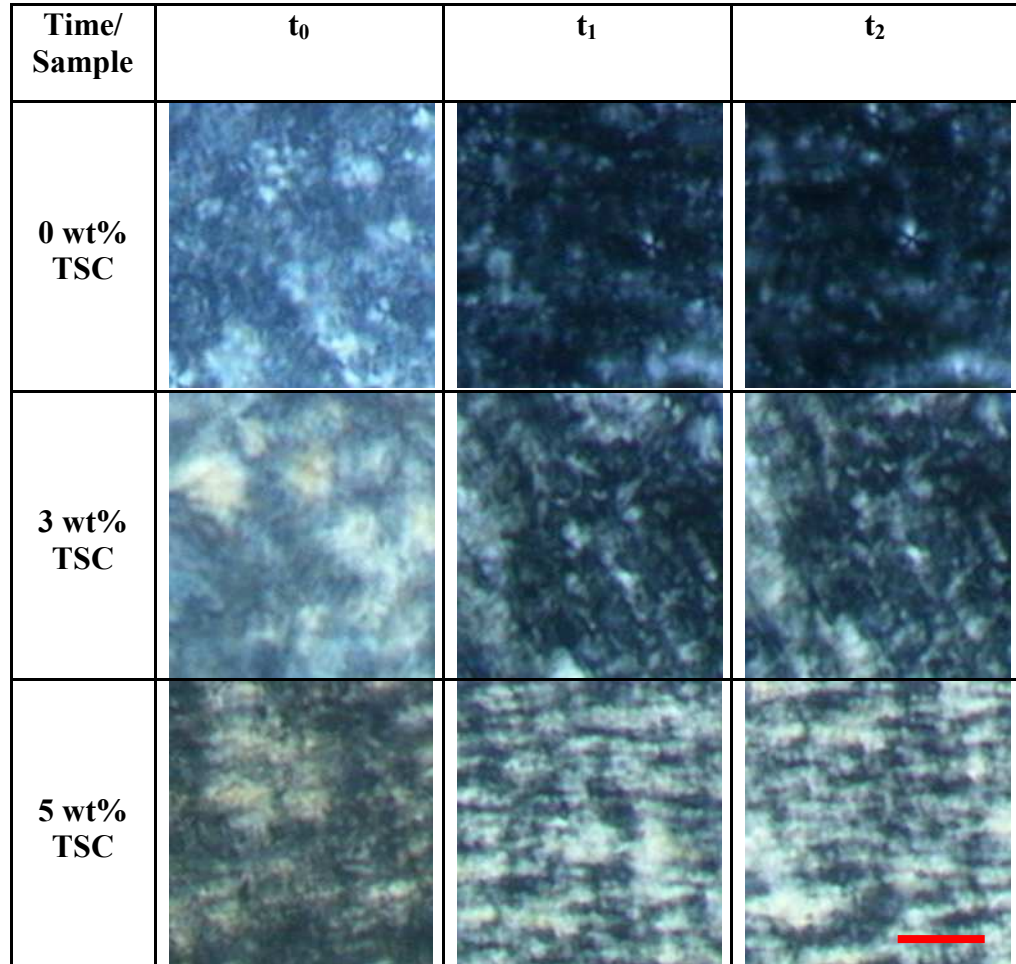
Figure 5.1.4: Optical micrographs viewed through crossed polars for the 0, 3 and 5 wt% TSC samples (5 months aged) at 25°C, showing the structural orientation caused by the application of extensional flow. The optical micrographs obtained before pressure was applied to the cover slip (t_0), immediately and 15mins after pressing the cover slip (t_1 and t_2 respectively). The scale bar represents 100μm.

Insignificant changes have been observed in the optical micrographs for all the samples after one day have been left to relax. It is noteworthy that the process of the alignment of the layers starts at the liquid/glass interface and is a time consuming process. The process of alignment is affected by the domain-domain interactions within the phase. The time required for such orientation process is closely related with the elasticity of the system.

Therefore, the orientation process observed in a lamellar system closed between two glass plates is a general rheological attribute of the system.

5.1.4 Discussion

Giving consideration to the observations thus far, it seems likely that there are two possible factors influencing the phase structure. The first is the influence of the electrolyte level and the second is the shear history of the sample.

Observations of the samples by light microscopy and on their physical appearance were performed over 5 months period. All samples (except the 5 wt% TSC sample) appeared homogeneous with insignificant changes in microscopic appearance. Considering each of the optical micrographs as a typical representation of the sample overall it can be said that there are definite aging effects, although seemingly random, with defects over a small distance scale (see Figures 5.1.2a and 5.1.2b). Changes in the brightness of the textures can be explained as changes in the alignment of the layers.

The samples exhibit birefringence, this has previously been observed in systems that are thought to be lamellar in nature[6]. Maltese crosses were present in all cases however there were changes in the size and the arrangement of the layers being observed with increasing electrolyte level. As shown in Figure 5.1.1 the structural characteristics of the lamellar phases observed in this study are strongly depended on the electrolyte level. The microscopic appearance of the optical micrographs for the 0 to 3 wt% TSC samples (mosaic textures) indicates a single continuous lamellar phase with flexible bilayers, each of them characterised by a director with random orientation which defines the main orientation of the phase. As the layers are liquid-like and slide over one another, they can easily be curved, while keeping for energetic reasons a constant thickness. Defects in the bilayers are easily detected on the basis of Maltese crosses thus from a microscopic point of view the phase looks irregular.

The grainy lamellar textures seen for the 4 and 5 wt% TSC samples suggest that these samples can be a two-phase system, *i.e.* a lamellar dispersion (vesicles and excess isotropic solution). In light microscopy large structures such as large vesicles are flattened between the glasses. Therefore, large vesicles will not show any internal structure. Maltese crosses

as seen in these optical micrographs indicate a domain with radial symmetry. Sometimes the vesicles are large compared to the thickness of the sample thus the layers in the centre of the vesicle are forced to align parallel to the surface of the slide and dark pseudo-isotropic bands are observed.

Our results reveal that the amount of extensional flow induced in the lamellar systems has an important effect on the alignment process thus an impact on the lamellar microstructure. This work is of particular relevance for industrial processes where the amount of extensional flow, shear flow and the age of the product may be important if changes in microstructure observed. Thereby, the effect of all the factors mentioned above on the microstructure, is important to be considered throughout this work.

In order to arrive to a more conclusive decision, the two-phase lamellar dispersion as well as all the other samples were investigated with other techniques like small angle X-ray scattering and ^{2}H NMR spectroscopy.

5.2 Small-angle X-ray Scattering (SAXS)

5.2.1 Introduction

SAXS experiments are used as the lamellar structures usually show characteristic Bragg reflections in the low-angle region in the ratio of d: $d/2$: $d/3$: $d/4$… besides the diffuse reflection with spacing corresponding to 4.5Å. The diffraction patterns of such reflections indicate a tendency for preferred orientation of the lamellar bilayers within the sample parallel to the container walls. Often with aqueous systems only the first reflection is visible, while the intensity falls off sharply for the higher orders.

The lamellar structure is composed of an alternation of double layers of amphiphilic molecules separated by water layers as shown in Figure 5.2.1.
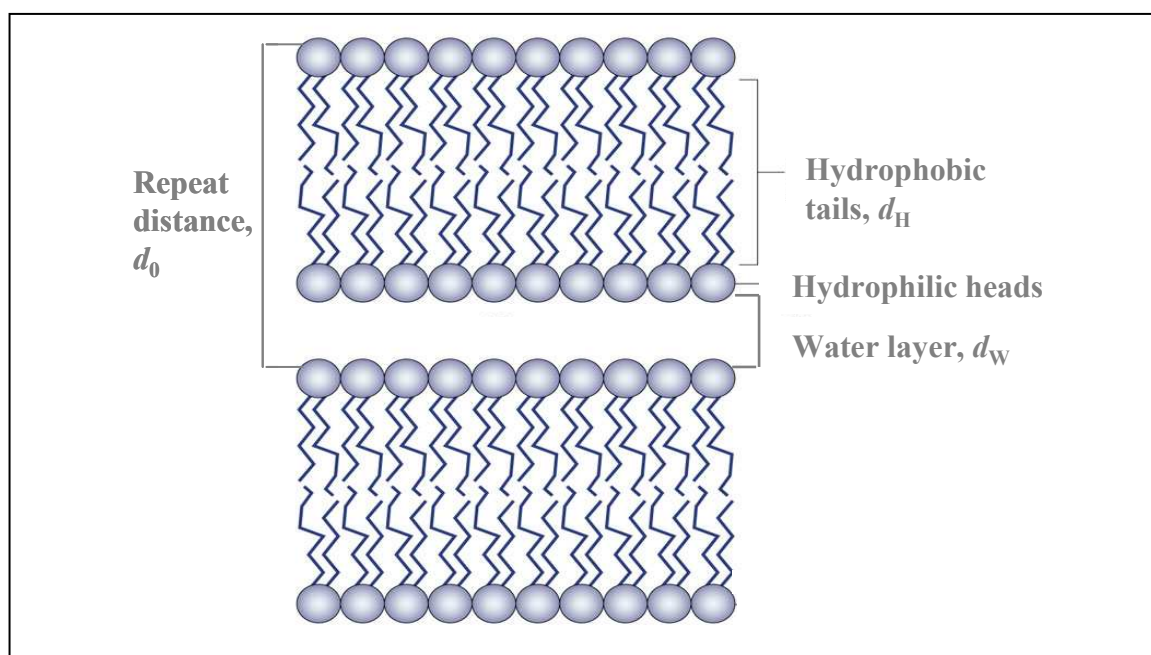
Figure 5.2.1: Schematic representation of the structure of the lamellar phase, where d_0, is the repeat distance (d-spacing), d_H and d_W are the thickness of the alkyl chains and water layer respectively.

Information regarding the structure of the lamellar phase formed and the structural parameters will be made through analysis of the obtained diffraction pattern.

5.2.2 Experimental details

Samples were prepared by mixing the appropriate weights of surfactant, electrolyte and distilled water as described in Chapter 4. All the samples were kept undisturbed for 1 week because as mentioned before the complete built-up of the liquid crystalline structure is a time-consuming process[12, 13]. After standing at room temperature for one week, samples were loaded into 1mm diameter Lindemann glass capillary tubes and care was taken to limit the exposure to air. The tubes were then flame sealed. SAXS measurements were carried out one day after filling the tubes.

SAXS experiments were carried out at the Synchrotron Radiation Source (SRS) at Daresbury Laboratory, UK. The detector distance for SAXS was maintained at 1m and the wavelength was 1.54Å. A Linkam hot stage was used to hold each of the Lindemann tubes and this was arranged in such a way that the X-ray beams impinges on a spot on the Lindemann tube. The temperature on the hot stage was controlled using a liquid nitrogen connected pump and a temperature controller. The sample temperature is controlled to $\pm 0.5°C$. The effect of temperature on the microstructure of the samples was studied by heating and cooling the samples from 25 to 100°C at a rate of $5°Cmin^{-1}$ with 1 minute to equilibrate at each temperature. The temperature of interest is ca. 25°C, as this is the approximate temperature during post processing, storage and transportation of the final product. The calibration standard used is wet rat tail.

5.2.3 Results

X-ray scattering measurements were carried out for the 0, 1, 3 and 5 wt% TSC samples on a heat-cool cycle from 25 to 100°C and subsequently cooled back to 25°C. Data were collected at a range of temperatures, including 25, 50, 75 and 100°C. The results are tabulated for ease of reference and are presented in Table 5.2.1.

Temp. / °C	0 wt% TSC		1 wt% TSC		3 wt% TSC		5 wt% TSC	
	d/2	d_0	d/2	d_0	d/2	d_0	d/2	d_0
25	23.5	46.7	23.4	45.5	23.3	46.7	20.0	39.4
50	22.6	44.3	22.6	45.4	22.4	45.4	19.8	39.3
75	22.0	44.9	22.4	43.7	22.4	44.9	19.5	38.9
100/100	21.8	43.7	21.8	43.3	21.8	43.7	19.3	38.4
75	21.3	41.7	22.1	42.7	22.6	44.9	19.2	38.4
50	22.4	44.9	22.6	44.9	22.4	44.9	19.7	38.9
25	23.1	45.5	22.9	46.7	23.1	46.1	20.1	39.4

Table 5.2.1: Tabulated *d*-spacing (Å) from variable temperature SAXS scans (where red colour on heating and blue colour on cooling cycle).

On visual inspection the X-ray diffraction pattern for all the samples displays two reflections which appear to be in a 2:1 ratio of the corresponding distances, which is typical for one-dimensional lamellar phases. The diffraction patterns collected for the 0, 1, 3 and 5 wt% TSC samples (1 week aged) at 25°C are shown in Figure 5.2.2.
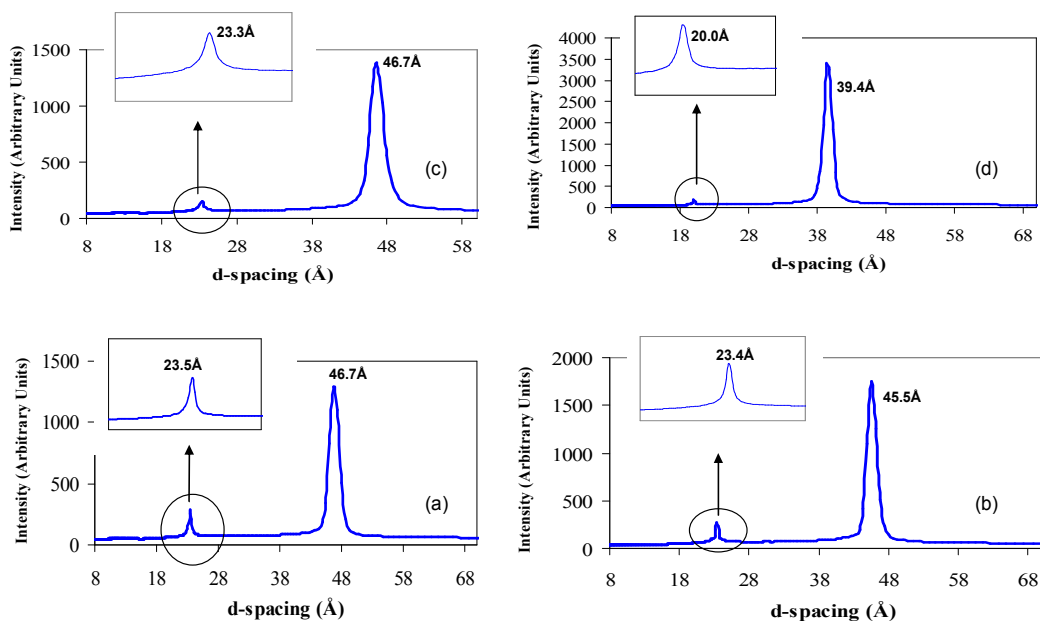
Figure 5.2.2: SAXS diffraction patterns for (a) the 0 wt% TSC sample, (b) the 1 wt% TSC sample, (c) the 3 wt% TSC sample and (d) the 5 wt% TSC sample. All the SAXS experiments were carried out at 25°C. The d_0 and $d/2$ values are indicated.

The peak positions of the lamellar phases for the 0, 1 and 3 wt% TSC samples did not vary significantly. Thus the repeat distances in the lamellar phase remain fairly constant as shown in Table 5.2.1. The term lamellar repeat distance refers to the d-spacing indicated as d_0 in Figure 5.2.1. A small decrease in d-spacing is observed for the 5 wt% TSC sample. This suggests that until a certain salt concentration in the system, the d-spacing values are rather similar. Above this concentration d-spacing starts to decrease. This possibly marks the onset of the transition from a single lamellar to a lamellar dispersion (vesicles with a significant excess of isotropic phase).

Selected 2-D scattering images corresponding to the 0, 1, 3 and 5 wt% TSC samples at 25°C, representative of the data obtained, are shown in Figure 5.2.3. It should be noted that all the experiments were performed on Station 2.1 at Daresbury SRS where the beam centre is at the top of the image.

Intensity (arbitrary units)
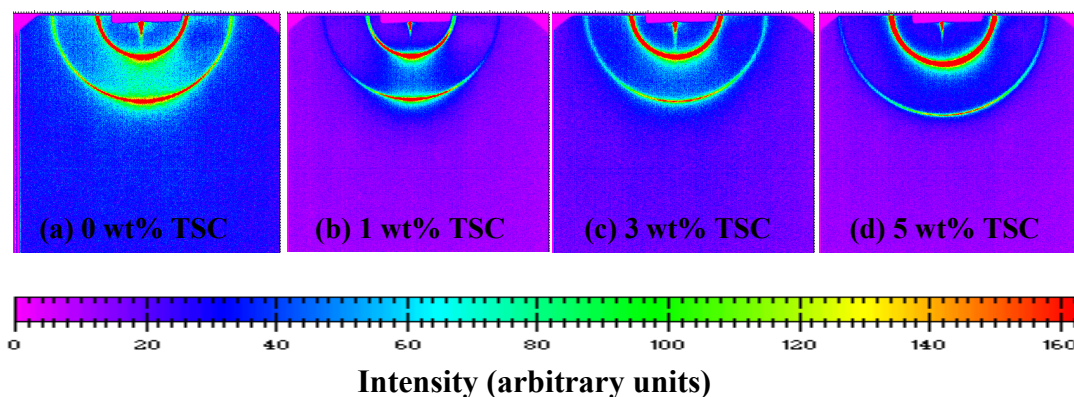
Figure 5.2.3: X- ray diffraction (XRD) (SAXS) 2-D scattering images for (a) the 0 wt% TSC sample, (b) the 1 wt% TSC sample, (c) the 3 wt% TSC sample and (d) the 5 wt% TSC sample at 25°C.

As can be seen in Figure 5.3.2 the 2-D scattering images for the 0 and 1 wt% TSC samples give an indication of preferred orientation parallel to the glass wall of the capillary tube (diffraction rings show distinct regions of maximum and minimum intensity). This suggests that the lamellar phase must be continuous throughout the sample, otherwise would not give an indication of preferred orientation. Thus the 0 and 1 wt% TSC samples can be a single lamellar phase. However, the 2-D scattering image for the 3 wt% TSC sample gives a lower intensity distinct region indicating that the aligned fraction of material in this system might be smaller. A noteworthy observation is that the 2-D scattering image for the 5 wt% TSC sample gives no indication of preferred orientation. Thus, it can be said that this is a two-phase system with vesicles and an excess of isotropic phase.

The next step was to extend the X-ray studies to include variable temperature measurements. The X-ray diffraction patterns are represented in the following paragraphs according to the concentration of salt in the sample.

A series of diffraction patterns collected during a heat-cool cycle for the 0 wt% TSC sample is shown in Figure 5.2.4. Peak positions did not vary significantly on heating. This suggests that the phase is stable upon heating.

Figure 5.2.4: XRD (SAXS) on Station 2.1 for the 0 wt% TSC sample during the heat-cool cycle from 25 to 100°C and subsequently cooled back to 25°C.

At 25°C the lamellar repeat distance is 46.7Å and it starts to decrease with increasing temperature, reaching 44.3Å at 50°C. There was further decrease in the magnitude of the *d*-spacing at 75°C, which continued as the sample heated to 100°C. During cooling, the magnitude of the *d*-spacing increases but did not match with their respective values obtained during heating (Figure 5.2.4). This may be due to slow re-accommodation of the water into the bilayers.

Selected 2-D scattering images for the 0 wt% TSC sample from 25 to 100°C and subsequently cooled back to 25°C are shown in Figure 5.2.5.

Figure 5.2.5: XRD (SAXS) 2-D scattering images for the 0 wt% TSC sample during heat-cool cycle from 25 to 100°C and subsequently cooled back to 25°C.

The scattering rings obtained when cooled back to 25°C gives lower intensity distinct region indicate that changes occurred in the rearrangement of the domains. This difference is possibly due to reformation of the phase as the sample re-accommodates the bilayer water and relaxes to its original structure with time.

Shown in Figure 5.2.6 is the X-ray diffraction pattern for the 1 wt% TSC sample. The data were qualitatively similar to the behaviour observed for the 0 wt% TSC sample.
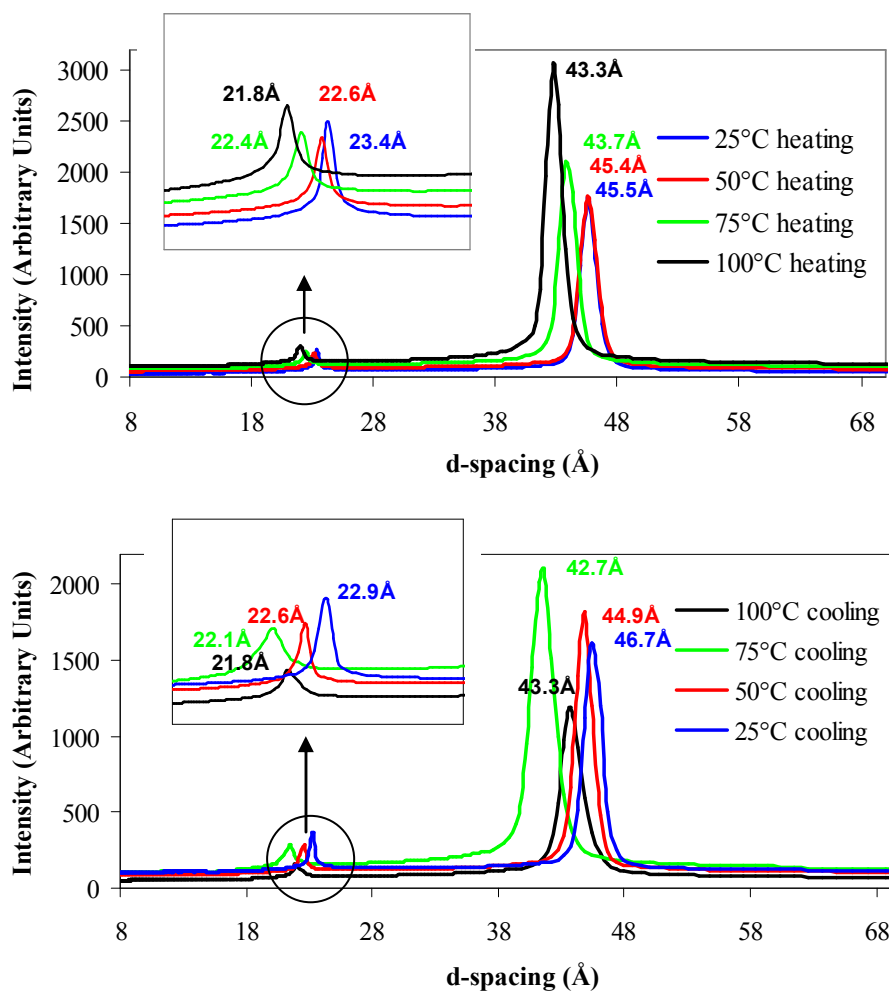
Figure 5.2.6: XRD (SAXS) on Station 2.1 for the 1 wt% TSC sample during a heat-cool cycle from 25 to 100°C and subsequently cooled back to 25°C.

The lamellar phase starts at a *d*-spacing of 45.5Å at 25°C and remains constant until 50°C when it gradually starts to decrease with increasing temperature, reaching 43.7Å at 75°C. Upon further heating to 100°C the *d*-spacing decreases at 43.3Å. Overall, it was shown that the *d*-spacing decreases with increasing temperature. However, the changes in the *d*-spacing values suggest that the lamellar region remains fairly unchanged upon heating.

The 2-D scattering images obtained during the heat-cool cycle from 25 to 100°C and subsequently cooled back to 25°C are shown in Figure 5.2.7.

Intensity (arbitrary units)
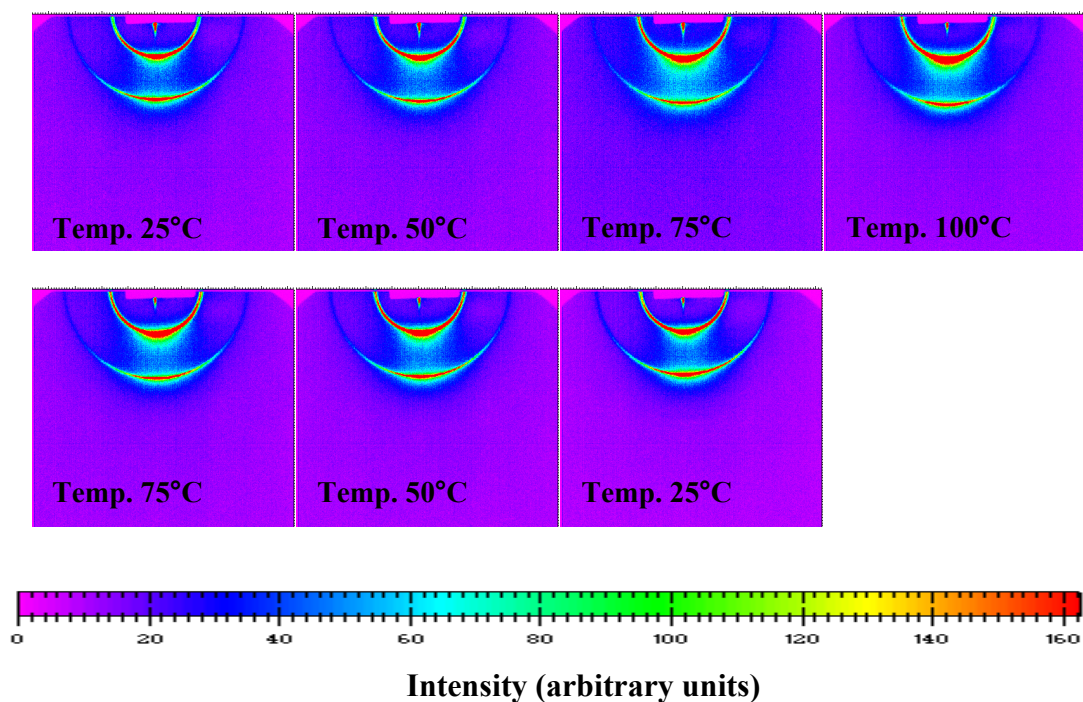
Figure 5.2.7: XRD (SAXS) 2-D scattering images for the 1 wt% TSC sample during a heat-cool cycle from 25 to 100°C and subsequently cooled back to 25°C.

Variable temperature X-ray diffraction experiments were also carried out on the 3 wt% TSC sample. The nature of the X-rays was similar to those previously observed. The X-ray diffraction pattern obtained during heating from 25 to 100°C is shown in Figure 5.2.8.
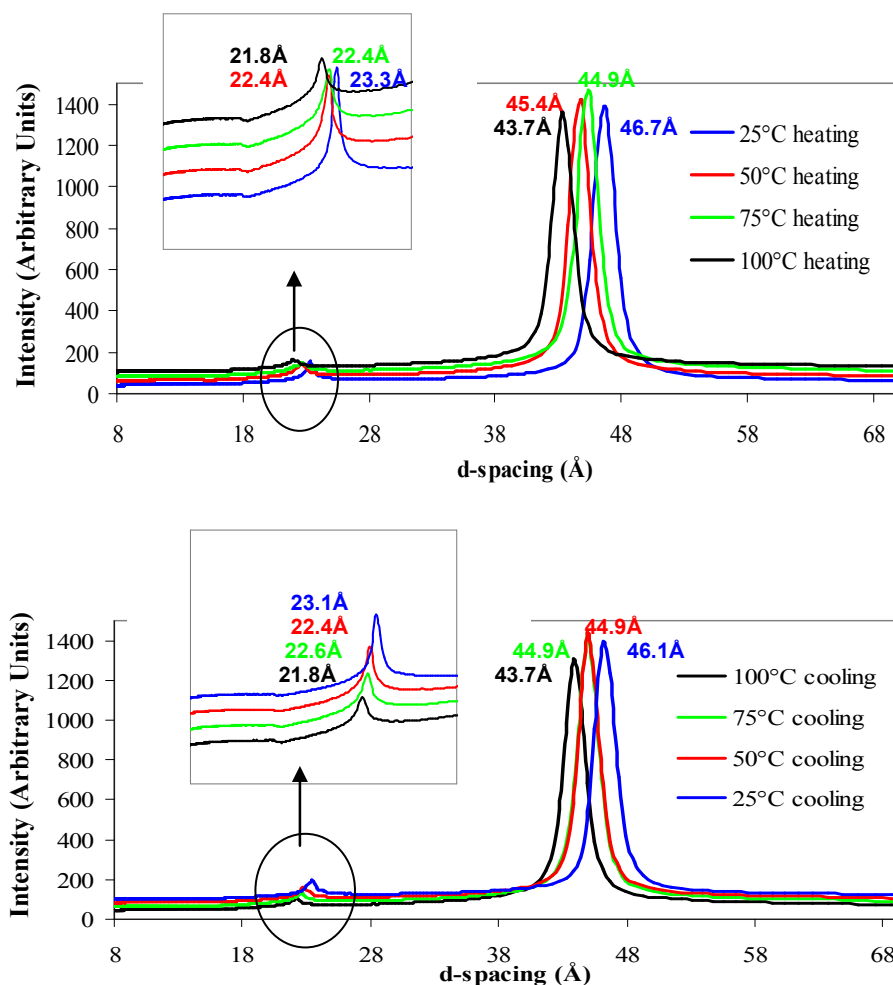
Figure 5.2.8: XRD (SAXS) on Station 2.1 for the 3 wt% TSC sample during a heat-cool cycle from 25 to 100°C and subsequently cooled back to 25°C.

The lamellar phase starts at a *d*-spacing of 46.7Å at 25°C and decreases with increasing temperature. Upon heating to 50°C the *d*-spacing decreases at 45.4Å. Further heating to 75°C results to a slight decrease of the *d*-spacing at 44.9Å. Upon further heating to 100°C the *d*-spacing decreases at 43.7Å.

During cooling, the magnitude of *d*-spacing increases without any significant changes in the peak position and shape. The *d*-spacing values did not match with their respective values during heating but are fairly similar. The X-ray diffraction patterns obtained during cooling are shown in Figure 5.2.8.

The 2-D scattering images obtained during the heat-cool cycle from 25°C to 100°C and subsequently cooled back to 25°C are shown in Figure 5.2.9.

Intensity (arbitrary units)
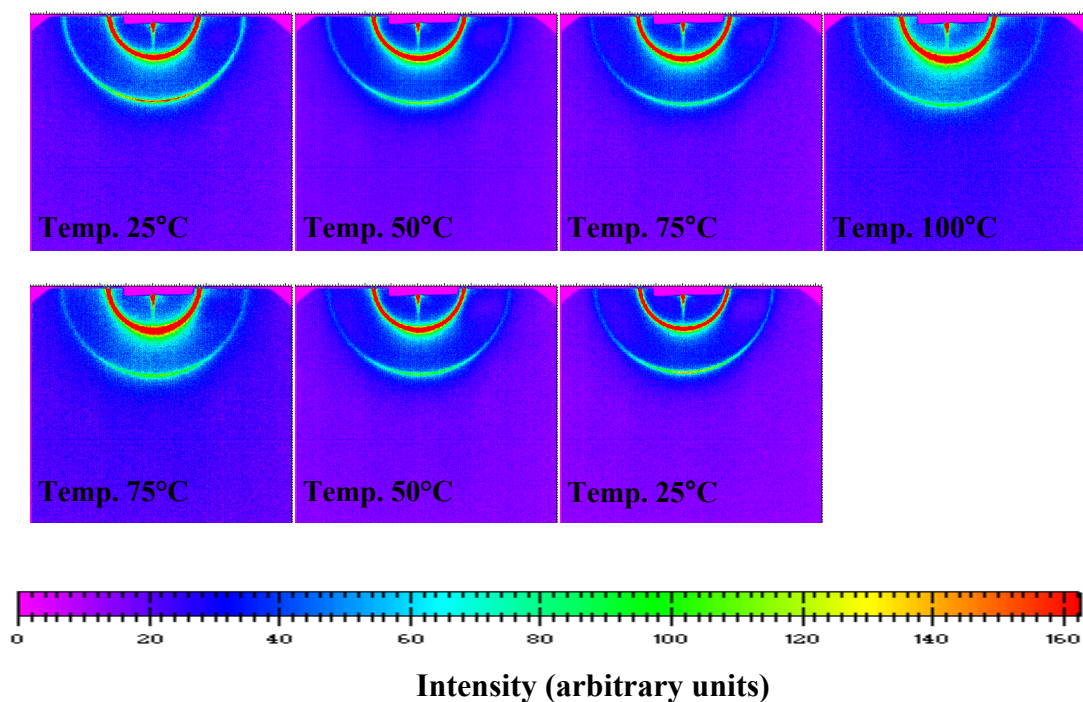
Figure 5.2.9: XRD (SAXS) 2-D scattering images for the 3 wt% TSC sample during a heat-cool cycle from 25 to 100°C and subsequently cooled back to 25°C.

Illustrated in Figure 5.2.10 is the X-ray diffraction pattern obtained for the 5 wt% TSC sample during a heat-cool cycle from 25 to 100°C and subsequently cooled back to 25°C. The lamellar phase starts at a *d*-spacing of 39.8Å at 25°C and decreases with increasing temperature. Upon heating to 50°C the *d*-spacing decreases at 39.3Å. Further heating to 75°C results to a decrease of the *d*-spacing at 38.9Å. Upon further heating to 100°C the *d*-spacing slightly decreases at 38.4Å.
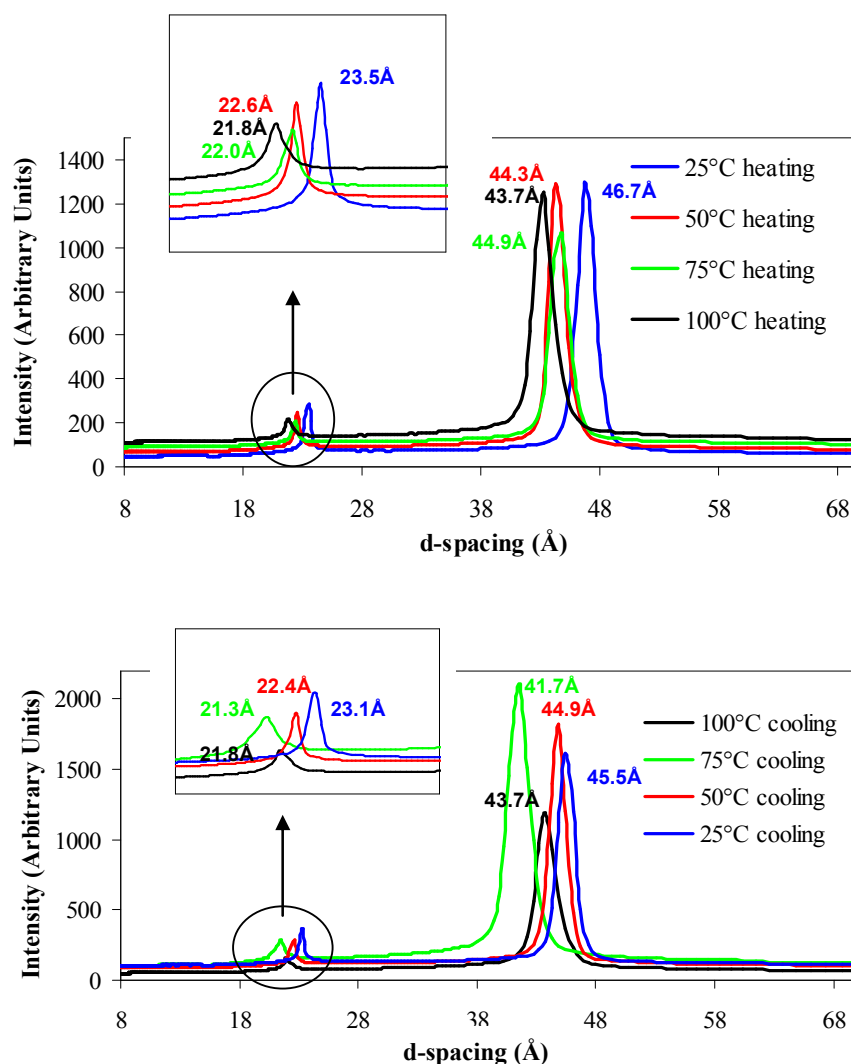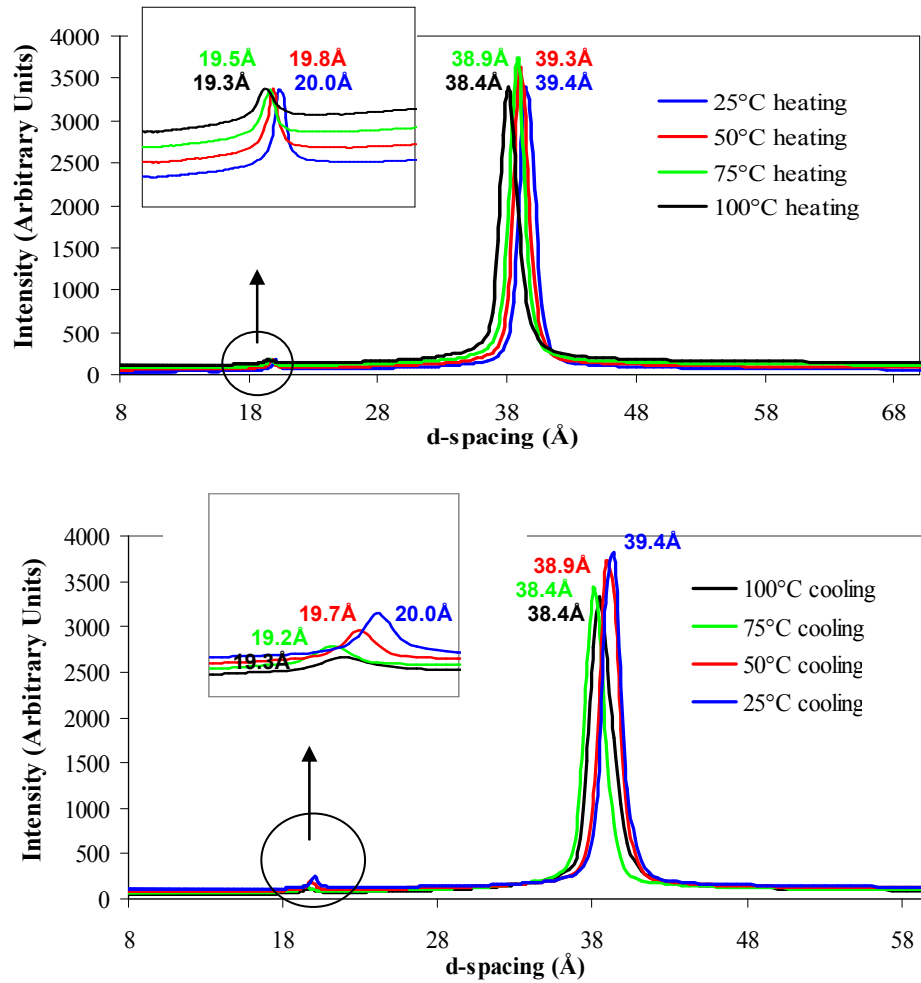
Figure 5.2.10: XRD (SAXS) on Station 2.1 for the 5 wt% TSC sample during a heat-cool cycle from 25 to 100°C and subsequently cooled back to 25°C.

On cooling, the magnitude of the *d*-spacing increases without any significant changes in the peak position and shape. The X-ray diffraction pattern obtained during cooling is shown in Figure 5.2.10.

The 2-D scattering images obtained during the heat-cool cycle from 25 to 100°C and subsequently cooled back to 25°C are shown in Figure 5.2.11.

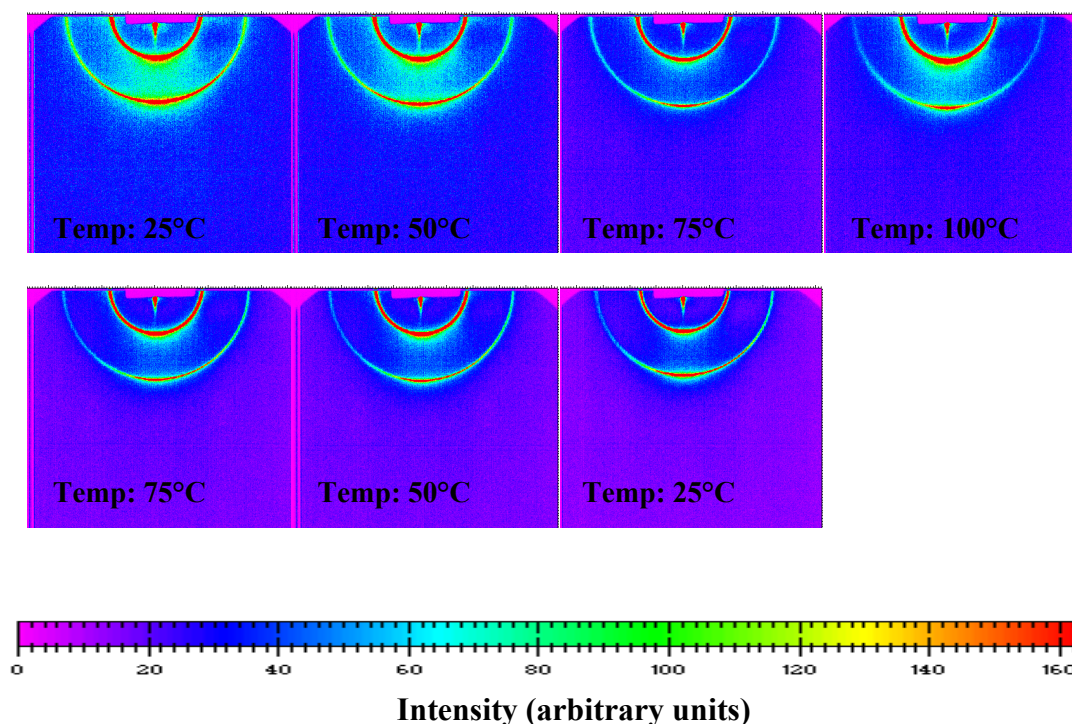**Intensity (arbitrary units)**
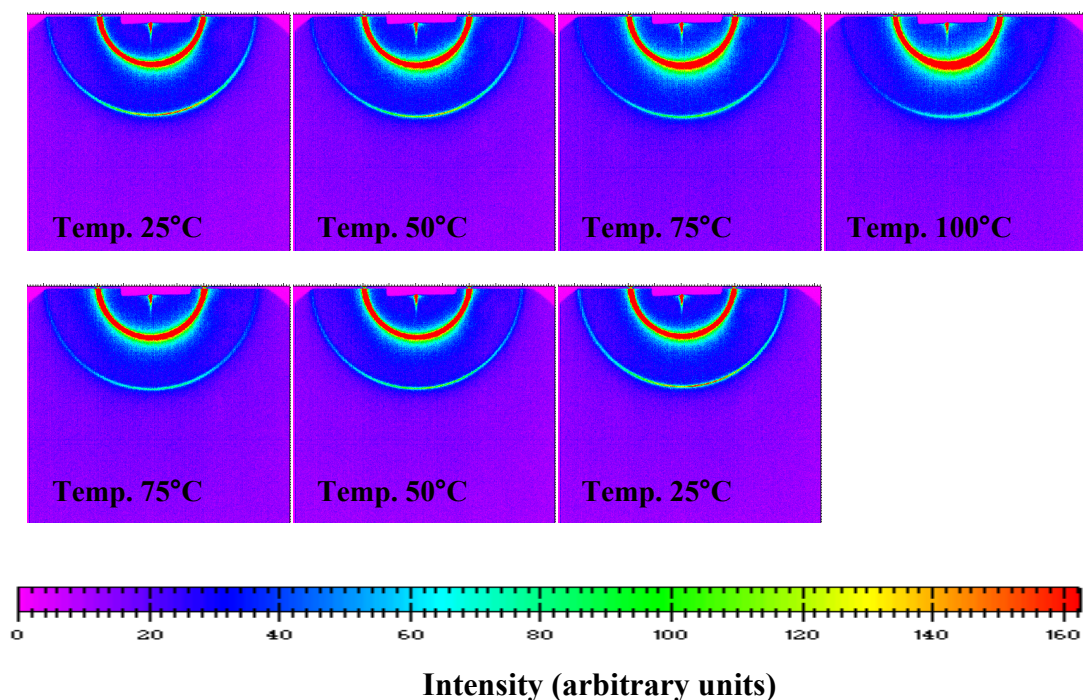
Figure 5.2.11: XRD (SAXS) 2-D scattering images for the 5 wt% TSC sample during heat-cool cycle from 25 to 100°C and subsequently cooled back to 25°C.

5.2.4 Discussion

SAXS experiments for the 0, 1, 3 and 5 wt% TSC samples were carried out to investigate the internal microstructure of the liquid crystalline phase as a function of salt concentration in the system.

On visual inspection the X-ray diffraction pattern for all the samples displays two reflections which appear to be in the 2:1 ratio of the corresponding distances, which is typical for one-dimensional lamellar phase. A crucial feature of the X-ray data is that the *d*-spacing for the 0, 1 and 3 wt% TSC samples are nearly identical but the *d*-spacing for the 5 wt% TSC sample is 7Å smaller than the electrolyte free system (see Table 5.2.1). This suggests that any changes occur in the system upon addition of salt are not affecting the *d*-spacing thus the macroscopic lamellar structure. However, above a certain level of electrolyte (5 wt% TSC) distinct differences occur. It seems reasonable that adding electrolyte would firstly disrupt the strong repulsive forces between the head groups and above a certain amount of salt would change the head group hydration level.

X-ray scattering measurements were carried out as a function of temperature with heat-cool cycles from 25 to 100°C and subsequently cooled back to 25°C. As expected, the X-ray results were dependent on temperature. Overall it can be said that as the temperature is increased there is a decrease in the *d*-spacing. However, at the higher temperatures the quantity of lamellar structure remaining was sufficient to produce a significant scattering pattern. This is also evidenced by the homogeneous alignment of the rings in the 2-D scattering images.

5.3 Deuterium Nuclear Magnetic Resonance (^{2}H NMR) Spectroscopy

5.3.1 Introduction

In this research as discussed in Section 4.2.5, the deuterium nucleus ^{2}H, with I=1 is used. The ^{2}H NMR spectra will exhibit a multiplet of $2I$ equally spaced peaks for each anisotropic phase present. Thus for the spectrum with a doublet and a central peak (see Figure 5.3.1) the doublet is formed from the anisotropic phase in the system, and the singlet is derived from isotropic media. The isotropic medium produces a narrow single peak in this case because the local domain is small enough to allow water molecules to experience different orientations with such rapidity (on the NMR timescale) that the doublet splitting will be averaged to zero, giving a central isotropic peak. Any isotropic media such as micellar solution in this study will make an additional contribution to the singlet.

When larger anisotropic domains are present the dynamics become slower and the quadrupole splitting appears. In this case the water molecules no longer sample all the orientations, so the quadrupole interaction is not averaged to zero. Such a unit cell corresponds to an almost randomly distributed lamellar phase spectrum (*i.e.* a deuterium 'powder' spectrum).
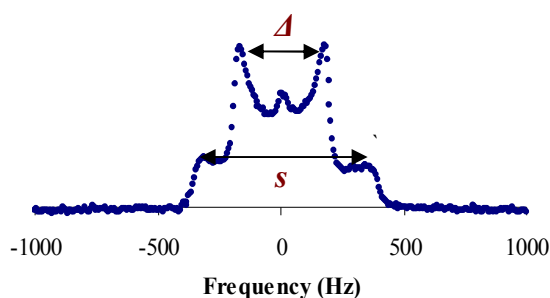
Figure 5.3.1: ^{2}H NMR spectrum with a quadrupole splitting Δ and the corresponding shoulders *s*. The small isotropic peak in the centre of the spectrum is evident the isotropic contribution to the NMR spectrum.

As mentioned above in anisotropic media such as randomly oriented lamellar mesophases, the quadrupole interaction of the deuterium nucleus with its surrounding electric field gradients, gives multiplet resonances ($2I$ peaks). The magnitude of the separation between

the adjacent resonance lines is termed the quadrupole splitting and its magnitude Δ for a 'powder' pattern is given by Equation 5.3.1.

$$\Delta = \frac{3}{2}\frac{eQV}{h} = \frac{3}{2}\frac{e^2qQ}{h}\frac{1}{2}\left(3\cos^2\Theta_0 - 1\right)$$ **Equation 5.3.1**

where Θ is the angle between the axis of the rotational symmetry and the magnetic field and e^2qQ/h is the quadrupole coupling constant E_Q.

A number of parameters are needed to interpret the NMR data. The main structure parameter is obtained from the observed quadrupole splitting Δ in terms of an order parameter S as shown in Equation 5.3.2. S is an order parameter describing time-averaged angle θ. The order parameter S is given by Equation 5.3.2.

$$S = \frac{1}{2}\left\langle 3\cos^2\theta - 1\right\rangle$$ **Equation 5.3.2**

where θ is the angle between the instantaneous direction of the electric field and the director of the liquid crystal (the long molecular axis of liquid crystalline samples).

The value of the quadrupole splitting can be used to differentiate between liquid crystalline phases. Furthermore, S is a time-averaged parameter thus any dynamical process occurs in a timescale shorter than $1/\Delta$, the value of the quadrupole splitting decreases and the spectrum line shape will turn into a broad single peak. The timescale of the residual quadrupole interaction depends on the interface curvature. A flat surface is the limiting case for infinitely slow dynamics. Since Δ depends on the director orientation, samples with a random distribution of director axes (so all values of θ contribute to the spectrum) give rise to characteristic powder 'Pake' spectra (see Section 4.2.5). However, a macroscopically aligned sample gives rise to a spectrum with a simple doublet of peaks with a splitting given by the fixed value of θ.

For our purposes, the changes in ^{2}H NMR line shape have been analysed to collect the information we are looking for. This is because the timescale of the residual quadrupole interaction, which determines the ^{2}H NMR line shape, ranges from a fast-motional regime

to the slow-motional regime depending on the curvature of the interface. Thus the ^{2}H NMR line shape is dependent on the microstructure of the mesophase and hence the sample composition.

5.3.2 Experimental details

For the ^{2}H NMR measurements, the samples (see Chapter 4 for sample preparation) were filled into NMR tubes of 10mm diameter. Care was taken that the samples did not contain any air bubbles. The tubes were initially sealed with an NMR tube cap and stored at room temperature for a day to ensure that all the material (surfactant/water/salt) was in the bottom of the tube.

For the NMR experiment is important to ensure that all the sample is within the RF coil of the NMR probe although as the probe is encased this cannot be seen. Previous work on the same ^{2}H NMR probe has shown that the optimum sample height is 8mm[14].

Typically 2048 scans were acquired for one spectrum, with relaxation delays of 0.4-0.5s between scans. Thus each NMR measurement took ca. 60mins. The number of data points acquired during measurements is 16384 and the spectra width is 100000Hz. For each series of experiments fresh samples were used by filling the sample into the same height and trying to minimize any shear histories arising from stresses during the filling procedure. Temperature controller was connected to the NMR spectrometer to control the temperature during the experimental run. The accuracy is estimated to be ±0.5°C.

^{2}H NMR experiments were conducted a day (sample is indicated as fresh), 1, 5 and 35 weeks after the sample preparation to investigate the effect of ageing on the NMR line shapes hence the microstructure of the lamellar mesophase. For these experiments the samples chosen were of concentrations of 0, 1, 2, 3, 4 and 5 wt% TSC in heavy water (^{2}H$_2$O).

Quadrupole splittings were obtained from the free induction decay (FID) following a signal averaging to improve the signal-to noise ratio. The results were then converted to a frequency-domain signal by a Fourier transformation.

5.3.3 Results

The dependence of the deuterium quadrupole splitting on the sample composition, sample age and temperature was investigated. Changes in the spectral line shape with sample composition, age and temperature have been utilised to monitor changes in the lamellar microstructure and curvature.

Firstly, we investigated the effect of surfactant concentration on the NMR line shape. The systems were prepared to have different weight ratios of amphiphile to aqueous (^2H_2O) solution. The amphiphile system was composed by 2/1/1 LAS/SLES/NI (surfactant system) (see Chapter 4). The compositions chosen were the 47, 50 and 53 wt% surfactant system to ^2H_2O. The spectra obtained are shown in Figure 5.3.2.

Well defined quadrupolar splitting patterns are evident for all 47, 50 and 53 wt% surfactant samples, with a characteristic well defined powder spectrum (Figure 5.3.2) from which can be taken the quadrupolar splitting Δ and the corresponding shoulders s. As can be seen the changes in amphiphile-to-water weight ratio were small however they influence the ^2H NMR line shape. The samples are thought to favour the planar configuration at room temperature. However, the spectrum recorded for the 47 wt% surfactant sample shows two contributions, an isotropic region exhibiting a single peak with no quadrupolar splitting and a liquid crystalline contribution which shows a quadrupolar splitting. The isotropic peak is believed to be a tiny amount of water not incorporated within the aggregate (*i.e.* in a different location). Previous work[15] has also suggested that the fast diffusion of water molecules in different 'crystallites' results to an additional averaging of the quadrupole splitting hence giving a single isotropic peak.
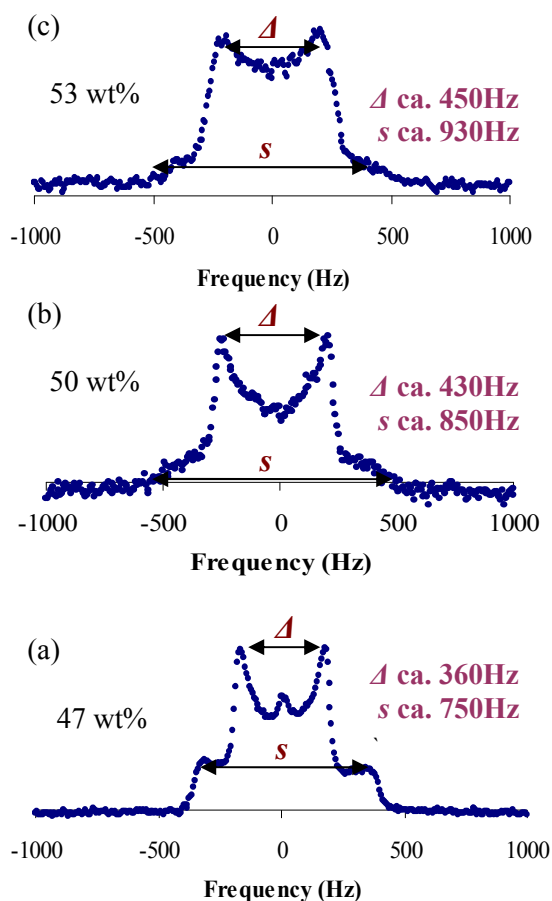
Figure 5.3.2: ^{2}H NMR spectra for varying wt% surfactant samples as labelled at 25°C. The compositions chosen were the 47, 50 and 53 wt% surfactant system to ^{2}H$_2$O (1day aged). The quadrupolar splitting Δ and the corresponding shoulders s are indicated.

As can be seen in Figure 5.3.2 the isotropic peak vanishes upon increasing the amount of surfactant in the system. Of equal import however, is the fact that the quadrupolar splittings behave uniformly upon surfactant loading in the system.

The composition selected for further investigation and to complete this study was the 53 wt% surfactant system to ^{2}H$_2$O.

The second factor is the effect of added electrolyte (TSC) in the system. The major observable change induced by the addition of electrolyte is a change in the appearance of the samples by eye, from a straw colour to a white colour. This might be due to a change in the state of the lamellar liquid crystalline phase from a planar state to a vesicular array. The most significant changes happened in the 3, 3.5, 4, 4.5 and 5 wt% TSC samples. Such a

141

change has in the past been related to a change from a planar configuration to vesicles under shear[16], and similar 'structuring' has been induced upon the addition of electrolytes in similar studies[17].

Changing the level of electrolyte also has an influence on the observed ^{2}H NMR line shape as shown in Figure 5.3.3. Quadrupole splittings with 'powder' phases (uniaxial) one dimensional periodicity were observed for the 0, 1 and 2 wt% TSC samples with no significant changes. The inner splitting of $\theta = 90°$, which corresponds to domains oriented perpendicular to the magnetic field, decreases ca. 80Hz upon addition of salt. However, the outer doublet decreases up to the addition of 2 wt% TSC indicating changes in the arrangement of the layers.

Upon further increase of salt level, a gradual transformation to a new line shape is observed. The spectrum obtained for the 2.5 wt% TSC sample is broader while, at the same time, its features become less distinct. The inner doublet vanishes and a broad single peak with a broader base appears (bell-like line shapes). The broad base observed for the 2.5 and 3 wt% TSC samples is not observed in the spectrum for the 3.5 wt% TSC sample. It has previously been suggested that the absence of shoulders may derived from a transition to an isotropically non-oriented liquid crystal array such as MLV's[18, 19].

The spectra obtained for the 3.5, 4 and 4.5 wt% TSC samples, show insignificant changes in the line-width-at-half-height. Slight changes on the line shape might be resulted by changes in the domain size and size polydispersity. The spectrum for the 5 wt% TSC sample displayed in Figure 5.3.3 shows evidence of both the isotropic peak and the beginning of the formation of a broad base peak. This line shape corresponds to a two-phase region of vesicles and excess of isotropic solution (aquatic electrolyte solution).
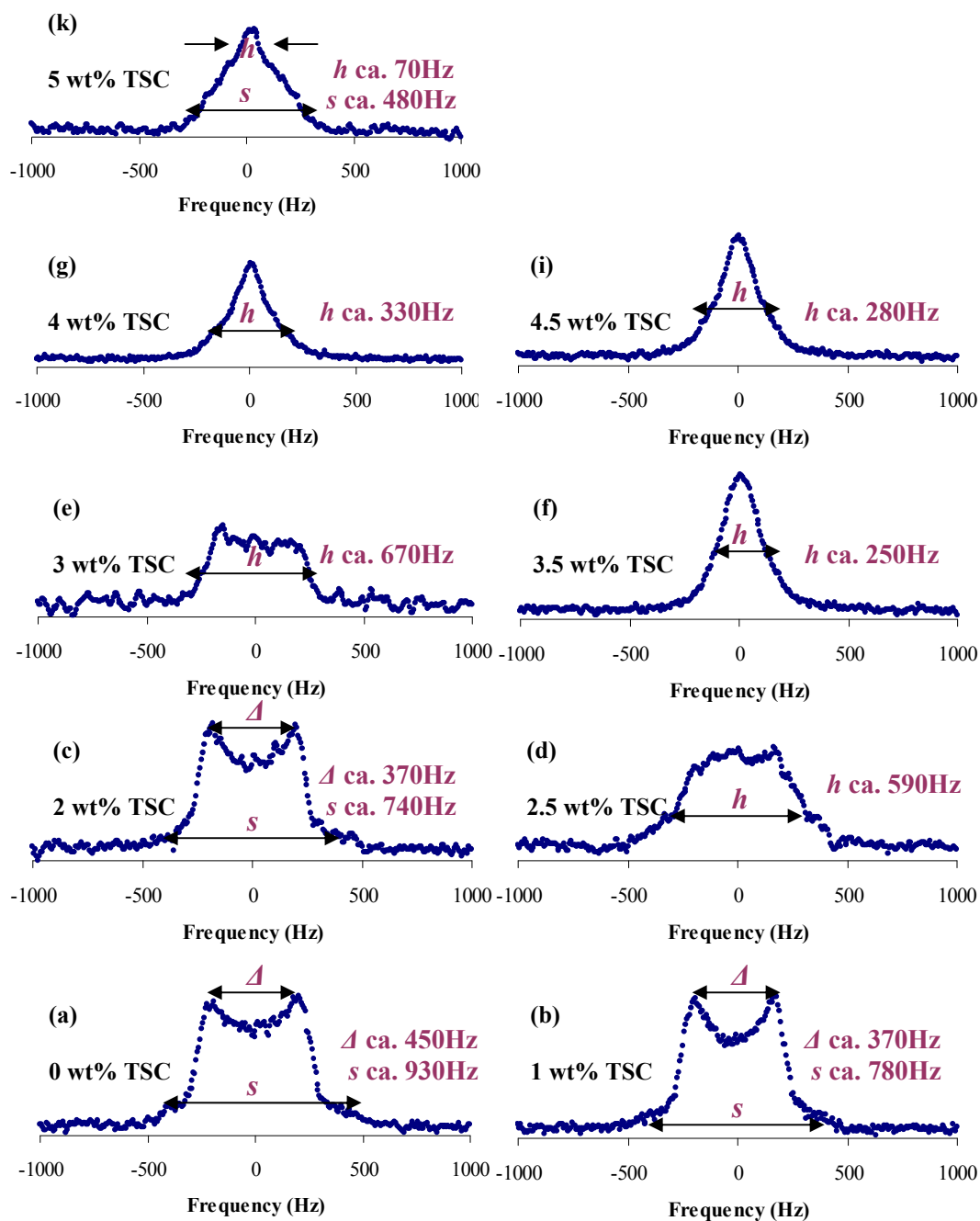
Figure 5.3.3: ^{2}H NMR spectra for varying wt% TSC as labelled at 25°C. The quadrupolar splitting $\varDelta$, the corresponding shoulders s and the width at half-height for isotropic regions h are indicated.

Another important factor investigated in this work is the temperature. The samples chosen for this investigation were the 0, 3 and 5 wt% TSC (1 day aged). Heat-cool cycles (25-50-25°C) have been completed every 5°C for all the samples. Care had to be taken to allow sufficient time (ca. 60mins) in order that the sample would reach thermal equilibrium

before the data were recorded at each temperature setting. A number of observations were made on the samples (see Figures 5.3.4a-c).

For the 0 wt% TSC sample, a small decrease in Δ is observed when the temperature is raised to 50°C (Figure 5.3.4a). When the temperature is dropped back to at ambient temperature insignificant changes are observed.

Figure 5.3.4a: Selected ^{2}H NMR spectra for the 0 wt% TSC sample (1day aged) subjected to a heat-cool experiment from 25 to 50°C and subsequently cooled back to 25°C (each 5°C equilibrated for ca. 60mins). The quadrupolar splitting Δ and the corresponding shoulders s are indicated.

Selected spectra for the 3 wt% TSC sample are shown in Figure 5.3.4b. The initial spectrum shows a broad peak with a weak quadrupolar splitting that vanishes when temperature is raised to 50°C. Upon heating to 50°C, a single broad isotropic peak presents with h at 240Hz. Similar spectra are shown for the sample after cooling to 25°C with h at 270Hz. The single peak formed after cooling does not alter significantly with time (NMR experimental scans were repeated after 2 days while the sample was left in the NMR probe). The line shape observed indicates that the motion of water molecules (the water motion to average the alignment around the bilayers) inside the lamellar liquid crystal upon heating is rapid, but not completely isotropic.
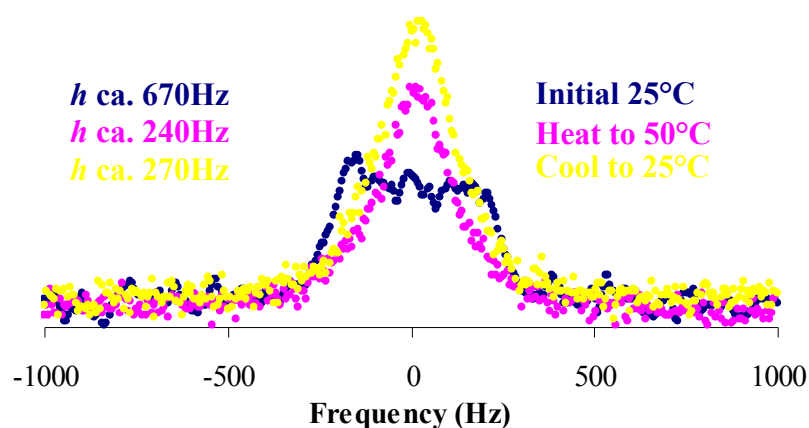
Figure 5.3.4b: Selected ^{2}H NMR spectra for the 3 wt% TSC sample (1day aged) subjected to a heat-cool experiment from 25 to 50°C and subsequently cooled back to 25°C (each 5°C equilibrated for ca. 60mins). The width at half-height for isotropic regions *h* is indicated.

For the 5 wt% TSC sample a bell-like line shape NMR spectrum was initially obtained at 25°C. This suggests the existence of a two-phase region (vesicles and an excess of aquatic electrolyte solution). Upon heating, a broader isotropic peak is observed (see Figure 5.3.4c).
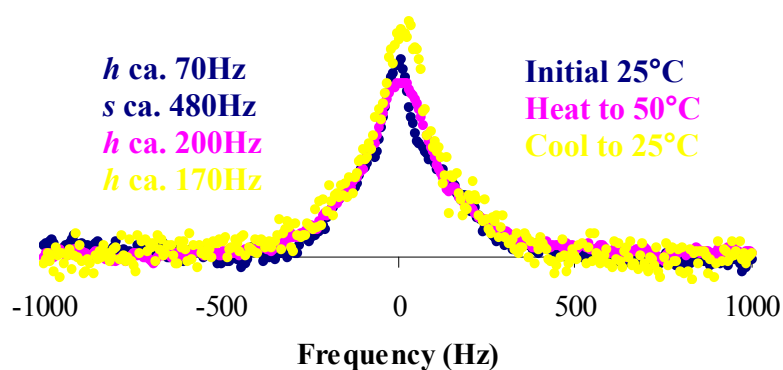
Figure 5.3.4c: Selected ^{2}H NMR spectra for the 5 wt% TSC sample (1day aged) subjected to a heat-cool experiment from 25 to 50°C and subsequently cooled back to 25°C (each 5°C equilibrated for ca. 60mins). The width at half-height for isotropic regions *h* is indicated.
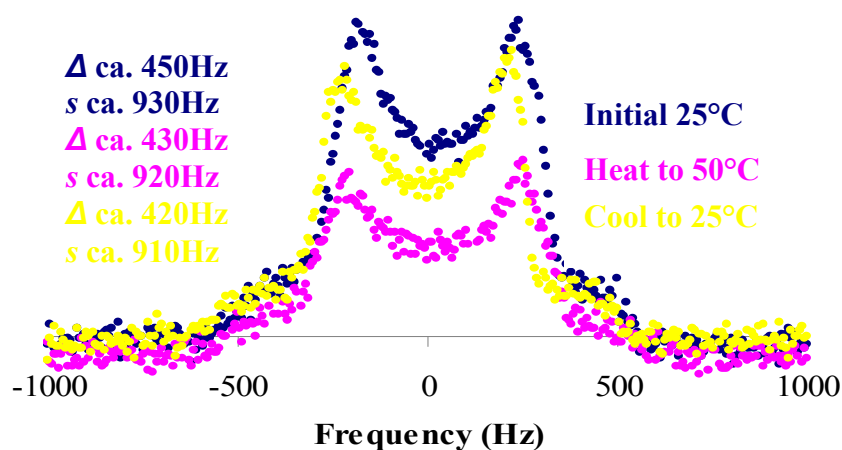
The quadrupolar spitting *Δ*, the corresponding shoulders width *s* and the width at half-height *h* as shown in Figures 5.3.4a-c for every surfactant sample and selected temperatures have been tabulated and shown in Table 5.3.1. As can be seen from Table 5.3.1 insignificant changes in the splittings are observed for the 0 wt% TSC sample with respect to temperature. A gradual decrease in *h* is observed when the 3 wt% TSC sample was heated to 50°C. However, insignificant changes are observed upon cooling back to 25°C. A noteworthy observation is that upon heating the bell-like line observed for the 5 wt% TSC sample changes to a single narrow line. Insignificant changes are observed in *h* upon further heating and cooling back to ambient temperature for the 5 wt% TSC sample.

Sample	Temperature/°C Upon Heating					
	25°C	30°C	35°C	40°C	45°C	50°C
0 wt% TSC	*Δ* ca. 450Hz *s* ca. 930Hz	*Δ* ca. 430Hz *s* ca. 900Hz	*Δ* ca. 430Hz *s* ca. 900Hz	*Δ* ca. 430Hz *s* ca. 900Hz	*Δ* ca. 420Hz *s* ca. 920Hz	*Δ* ca. 430Hz *s* ca. 920Hz
3 wt% TSC	*h* ca. 670Hz	*h* ca. 260Hz	*h* ca. 265Hz	*h* ca. 250Hz	*h* ca. 240Hz	*h* ca. 240Hz
5 wt% TSC	*h* ca. 70Hz *s* ca. 480Hz	*h* ca. 170Hz	*h* ca. 190Hz	*h* ca. 190Hz	*h* ca. 180Hz	*h* ca. 200Hz

Sample	Temperature/°C Upon Cooling					
	50°C	45°C	40°C	35°C	30°C	25°C
0 wt% TSC	*Δ* ca. 430Hz *s* ca. 920Hz	*Δ* ca. 420Hz *s* ca. 930Hz	*Δ* ca. 420Hz *s* ca. 920Hz	*Δ* ca. 420Hz *s* ca. 910Hz	*Δ* ca. 410Hz *s* ca. 900Hz	*Δ* ca. 420Hz *s* ca. 910Hz
3 wt% TSC	*h* ca. 200Hz	*h* ca. 240Hz	*h* ca. 240Hz	*h* ca. 220Hz	*h* ca. 240Hz	*h* ca. 270Hz
5 wt% TSC	*h* ca. 200Hz	*h* ca. 190Hz	*h* ca. 180Hz	*h* ca. 180Hz	*h* ca. 160Hz	*h* ca. 170Hz

Table 5.3.1: The quadrupolar splitting *Δ*, the corresponding shoulders *s*, and the line-width-at-half-height *h*, as a function of temperature for varying wt% TSC samples subjected to a heat-cool cycle (25-50-25°C). The samples (1 day aged) were allowed to equilibrate in spectrometer at 25°C overnight before cycle run with each temperature recorded (every 5°C) given an equilibrium time of ca. 60mins.

As this work is of particular relevance for industrial process it is important to investigate the effect of history (age and storage conditions) on the system microstructure. These studies have been completed regarding sample age over 5 and 35 weeks period. ^{2}H NMR measurements were performed for the 0, 1, 2, 3, 4 and 5 wt% TSC samples to monitor sample changes over time. Before discussion of the spectra it should be emphasised that only one sample of each composition has been loaded into the NMR tube and tested on varying dates. For all the samples the fresh (1 day aged) and the 5 weeks aged spectra are displayed in Figure 5.3.5. The spectra for the 5 and 35 weeks aged samples are displayed in Figure 5.3.6.
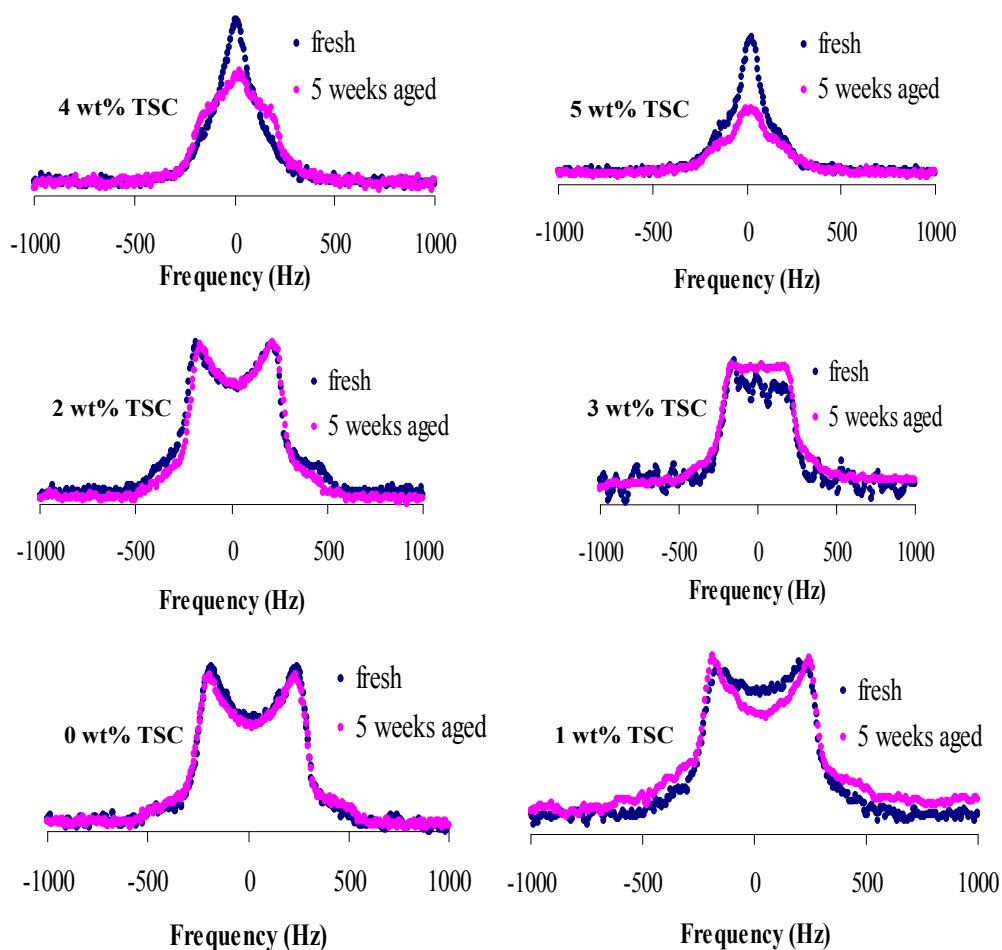
Figure 5.3.5: ^{2}H NMR spectra for all 0 to 5 wt% TSC surfactant samples recorded for the fresh (1day aged) and the five weeks aged samples at 25°C. The quadrupolar splitting Δ, the corresponding shoulders s and the width at half-height for isotropic regions h for every surfactant sample and age have been tabulated and plotted in Table 5.3.2.

As shown in Figure 5.3.5 well defined quadrupolar splitting patterns are evident for the 0, 1 and 2 wt% TSC samples with a characteristic powder spectrum from which can be taken the quadrupolar splitting Δ and the corresponding shoulders s. The 0, 1 and 2 wt% TSC samples clearly develop as the weeks progress with a better defined powder patterns after 5 weeks as is shown in Figure 5.3.5. Viewing Figure 5.3.5, it can be said that the structure of the 3 wt% TSC sample develops and the Δ splitting becomes less distinct as the sample ages. The ^{2}H NMR spectra recorded for the 4 and 5 wt% TSC samples show bell-like line shapes gradually develop into broader line shapes.
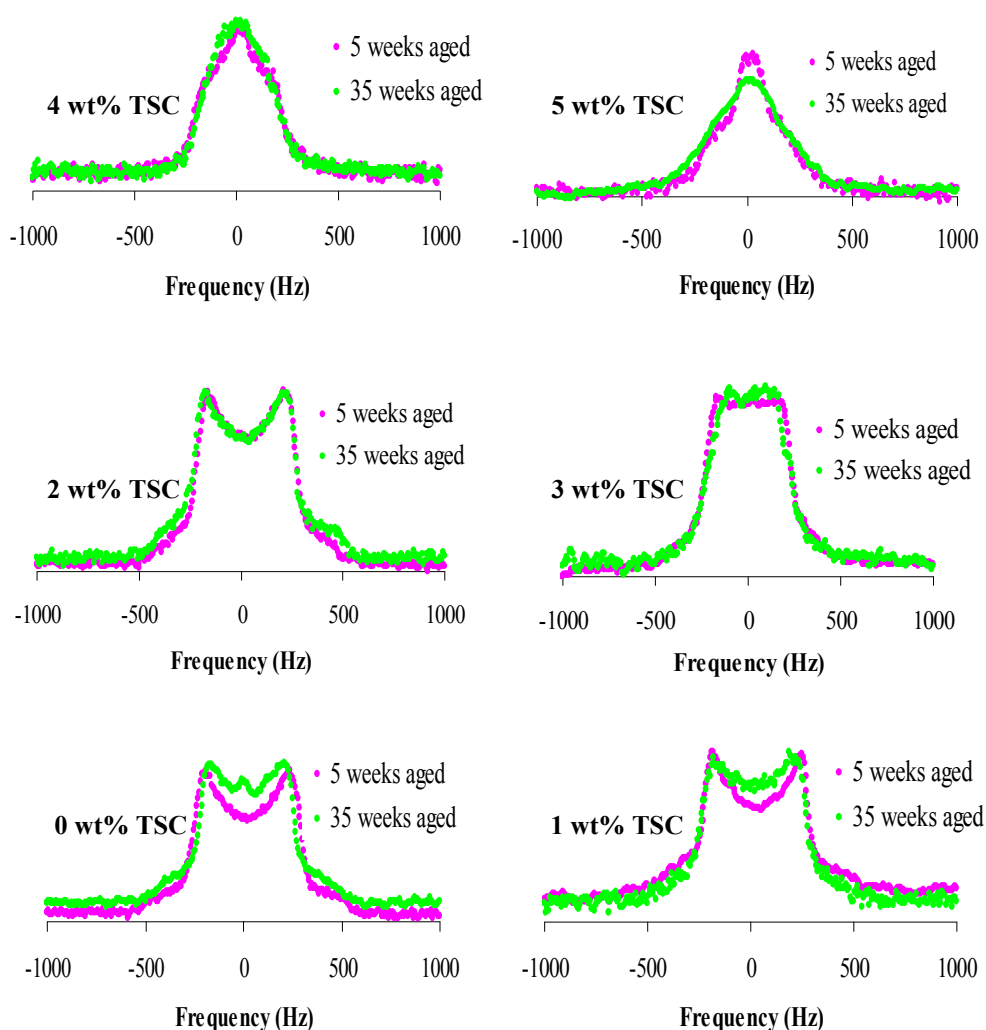
Figure 5.3.6: ^{2}H NMR spectra for all the samples range from 0 to 5 wt% TSC recorded after 5 and 35 weeks at 25°C. The quadrupolar splitting Δ, the corresponding shoulders s and the width at half-height for isotropic regions h for every surfactant sample and age have been tabulated and plotted (see Table 5.3.2).

The NMR data (see Table 5.3.2) suggest that the age and storage conditions appear to have little influence on the microstructure thus the NMR line shape. The quadrupolar spitting Δ, the corresponding shoulders width s and the width at half-height h as shown in Figures 5.3.5 and 5.3.6, for every surfactant sample and age have been tabulated and shown in Table 5.3.2.

wt% TSC	Obtained values (Hz)	Age of the sample (days)			
		1	7	35	245
0	h	-	-	-	-
	Δ	ca. 450	ca. 410	ca. 430	ca. 360
	s	ca. 930	ca. 890	ca. 870	ca. 750
1	h	-	-	-	-
	Δ	ca. 370	ca. 390	ca. 520	ca. 410
	s	ca. 780	ca. 820	ca. 950	ca. 830
2	h	-	-	-	-
	Δ	ca. 370	ca. 380	ca. 390	ca. 390
	s	ca. 740	ca. 750	ca. 780	ca. 870
3	h	ca. 670	-	ca.520	ca. 480
	Δ	-	-	-	-
	s	-	-	-	-
4	h	ca. 330	ca. 390	ca. 410	ca. 420
	Δ	-	-	-	-
	s	-	-	-	-
5	h	ca. 70	ca. 100	ca. 110	ca. 420
	s	ca. 480	ca. 460	ca. 430	-

Table 5.3.2: The quadrupolar splitting Δ values, the corresponding shoulders width s and the width at half-height h values at 25 °C for all the samples recorded over 35 weeks period were obtained from ^{2}H NMR spectra.

5.3.4 Discussion

Our goal in studying ^{2}H NMR quadrupole splittings of the lamellar phase formed by the surfactant system under investigation was to obtain information on the lamellar microstructure under various conditions. ^{2}H NMR offers a powerful tool for identification

of the phase transitions that occur as a function of composition, temperature and sample history.

For this study, the changes in ^{2}H NMR line shapes have been discussed in order to interpret the NMR observables such as the quadrupolar splitting Δ and the NMR line shape in a consistent way. The recurring argument when considering the morphology of the lamellar microstructure is the question surrounding whether the system is in planar state or a vesicular state. The use of splitting parameters to obtain information on lamellar microstructure is based on the assumption that the water binding to the aggregate surfaces is so affected by aggregate shape and composition variation of the phases that this considerably affects the quadrupolar splitting.

From the NMR data composition does appear to be an important driving force for the 'structuring' of the lamellar phase. Firstly, the effect of surfactant concentration on the NMR line shape has been investigated. There is no doubt that in systems shown in Figure 5.3.2 even small change in amphiphile-to-water weight ratio can influence the spectral line shape. As shown in Figure 5.3.2 all systems are thought to favour the planar configuration. An important observation is that the quadrupolar splitting behaves uniformly upon surfactant loading in the system. The 47 wt% surfactant sample is thought to favour the planar configuration with the co-existence of an isotropic phase indicative by the single peak.

The second factor investigated was the effect of added electrolyte. Our results reveal that changing the level of electrolyte has an influence on the microstructure of the lamellar phase. From the spectra obtained, it can be clearly seen that the change from a planar lamellar phase to highly curved phase is accompanied by a significant change in the ^{2}H NMR line shape. Well defined quadrupolar splitting patterns are evident for all 0, 1 and 2 wt% TSC samples (see Figure 5.3.3) with characteristic well defined powder spectra. These 'Pake' spectra are attributed to a lamellar phase with large domains which have random orientation. This may explain the fact that from a macroscopic point of view the microstructure looks irregular and with structural defects (Maltese crosses and oily streaks when viewed under polarising microscope). The ^{2}H NMR line shapes obtained for the 0, 1 and 2 wt% TSC samples are very similar with no significant changes in the splitting of $\theta =$

90°, which corresponds to domains oriented perpendicular to B_o. This is strong evidence that there is no significant structural modification in the lamellar microstructure by changing the level of the electrolyte in the system up to 2 wt%. However, the outer doublet begins to disappear suggesting that a reduction in the domain size occurred.

At significant electrolyte level the system exhibits some surprising behaviour, particularly deviations from the behaviour exhibited by the electrolyte free system. The ^{2}H NMR spectrum recorded for the 2.5 wt% TSC sample shows a gradual transformation to a new line shape (see Figure 5.3.3). The spectrum is broader while, at the same time, its features become less distinct. The inner doublet vanishes and a broad single peak with a broader base appears (bell-like line shape). However, the broad base observed for the 2.5 and the 3 wt% TSC samples is not observed in the spectrum recorded for the 3.5 wt% TSC sample. This might be attributed to the formation of a fully developed structure of close-packed vesicles caused by the addition of electrolyte at a significant level.

As can be seen from the spectra obtained for the 3.5, 4 and 4.5 wt% TSC samples (Figure 5.3.3) insignificant changes in the line-width-at-half-height are observed. Slight changes in the line shape might be resulted by changes in the domain size. However, the spectrum recorded for the 5 wt% TSC sample shows evidence of both the isotropic peak and the beginning of the formation of a broad base peak. This line shape corresponds to a two-phase region one consisted of vesicles and one consisted of excess of aquatic electrolyte solution.

Overall, our results show that composition does affect the NMR spectral line shape as well as the splittings. The changes in the microstructure can be explained in terms of a continuous transition to a stronger interface curvature followed by a separation of the spectrum into different components (vesicles and excess micellar solution).

Of equal import to composition effect is the effect of domain size. Our results suggest that the ^{2}H NMR line shape is not affected only by the composition of the system but also the domain size has an effect on it. If the domain size is small then diffusion of water molecules between domains of different orientation takes place during the measurement. As a result the quadrupole splitting decreases or even a vanishing of the splitting is

observed. Previous work[15] has also suggested that the fast diffusion of water molecules in different 'crystallites' leads to an averaging of Δ thus giving an isotropic signal.

The explanation put forward for this transition has to do with the salting out behaviour of the electrolyte (TSC) and the availability of water. The salting out behaviour is thought to be caused by electrolyte being less soluble in head group region. In previous studies head group interactions have been proposed as an important contributor to changes in the phase behaviour[16, 25]. When electrolyte is added to the system probably due to head group interactions, is less soluble so the surfactant activity increases. This in turn will increase the degree of phase separation between an electrolyte rich and surfactant rich region in order to maintain equality of the chemical potential.

Another possible explanation for the transformation to the new line shape is that the addition of the electrolyte might be resulted to the stabilisation of the defects present in the structure and thus the structure looks smaller in one dimension. However, this is less favourable. It has previously been suggested that the loss of definition in the ^{2}H NMR line shape may be derived from a transition to an isotropically non-oriented liquid crystal array such as MLV and is similar to the impact of shear[19, 23]. Hence, the broad peak can be assigned to the state of strong curved interface that might be the state of large close-packed vesicles. Combined with the results obtained from optical microscopy and SAXS it can be assumed that the size of the vesicles is restricted by the curvature of the bilayers.

In this work, Professor Westlund, P. O applied a model[26] to our system in order to demonstrate how the calculated heavy water line shapes change with the curvature of the hydrated interface and thus the composition of the system. As mentioned before the ^{2}H NMR line shape of an isotropic phase refers to fast isotropic modulations, and corresponds to a narrow isotropic signal. On the other hand, a curved (or randomly distributed) lamellar phase displays a ^{2}H NMR powder spectrum with a characteristic quadrupole splitting.

The aim of this model is to demonstrate that a ^{2}H NMR line shape analysis is a valuable approach which improves the molecular picture of lipid hydration. The lipid hydration of different phases may thus be described with respect to local ordering of hydrated water. The local order and dynamics of the bound water are, however changing between different interfaces. This indicates that local interactions of water with the head group are much

dependent on the actual phase composition. A simple calculation where the modulation of the quadrupole interaction is assumed along the normal of the aggregate interface is presented in Appendix II. It can be concluded that as the aggregate interface get more and more curved the modulation of the partial averaged quadrupole interaction of the bilayer interface goes from the 'Pake powder' pattern to an isotropic signal. This suggests that sufficient fast rotational diffusion of water molecules takes place in the NMR time scale and thus corresponds to small enough curved domains where the water molecules exchange fast around the curved interfaces.

The effects of temperature as well as the history effect were also investigated. As it can be seen in Figure 5.3.4a the spectral line shape remains unchanged with increasing temperature for the 0 wt% TSC sample. Insignificant changes have been recorded. Considerations, of ^{2}H NMR line shape and estimates of the splittings as well as the X-ray data indicate the insignificance of temperature effect on the electrolyte free system. However, for the 3 wt% TSC sample marked differences in h can be seen (see Table 5.3.1). The decrease in h observed at high temperatures probably reflects a decrease in the domain size or a decrease in the density of defects. Clearly for the 5 wt% TSC samples there is a little change in h with respect to temperature. It is noteworthy that the presence of a two-phase region which was indicated by the spectral line shape, observed for the 5 wt% TSC sample at ambient temperature, is not obtained when the temperature dropped back to 25°C after heating. The broad isotropic peak is retained on cooling and does not alter significantly with time.

The effect of history (age and storage conditions) appears to have little influence on the ^{2}H NMR line shape. Previous studies[27] report that the orientations of the domains and their size have an effect on the ^{2}H NMR line shape. Viewing both spectra shown in Figures 5.3.5 and 5.3.6 it is evident that the domain size slightly increases as the samples age. However, the line shapes for the 4 and 5wt% TSC samples indicate that the domains are remaining small enough such that diffusion of water between them takes place during the measurement.

5.4 Summary

Both optical microscopy and SAXS investigations reported in here give clear evidence of the existence of the lamellar phase in the systems in question. Our results reveal that the lamellar phase microstructure depending on the salt level may form a single layered lamellar or a lamellar dispersion.

The sensitivity of NMR spectral line shape to phase transitions was used for the investigation of the effect of sample composition, age and temperature on the lamellar microstructure. Using this technique, we showed that the transition from planar layered lamellar to liposomes is accompanied by significant change in the NMR spectral line shape. NMR spectroscopy also identified the onset to a more curved lamellar phase and a lamellar dispersion phase upon addition of electrolyte to the system.

Our results reveal that the effect of history (age and storage conditions) appears to have little influence on the lamellar structure. However, although the optical micrographs have displayed texture variety throughout the time period of investigation this does not sufficiently alter the appearance of the NMR spectrum. Thus an indication that the structure became better developed but with insignificant changes in the domain size.

Coupling these experimental techniques provides evidence that the electrolyte free system consisting of a single continuous lamellar phase with flexible bilayers and random orientation. Upon addition of salt changes in the microstructure can be explained in terms of a continuous transition to a lamellar microstructure with stronger interface curvature followed by a two-phase lamellar dispersion consisting of vesicles and excess micellar solution.

5.5 References

1.   Hartshorne, N. H., *The microscopy of liquid crystals*. Microscope Publications: London, 1974; Vol. 48.

2.   Winsor, P. A., Binary and multicomponent solutions of amphiphilic compounds. Solubilisation and the formation, structure, and theoretical significance of liquid crystalline solutions. *Chemical Reviews* **1968,** 68, (1), 1-40.

3.   Diat, O., Roux, D., Nallet, F., Effect of shear on a lyotropic lamellar phase *Journal de Physique II* **1993,** 3, (9), 1427.

4.   Dimitrova, G. T., Tadros, T. F., Luckham, P. F., Investigations of the Phase Changes of Nonionic Surfactants Using Microscopy, Differential Scanning Calorimetry and Rheology. 1. Synperonic A7, a C13/C15 Alcohol with 7 mol of Ethylene Oxide. *Langmuir* **1995,** 11, 1101-1111.

5.   Dimitrova, G. T., Tadros, T. F., Luckham, P. F., Kipps, M. R., Investigations into the Phase Behavior of Nonionic Ethoxylated Surfactants Using 2H NMR Spectroscopy. *Langmuir* **1996,** 12, 315-318.

6.   Candau, F., Ballet, F., Debeauvais, F., Wittmann, J., Structural Properties and Topological Defects of Swollen Polymeric Mesophases: Low Angle X-Ray Diffraction and Optical Microscopic Studies. *Journal of Colloid and Interface Science* **1982,** 87, (2), 356-374.

7.   Gallegos, C., Nieto, M., Nieto, C., Muñoz, J., Influence of surfactant concentration on the time-dependent rheological behavior of the lamellar liquid crystal *Progress in Colloid and Polymer Science* **1991,** 84, 236-240.

8.   Penfold, J., Staples, E., Lodhi, A. K., Tucker, I., Tiddy, G. J. T., Shear-Induced Transformations in the Lamellar Phase of Hexaethylene Glycol Monohexadecyl Ether. *Journal of physical chemistry* **1997,** 101, (1), 66-72.

9.   Alcantara, M., Vanin, J., Rheological properties of lyotropic liquid crystals. *Colloids and Surfaces A: Physicochemical and Engineering Aspects* **1995,** 97, 151-156.

10.   Valiente, M., Influence of a cationic surfactant on the phase behavior of C12E4/hexanol/water system at low surfactant concentration. *Colloids and Surfaces A: Physicochemical and Engineering Aspects* **1995,** 105, 265-275.

11.   Horanyi, T., Halasz, L., Palinkas, J., Nemeth, Z., Relationship between optical and rheological properies of polymer-added lamellar liquid-crystalline systems. *Langmuir* **2004,** 20, 1639-1646.

12.   Macdonald, P. M., 2H NMR and polyelectrolyte–surfactant interactions: from micelles to monolayers to membranes. *Colloids and Surfaces A: Physicochemical and Engineering Aspects* **1999,** 147, (1-2), 115-131.

13.   Chidichimo, G., Vaz, N. A. P., Yaniv, Z., Doane, J. W., Investigation of the Ribbon Structure of a Lyotropic Liquid Crystal by Deuterium Nuclear Magnetic Resonance. *Physical Review Letters* **1982,** 49, (26), 1950-1954.

14.   Dutton, H. M. The behaviour of surfactant lamellar and gel phases under flow. The University of Manchester, Manchester, 2007.

15.   Lindblom, G., Lindman, B., Tiddy, G. J. T. , Ion binding studied using quadrupole splittings of sodium-23(1+) ions in lyotropic liquid crystals. The dependence on surfactant type. *Journal of the American Chemical Society* **1978,** 100, (8), 2299-2303.

16.   Sein, A., Engberts, J. B. F. N., Micelle to Lamellar Aggregate Transition of an anionic surfactant in dilute aqueous solution induced by alkali-metal chloride and tetraalkyl ammonium chloride salts. *Langmuir* **1995,** 11, 455-465.

17.   Sein, A., Engberts, J. B. F. N., Van der Linden, E., Van de Pas, J. C., Lyotropic phases of dodecylbenzenesulfonates with different counterions in water. *Langmuir* **1996,** 12, 2913-2923.

18.   Heaton, N. J., Althoff, G., Kothe, G., Observation of lateral diffusion in biomembranes by excitation transfer P-31 NMR: Estimetion of vesicle size distributores. *Journal of physical chemistry* **1996,** 10, 4944-4953.

19.   Blum, F. D., Franses, E. I., Rose, K. D., Bryant, R. G., Miller, W. G., Structure and Dynamics in Lamellar Liquid Crystals. Effect of Agitation and Aging on Deuterium NMR Line Shapes. *Langmuir* **1987,** 3, (4), 448-452.

20.   Rendall, K., Tiddy. G. J. T., Interaction of water and oxyethylene groups in lyotropic liquid-crystalline phases of poly(oxyethylene) n-dodecyl ether surfactants studied by 2H nuclear magnetic resonance spectroscopy. *Journal of the Chemical Society, Faraday Transactions 1: Physical Chemistry in Condensed Phases* **1984,** 80, 3339 - 3357.

21.   Fischer, P., Schmidt, C., Finkelmann, H., Amphiphilic liquid-crystalline networks - phase behavior and alignment by mechanical fields. *Macromolecular rapid communication* **1995,** 16, (6), 435-447.

22.   Medronho, B., Shafaei, S., Szopko, R., Miguel, M. G., Olsson, U., Schimdt, C., Shear induced transitions between a planar lamellar pahse and multilamellar vesicles: Continuous versus discontinuous transformation. *Langmuir* **2008,** 24, 6480-6486.

23.   Heaton, N. J., Althoff, G., Kothe, G., Observation of Lateral Diffusion in Biomembranes by Excitation Transfer 31P NMR: Estimation of Vesicle Size Distributions. *Journal of physical chemistry* **1996,** 100, 4944-4953.

24.   Auguste, F., Douliez, J. P., Bellocq, A. M., Dufourc, E. J., Gulik-Krzywicki, T., Evidence for Multilamellar Vesicles in the Lamellar Phase of an Electrostatic Lyotropic Ternary System. A Solid State 2H-NMR and Freeze Fracture Electron Microscopy Study. *Langmuir* **1997,** 13, 666-672.

25.   Ockelford, J., Timimi, B. A., Narayaki, K. S., Tiddy, G. J. T., An upper critical - point in Lamellar Liquid Crystalline phase. *Journal of physical chemistry* **1993,** 97, (1993), 6767-6769.

26.   Westlund, P. O., Line shape Analysis of NMR Powder Spectra of 2H2O in Lipid Bilayer Systems. *Journal of Physical chemistry B* **2000,** 104, 6059-6064.

27.   Müller, S., Börschig, C., Gronski, W., Schmidt, C., Roux, D, Shear-Induced States of Orientation of the Lamellar Phase of C12E4/Water. *Langmuir* **1999,** 15, 7558-7564.

Chapter 6

Characterisation of the mixed surfactant system during and after the application of shear

Shear can be applied to any system and if sufficiently high will cause the sample to flow. It is important for this work to recognise that a sample may flow due to extensional forces and shear. Studies on the influence of shear on lyotropic lamellar phases have revealed many interesting results such as the transition from parallel to perpendicular orientation when changing the shear rate, the formation of liposomes *etc* [1, 2].

A comprehensive summary of studies on the rheological behaviour and the optical properties of lamellar systems is given by Chen *et al* [3, 4]. According to other authors [5-8], the lamellar becomes more ordered by shear flow. Diat and co-workers [1] have found that shear induced the formation of MLVs in a defective lamellar phases. The size of these vesicles is controlled by the shear rate [9]. The effects of shear flow are summarised in a so-called shear diagram suggested by Diat *et al* [1].

The following Sections will be structured according to the different techniques used to investigate the transition from planar lamellar phase to MLVs. The shear induced transitions were studied by the Linkam Optical Shear Cell, AT Rheometer and by ^{2}H Rheo-NMR, as a function of the composition, the age and the shear rates applied into the samples. Samples chosen were those containing 0, 3 and 5 wt% TSC in ^2H_2O.

6.1 Linkam CSS-450 Optical Shear Cell

6.1.1 Experimental Details

Throughout this work a Linkam CSS-450 shear cell was used in order to carry out rheological experiments under the light microscope. Shear has been applied onto the sample by a stepper motor that drives the bottom window of the shearing cell (see Figure 4.2.3). A parallel plate arrangement, with a static and a rotating disc was used. The discs

are made of transparent material, so as to allow the passage of light (see Figure 4.2.3). The sample is placed between two windows that are in close thermal contact with silver heaters.

All experiments performed have been under steady shear mode with the gap setting of the shear cell at 200μm and the temperature controlled at 25°C. Throughout this work the shear cell rotates clockwise. However it should be noted that as this is a parallel-plate arrangement there are varying shear rates across between the plates (maximum shear at the edge, minimum at the centre). The viewing of the sample is through the aperture hole in the top plate so only a small proportion of the sample is seen.

The samples selected for shear characterisation are the 0, 3 and 5 wt% TSC samples (5 months aged). All the samples were prepared as described in Section 4.1.2. Two different experimental set-ups were performed in order to characterise the phase behaviour immediately after shearing is stopped and while shearing the sample.

In all experiments the shear rate ranges from 1 to $200s^{-1}$. Each shear rate was applied to the sample for 5mins to observe the differences between the optical micrographs taken for the resting sample and that taken immediately after shearing is stopped or during shearing in relation to the alignment of the lamellar layers and the possible formation of liposomes.

6.1.2 Results

Shown in Figure 6.1.1 are the optical micrographs obtained for the 0 wt% TSC sample immediately after shearing is stopped. At rest (prior to shear) and at low shear rate up to $1s^{-1}$ a long range texture is present with Maltese crosses which are indicative of defects. The dark bands correspond to homeotropic regions and thus indicate the variation of the optical director with respect to the direction of flow.
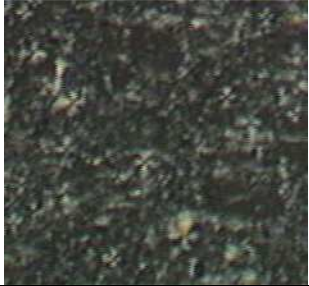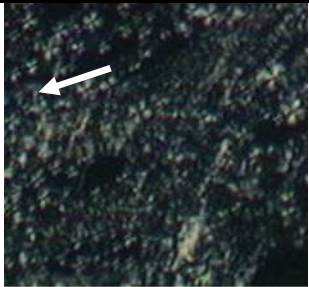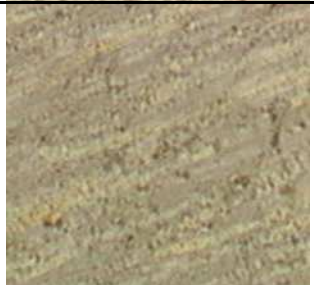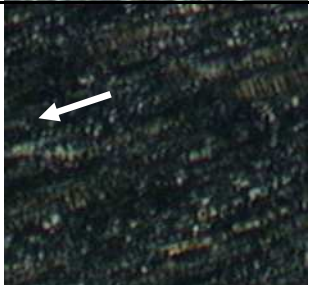
Shear rate/ (s^{-1})	Uncrossed polars	Crossed polars
0s^{-1}		
1s^{-1}		
10s^{-1}		
100s^{-1}		
200s^{-1}		

Figure 6.1.1: Optical micrographs for the 0 wt% TSC sample (5 months aged) immediately after shearing is stopped at 25°C. Each shear rate was applied to the sample for 5mins. The arrow indicates the direction of flow and the scale bar represents 100μm.

As the shear rate increases ($10s^{-1}$) the alignment of the sample is more evident with less Maltese crosses suggesting that defects are reduced. At higher shear rates ($> 100s^{-1}$) the layers whip around with the director perpendicular to the flow. In the texture parallel bands can be seen pointing along the shear direction. At highest shear rates shown here ($200s^{-1}$) the diameter of these bands gets smaller thus the sample no longer shows birefringence. The optical micrographs shown at left hand site show the polarisers uncrossed demonstrating the presence of material under the microscope.

Selected optical micrographs for the 3 wt% TSC sample (5 months aged) are shown in Figure 6.1.2 below. At rest (prior to shear) a characteristic mosaic texture is observed with no sign of structure. Spherical air bubbles and birefringent domains suggest the existence of a lamellar liquid crystalline phase. As the shear rate is increased to $1s^{-1}$ the sample flows to the direction of shear and more birefringent particles are present, indicating the presence of defects in the structure or even the presence of highly curved domains.

At higher shear rate ($10s^{-1}$) the spherical air bubbles observed become elongated in the flow direction underlining changes in the lamellar phase. As the shear rate is increased air bubbles become smaller and ellipsoidal. Additionally, at the highest shear rates shown here (100 and $200s^{-1}$) the sample no longer shows birefringence. This is because at the highest shear rates the domain size becomes so small that it is no longer possible to observe the domain's birefringence.

Figure 6.1.2: Optical micrographs for the 3 wt% TSC sample (5 months aged) immediately after shearing is stopped at 25°C. Each shear rate was applied to the sample for 5mins. The arrow indicates the direction of flow and the scale bar represents 100μm.

161

The 5 wt% TSC sample exhibited similar behaviour. The optical micrographs obtained for the 5 wt% TSC sample when shearing is stopped are shown in Figure 6.1.3. At rest (prior to shear) a long range texture is present with different coloured bands indicate the present of a lamellar dispersion. These bands indicate the variation of the optical director within the sample. As the shear rate is increased ($1s^{-1}$) the sample starts to move without any significant evidence of alignment. The coloured bands decrease in width and a uniform mosaic texture is present.

At higher shear rates ($10s^{-1}$) light and dark coloured bands are present with air bubbles in the flow direction. At highest shear rates ($> 100s^{-1}$) it is probable that the domain size becomes so small that is no longer possible to resolve the system birefringence. The sample director is thought to be aligned along the flow direction and thus appearing isotropic. The sample is observed under polarisers slightly uncrossed demonstrating the presence of material.

Shear rate/ (s^{-1})	Uncrossed polars	Crossed polars
$0s^{-1}$		
$1s^{-1}$		
$10s^{-1}$		
$100s^{-1}$		
$200s^{-1}$		

Figure 6.1.3: Optical micrographs for the 5 wt% TSC sample (aged 5 months) immediately after shearing is stopped at 25°C. Each shear rate was applied to the sample for 5mins. The arrow indicates the direction of flow and the scale bar represents 100μm.

All samples selected exhibited similar behaviour while viewing under shear. Optical micrographs taken using a CCD camera with a shutter speed of 15-25 frames/s. Samples were controlled at 25ºC and exerted to shear rates from 1 to 200s^{-1}. Each shear rate was applied to the sample for 5mins. Selected optical micrographs of reasonable quality are displayed in the following figures (Figure 6.1.4-6).

Viewing the optical micrographs for the 0 wt% TSC sample shown in Figure 6.1.4 it can be seen that prior to shear and at very low shear rate (1s^{-1}) the sample is stable and a mosaic texture with Maltese crosses is present suggesting defects in the structure. The oily streaks indicate the variation of the optical director with respect to the direction of shear flow[10] and the optically extinct bands has been noted by others[11]. At higher shear rates (50 and 100s^{-1}) dark and light bands are pushed together and merge. At highest shear rates shown here (150 and 200s^{-1}) a layered texture can be seen.

Shear rate/ (s^{-1})	Crossed polars	Shear rate/ (s^{-1})	Crossed polars
$0s^{-1}$		$50s^{-1}$	
$1s^{-1}$		$100s^{-1}$	
$5s^{-1}$		$150s^{-1}$	
$10s^{-1}$		$200s^{-1}$	

Figure 6.1.4: Optical micrographs for the 0 wt% TSC sample taken while shearing at 25ºC. Each shear rate was applied to the sample for 5mins. The arrow indicates the direction of flow and the scale bar represents 100μm.

Shown in Figure 6.1.5 are the optical micrographs taken for the 3 wt% TSC sample. At rest a characteristic mosaic texture of non-oriented lamellar phase is observed. Increasing the shear rate to $1s^{-1}$ introduces large birefringent domains and no characteristic texture can be seen. Similar textures are observed when comparing 5 and $10s^{-1}$.

Increasing further to $50s^{-1}$ the texture becomes more ordered to the direction of flow. Light and dark bands indicate the variation of the optical director with respect to the direction of

shear flow. At highest shear rates shown here (150 and 200s^{-1}) the domain size becomes so small that is no longer possible to resolve the systems birefringence.

Shear rate/ (s^{-1})	Crossed polars	Shear rate/ (s^{-1})	Crossed polars
0s^{-1}		50s^{-1}	
1s^{-1}		100s^{-1}	
5s^{-1}		150s^{-1}	
10s^{-1}		200s^{-1}	

Figure 6.1.5: Optical micrographs for the 3 wt% TSC sample taken while shearing at 25ºC. Each shear rate was applied to the sample for 5mins. The arrow indicates the direction of flow and the scale bar represents 100μm.

The optical micrographs taken for the 5 wt% TSC sample are displayed in Figure 6.1.6. At rest and at very low shear rates (< 5s^{-1}) a mosaic texture with coloured bands is observed. The coloured bands indicate the present of a lamellar dispersion. Increasing the shear rate

to 10s^{-1} the sample moves to the direction of flow. Similar behaviour is observed at 50s^{-1}. Further increase to the highest shear rates observed here (100-200s^{-1}) no characteristic texture is seen.

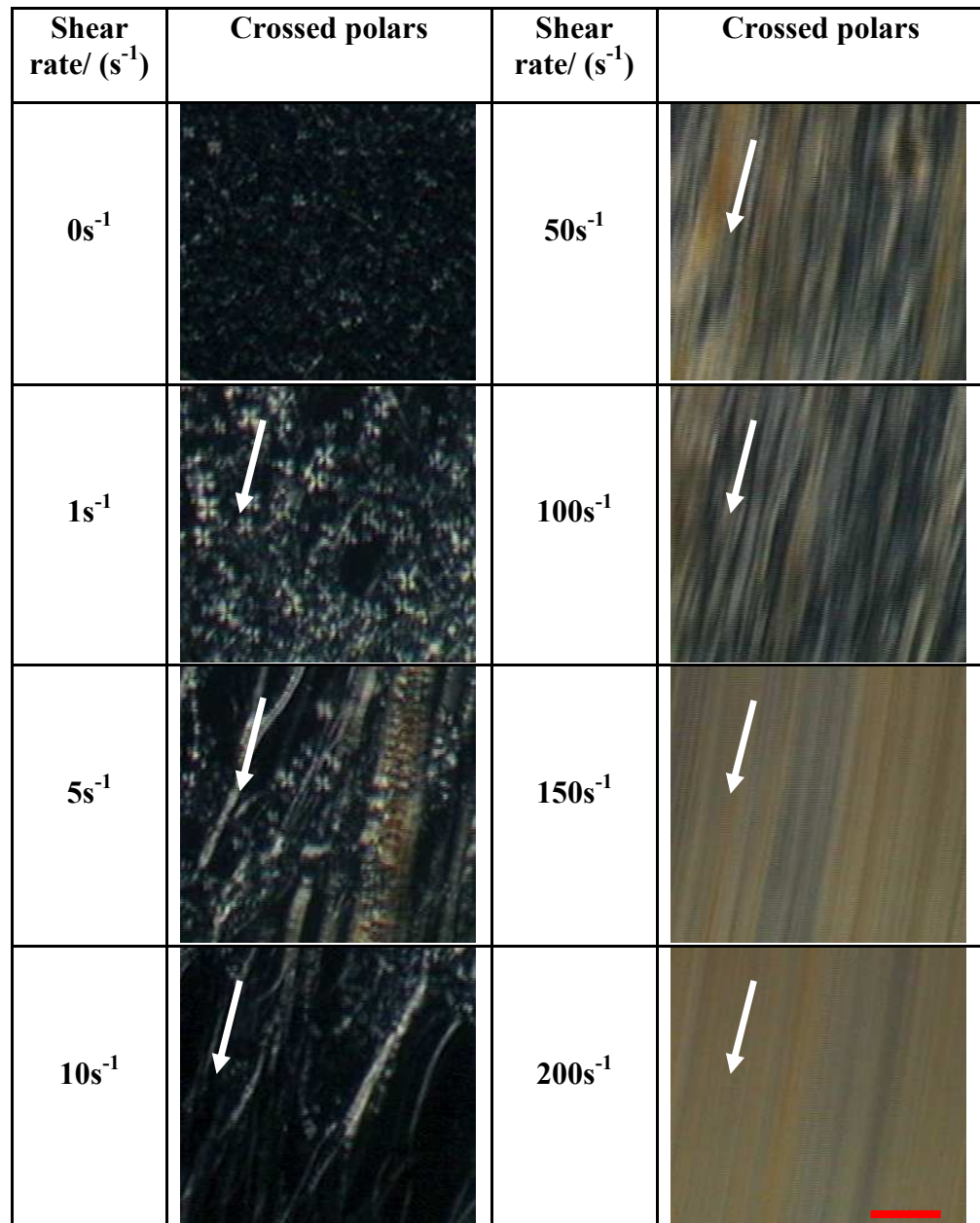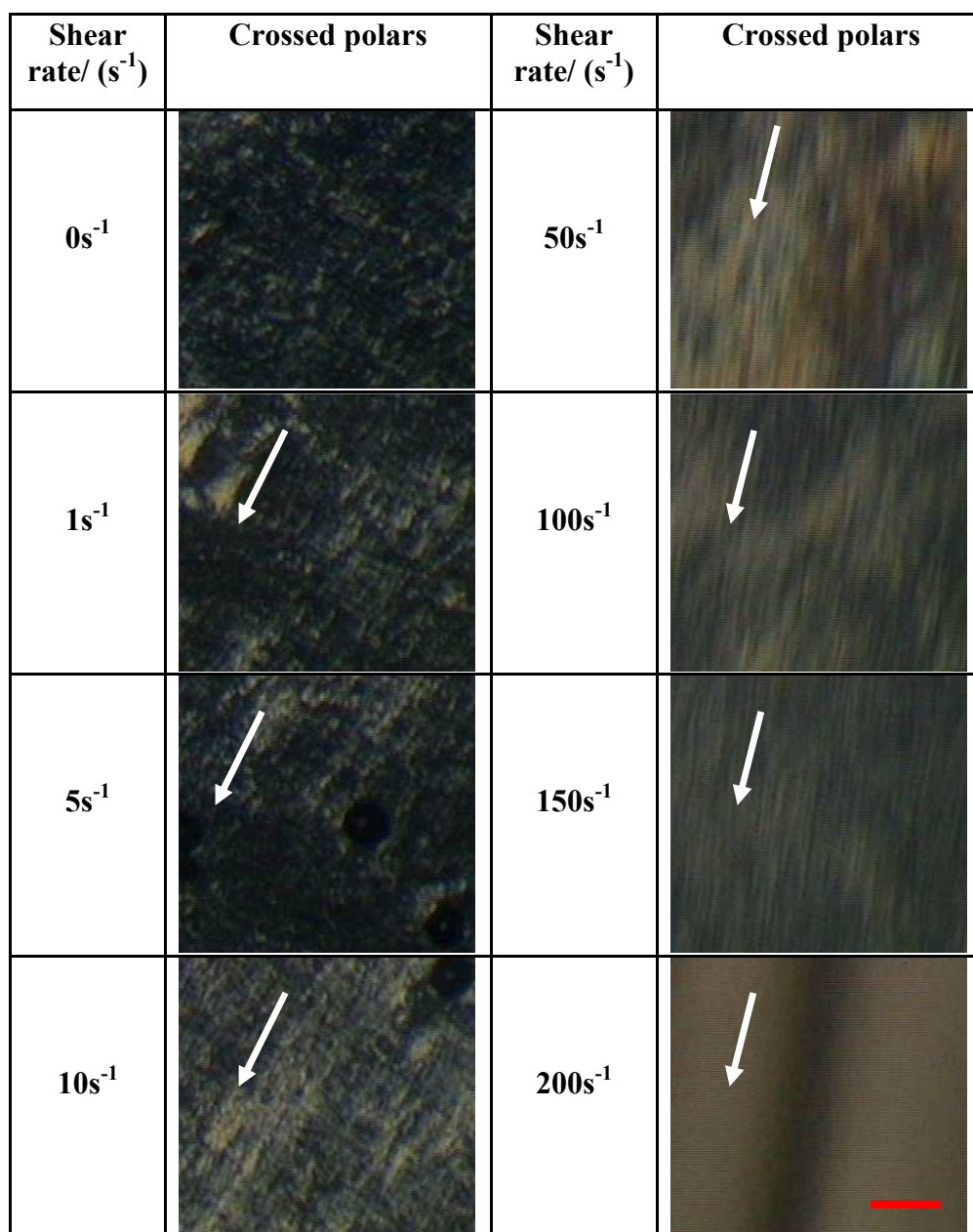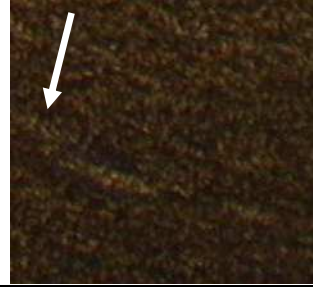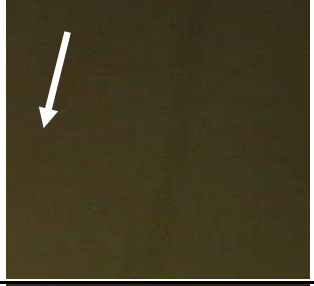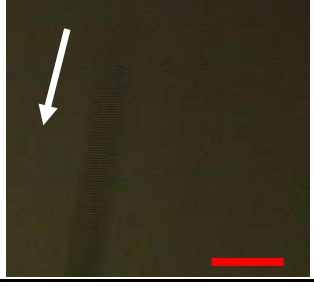| Shear rate/ (s^{-1})	Crossed polars	Shear rate/ (s^{-1})	Crossed polars
0s^{-1}		50s^{-1}	
1s^{-1}		100s^{-1}	
5s^{-1}		150s^{-1}	
10s^{-1}		200s^{-1}	

Figure 6.1.6: Optical micrographs for the 5 wt% TSC sample taken while shearing at 25ºC. Each shear rate was applied to the sample for 5mins. The arrow indicates the direction of flow and the scale bar represents 100μm.

6.1.4 Discussion

Previous studies (although not performed on a Linkam Shear Cell) on the influence of shear flow on lyotropic lamellar phases can be compared with similar results observed. It was shown by many research groups[5-8, 12] that shearing can cause orientation in lamellar phases. The first studies by Diat *et al*[1] suggested three states of orientation, a parallel at both low and high shear rates and a vesicle state at intermediate shear rates.

The formation of vesicles has been found in a broad range of surfactant systems and seems to start only from parallel orientation. It is believed that the lamellar layers always tend to arrange parallel to the plane of shear in order to minimise their mechanical resistance. According to previous studies on MLVs size, the size of shear induced MLVs is correlated with the shear rate[1]. Roux and co-workers[13] reported a transition from a population of small vesicles to a population with bigger vesicles by increasing the shear rate while Hoffmann *et al*[14] found a transition from MLVs into small uni-lamellar vesicles (ULV) at high shear rates.

Previous studies already proved the shear induced formation of MLVs in defective lamellar phases[9]. However, Gustafsson *et al*[15] suggested that the membrane defects might hinder the MLVs formation. Some other authors suggested that defects are responsible for the differences in the onset of the vesicle formation and that the vesicular state is a state of the lamellar phase with a well defined concentration and distribution of defects.

Further literature reviews[1, 13, 16] also noted the shear impact on the lamellar phases at various shear rates. The transition from parallel to perpendicular orientation was found in a broad range of shear rates therefore, the co-existence of two different lamellar orientations was assumed. In some cases it was found that a parallel orientation exists at low and high shear rates[1], whereas a transition from parallel to perpendicular orientation was reported, independent of the formation of vesicles[17, 18].

Here we have observed different shear induced orientations of the lamellar phases. It is believed that shear slowly induces a change in morphology from extended bilayers (very large domains in the electrolyte free system) to liposomes. At intermediate shear rates the liposomes arrange behind each other in the flow direction. At higher shear rates the stripes

shown in the optical textures are believed to be parallel lines of liposomes. The more shear the sample experiences, the more stripes can be seen in the textures.

An important question when considering the phase microstructure of the complex systems studied in this work is the effect of shear on the microstructure. Although there is little evidence of vesicles from these optical micrographs the differences observed after shear was applied onto the system suggest structural transitions within the lamellar phase. Evidence for structural transitions of the lamellar phase is more likely to be discussed in the following Sections throughout this Chapter.

6.2 Rheology

6.2.1 Introduction

Rheology by definition is the science of the deformation and flow of matter[19, 20]. This has been studied through oscillation and viscometry tests. The tests allow the establishment of sample characteristics such as the viscoelastic behaviour, whether the sample is shear thinning or shear thickening, and enables the determination of the power law index required for the Rheo-NMR calculations (Appendix III).

Oscillation test is a dynamic test which oscillates the sample though fixed stress/strain to determine the viscoelasticity. Oscillation tests include the amplitude sweep step and the frequency sweep step. The amplitude sweep identifies the linear viscoelastic region (LVR) which is an indication of how tough the material is (long LVR enables the sample to 'absorb' a broader range of deformations before the structure breaks down). Frequency sweep measures the phase angle, δ, complex modulus, G^*, storage (elastic) modulus, G', loss (viscous) modulus G'' and the dynamic viscosity, $|\eta^*|$, based on a fixed amplitude. These properties can be measured as a function of time, frequency and/or amplitude of shear and temperature.

Viscometry tests are simple rotational shear experiments and are destructive tests as the sample must flow. The flow behaviour can be described using shear profile which measures instantaneous viscosity as a function of shear stress, temperature and time.

The effects of flow on lyotropic lamellar phases have been widely studied[1, 17, 21, 22]. It has been shown that under shear some rearrangements of the lamellar domains occur which lead to well-defined steady-state orientations. The effects of the shear flow are summarised in a so-called shear diagram suggested by Diat *et al*[21].

In this work we study the coupling of the sample composition and the rheological properties of the lamellar phases. Furthermore this study correlates the formation of MLVs to the defect density in the lamellar phases.

6.2.2 Experimental Details

Throughout this work a TA (thermal analysis) instrument, AR 2000, was used for rheological measurements of the samples. The rheometer is a cone and plate system with 40 mm plate and 53 μm gap (Section 4.2.4).

Two different types of rheological measurements were performed in this work:

1) Oscillatory tests were performed with a stress controlled amplitude sweep at a relatively low frequency (6.28rad.s^{-1}) and a frequency sweep at constant strain inside the linear viscoelastic region (LVR).

2) Steady-state flow measurements (viscometry tests) were performed as a function of shear rate and shear stress.

The samples selected for shear characterisation are the 0, 3 and 5 wt% TSC samples. All the samples were prepared as described in Section 4.1.2. Before any rheological measurement, all samples were kept undisturbed for 10 days because the complete build-up of the liquid crystalline structure is a time-consuming process[23]. For the rheological measurements it was assumed that all the samples have the same shear history and were left for 10 minutes in the rheometer cell before any measurement. All the rheological tests were performed at 25°C and at least two replicates of each test were done.

6.2.3 Results

Amplitude sweep experiments were performed on all the samples at a constant frequency of 6.28rad.s^{-1}. In each of the experiments, the stress (amplitude) was varied from ca. 0.01 to ca. 500Pa. Representative plots of elastic modulus G' and viscous modulus G'' as a function of the applied stress are shown in Figures 6.2.1.
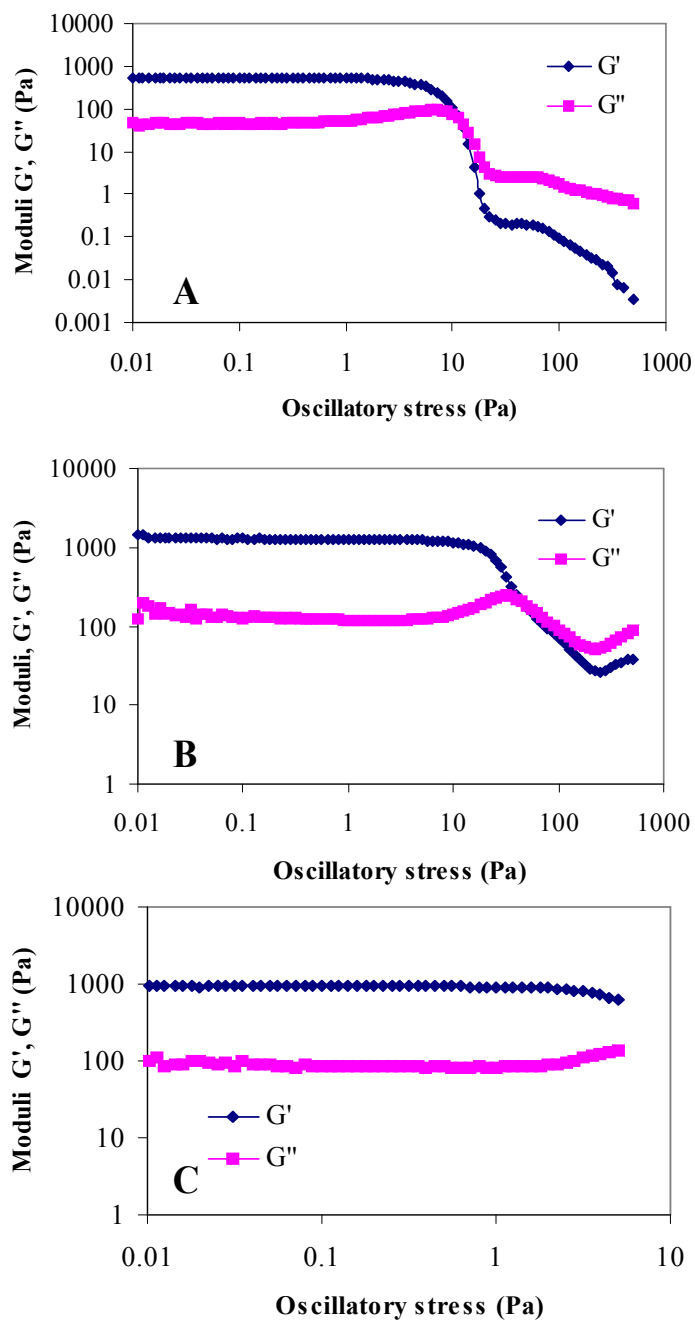
Figure 6.2.1: Amplitude (stress) sweep tests as a function of the applied stress showing the soft-solid behaviour (LVR, $G' > G''$) and the viscoelastic liquid behaviour (NLVR $G' < G''$) for (A) the 0 wt% TSC sample, (B) the 3 wt% TSC sample and (C) the 5 wt% TSC sample.

The elastic modulus, G', is a measure of the deformation energy stored in the sample during the shear process, whereas the viscous modulus, G'', is a measure of the deformation energy used up and lost to the sample. At low stress values, the elastic modulus, G', and the viscous modulus, G'', are constant and the sample exhibited a soft

solid behaviour with $G' > G''$. This regime is known as the linear viscoelastic region (LVR).

As oscillation testing monitors the dynamic properties of the sample only (*i.e.* the sample should not flow) therefore further experiments, the frequency sweep tests, are performed within the LVR at a constant strain.

Typical results of the storage modulus, loss modulus, and complex dynamic viscosity as a function of the frequency in the LVR can be seen in Figure 6.2.2.
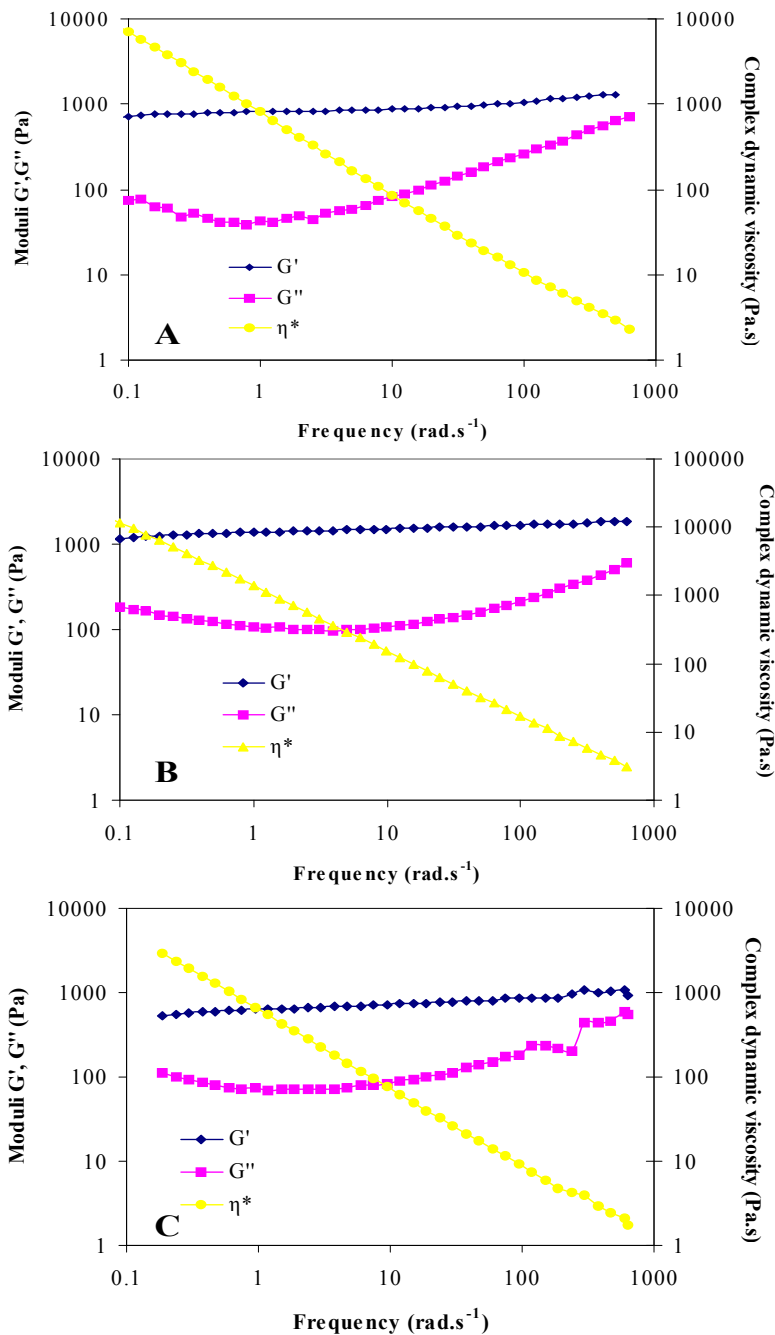
Figure 6.2.2: Evaluation of the storage modulus (*G'*), the loss modulus (*G''*) and the complex dynamic viscosity |η*| as a function of frequency for the systems containing (A) 0 wt% TSC, (B) 3 wt% TSC and (C) 5 wt% TSC.

As can be observed in Figure 6.2.2 in all cases the frequency dependence of *G'* and *G''* was always similar. Thus, almost constant values of *G'* and a clear minimum in *G''* can be detected for the systems. In all cases the system is more elastic than viscous in the range of frequency investigated, and the storage modulus is higher by about one order of magnitude

than the loss modulus. While the storage modulus has a weak dependence on the applied frequency, the loss modulus shows a minimum. The complex viscosity, |η*|, which represents the flow resistance of the sample, in all cases is strongly frequency dependent: the higher the frequency, the lower is the complex viscosity. Similar results have been found in the literature for systems with different types of surfactants[24, 25].

Oscillatory measurements were performed as a function of frequency for samples with different ages (Figure 6.2.3). Comparing the sample ages at 25°C the recorded parameters are very similar indeed. These results are in a good agreement with previous studies where it was pointed out that the rheological properties of samples were not influenced by time.
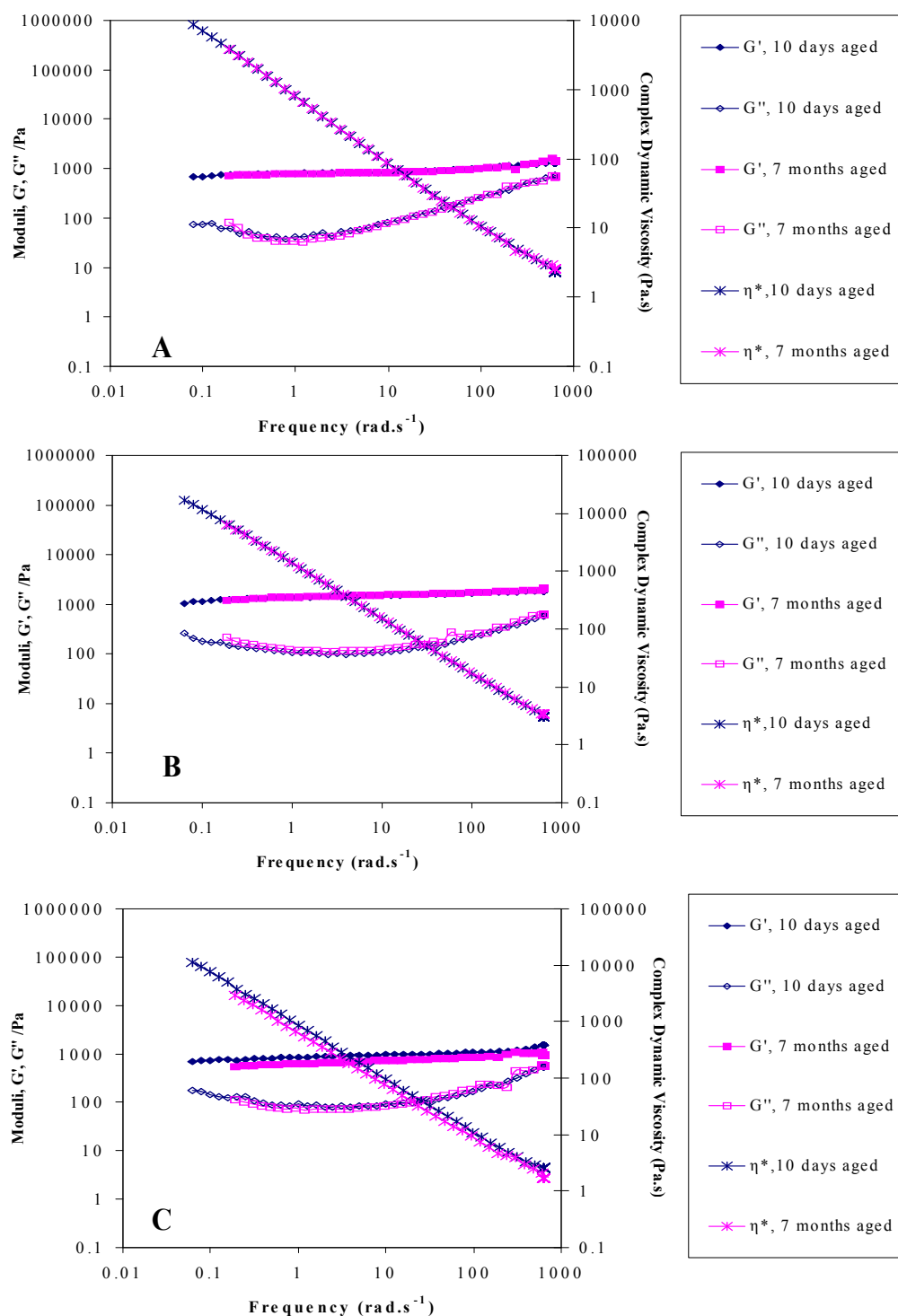
Figure 6.2.3: Evaluation of the storage modulus (*G'*), the loss modulus (*G''*) and the complex dynamic viscosity |η*| as a function of frequency. The effect of aging on the rheological properties of the samples (10 days and 7 months aged) was investigated. The systems containing (A) 0 wt% TSC, (B) 3 wt% TSC and (C) 5 wt% TSC.

Steady state measurements were performed at 25°C for all samples to investigate the flow properties of the systems. The flow properties are rather similar for all the samples,

although for higher and intermediate values of shear rates, viscosity curves depend on composition (see Figure 6.2.4).
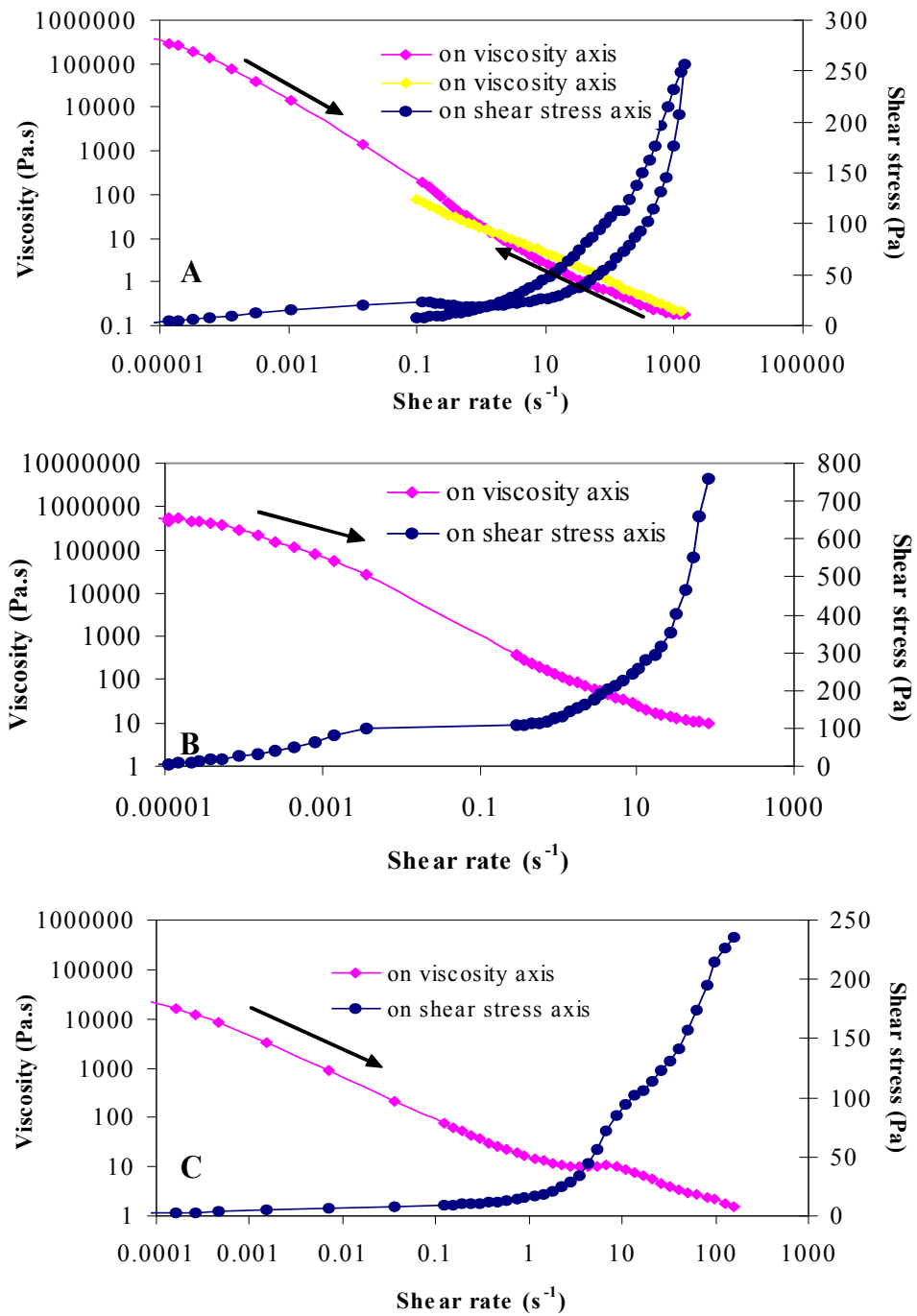
Figure 6.2.4: Log plot of viscosity and shear stress versus shear rate for samples at 25°C containing (A) 0 wt% TSC, (B) 3 wt% TSC and (C) 5 wt % TSC with all samples aged 10 days.

Flow curves are greatly dependent on a composition showing shear thinning behaviours. Shear thinning behaviour is noted in steady flow measurements with the overall reduction of the viscosity as the shear rate increases. As shown in Figure 6.2.4 (A) the sweep down curve for the 0 wt% TSC sample exhibited a hysteresis instead of overlapping the viscosity profile of the sweep up operation. The hysteresis loop is a clear indication that the sample exhibits complex non-Newtonian flow. In order to investigate the time dependence on the viscosity build-up the same steady state experiment was performed for the 0 wt% TSC sample but the sweep down operation was carried out after the sample relaxed for 14hrs on the shear cell (see Figure 6.2.5).
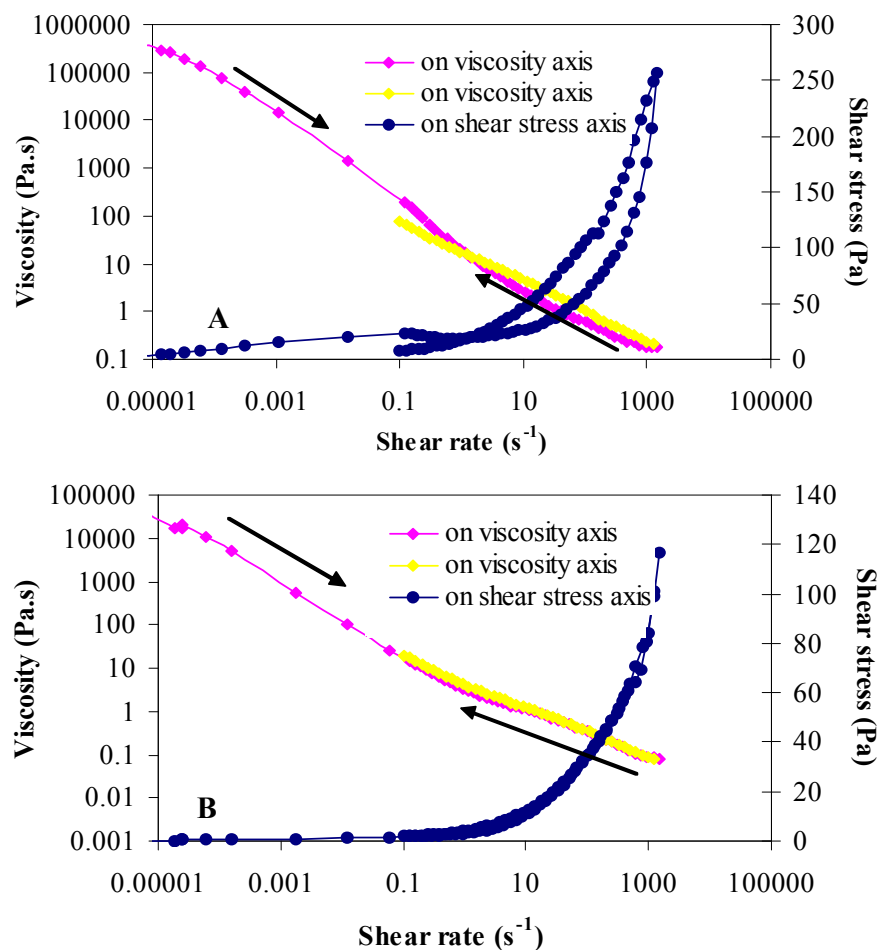
Figure 6.2.5: Steady state measurements as a function of shear rate performed for the 0 wt% TSC sample at 25°C. (A) The sweep down operation was carried out immediately after the sweep up step is stopped and (B) the sweep down operation was carried out 14hrs after the sweep up step is stopped. The sample was left in the shear cell to relax.

For the cases of 3 and 5 wt% TSC samples, the system can not accommodate the stress applied and so the material is forced out from the shear cell. Similar behaviour was observed when the steady state measurements were performed through the use of a cylindrical rheometer.

A noteworthy result observed in Figure 6.2.4 is that at higher shear rates there is a sharp increase in the shear stress with the shear rate. This is widely considered to be a change from planar bilayer arrangement to a multi-lamellar vesicles arrangement (MLVs)[1, 26].

The stress sweep up and down experiment on the samples is shown in Figure 6.2.6.
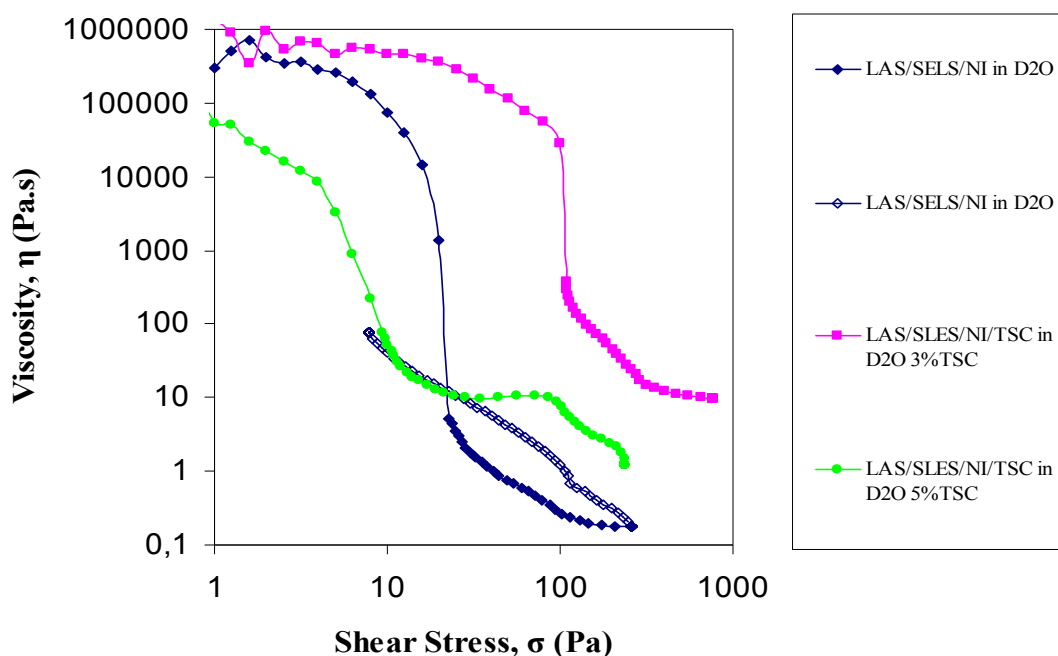
Figure 6.2.6: Stress sweep up (solid symbols) and sweep down (open symbols) experiment.

As the shear stress increased from ca. 1Pa, the viscosity remained almost constant for the 0 and 3 wt% TSC samples, until a stress of ca. 10Pa and ca. 80Pa for the 0 and the 3 wt% TSC sample respectively is applied. This is known as the first Newtonian plateau. Shear thinning behaviour is observed for all the samples. The shear thinning regime appeared at different stress values. Shear thinning behaviour is noted in steady-state measurements with the overall reduction of the viscosity as the shear stress increases. As the stress increases the viscosity was decreased and finally reached a very low value. A second Newtonian plateau is then observed after the shear thinning regime for the 3 and 5 wt%

TSC samples. In the second Newtonian plateau, the viscosity remains fairly low and constant. However, in the case of the 3 and 5 wt% TSC samples, the magnitude of the stresses past the shear thinning regime was so high that the samples could no longer accommodate the stresses and consequently the sweep down step was not observed when using the cone and plate geometry.

From the 0 wt% TSC sample behaviour in the sweep up operation, the first point to conclude is that the sample exhibits the first Newtonian plateau and is shear thinning in nature. In the sweep down operation the viscosity did not superimpose the same path of the sweep up operation. This is to say that the sample exhibited hysteresis with an increased viscosity profile in the sweep down operation.

Based on the flow behaviour in the sweep down operation it can be said that the sweep up operation deformed the sample to such an extent that the removal of stresses does not change the structure immediately. The reformation of the structure is time dependent.

Similar behaviour was observed for the 3 wt% TSC sample. However, the first Newtonian plateau ends at higher shear stresses than the plateau observed in the electrolyte-free flow curve. It is noteworthy that the 3 wt% TSC sample exhibited a second Newtonian plateau however the sweep down operation could not occurred as the sample was forced out from the shear cell.

This behaviour was also noted for the 5 wt% TSC sample. The flow curve observed in Figure 6.2.6 for the 5 wt% TSC sample has two steps. This curve is a characteristic flow curve for a lamellar dispersion system.

As mentioned before when observed Figure 6.2.4 strangely for these systems the viscosity is lower for the system with the higher wt% salt. That it can be due to the effect of shear history on these lamellar systems. This is thereby a good example of the need to eliminate the shear history effect.

The flow behaviour of the systems was investigated at varying ages. The effect of aging on the flow behaviour is shown in Figure 6.2.7. Overall it can be seen that the flow properties are rather similar between the fresh (10 days aged) and the 7 months aged samples.
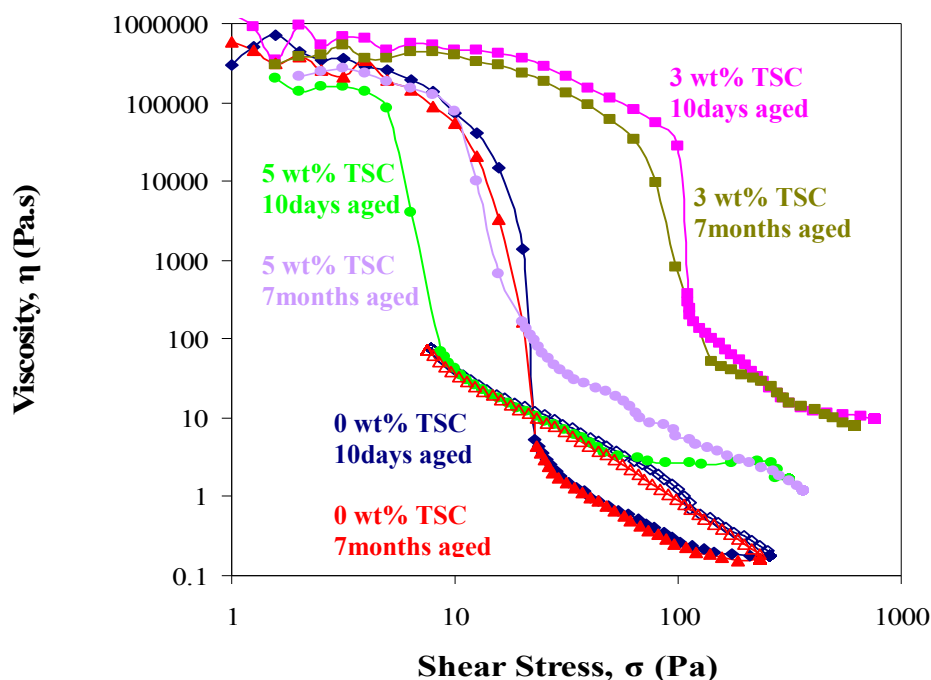
Figure 6.2.7: Stress sweep up (solid symbols) and sweep down (open symbols) experiment for all samples showing the ageing effect on flow curves.

However, a noteworthy observation is the difference observed in the flow curve of the 5 wt% TSC sample. As previously mentioned it seems likely that the 5 wt% TSC system is a lamellar dispersion. As shown in Figure 6.2.7 after 7 months the flow curve is changed. That might be suggesting changes in the structure of the system or changes in the size of the domain present in the lamellar dispersion.

6.2.3 Discussion

The linear viscoelastic behaviour of the lamellar liquid crystalline systems was investigated as a function of sample composition and age. As shown in Figure 6.2.2 the lamellar phase for all the cases is characterised by a small linear viscoelastic range. This has previously been demonstrated by Robles-Vasquez *et al*[27]. The values of G' are almost constant and a clear minimum in G'' is been detected for all the systems. Overall, all the samples can be described as soft-solid with $G' > G''$.

The elasticity of the lamellar phases may attribute to the structure units formed. Here is assumed that the structure units are organised in sheets, which although they can slide over each other, the mobility of the chains within the sheet is more restricted.

This mechanical spectrum corresponds to the 'plateau' region observed in steady-state flow curves. This plateau has been related to the formation of an elastic structural network due to the interactions between liquid-crystalline domains.

Comparing the rheological properties (G', G'' and $|\eta^*|$) of the samples at varying ages it can be said that they are not influenced by time.

The flow behaviour of the systems was investigated as a function of shear rate, shear stress and age. The flow properties are rather similar for the 0 and 3 wt% TSC samples, although for higher and intermediate values of shear rates, viscosity curves depend on composition.

Based on the shape of the flow curve, the first point to conclude is that the 0 and 3 wt% TSC samples exhibit the first Newtonian plateau and are shear thinning in nature. In the first Newtonian plateau, the elastic components of the viscoelastic material offer a great resistance to the applied shear stress. The low magnitude applied stresses produced less strain in the 3 wt% TSC sample, which was resisted by the sample probably because it is more ordered than the 0 wt% TSC sample. At the end of the Newtonian plateau, the applied stress caused sufficient strain in both samples that are started to respond to the applied stresses. It seems likely that the induced stress has sheared the elastic components of the material and therefore the domains within the structure orient themselves in the direction of flow.

Once the orientation is sufficient and most of the elasticity in the sample is broken down, the sample offers very low resistance to the applied shear and reaches a shear thinning regime. In this regime the bilayers would slide against one another. In the literature the shear thinning behaviour has been related to the formation of ordered bilayer structures being aligned in the flow direction.

Moreover Mayer *et al* proposed that the first regime can be associated to the presence of oily streaks aligned in the flow direction. These observations are in a good agreement with the textures observed under optical shear cell at low shear rates $< 10\text{s}^{-1}$. However, in the case of 0 and 3 wt% TSC samples the flow curves are in a good agreement with the textures observed. It has been observed that the mosaic texture of the non-oriented lamellar

phases was clearly followed by the oily streaks texture at intermediate shear rates and, finally, the total alignment of this texture was observed.

The different shapes of flow curves seen can be explained on the basis of the resistance that the bilayers oppose to flow. The sweep down operation observed in the flow curve for the 0 wt% TSC sample could be explained on the basis that, at that point, some bilayers begin to close, resulting in the formation of vesicles.

As previously mentioned, flow properties of the lamellar systems are strongly dependent on composition. From the observations it can be concluded that the electrolyte free system is the most resistant to the formation of liposomes so it is believed that is furthest from the transition region.

In order to understand the rheology of such complex fluids, it is important to link the macroscopic viscosity to the mesophase structure. ^{2}H Rheo-NMR holds the promise of further information regarding any changes in the mesophase structure through changes in the ^{2}H NMR line shape (Section 6.3).

6.3 Rheological Deuterium Magnetic Resonance (^{2}H Rheo-NMR)

6.3.1 Introduction

While rheology involves mechanical measurement of flow properties, the really interesting questions concern the molecular basis of these properties. Under flow conditions, conformational distortion, reorganisation of mesophase structure and transition to another mesophase structure can result because of the competition between the molecular organisational dynamic and the external deformation[28-30].

^{2}H Rheo-NMR is capable of investigating molecular order and alignment through utilizing nuclear quadrupole interactions[31]. The interest in the molecular-mechanical deformation link has led to the ^{2}H Rheo-NMR technique in which the *in situ* flow is incorporated within the spectrometer detection system. ^{2}H Rheo-NMR holds the promise of further information regarding orientation and any changes in the mesophase structure through changes in the quadrupole splitting Δ and the ^{2}H NMR line shape.

The basic theory of ^{2}H NMR has been described in Section 4.2.5. However, is important to recall that the lineshape of the ^{2}H NMR spectra is governed by the quadrupole couplings between the deuterium nuclei (spin I=1) and the electric field gradients at the sites of the observed nuclei. The residual quadrupole splitting arise from the anisotropy of the rotational motions of the water molecules is given by Equation 6.3.1.

$$\Delta = \frac{3}{2}\frac{eQV}{h} = \frac{3}{2}\frac{e^2qQ}{h}\frac{1}{2}\left(3\cos^2\Theta_0 - 1\right)$$

Equation 6.3.1

where Θ is the angle between the axis of rotational symmetry and the magnetic field and e^2qQ/h is the quadrupole coupling constant, E_Q.

According to Equation 6.3.1 the ^{2}H NMR line shape depends on the orientational distribution of directors. A well aligned lamellar phase gives rise to a simple doublet. A disordered lamellar phase with an isotropic distribution of directors gives rise to the characteristic powder pattern also known as 'Pake' pattern (see Section 4.2.5). This will be used in order to understand how the mesophase structure is affected by shear flow. It has

been demonstrated that ^{2}H Rheo-NMR is a powerful tool for the study of shear-induced structures since the transition to another mesophase structure, the presence of defects and changes in the domain size have an impact on the ^{2}H NMR line shape.

6.3.2 Experimental details

For the ^{2}H Rheo-NMR measurements, the samples (1week aged) (see Section 4.1.2 for sample preparation) were filled into NMR tubes of 10mm diameter. Care was taken that the samples did not contain any air bubbles so that no flow occurred after reorientation of the samples. These were initially sealed with an NMR tube cap and stored in room temperature for a day to ensure that as much material (surfactant/water/salt) as possible was in the bottom of the tube. For each series of experiment reproducible initial conditions were achieved. Each sample was loaded in several NMR tubes according to the variety of the shear rates tested.

For ^{2}H NMR and ^{2}H Rheo-NMR experiment is important to ensure that the sample sits in the within the RF coil of the NMR probe although as the probe is encased this cannot be seen. Previous work has been done on the same ^{2}H NMR probe to determine the optimum sample height to ensure that the sample sits within the coils in the probe suggests that the sample height for experiments is 8mm[32]. Tests have been repeated for different sample heights to improve the signal to noise ratio and therefore increasing sensitivity even when the inner tube is loaded in the sample. Thus the useful sample height for Rheo-NMR experiments is determined to be 7mm.

^{2}H Rheo-NMR is performed using a homemade cylindrical couette cell (Rheo-NMR couette, see Figure 6.3.1) and the bench-top Maran Ultra Spectrometer. An advantage of the couette cell is the fact that solvent evaporation during the measurement is negligible. The inner radius of the cylinder is 2.5mm with a gap of 2mm. The rheological cell is located within the RF coils of the ^{2}H NMR probe and is driven by a stepper-motor gearbox. Shear is applied by rotating the inner tube. The shear rate is determined from the motor voltage setting as shown in Section 4.2.6 using the appropriate power law index given in Appendix III. The axis of the shear cell is aligned parallel to the magnetic field. All the NMR data have been taken at a controlled temperature of 25°C ±0.5°C.
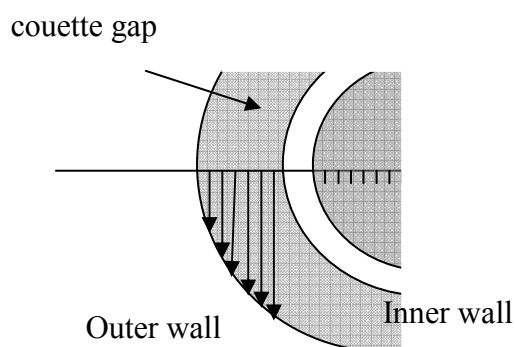
Figure 6.3.1: Schematic representation of the couette-like device which shears the sample[33]. The arrows indicate the different positions across the annular gap of the couette cell.

In order to perform both ^{2}H NMR and rheological experiments the sample was loaded in the ^{2}H NMR probe giving, essentially, the spectrum which indicates the structure on resting before loading the inner tube. To be able to identify any changes caused by extensional force exerted onto the sample spectra were taken after gently loading the inner tube. The sample stand in the ^{2}H NMR probe and several NMR experimental scans were recorded at zero shear rates for two days to record any changes upon addition of the inner tube. After two days, the sample was sheared for a given shear rate and shear time. The shear rate is determined from the motor voltage setting as shown in Appendix III.

The ^{2}H NMR experimental scans performed after shearing is stopped (except when the NMR experimental scans performed during the application of shear). Typically 2048 scans were acquired for one spectrum, with relaxation delays of 0.4-0.5s between scans. Thus each NMR measurement took ca. 60mins. The number of data points acquired during pulse is 16384 and the spectra width is 100000Hz. For each experimental shear rate setting fresh sample was loaded into the couette cell and care was taken to minimise any shear histories arise from stresses during the filling procedure.

Samples chosen were those containing 0, 3 and 5 wt% TSC in ^{2}H$_2$O with varying shear rates used to monitor changes through the lamellar liquid crystalline phase at 25°C. The spectra at varying shear rates and relaxation times have been displayed in the following Sections for each sample.

6.3.3 Results

<u>^{2}H Rheo-NMR results for the 0 wt% TSC sample</u>

Figure 6.3.2 shows the ^{2}H NMR spectra obtained for the electrolyte free system at zero shear rates at 25°C before and after gently loading the inner tube. It can be seen that the splitting in the spectrum decreases after adding the inner tube from ca. 450Hz to ca. 380Hz. It can be seen that the shoulders singularities are higher in intensity and the *s* value decreases from ca. 930Hz to ca. 880Hz.
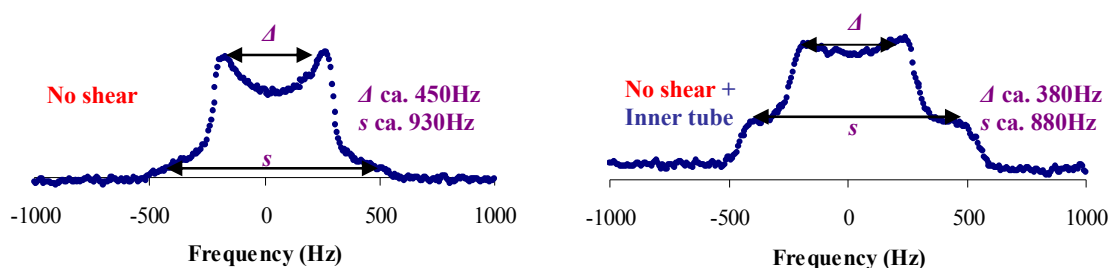
Figure 6.3.2: ^{2}H NMR spectra for the 0 wt% TSC sample at zero shear rates at a temperature of 25°C. The spectrum on the right hand recorded after gently loading the inner tube.

Experimental NMR scans were running for two days and insignificant changes were recorded in the spectral line shape. This is an indication of a stable state orientation. The spectrum recorded with the loaded inner tube represents the reference spectrum for the structural analysis.

Table 6.3.1 below shows the experimental settings for each rheological run at varying shear rates and shear time.

Experimental Conditions Sample: 0 wt%TSC		
Motor Voltage setting (V) and shear rate (s^{-1})	Time sheared for (hrs:mins)	Time relaxed for (hrs:mins)
2.5V ($68s^{-1}$)	00:05	25:00
5V ($137s^{-1}$)	00:05	25:00
5V ($137s^{-1}$)	00:15	25:00
10V ($274s^{-1}$)	00:05	25:00
10V ($274s^{-1}$)	00:15	25:00
10V ($274s^{-1}$)	25:00	Not recorded

Table 6.3.1: Experimental conditions for varying shear rates for the 0 wt% TSC sample at 25°C. The spectra are displayed below.

The effect of shear rate on the ^{2}H NMR line shape is shown in Figure 6.3.3. For this experiment sample of the same composition was loaded in three tubes and scans were performed after the inner tube was added in the sample. Each sample was sheared for 5mins at varying shear rates. In all the cases, the reference spectrum for the structural analysis is the spectrum recorded after loading the inner tube in the sample. The shear rates are indicated on the spectra.

Figure 6.3.3: ^{2}H NMR spectra for the 0 wt% TSC sample sheared at different shear rates for 5mins. The shear rates (s^{-1}) are given to the left of the spectra.

As can be seen from the individual spectra shown in Figure 6.3.3, a powder spectrum obtained after shearing the sample at 68s^{-1} for 5mins. The NMR spectrum of such two-dimensional powder has maxima at the frequencies of the initial inner splitting (for layers aligned with their normal perpendicular to the magnetic field) and at twice these frequencies (for layers oriented with their normal parallel to the magnetic field). The spectrum recorded when the sample sheared at 137s^{-1} for 5mins shows insignificant decrease in quadrupolar splitting. However, the spectral line shape and the quadrupolar splitting suggest that the curvature of the domains still is low thus making the reorientation motion slow. The line shape observed for the sample when sheared at 274s^{-1} for 5mins shows a gradual transformation to a new line shape. As can be seen in Figure 6.3.3 the lamellar doublet is no longer resolved and a broad single peak is observed.

Shown in Figure 6.3.4 are the characteristic NMR spectra obtained for the shear rates of 137 and 274s^{-1} for 15mins. A two-dimensional powder spectrum is observed suggesting that the structure is consisting of large domains of planar layers the normal axis of which is distributed perpendicular to the direction of flow. Godinho *et al*[34] have suggested, based on studies on a liquid crystal polymer system that after rapid deformation the degree of alignment in the sample is less than after slow deformation.
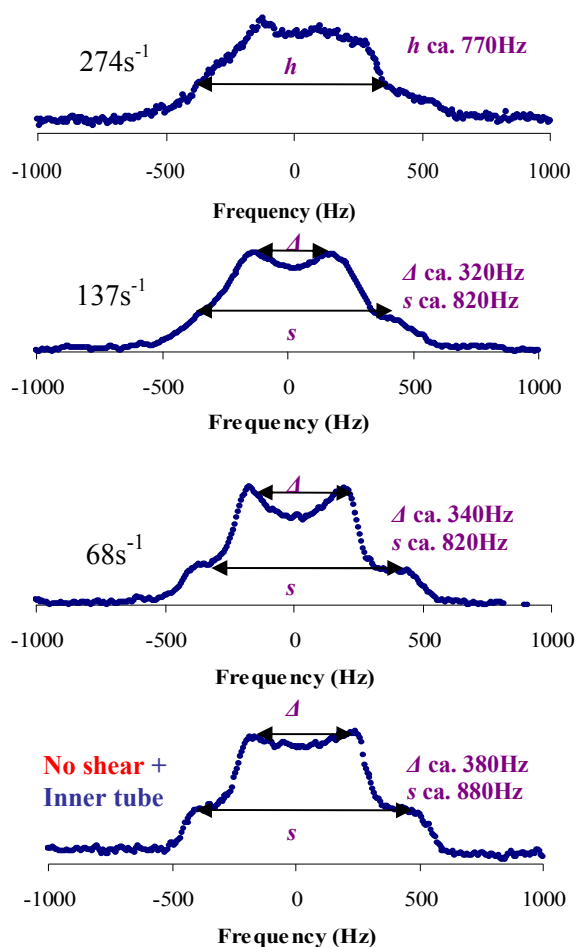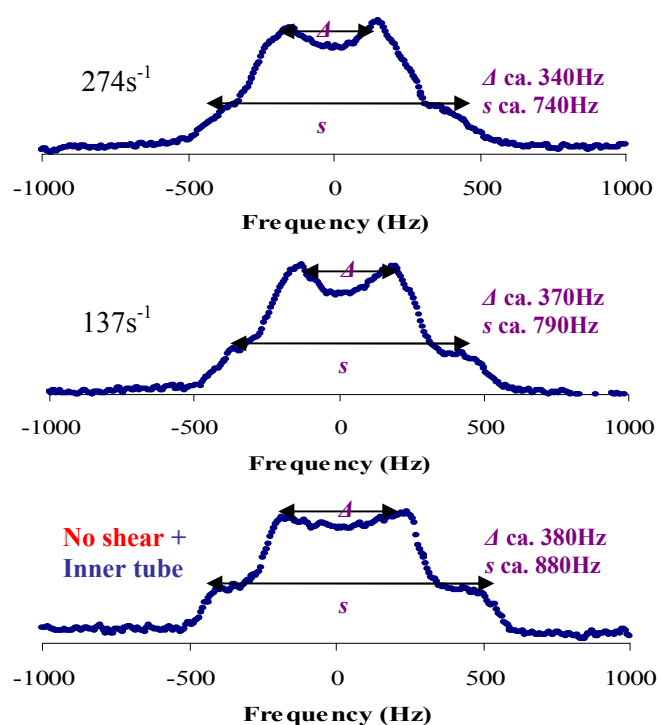

Figure 6.3.4: ^{2}H NMR spectra for the 0 wt% TSC sample sheared at different shear rates for 15mins. The shear rates (s^{-1}) are given to the left of the spectra.

Comparing the spectra after the application of shear for 5 and 15mins to the sample for the shear rate of 274s^{-1} shown in Figure 6.3.5 a gradual change in the spectral line shapes can be seen. The spectral line shape recorded after shearing the sample for 5mins indicates the transition to curved domains. However, after shearing the sample for 15mins a two-dimensional spectrum is observed indicating the anisotropic motions of the water molecules.
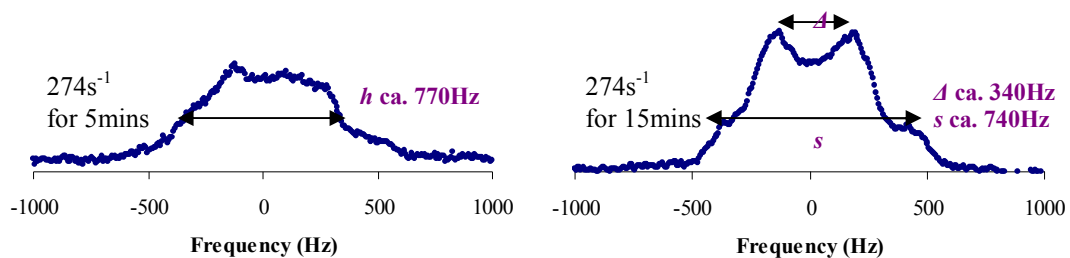
Figure 6.3.5: ^{2}H NMR spectra for the 0 wt% TSC sample sheared at 274s^{-1} for 5 and 15mins respectively.

These data suggest that the shear application into the lamellar phase results in more curved domains if the shear rate applied is sufficiently high and the shear time is relatively short (ca. 5mins).

The relaxation kinetics of the shear induced states is also investigated in this project. For all the relaxation studies the samples were sheared at a specific shear rate and time and then they were left in the NMR probe for approximately 35hrs.

Figure 6.3.6 and 6.3.7 show a series of ^{2}H Rheo-NMR spectra taken at varying times after shearing is stopped. The sample sheared at 137s^{-1} for 5 and 15mins respectively.

Figure 6.3.6: ^{2}H NMR spectra for the 0 wt% TSC sample sheared at 137s^{-1} for 5mins at 25°C before initiating the ^{2}H NMR experimental scans. The time of relaxation of the sample in hours (hrs) is indicated on the right hand side of each spectrum.

As can be seen from the spectra shear induced changes in the appearance of the spectral line shape although small changes recorded for Δ values. Note that for all the relaxation experiments the first spectrum obtained is 1hr after shearing is stopped (this is because each ^{2}H NMR measurement took ca. 60mins). On relaxation reorganisation of the structure is clearly shown after ca. 5hrs. Δ remains relatively unchanged although the appearance of shoulders becomes more obvious upon relaxation. The continuous change of the spectral line shape and the initial decrease of the splitting suggest that defects were formed after shearing the sample.

Shown in Figure 6.3.7 are the spectra recorded after shearing the sample at 137s^{-1} for 15mins. Comparing the data obtained from the relaxation kinetics in Figures 6.3.6 and 6.3.7 it can be said that the structure reorganises faster when the application of shear is longer and ends with the same line shape upon relaxation for 25hrs.

Figure 6.3.7: ^{2}H NMR spectra for the 0 wt% TSC sample sheared at 137s^{-1} for 15mins at 25°C before initiating the ^{2}H NMR experimental scans. The time of relaxation of the sample in hours (hrs) is indicated on the right hand side of each spectrum.

Upon increase of the shear rate to 274s^{-1} for 5mins, a transformation to a new line shape is observed (see Figure 6.3.8). The spectrum features become less distinct, the inner doublet vanishes and a broad single peak appears. The quadrupole splitting appears again after ca. 5hrs relaxation and after ca. 10hrs the spectrum recorded is a two-dimensional powder pattern. From the spectrum recorded upon relaxation for ca. 5hrs it seems that immediately after shearing is stopped most of the layers are oriented perpendicular to the magnetic field (in the direction of flow - inner doublet). Upon further relaxation a fraction of layers aligns parallel to the magnetic field, thus the intensity of the shoulders increases. The quadrupole doublet with a well defined spectrum is fully recovered after relaxation of ca. 25hrs.
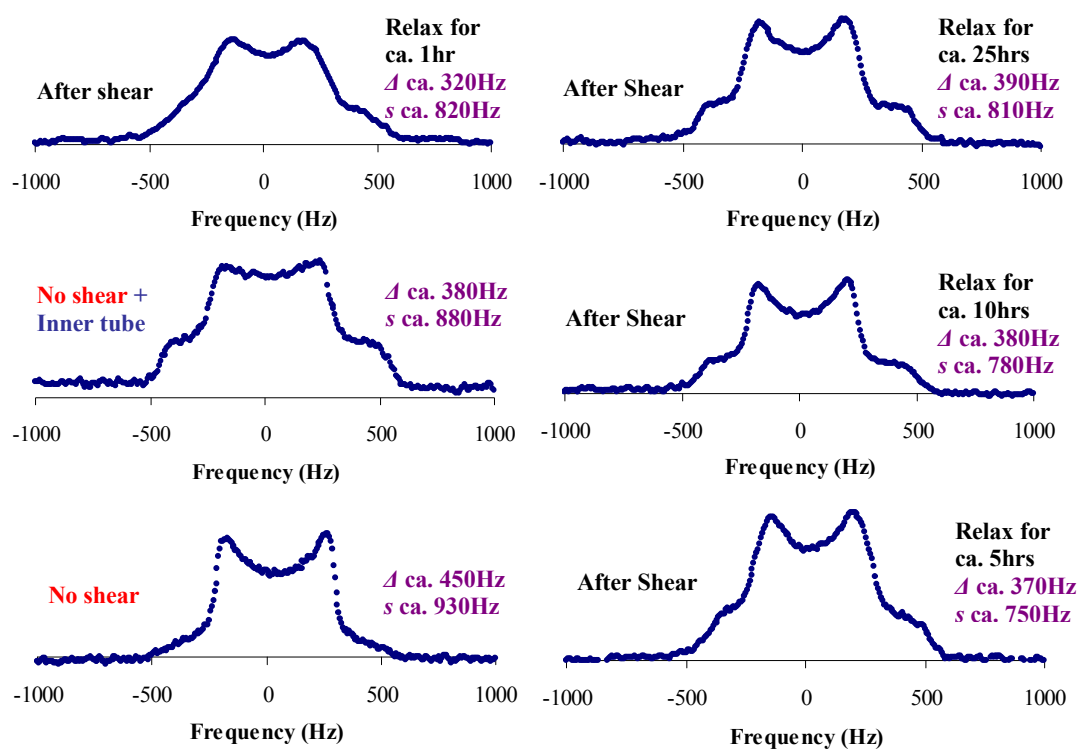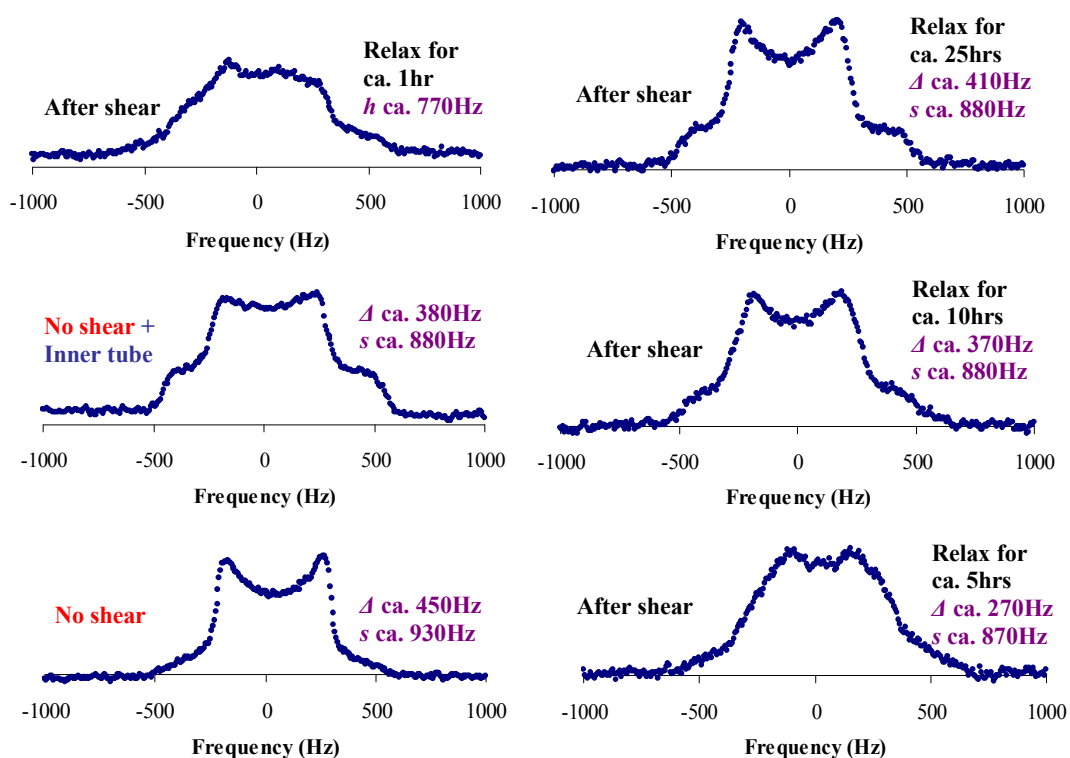
Figure 6.3.8: ^{2}H NMR spectra for the 0 wt% TSC sample sheared at 274s^{-1} for 5mins at 25°C before initiating the ^{2}H NMR experimental scans. The time of relaxation of the sample in hours (hrs) is indicated on the right hand side of each spectrum.

Similar changes in the ^{2}H NMR line shape occur when the sample sheared at 274s^{-1} for 15mins (see Figure 6.3.9). The powder pattern appears upon relaxation for ca. 10hrs indicating that the structure reorganises towards the classical lamellar phase.
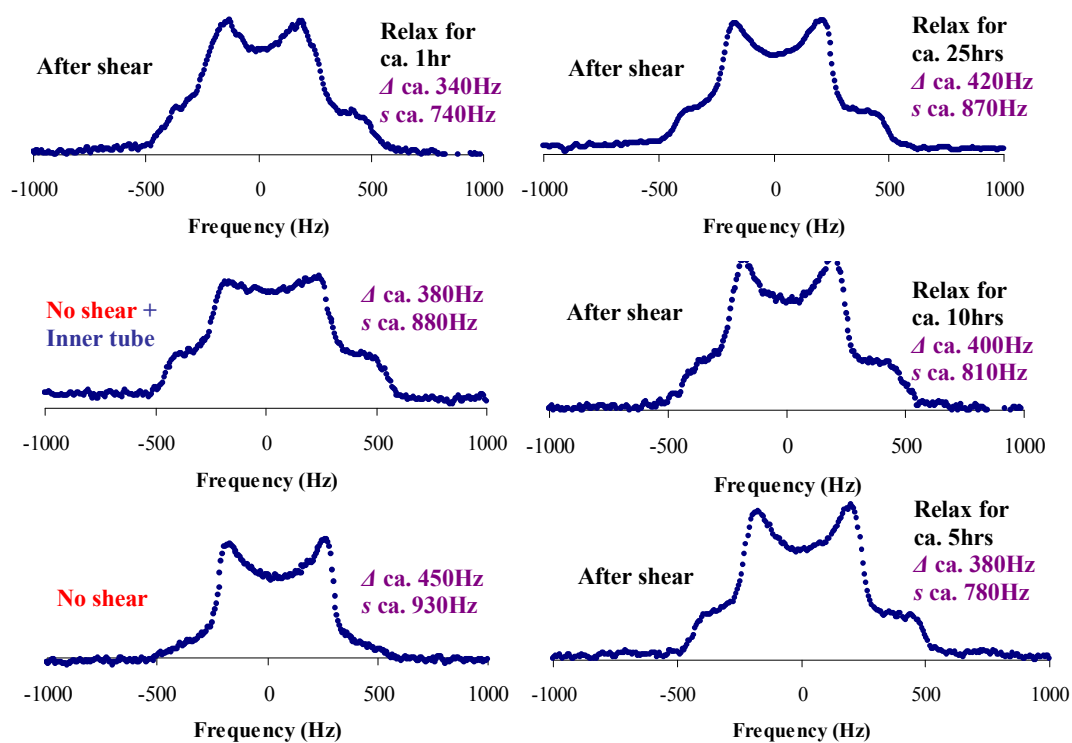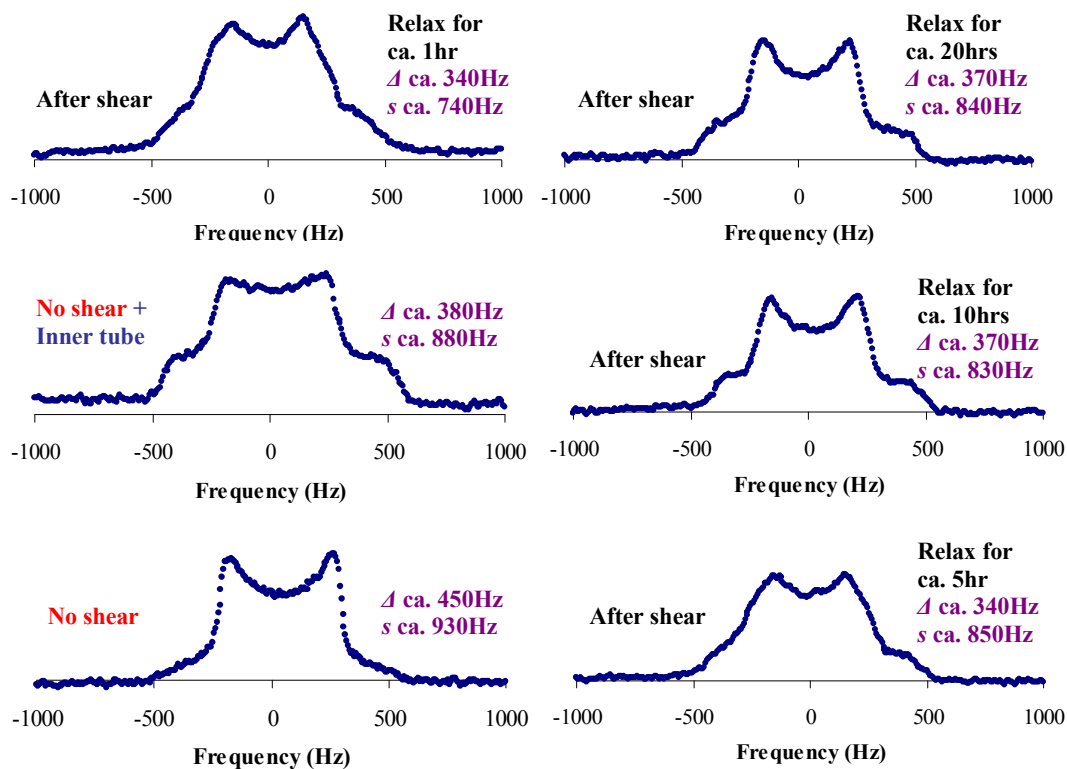
Figure 6.3.9: ^{2}H NMR spectra for the 0 wt% TSC sample sheared at 274s^{-1} for 15mins at 25°C before initiating the ^{2}H NMR experimental scans. The relaxation of the sample in hours (hrs) is indicated on the right hand side of each spectrum.

The final line shapes observed for the electrolyte free sample after relaxation for ca. 25hrs do not change for several hours, indicating a relatively stable state of orientation and molecular reorganisation of the lamellar liquid crystalline phase.

It has been observed that when scans performed during the application of shear at 274s^{-1} for 25hrs, $\varDelta$ remains relatively unchanged although the shoulder's intensity slightly changes. Figure 6.3.10 indicates that the application of shear does not alter the spectrum appearance with the 'Pake' powder pattern evident throughout the experimental run.
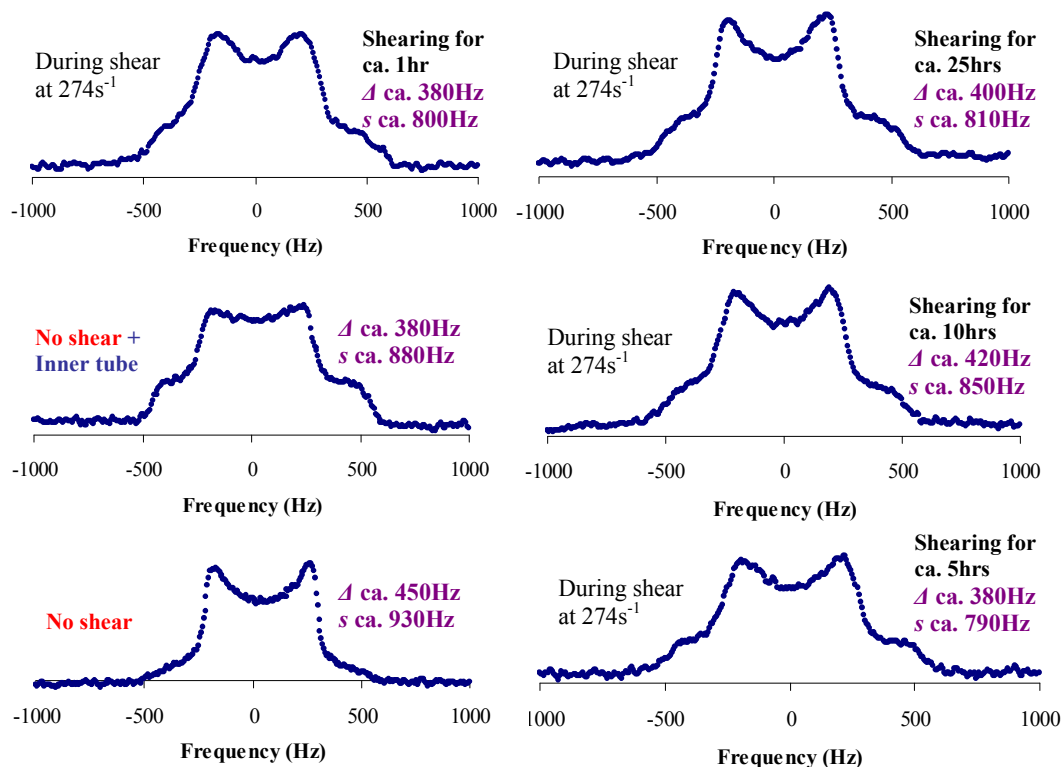
Figure 6.3.10: ^{2}H NMR spectra for the 0 wt% TSC sample sheared at 274s^{-1}. The scans performed during the application of shear for 25hrs.

^{2}H Rheo-NMR results for the 3 wt% TSC sample

As discussed in Section 5.3 upon addition of electrolyte up to 3 wt% a gradual change in the ^{2}H NMR line shape is observed. Our ^{2}H NMR data suggest that this change is due to the formation of more curved domains. The lack of clear splitting may be due to either different degrees of order in different domains or to domains with the same internal order but powder-like alignment.

Before any ^{2}H Rheo-NMR scans the effect of the added inner tube on the spectrum line shape was investigated. The inner tube was gently loaded in the sample and scans were recorded over 2 days. Figure 6.3.11 shows the spectra obtained before and after the addition of the inner tube. As can be seen from the spectra shown in Figure 6.3.11 a flat-topped line is obtained after the addition of the inner tube. The flat-topped line evolves some liquid crystalline structure.
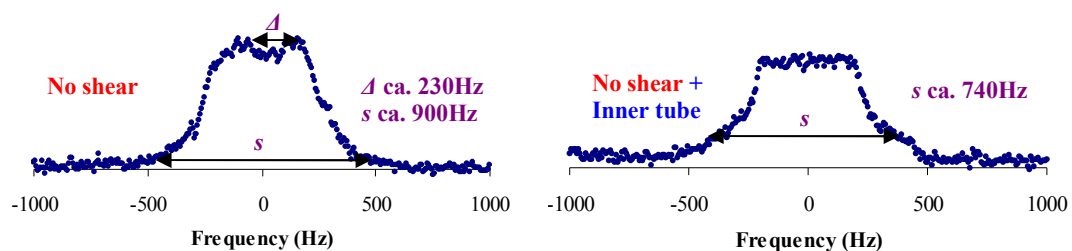
Figure 6.3.11: ^{2}H NMR spectra for the 3 wt% TSC sample at zero shear rates at a temperature of 25°C. The spectrum on the right hand recorded after gently loading the inner tube.

The relation between the size of the domains and the ^{2}H NMR line shape has been investigated by varying shear rates and shear time period. Although there is not a quantitative relation between spectrum line width and MLVs size, it is known that the line width is proportional to the MLVs size[35].

Table 6.3.2 below shows the experimental settings for each rheological run at varying shear rates and shear time period.

Experimental Conditions Sample: 3 wt%TSC		
Motor Voltage setting (V) and shear rate (s^{-1})	Time sheared for (hrs:mins)	Time relaxed for (hrs:mins)
2.5V (45s^{-1})	00:05	25:00
5V (91s^{-1})	00:05	25:00
5V (91s^{-1})	00:15	25:00
10V (182s^{-1})	00:05	25:00
10V (182s^{-1})	00:15	25:00
10V (182s^{-1})	25:00	Not recorded

Table 6.3.2: Experimental conditions for varying shear rates for the 3 wt% TSC sample at 25°C. The spectra are displayed below.

Figure 6.3.12 shows the ^{2}H NMR spectra for the sample sheared at varying shear rates for 5mins. In all the cases, the reference spectrum for the structural analysis is the spectrum recorded after loading the inner tube in the sample. The shear rates are indicated on the spectra.
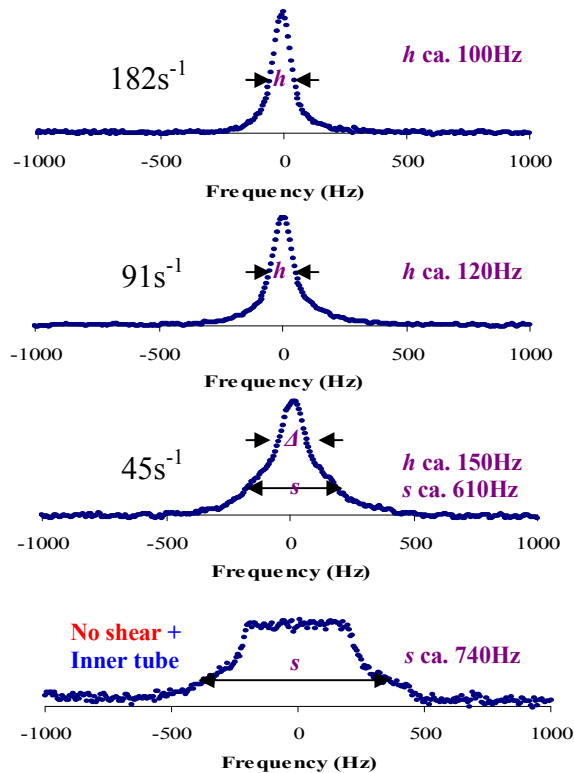
Figure 6.3.12: ^{2}H NMR spectra for the 3 wt% TSC sample sheared at different shear rates for 5mins. The shear rates (in s^{-1}) are given to the left of the spectra.

In all cases after shearing the sample the spectrum obtained is narrower than the reference spectrum. When a constant shear rate was applied to the sample, a gradual change in the ^{2}H NMR line shape recorded. The spectrum displayed for the sample sheared at 45s^{-1} shows the co-existence of a two-phase region, an isotropic peak with evidence of liquid crystalline structure towards the bottom of the peak. When the samples were sheared at 91 and 182s^{-1} respectively relatively sharper line shapes without the broad bottom were observed.

Figure 6.3.13 below shows the spectra obtained for the sample sheared at 91 and 182s^{-1} for 15mins.
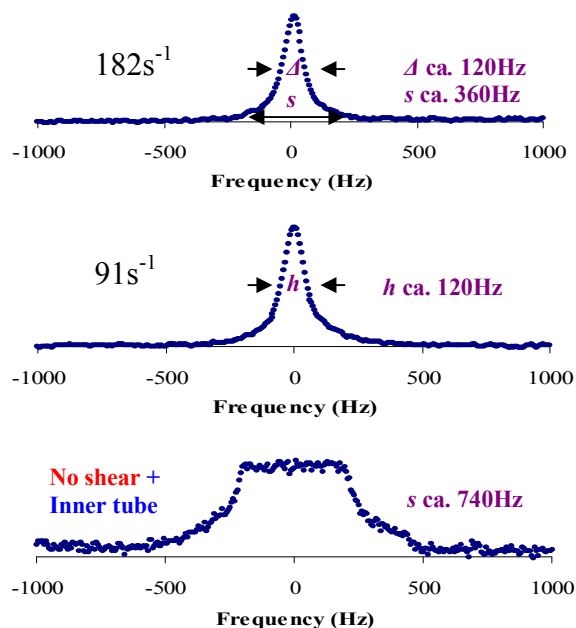
Figure 6.3.13: ^{2}H NMR spectra for the 3 wt% TSC sample sheared at different shear rates for 15mins. The shear rates (in s^{-1}) are given to the left of the spectra.

As can be seen in Figure 6.3.14 shear induced insignificant changes in the line width at half height (*h*). However, a closer inspection of the spectra reveals that after slow deformation shoulders are present in the spectrum. A possible explanation for that is the present of defects in the direction of flow. Additionally, shoulders may indicate the formation of big lamellar 'lumps' or big vesicles.
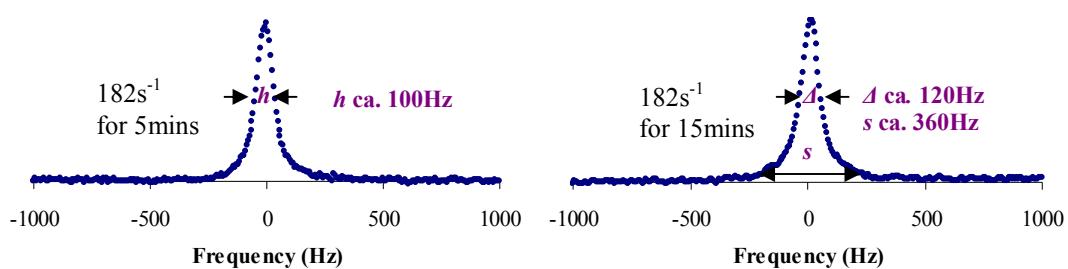
Figure 6.3.14: ^{2}H NMR spectra for the 3 wt% TSC sample sheared at 182s^{-1} for 5 and 15mins respectively.

Figure 6.3.15 and 6.3.16 show a series of ^{2}H Rheo-NMR spectra taken at varying times after shearing is stopped. The sample sheared at 91s^{-1} for 5 and 15mins respectively.

Figure 6.3.15: ^{2}H NMR spectra for the 3 wt% TSC sample sheared at 91s^{-1} for 5mins at 25°C before initiating the ^{2}H NMR experimental scans. The relaxation of the sample in hours (hrs) is indicated on the right hand side of each spectrum.

As can be seen from the spectra shown in Figure 6.3.15 a narrower single peak obtained after shearing is stopped. The single peak undergoes a continuous change of shape and its width increases upon relaxation. The changes in the line shape and the width of the peak indicate that the size of the structure is getting bigger until a final steady state is reached at ca. 25hrs. However, the recorded spectra showed that the re-formation of the structure only started, approximately, ca. 5-10hrs after shearing is stopped.

When shearing the sample at 91s^{-1} for 15mins (see Figure 6.3.16) similar spectra obtained. However, the relaxation seems to be slower after rapid deformation. The reorganisation of the structure only started, approximately, 25hrs after shearing is stopped. The line width at half height *h* remains almost unchanged upon relaxation for ca. 10hrs. The spectrum recorder after relaxing for ca. 25hrs shows a significant increase in *h* of ca. 100Hz.
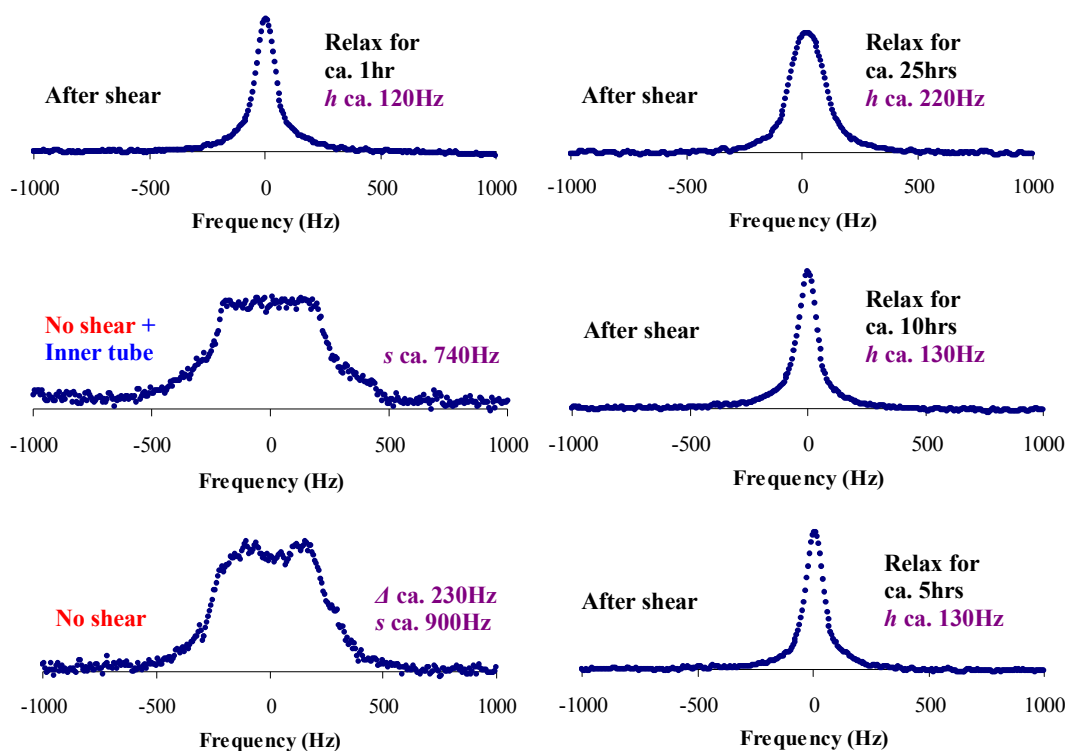
Figure 6.3.16: ^{2}H NMR spectra for the 3 wt% TSC sample sheared at 91s^{-1} for 15mins at 25°C before initiating the ^{2}H NMR experimental scans. The relaxation of the sample in hours (hrs) is indicated on the right hand side of each spectrum.

Upon increase of the shear rate to 182s^{-1} for 5mins a single narrow line is observed after relaxing for 1hr (see Figure 6.3.17). The structural relaxation was found to be considerably fast, approximately, 5hrs after shearing is stopped. Comparing the spectra recorded when the sample sheared at low (91s^{-1}) and high (182s^{-1}) shear rate for 5mins it can be concluded that the shear rates influence the relaxation process. Hence, the stability of the shear induced structure.
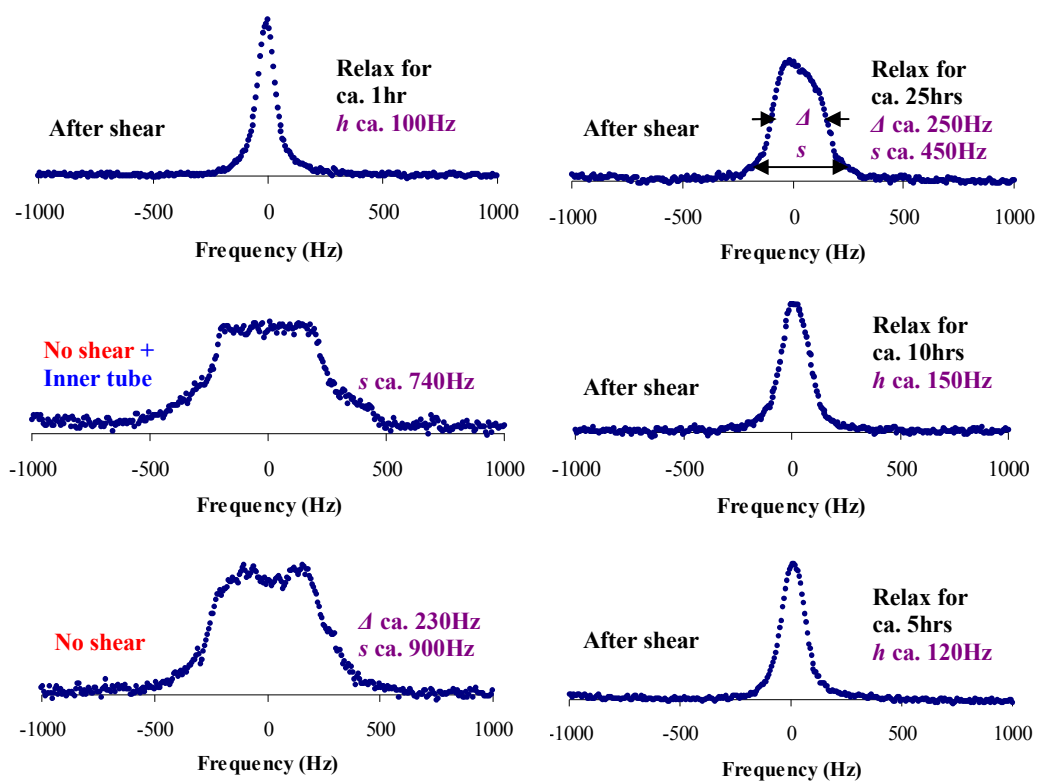
Figure 6.3.17: ^{2}H NMR spectra for the 3 wt% TSC sample sheared at 182s^{-1} for 5mins at 25°C before initiating the ^{2}H NMR experimental scans. The relaxation of the sample in hours (hrs) is indicated on the right hand side of each spectrum.

Similar changes in the ^{2}H NMR line shapes are shown in Figure 6.3.18. The spectra obtained after shearing is stopped. The sample was sheared at 182s^{-1} for 15mins.
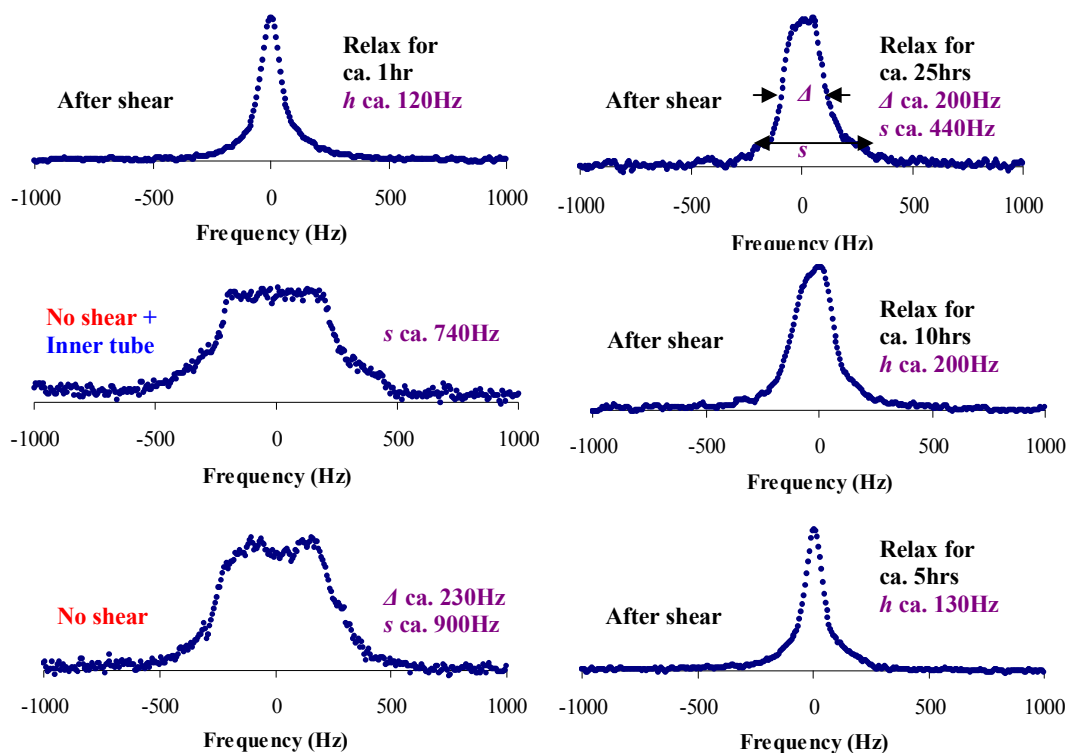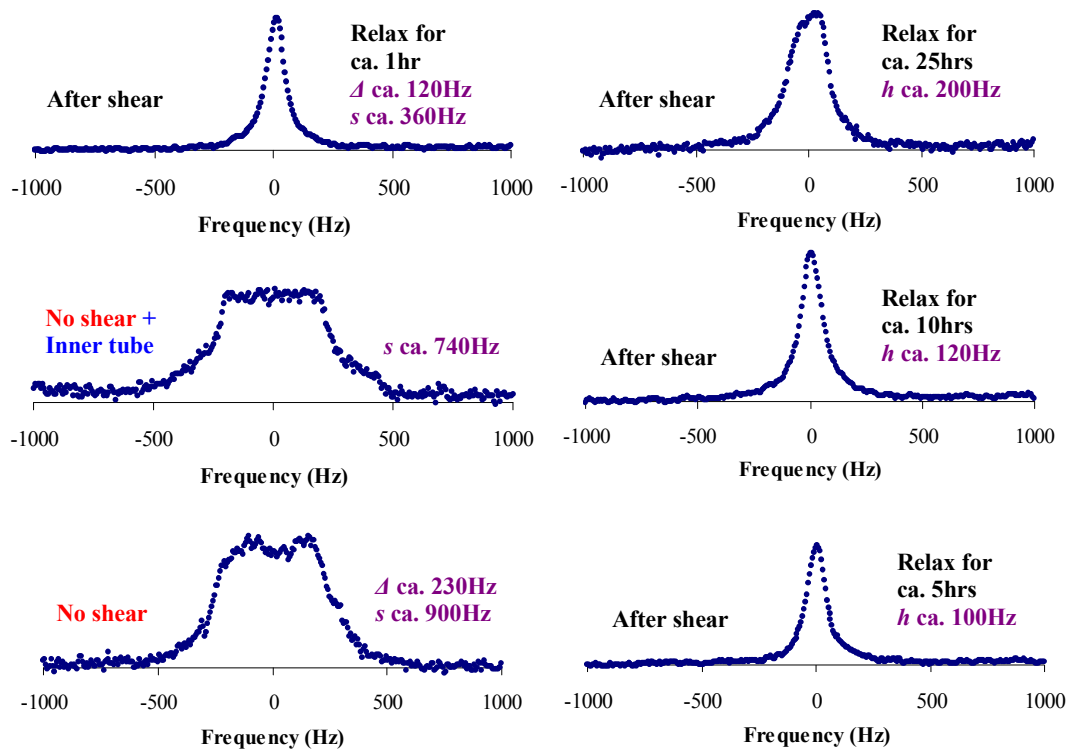
Figure 6.3.18: ^{2}H NMR spectra for the 3 wt% TSC sample sheared at 182s^{-1} for 15mins at 25°C before initiating the ^{2}H NMR experimental scans. The relaxation of the sample in hours (hrs) is indicated on the right hand side of each spectrum.

When scans performed during the application of a shear rate of 182s^{-1} to the sample for 25hrs (see Figure 6.3.19) significant changes in the ^{2}H NMR line shapes were recorded. After shearing for ca. 1hr a single peak appears with the shoulder singularities indicate the anisotropy of the motions of the water molecules. When further shearing for ca. 10hrs a broader line shape is observed. An increase in the line width at half height of ca. 70Hz is noted. After ca. 25hrs shearing the recorded spectrum shows a flat-topped line with an *h* at ca. 270Hz.
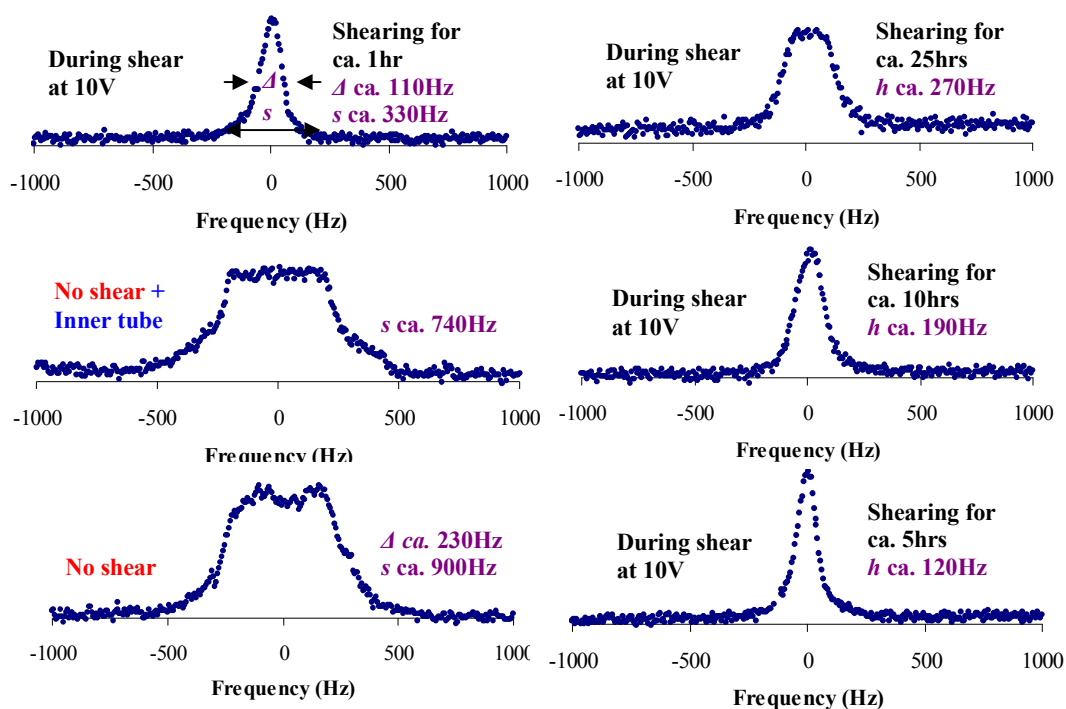
Figure 6.3.19: ^{2}H NMR spectra for the 3 wt% TSC sample sheared at 182s^{-1}. The scans performed during the application of shear for 25hrs.

A reasonable explanation for the differences in half height line widths after relaxation is related to the polydispersity of the domain size.

^{2}H Rheo-NMR results for the 5 wt% TSC sample

The ^{2}H NMR spectrum obtained for the 5 wt% TSC sample displayed in Figure 6.3.20 shows evidence of both the isotropic peak and the beginning of the formation of a broad base peak. This line shape corresponds to a two-phase region of vesicles/liposomes and excess isotropic solution.

Before any ^{2}H Rheo-NMR experiment the effect of the added inner tube on the ^{2}H NMR line shape was investigated. The inner tube was gently loaded in the sample and scans were recorded over 2 days. Figure 6.3.20 shows the spectra obtained before and after the addition of the inner couette tube.
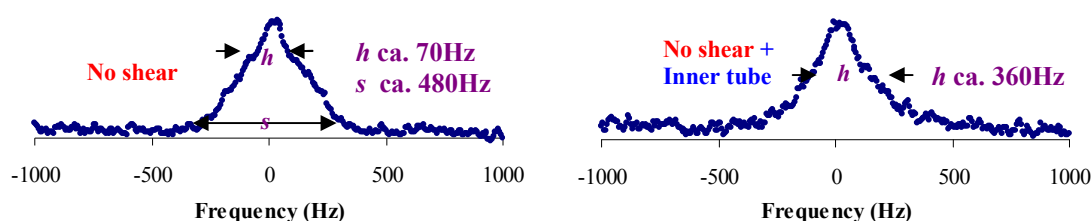
Figure 6.3.20: ^{2}H NMR spectra for the 5 wt% TSC sample at zero shear rates at a temperature of 25°C. The spectrum on the right hand recorded after gently loading the inner tube.

The spectrum obtained after gently loading the inner tube is slightly different than before. The isotropic peak at the top of the peak is not as distinct as before. This can be a consequence of a change in the degree of order in the domains or a change in the domain size.

Different shear rates applied to the sample over different shear time period to investigate the effect of shear on the NMR line shape thus if vesicles formed indeed, and the polydisperisty of the MLVs.

Table 6.3.3 below shows the experimental settings for each rheological run at varying shear rates and time period.

Experimental Conditions Sample: 5 wt%TSC		
Motor Voltage setting (V) and shear rate (s^{-1})	Time sheared for (hrs:mins)	Time relaxed for (hrs:mins)
2.5V (43s^{-1})	00:05	25:00
5V (86s^{-1})	00:05	25:00
5V (86s^{-1})	00:15	25:00
10V (173s^{-1})	00:05	25:00
10V (173s^{-1})	00:15	25:00
10V (173s^{-1})	25:00	Not recorded

Table 6.3.3: Experimental conditions for varying shear rates for the 5 wt% TSC sample at 25°C. The spectra are displayed below.

Shown in Figure 6.3.21 are the ^{2}H NMR spectra for the sample sheared at varying shear rates for 5mins. In all the cases, the reference spectrum for the structural analysis is the spectrum recorded after loading the inner tube in the sample. The shear rates are indicated on the spectra.
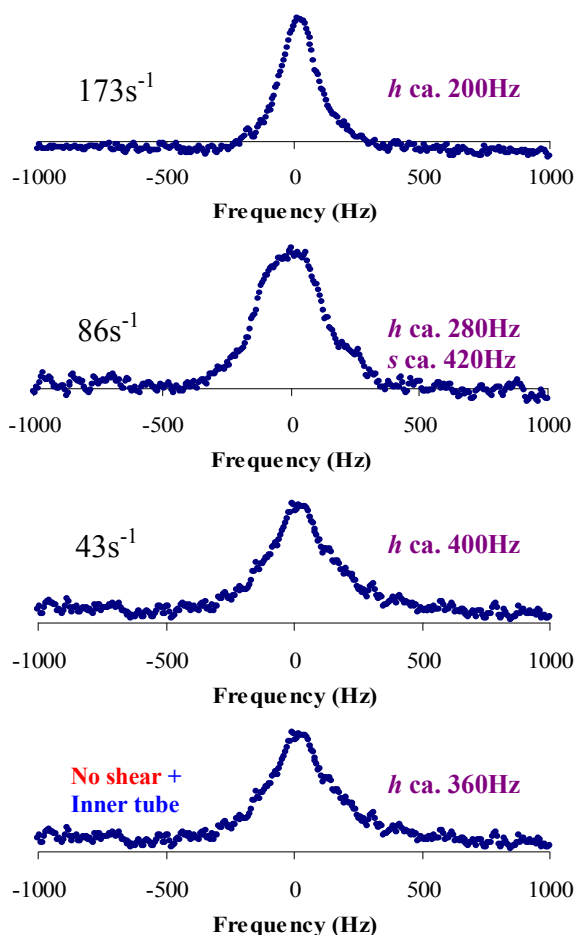
Figure 6.3.21: ^{2}H NMR spectra for the 5 wt% TSC sample sheared at different rates for 5mins. The shear rates (in s^{-1}) are given to the left of the spectra.

From the spectra displayed in Figure 6.3.21 it is evident that shear induced changes in the domain size as can be observed from the differences in h values. When the sample sheared at 43s^{-1} a similar line width is observed. Upon increasing the shear rate to 86s^{-1} changes in h values were observed and shoulders appeared indicating the larger structures formed. Upon further increase of the shear rate up to 173s^{-1} a narrower peak appears and a decrease in h is observed. The further decrease of h as seen in Figure 6.3.21 can be due to further decrease of the vesicle size at higher shear rates.

However, not only the shear rate but also shear time period has an effect on the ^{2}H NMR line shape. Figure 6.3.22 shows the spectra obtained at varying shear rates when the sample sheared for 15mins.
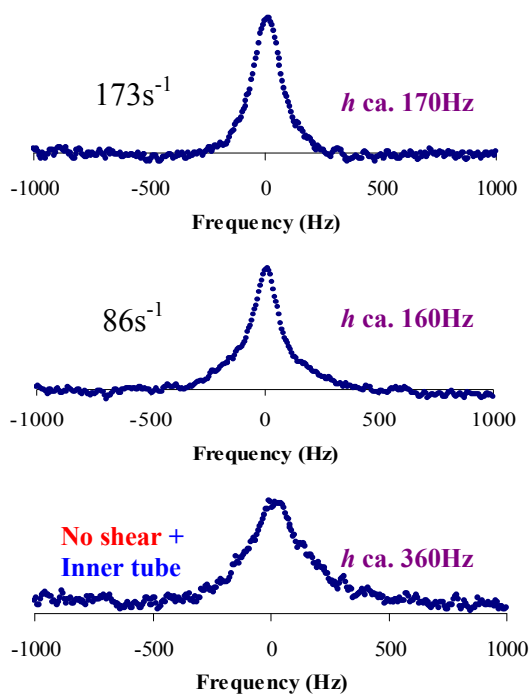
Figure 6.3.22: ^{2}H NMR spectra for the 5 wt% TSC sample sheared at different shear rates for 15mins. The shear rates (in s^{-1}) are given to the left of the spectra.

Comparing the spectra obtained after shearing the sample for 5 and 15mins (see Figure 6.3.21 and 6.3.22) a decrease in h is observed when the sample sheared at 86s^{-1} for 15mins. On the other hand, no significant changes observed when the sample sheared at 173s^{-1} for 5 and 15mins. This confirms the notion that at lower shear rates shear needs to be applied for longer.

The shear induced structures, however, are not stable as can be concluded from the ^{2}H NMR line shape occur in time evidencing the structural relaxation towards the two-phase region. Figure 6.3.23 shows the spectra obtained for the sample sheared at 86s^{-1} for 5mins. The spectra were recorded after shearing is stopped.

Figure 6.3.23: ^{2}H NMR spectra for the 5 wt% TSC sample sheared at 86s^{-1} for 5mins at 25°C before initiating the ^{2}H NMR experimental scans. The relaxation of the sample in hours (hrs) is indicated on the right hand side of each spectrum.

The first spectrum obtained 1hr after shearing is stopped shows a broad single peak of *h* at ca. 280Hz. A broad base is apparent in the spectrum that remains upon relaxation. After relaxing for ca. 5hrs insignificant changes are observed. However, the recorded spectra showed that the re-arrangements in the structure to relax back started, approximately, 10hrs after shearing is stopped. The spectral line shape recorded after relaxing for 25hrs indicates a two-phase region thus vesicles and an excess isotropic phase. It is important to note that the broad base remains unchanged upon relaxation. This suggests that there are insignificant changes in the liquid crystalline phase.

Shown in Figure 6.3.24 are the spectra obtained for the sample sheared at 86s^{-1} for 15mins. The spectra were recorded after shearing is stopped.
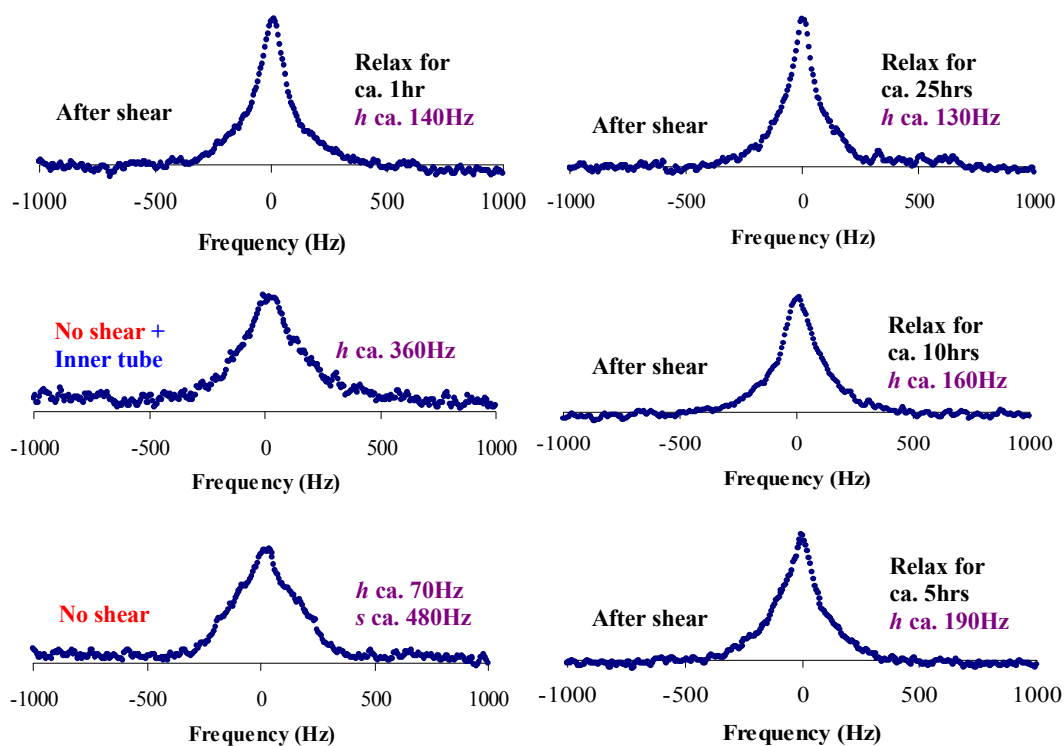
Figure 6.3.24: ^{2}H NMR spectra for the 5 wt% TSC sample previously sheared at $86s^{-1}$ for 15mins at 25°C before initiating the ^{2}H NMR experimental scans. The relaxation of the sample in hours (hrs) is indicated on the right hand site of each spectrum.

Figure 6.3.24 shows that the application of shear for 15mins results in insignificant changes in *h* values. Moreover, during relaxation insignificant changes in *h* are observed. The spectral line shape displayed in Figure 6.3.24 suggest that after shearing is stopped the shear-induced structure consists of small spherical domains and the broad base indicates that some liquid crystalline phase is present.

The spectra recorded when the sample was sheared at $173s^{-1}$ for 5mins are shown in Figure 6.3.25.
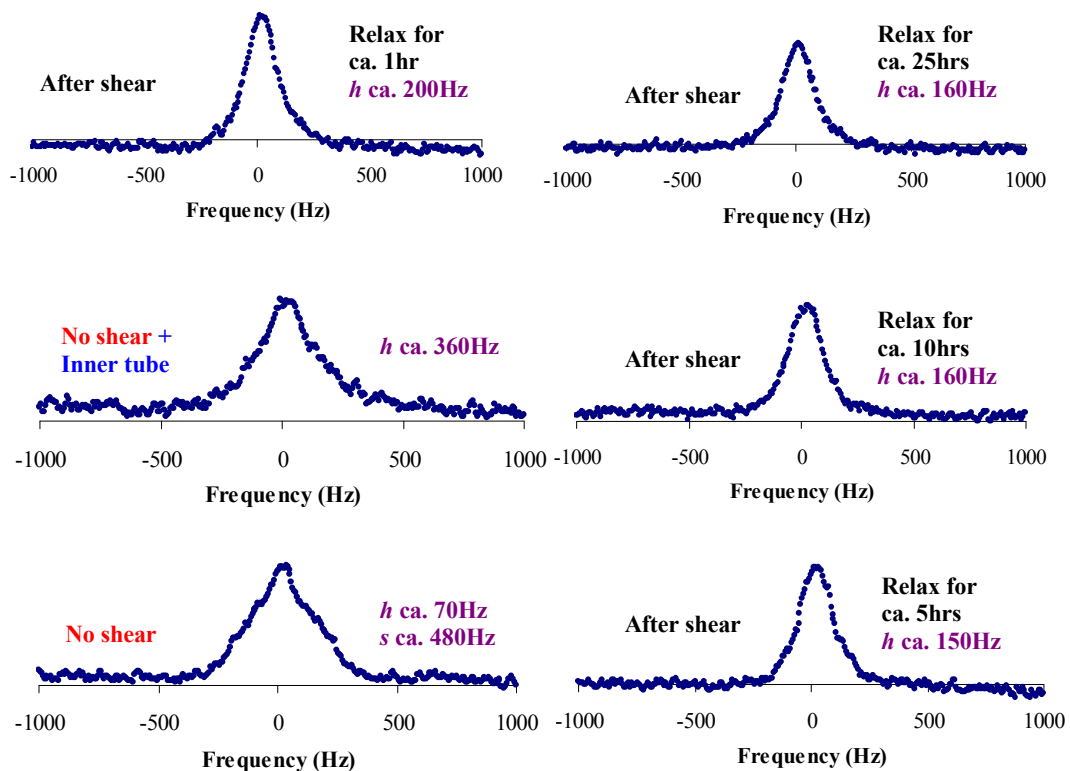
Figure 6.3.25: ^{2}H NMR spectra for the 5 wt% TSC sample sheared at 173s^{-1} for 5mins at 25°C before initiating the ^{2}H NMR experimental scans. The relaxation of the sample in hours (hrs) is indicated on the right hand side of each spectrum.

The spectral line shapes shown in Figure 6.3.25 suggest that the shear induced a stable structure. Small changes are observed in *h* values upon relaxation. Additionally, the ^{2}H NMR line shape changes slightly on the top of the peak upon relaxation.

When the sample sheared at 137s^{-1} for 15mins different results can be seen upon relaxation (see Figure 6.3.26). A narrow peak is observed after relaxing for ca. 1hr that is gradually transformed to a broad peak, approximately, ca. 10hrs after shearing is stopped.
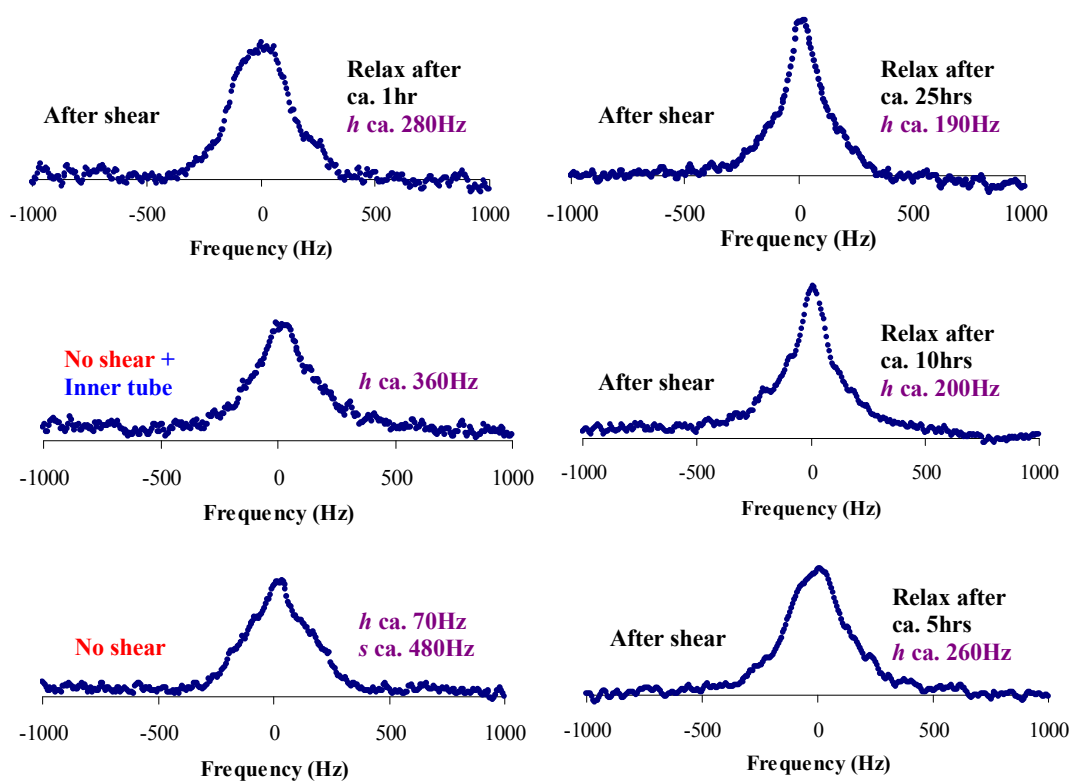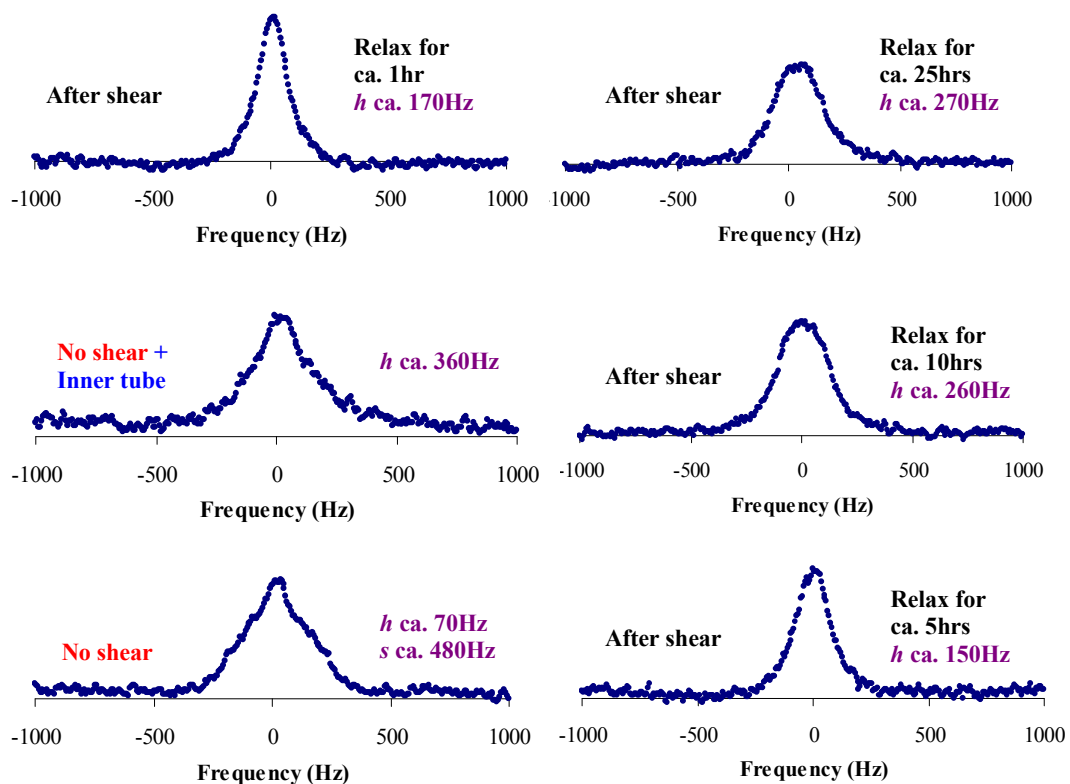
Figure 6.3.26: ^{2}H NMR spectra for the 5 wt% TSC sample sheared at 173s^{-1} for 15mins at 25°C before initiating the ^{2}H NMR experimental scans. The relaxation of the sample in hours (hrs) is indicated on the right hand side of each spectrum.

The results listed above for the 5 wt% TSC sample confirms the notion that higher shear rates are required for high viscosity samples or shear needs to be applied for longer.

In order to understand the effect of shear time on the ^{2}H NMR line shape scans were performed during shear application for 25hrs. The spectra obtained are displayed in Figure 6.3.27.
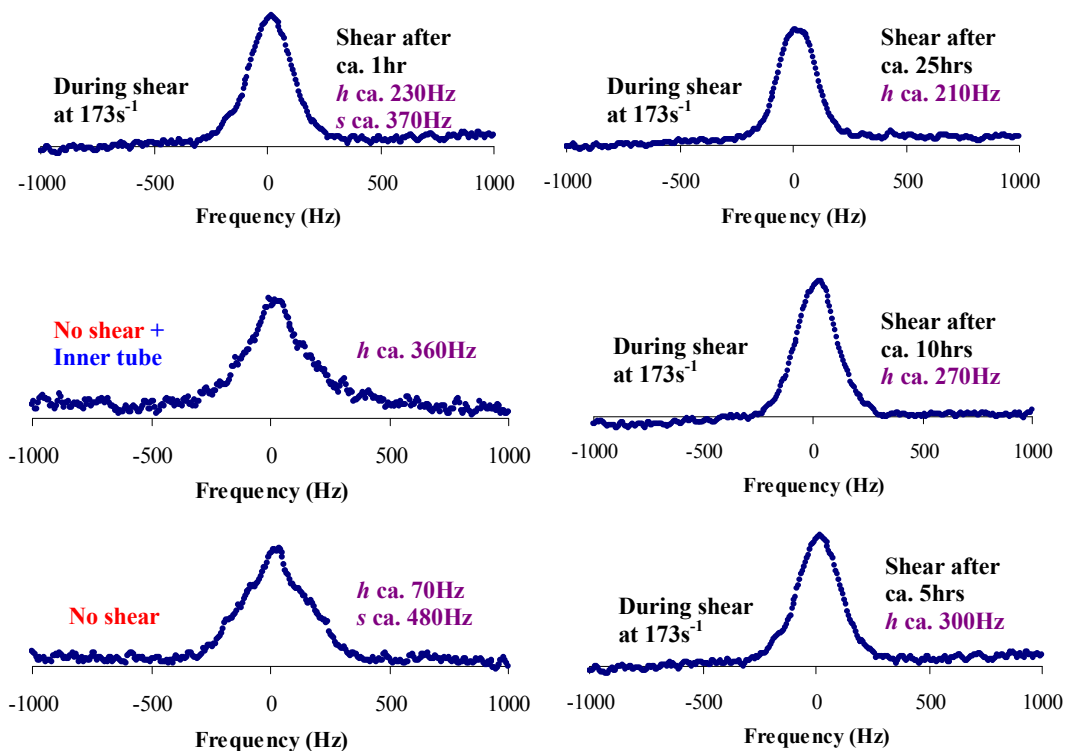
Figure 6.3.27: ^{2}H NMR spectra for the 5 wt% TSC sample sheared at 173s^{-1}. The scans performed during the application of shear for 25hrs.

There are insignificant changes in *h* when a shear rate of 173s^{-1} is applied for 25hrs as shown in Figure 6.3.27. However, the overall ^{2}H NMR line shape during shear has changed to a single broad line. The isotropic peak with the broad base vanishes after shearing for ca. 1hr.

It is important to mention that a separation of the spectral line shape into different components is not observed during the application of shear or even after 2days relaxation. This indicates that the sample remains homogeneous, as opposed to the two-phase line shape observed before the application of shear.

All the results shown so far are highly reproducible if the same raw materials and shear history are applied.

6.3.4 Discussion

The relation between shear and changes in conformation and orientation of the domains can be extended with ^{2}H Rheo-NMR studies. ^{2}H Rheo-NMR experiments have been performed in order to understand how the mesophase structure is affected by shear flow. The ^{2}H NMR line shape and the characteristic values obtained from the spectra have been used to obtain information regarding the effect of shear rate and shear time on the lamellar structure. Any changes in the ^{2}H NMR line shape are discussed in terms of mesophase structure, shear alignment and structural reorganization.

^{2}H Rheo-NMR discussion for the 0 wt% TSC sample

For all the samples spectra were taken before and after adding the inner tube to note any changes caused by the extensional force exerted onto the sample. As can be seen from the changes in ^{2}H NMR line shape after loading the inner tube, shown in Figure 6.3.2, the extensional force exerted onto the sample causes dramatic changes of the director distribution fraction. The intensity of the shoulders becomes more visible at the maximum quadrupole splitting, corresponding to $\theta = 0°$, suggesting that after loading the inner tube more layers become aligned with their normal axis parallel to the magnetic field. A closer inspection of the ^{2}H NMR spectra in Figure 6.3.2 reveals that the inner splitting becomes smaller. This decrease of the motionally averaged coupling indicates that the water molecules probe a more curved surface by their lateral diffusion in the hydrophilic layer. This can be due to the presence of defects or to an increase of undulation of the bilayers as the inner tube is loaded in the sample.

From the ^{2}H NMR line shapes measured at different shear rates we can clearly distinguish three different shear induced states (see Figure 6.3.3). The first shear induced states show a preferred orientation of the lamellar with the layer normal perpendicular to the magnetic field thus leads to the inner splitting. This alignment is observed for the sample when sheared at 68s^{-1}. At intermediate shear rates (137s^{-1}) the spectrum distinct features became less obvious. This can be due to the presence of defects in the shear induced structure or due to some bilayers fold to form liposomes. At higher shear rated, (274s^{-1}), a gradual transformation to a new line shape is observed and its features become less distinct. This shear induced state can be due to the formation of vesicles at high shear rate. Vesicles have strong curvature and so the diffusion of water molecules along the bilayers have a rotary

component which has previously been noted to have a dramatic effect on the ^{2}H NMR line shape with a decrease or vanishing of the splitting[36-38]. Lukaschek and co-workers proposed that the observed relatively broad but featureless lines are due to the formation of large multilamellar vesicles. A distribution of averaged quadrupole splittings is expected for large MLVs thus while diffusion in the inner shells leads to isotropic averaging, diffusion in the outer shells covers only part of the vesicle bilayer leads to a residual splitting. Consequently, it is reasonable to believe that the broad featureless lines are superposition of spectra with different splittings.

The ^{2}H NMR line shapes shown in Figures 6.3.7 and 6.3.9 suggest a continuous relaxation process from vesicles to planar lamellar with less defects and dislocations. The observed fast relaxation gives indication of something less organised and unstable.

^{2}H Rheo-NMR discussion for the 3 wt% TSC sample

From the ^{2}H NMR line shape measured for the 3 wt% TSC sample after gently loading the inner tube a flat-topped line can be observed (see Figure 6.3.11). It is noteworthy that the lack of splittings and the shoulders *s* can be due to a polydomain structure. The lack of splitting may be due to different degrees of order in different domains that are aligned parallel to the magnetic field. Another reasonable explanation for the lack of splitting is related to the formation of large MLVs.

All results taken from ^{2}H NMR line shapes measured during and after shearing the sample show the development of new shear induced structures. The exact nature of the structures is not known, but there is some evidence that MLVs aligned parallel to the direction of flow may be involved. Our results suggest that the formation of MLVs is dependent on shear rate and shear time period. At low shear rate (see Figure 6.3.12) the structure break to a polydomain structure as suggested from the spectrum obtained at 45s^{-1}. The ^{2}H NMR line shape indicates that vesicles are present with different sizes. Another possible explanation for the ^{2}H NMR line shape is the co-existence of vesicles and excess isotropic solution. At higher shear rates sharper lines are observed. This suggests that the formation of vesicles as well as the vesicle size is controlled by shear rate. This was also observed by Roux and co-workers who found that the vesicle diameter scales with shear rate inverse square root. The decrease of the size under increasing shear rate has also been observed by Bergmeier *et al*[39].

The data collected upon structural relaxation are crucially dependent on the initial shear induced structure. Upon relaxation broader lines are observed. A reasonable explanation is related to polydispersity. Theoretical studies, done by Ramos *et al*[40] argue about the possibility of having vesicles arranged in such an array where small MLVs fill the free space between big MLVs. This polydispersed array is known as the 'Apollonian packing'.

<u>^{2}H Rheo-NMR discussion for the 5 wt% TSC sample</u>

It has already been established that the bell-like line shape observed in the spectrum for the 5 wt% TSC sample indicates the transformation to a different microstructure rather than the planar lamellar bilayers.

Rheo-NMR data suggest that the shear rate has an effect on the domain size. At low shear rate ($43s^{-1}$) a two-phase region is observed indicate that the shear rate or the shear time period is not sufficient to induce any changes in the sample. At intermediate shear rates ($86s^{-1}$) a broad line is observed indicates changes in the domain size or a polydispersed vesicle phase. At higher shear rates ($173s^{-1}$) a narrower line is observed which can be due to smaller vesicles. In agreement with previous work done by other groups, we find that the vesicle size is controlled by shear rate[34, 35, 41]. The MLVs formed at higher shear rate are smaller than the ones formed at the lower shear rate as demonstrated by the ^{2}H NMR narrower line shapes shown in Figure 6.3.21. These results parallel the findings of Roux and co-workers[21] who found that in a certain range of shear rate the lamellar phase of various systems organizes into spherical MLVs of well-controlled size.

6.4 Summary

In this Chapter the rheological behaviour of the 0, 3 and 5 wt% TSC samples was investigated. A range of techniques, including, Linkam optical shear cell, rheometer and ^{2}H Rheo-NMR spectroscopy was used to determine the microstructure of the shear induced states. The rheological characterisation involved fundamental experiments investigating the effect of shear rate, shear time and age on the lamellar microstructures. In addition, the reorganisation of the structures after the application of shear was studying by ^{2}H Rheo-NMR spectroscopy.

Coupling the results from shear studies it can be said that the basic microstructure of the electrolyte free system is a single lamellar phase with a random distribution of planar, partially flexible sheets and defects. These sheets, which are stacks of bilayers, slide against one another when shear applied into the system. Optical shear cell textures suggest shear slowly induces changes in morphology from very large domains (extended bilayers) to liposomes. At high shear rates stripes observed in the optical textures which are parallel lines of liposomes.

In the context of the rheological characterisation of the electrolyte free system it was shown that at low shear rates the structure reorganises and orients to the direction of shear. At intermediate shear rates it seems likely that once the orientation is sufficient the structure brakes down and reaches a shear thinning regime. In this regime the bilayers would slide against one another and it is seems likely as shown from Rheo-NMR analysis that some bilayers fold to form vesicles/liposomes. At higher shear rates it is believed that large vesicles are formed and their size and polydispersity are shear rate and shear time dependent.

From the results listed in Chapter 5 it seems likely that the 3 wt% TSC sample consists of large liposomes. During shear process at low shear rates these large domains can accommodate the applied shear stresses. At intermediate shear rates the co-existence of liposomes of different sizes was evidenced. At higher shear rates liposomes became smaller and so the sample no longer shows birefringence. Rheo-NMR results suggested that the size of the vesicles is shear rate and shear time dependent. These results are in a good agreement with the work done by Zipfel *et al*[17] suggesting that the vesicle size depends on the shear rate.

Similar behaviour was observed for the 5 wt% TSC sample which was established as a lamellar dispersion (see Chapter 5). The Rheo-NMR studies revealed that the size and the polidispersity of the vesicles formed after the application of shear are again shear rate and shear time dependent. Flow curve analysis show two-Newtonian plateaus indicating that the system is a lamellar dispersion possibly consists of large vesicles and excess isotropic solution.

Overall, our results from shear studies highlight the importance of the microstructure's morphology. The hypothesis put forward is that transitions between higher and lower viscosity states are related to changes from a defective layered lamellar to liposomes. The size of the liposomes is shear rate and shear time dependent. With Rheo-NMR experiments we have shown that the structure reorganises after the application of shear however never reaches the original state (structure before the application of shear).

An important result is that the aging process appears to have little influence on the rheological behaviour of the 0 and 3 wt% TSC samples. However, the flow curve recorded for the 5 wt% TSC sample (5 months aged) shown significant deviation from the flow curve recorded for the fresh sample. Thus changes in the size of the domains in the lamellar dispersion. This parallel the results from studies of the aging effect on the ^{2}H NMR spectral line shape discussed in Section 5.3.

6.5 References

1.   Diat, O., Roux, D., Nallet, F., Effect of shear on a lyotropic lamellar phase *Journal de Physique II* **1993,** 3, (9), 1427.

2.   Penfold, J., Staples, E., Lodhi, A. K., Tucker, I., Tiddy, G. J. T. , Shear-Induced Transformations in the Lamellar Phase of Hexaethylene Glycol Monohexadecyl Ether. *Journal of physical chemistry* **1997,** 101, (1), 66-72.

3.   Chen, Z. R., Issaian, A. M., Kornfield, J. A., Smith, S. D., Grothaus, J. T., Satkowski, M. M., Dynamics of Shear-Induced Alignment of a Lamellar Diblock: A Rheo-optical, Electron Microscopy, and X-ray Scattering Study. *Macromolecules* **1997,** 30, 7096-7114.

4.   Chen, Z. R., Kornfield, J., Smith, S., Grothaus, J., Satkowski, M., Block Copolymers Pathways to Macroscale Order in Nanostructured. *Science* **1997,** 277, 1248.

5.   Franco, J. M., Munoz, J., Gallegos, C., Transient and Steady Flow of a Lamellar Liquid-Crystalline Surfactant/Water System. *Langmuir* **1995,** 11, (2), 669-673.

6.   Alcantara, M. R., Vanin, J. A., Rheological properties of lyotropic liquid crystals. *Colloids and Surfaces, A: Physicochemical and Engineering Aspects* **1995,** 97, (2), 151-156.

7.   Valiente, M., Influence of a cationic surfactant on the phase behavior of C12E4 /hexanol /water system at low surfactant concentration. *Colloids and Surfaces, A: Physicochemical and Engineering Aspects* **1995,** 105, 265-275.

8.   Lauger, J., Weigel, R., Berger, K., Hiltrop, K., Richtering, W., Rheo-small-angle-Light-Scattering Investigation of Shear-Induced Structural Changes in a Lyotropic Lamellar Phase. *Journal of Colloid and Interface Science* **1996,** 181, 521-529.

9.   Läugera, J., Weigela, R., Bergerb, K., Hiltropb, K., Richtering, W., Rheo-small-Angle-Light-Scattering Investigation of Shear-Induced Structural Changes in a Lyotropic Lamellar Phase *Journal of Colloid and Interface Science* **1996,** 181, (2), 521-529.

10.   Fischer, P., Schmidt, C., Finkelmann, H., Amphiphilic liquid-crystalline networks - phase behavior and alignment by mechanical fields. *Macromolecular rapid communication* **1995,** 16, (6), 435-447.

11.   Gleeson, H. In *The Physics of Liquid Crystals*, British Liquid Crystal Society, Hull, 2003; Hull, 2003.

12.   Stein, R. S., Wilson, P. R., Scattering of light by polymer films possessing correlated orientation fluctuations. *Journal of Applied Physics* **1962,** 33, 1914-1922.

13.   Sierro, P., Roux, D., Structure of a Lyotropic Lamellar Phase under Shear. *Physical Review Letters* **1997,** 78, 1496-1499.

14.   Bergmeier, M., Gradzielski, M., Hoffmann. H., Mortensen, K. , Behaviour of a Charged Vesicle System under the Influence of a Shear Gradient: A Microstructural Study. *Journal of physical chemistry* **1998,** 102, (16), 2837-2840.

15.   Gustafsson, J., Orädd, G., Nyden, M., Hansson, P., Almgren, M., Defective Lamellar Phases and Micellar Polymorphism in Mixtures of Glycerol Monooleate and Cetyltrimethylammonium Bromide in Aqueous Solution. *Langmuir* **1998,** 14, (18), 4987-4996.

16.   Diat, O., Roux, D., Nallet, F., "Layering" effect in a sheared lyotropic lamellar phase. *Physical Review E: Statistical Physics, Plasmas, Fluids, and Related Interdisciplinary Topics* **1995,** 51, 3296-3299.

17.   Berghausen, J., Zipfel, J., Lindner, P., Richtering, W., Shear-induced orientations in a lyotropic defective lamellar phase. *Europhysics Letters* **1998,** 43, (6), 683-689.

18.   Zipfel, J., Berghausen, J., Lindner, P., Richtering, W., Influence of Shear on Lyotropic Lamellar Phases with Different Membrane Defects. *Journal of Physical Chemistry B* **1999,** 103, (15), 2841-1849.

19.   Barnes, H., Hutton, J. F., Walters, K., *An Introduction to Rheology*. Elsevier: New York, 1989.

20.   Barnes, H. A., *A Handbook of Elementary Rheology*. Instiute of Non-Newtonian Fluid Mechanics, University of Wales: Aberystwyth, 2000.

21.   Diat, O., Roux, D., Nallet, F., Effect of shear on a lyotropic lamellar phase. *Journal de Physique II* **1993,** 3, (9), 1427.

22.   Zilman, A. G., Granek, R., Undulation instability of lamellar phases under shear: A mechanism for onion formation? *European Physical Journal B: Condensed Matter Physics* **1999,** 11, (4), 593-608.

23.   Dimitrova, G. T., Tadros, F., Luckham, P. F., Kipps, M. R. , Investigations into the Phase Behavior of Nonionic Ethoxylated Surfactants Using 2H NMR Spectroscopy. *Langmuir* **1996**, 315-318.

24.   Alfaro, M. C., Guerrero, A., Munoz, J., Dynamic Viscoelasticity and flow behaviour of a Polyoxyethylene Glycol Nonylphenyl Ether/toluene/water system. *Langmuir* **2000,** 16, 4711-4719.

25.   Horanyi, T., Halasz, L., Palinkas, J., Nemeth, Z., Relationship between Optical and Rheological Properties of Polymer-Added Lamellar Liquid-Crystalline Systems. *Langmuir* **2004,** 20, (5), 1639-1646.

26.   Oliviero, C., Coppola, L., Gianferri, R., Nicotera, I., Olsson, U., Dynamic phase diagram and onion formation in the system C10E3/D2O. *Colloids and Surfaces A: Physicochemical and Engineering Aspects* **2003,** 228, (1-3), 85-90.

27.   Cordobes, F., Franco, J.M., Gallegos, C., Rheology of the lamellar liquid-crystalline phase in polyethoxylated alcohol/water/hetane systems. *Grasas y Aceites* **2005,** 56, 96 -105.

28.   Doi M., Edwards, S. F., *The theory of polymer dynamics*. Oxford University Press: Oxford, 1987.

29.   Marrucci, G., Rheology of liquid crystalline polymers. In *Theodretical Challenges in the dynamics of Complex Fluid*, Mcleish, T., Ed. Kluwer Press: Dordrect, 1997; pp 141-158.

30.   Callaghan, P. T., Rheo-NMR. In *Modern Magnetic Resonance* Publisher Springer Netherlands MacDiarmid Institute for Advanced Materials and Nanotechnology, Victoria University of Wellington, New Zealand, 2006; pp 383-388.

31.   Siebert, H., Grabowski, D. A., Schmidt, C., Rheo-NMR study of a non-flow-aligning side-chain liquid crystal polymer in nematic solution *Rheologica Acta* **1997,** 36, 618.

32.   Dutton, H. M. The behaviour of surfactant lamellar and gel phases under flow. The University of Manchester, Manchester, 2007.

33.   Callaghan, P., Rheo-NMR: A New Window on the Rheology of Complex Fluids. In Grant, D. M., Harris, R. K., Ed. John Wiley and Sons: Chichester, 2002.

34.   Lukaschek, M., Grabowski, D. A., Schmidt, C., Shear-Induced Alignment of a Hexagonal Lyotropic Liquid Crystal as Studied by Rheo-NMR. *Langmuir* **1995,** 11, 3590-3594.

35.   Schmidt, G., Muller, S., Schmidt, C., Richtering, W., Rheo-optical investigations of lyotropic mesophases of polymeric surfactants. *Rheologica Acta* **1999,** 38, (6), 486-494.

36.   Heaton, N. J., Althoff, G., Kothe, G., Observation of lateral diffusion in biomembranes by excitation transfer P-31 NMR: Estimtion of vesicle size distributores. *Journal of physical chemistry* **1996,** 10, 4944-4953.

37.   Blum, F. D., Franses, E. I., Rose, K. D., Bryant, R. G., Miller, W. G., Structure and Dynamics in Lamellar Liquid Crystals. Effect of Agitation and Aging on Deuterium NMR Line Shapes. *Langmuir* **1987,** 3, (4), 448-452.

38.   Filippelli, L. M., B., Rossi, C. O., Miguel, M. G., Olsson, U., Metastability of Multi-Lamellar Vesicles in a Nonionic System. *Molecular Crystals and Liquid Crystals* **2009,** 500 166-181

39.   Dhez, O., Nallet, F., Diat, O., Influence of screw dislocations on the orientation of a sheared lamellar phase. *Europhysics Letters* **2001,** 55, 821-826.

40.   Ramos, L., Roux, D., Olmsted, P. D., Cates, M. E., Equilibrium onions? *Europhysics Letters* **2004,** 66, (6), 888-894.

41.   Auguste, F., Douliez, J. P., Bellocq, A. M., Dufourc, E. J., Gulik-Krzywicki, T., Evidence for Multilamellar Vesicles in the Lamellar Phase of an Electrostatic Lyotropic Ternary System. A Solid State 2H-NMR and Freeze Fracture Electron Microscopy Study. *Langmuir* **1997,** 13, 666-672.

Chapter 7

Conclusions and Future Work

The overall aim of this thesis was to develop a better understanding between the microstructure and the rheology of mixed surfactant lamellar systems. The results have already been summarised throughout this thesis (at the end of Chapter 5 and 6). This Chapter will therefore attempt to draw overall conclusions from the work carried out and make suggestions for future work in this area. Future work will be discussed in Section 7.2.

7.1 Conclusions

During the course of this work we have investigated the effects of electrolyte concentration, temperature, age and shear on the lamellar phase microstructure. The detailed characterisation of the mixed surfactant systems has led to an understanding of the complex lamellar microstructure.

7.1.1 Static studies

Optical microscopy and SAXS studies give clear evidence of the existence of the lamellar phase in the systems in question. Our results reveal that the lamellar phase microstructure depending on the salt level may form a single layered lamellar or a lamellar dispersion. A crucial feature from SAXS data is that the *d*-spacing for the 0, 1 and 3 wt% TSC samples are nearly identical but the *d*-spacing for the 5 wt% TSC sample is 7Å smaller than the electrolyte free system.

Based on the ^{2}H NMR spectral line shape analysis it was shown that upon addition of salt changes in the lamellar phase microstructure occurred. These changes can be explained in terms of a continuous transition to a lamellar microstructure with stronger interface curvature followed by a two-phase lamellar dispersion consisting of vesicles and excess micellar solution. ^{2}H NMR spectroscopy identified the onset to a curved lamellar phase (~2.5 wt% TSC) and a lamellar dispersion phase (~4.5 wt% TSC) upon addition of electrolyte to the system. By combining the results from SAXS and NMR we assume that

the decrease in *d*-spacing and the collapse of the deuterium powder pattern is due to the formation of vesicles.

The possible explanations put forward for this transition has to do with: firstly, the addition of salt creates defects at which the water could move isotropically. These defects might be expected to heal with time, but this type of behaviour was not observed. Secondly, upon addition of salt, the domain size of the lamellar bilayers may be reduced, with most of the material found in vesicles/liposomes.

The results listed in Chapter 5 provide evidence that the electrolyte free system consists of a single lamellar phase with a random distribution of planar, partially flexible sheets and defects. These sheets, which are stacks of bilayers, slide against one another when shear applied into the system. At significant electrolyte level (~2.5 wt% TSC) the lamellar liquid crystalline phase consists of large domains of various orientations and vesicles of a broad size distribution. ^{2}H NMR spectral line shape analysis reveal that the size of the vesicles decreases with increasing electrolyte level. However, no relation could be drawn between the size distribution or the vesicle size and the NMR line shape. Overall, all the static evidence that gives a guide to lamellar phase morphology, optical microscopy, SAXS and ^{2}H NMR, suggest that the addition of electrolyte LAS/SLES/NI system drives a transformation to MLVs.

The effect of aging on the lamellar phase microstructure was investigated using optical microscopy and ^{2}H NMR spectroscopy. The optical micrographs and the ^{2}H NMR spectral line shape suggest that the lamellar microstructure was developed but with insignificant changes in the domain size.

In this study we have also investigated the effect of temperature on lamellar phase microstructure using SAXS and ^{2}H NMR spectroscopy. Our results reveal that little changes occurred in the lamellar microstructure upon temperature variation. It is noteworthy that even at the higher temperatures (~100°C) the quantity of lamellar structure remaining was sufficient to produce a significant scattering pattern. This is also evidenced by the homogeneous alignment of the rings in the 2-D scattering images. The changes in the ^{2}H NMR spectral line shape recorded for the 3 and 5 wt% TSC samples are believed to be due to changes in the size of the domains.

At this point it is important to note that even in static studies shear is involved. For example, when using optical microscopy the sample on a slide is compressed under the cover slip. The Lindeman tube (for SAXS) and the NMR tube are loaded with a spatula and this leads to structuring of the samples. However our results shown that when low shear is applied as in optical shear cell and rheology experiments this structuring can be reversed.

7.1.2 The shear effect

The rheological behaviour of the 0, 3 and 5 wt% TSC samples was investigated using Linkam optical shear cell, the AR 2000 rheometer and ^{2}H Rheo-NMR spectroscopy. The rheological characterisation involved fundamental experiments investigating the effect of shear rate, shear time and age on the lamellar microstructures. In addition, the relaxation of the shear-induced structures was studying by ^{2}H Rheo-NMR spectroscopy.

Studies on the optical shear cell suggest that shear slowly induces a change in morphology from extended bilayers (very large domains in the electrolyte free system) to liposomes. At intermediate shear rates the liposomes arrange behind each other in the flow direction. At higher shear rates the stripes shown in the optical textures are believed to be parallel lines of liposomes. The more shear the sample experiences, the more stripes can be seen in the textures.

Oscillatory rheology of the samples suggested that all the samples can be described as soft-solid with $G' > G''$. The elasticity of the lamellar phases may attribute to the structure units formed. Here is assumed that the structure units are organised in sheets, which although they can slide over each other, the mobility of the chains within the sheet is more restricted.

Simple stress sweeps for all the samples identified the first Newtonian plateau and the shear-thinning regime. The flow curve analyses for all the samples suggest that the flow properties of the lamellar systems are strongly dependent on composition. From the observations it can be concluded that the electrolyte free system is the most resistant to the formation of liposomes so it is believed that is furthest from the transition region. The shear profile for the 3 and 5 wt% TSC samples suggest that the electrolyte interacts with

the bilayers to make the formation of liposomes more favourable than in the electrolyte free system, though an external driving force (*i.e.* shear) is still required.

The effect of aging on the rheological behaviour of the samples was demonstrated using oscillatory rhelology and flow curves. Comparing the rheological properties (*G'*, *G''* and $|\eta*|$) of the samples at varying ages it can be said that they are not influenced by time. An important result is that the aging process appears to have little influence on the flow curves of the 0 and 3 wt% TSC samples. However, the flow curve recorded for the 5 wt% TSC sample (5 months aged) shown significant deviation from the flow curve recorded for the fresh sample. Thus an indication that changes in the size of the domains in the lamellar dispersion occurred. This parallel the results from ^{2}H NMR line shape analysis for the samples of different ages.

The relation between shear and changes in conformation and orientation of the domains has been investigated using Rheo-NMR. Rheo-NMR studies revealed that the size and the polidispersity of the liposomes formed after the application of shear are shear rate and shear time dependent. The relaxation kinetics of the shear-induced structures has been investigated. Rheo-NMR experiments have shown that the structure reorganises after the application of shear however never reaches the original state (structure before the application of shear). Rheo-NMR results suggested a continuous relaxation process from liposomes to planar lamellar with less defects and dislocations. The observed fast relaxation gives indication of something less organised and unstable.

7.2 Future Work

The work detailed in this thesis developed an understanding of the relation between the microstructure and the rheology of the mixed surfactant lamellar system. This work established a good knowledge of the mixed surfactant lamellar phases of interest in terms of their microstructure, their link to rheology, aging and temperature effects.

A detailed study of the changes of the microstructure on application of shear could be proposed as an interesting avenue for future work. For such studies, Linkam CSS-450 optical shear cell could be used in combination with SAXS. Both oscillatory and steady state rheology experiments could be carried out.

With regards to the temperature experiments described in this work, it would be of interest to study the effect of temperature on shear-induced structures.

An important next step would be to use Cryogenic Scanning Electron Microscopy (cryo SEM). Cryo SEM is utilised to investigate areas not visible with a normal microscope. This would help in improving the knowledge of defects and to gain an overall understanding of what is going on within the lamellar bilayers. With regards to shear effects it would be of interest to use cryo SEM in combination with shear.

One further avenue to be explored is microrheology. This technique studies the thermal motion of small particles in a material in order to extract the rheological properties. It would allow a better understanding of the relation between the microstructure and the rheological properties of mixed surfactant lamellar systems. An advantage of this technique is that is only requires a small quantity of material.

Appendix I

In the case of the 0 wt% TSC sample, 53/47 surfactant mixture/water

53 wt% of 2/1/1 LAS/SLES/$C_{12}EO_6$ thus 26.5/13.25/13.25 LAS/SLES/$C_{12}EO_6$

For the calculations of the thickness of bilayer water (d_W), thickness of the bilayer (d_H) and area per surfactant molecule (a_0), consider the following

Z_X = wt% of X in the sample

wt% of LAS, Z_{LAS}=26.5*40/100=10.6

wt% of SLES, Z_{SLES}=13.25*70/100=9.275

wt% of $C_{12}EO_6$, Z_{C12EO6}=13.25

wt% of water in the system=100-wt%(LAS+SLES+$C_{12}EO_6$)=66.875

Molar mass of LAS, S_{LAS}=326

Molar mass of SLES, S_{SLES}=420

Molar mass of $C_{12}EO_6$, S_{C12EO6}=450.65

Number of moles of surfactant in 1g of sample (m_s)=

$Z_{LAS}/100*S_{LAS} + Z_{SLES}/100*S_{SLES} + Z_{C12EO6}/100* S_{C12EO6}$=0.8*10^{-3}

Molar mass of the head groups of LAS, G_{LAS}=80

Molar mass of the head groups of SLES, G_{SLES}=132

Molar mass of the head groups of $C_{12}EO_6$, G_{C12EO6}=281

Molar mass of non-polar groups of LAS, H_{LAS}=246

Molar mass of non-polar groups of SLES, H_{SLES}=288

Molar mass of non-polar groups of $C_{12}EO_6$, H_{C12EO6}=169.65

Density of water, ρ_W=1kg/m^{-3}

Density of non-polar groups, ρ_H=0.8kg/m^{-3}

The weight fraction of non-polar region, $Z_H = Z_{H, LAS} + Z_{H, SLES} + Z_{H, C12EO6} =$

$H_{LAS}*Z_{LAS}/100*S_{LAS} + H_{SLES}*Z_{SLES}/100*S_{SLES} + H_{C12EO6}* Z_{C12EO6}/100*S_{C12EO6} = 0.1933$

The weight fraction of polar region, $Z_W = 1 - Z_H = 0.8067$

Volume fraction of non-polar region, $\varphi_H = \dfrac{Z_H/\rho_H}{Z_H/\rho_H + Z_W/\rho_W} = 0.3$

$d_0 = 46.7$Å (Section 5.2.3)

For lamellar phase

The thickness of the non-polar region, $d_H = \varphi_H*d_0 = 14.01$

The thickness of polar region, $d_W = \varphi_W*d_0 = (1-\varphi_H) d_0 = d_0 - d_H = 32,69$

Area per surfactant molecule, $\alpha_0 =$

$$\alpha_0 = \frac{2}{d_0}\left(\frac{Z_W}{\rho_W} + \frac{Z_H}{\rho_H}\right)\frac{10^{24}}{m_S N}(\text{Å}^2) = 42.4\text{Å}^2$$

Appendix II

An NMR line shape analysis has been performed on ^2H_2O molecules in the 3 wt% and 5 wt% TSC samples using the Stochastic Liouville Approach (SLA). The analysis has been done by Professor Westlund, P. O., Umea University, Sweden. The NMR model is presented in reference[1].

The stochastic Liouville equation is very useful in combination with complex dynamic models. In this work the SLA is used to a model system in order to demonstrate how calculated ^2H NMR line shapes change with the curvature of the surfactant/water interface.

The water dynamics at the interface is expected to be complex, involving lateral diffusion along the interface and chemical exchange between the 'bound' and 'free' water molecules of the interface. The 'bound' water molecules refer to hydration of the aggregate interface, whereas the 'free' water molecules are nonperturbed molecules with a zero quadrupole splitting. Hence, the 'bound' water molecules are diffusing among different binding sites thereby averaging over different site parameters into one effective order parameter S_0. This motion is characterised by correlation time τ_c.

Line shape calculations

The changes in ^2H_2O line shapes have been calculated by Westlund *et al.* in order to obtain informations about the timescale of the residual quadrupole interaction, which determines the NMR line shape. The timescale of the residual quadrupole interaction depends on the interface curvature. A flat surface is the limiting case for infinitely slow dynamics. Therefore, we expect that for any structural transitions within the lamellar liquid crystalline phase the correlation times along the aggregate/water interface are changing.

In order to generate the line shapes a cylindrical symmetry around the bilayer interface was assumed and that the quadrupole coupling constant χ is the same for both samples. This is because the local averaging outside the interface and the interactions with the salt are the same. It was also assumed that the translational diffusion coefficient is the same for ^2H_2O in both samples.

The translational diffusion coefficient D of ^2H_2O is related to the rotational diffusion coefficient d by:

$$d = D/r^2 \qquad (1)$$

where r is the radius of a sphere. The radius of a sphere becomes $r = \infty$ for a lamellar liquid crystalline phase. The rotational correlation time is

$$\tau_R = r^2/6D \qquad (2)$$

if we assume that the water molecules diffusion is the same for both systems (the 3 and 5 wt% TSC samples) the difference in rotational correlation function can be expressed as a difference in the radius r or the interface curvature h.

$$\frac{\tau_R(3\%TSC)}{\tau_R(5\%TSC)} = \frac{230}{400} = \frac{r^2\,(3\%TSC)}{r^2\,(5\%TSC)} \qquad (3)$$

Which may also be written in terms of the curvature $h = 1/r$

$$\frac{h(5\%TSC)}{h(3\%TSC)} = \sqrt{\frac{1}{1.74}} \qquad (4)$$

thus indicating that the curvature decreases or that the aggregates increase from 3 wt% to the 5 wt% TSC.

In Figure 1 the experimental line shape is very likely a sum of at least two line shapes one obtained for the 5 wt% TSC line shape and the second is a broader one with a larger quadrupolar coupling constant.
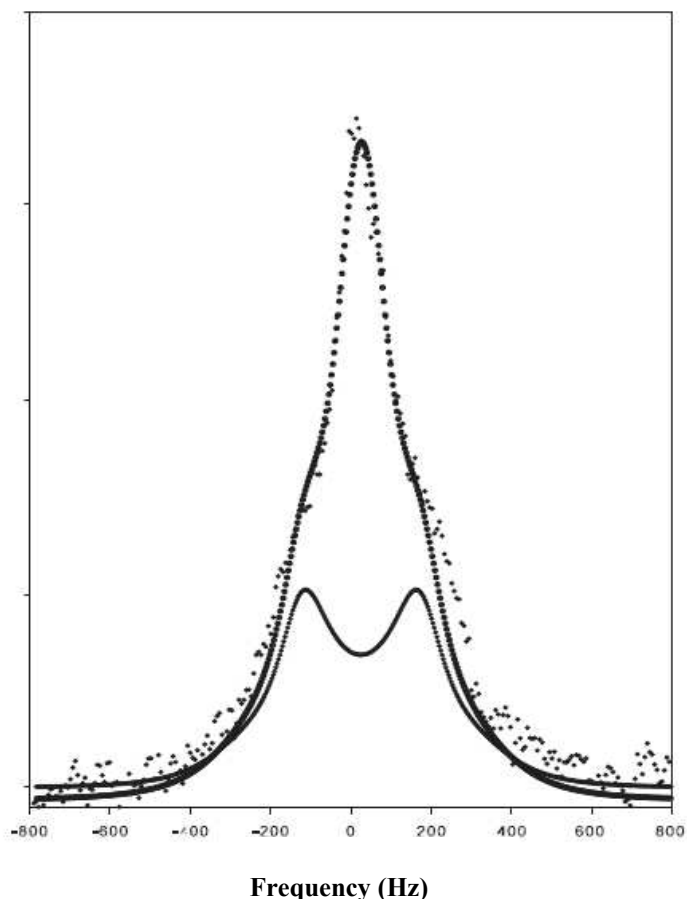
Frequency (Hz)

Figure 1: The ^{2}H NMR line shape for the 5 wt% TSC sample. A sum of two line shapes is observed consisted by the line shape recorded for the 5 wt% TSC sample and a broader line shape which is displayed as a solid line with a quadrupolar coupling constant of $\chi =$ 680Hz and reorientational correlation times $\tau_R = 1000\mu s$.

As shown in Figure 1 there are two different line shapes correspond to two different aggregate structures. One may consisted of micelles or vesicles small enough to allow water molecules to diffuse over the whole unit cell. This generates an isotropic broad signal. The second ^{2}H NMR line shape displayed in Figure 1 refers to an aggregate of increasing size or to an aggregate with lower curvature than before. The dynamics become slower as the curvature decreases and the quadrupole splitting appears when the water molecules no longer sample the whole unit cell.

The information content of ^{2}H line shapes from the SLA is limited. However, the changes observed in the ^{2}H NMR suggest changes in the curvature of the bilayers and in the domain

size. The line shape analysis must be combined with other methods in order to give conclusive information about an actual mechanism of a structural transition.

References

1.   Westlund, P. O., Line shape Analysis of NMR Powder Spectra of 2H2O in Lipid Bilayer Systems. *Journal of Physical chemistry B* **2000,** 104, 6059-6064.

Appendix III

The amount of shear applied into the samples is a vital parameter for this work. Therefore for Rheo-NMR experiments the power law of the couette cell (see Section 4.2.6) was determined using the AR 2000 rheometer. The power law index (n) is obtained from the slope (n-1) of a plot of the natural log of apparent viscosity versus the natural log of shear rate as shown in Equation 4.2.19.

The power-law model given in Equation 4.2.18 was used for a gap setting of $r_i/r_o = 0.55$. The radial velocity (rad/s) of the rotating tube is determined using a tachometer (outputted reading in rev/min)[1]. The results are shown in Figure 1.
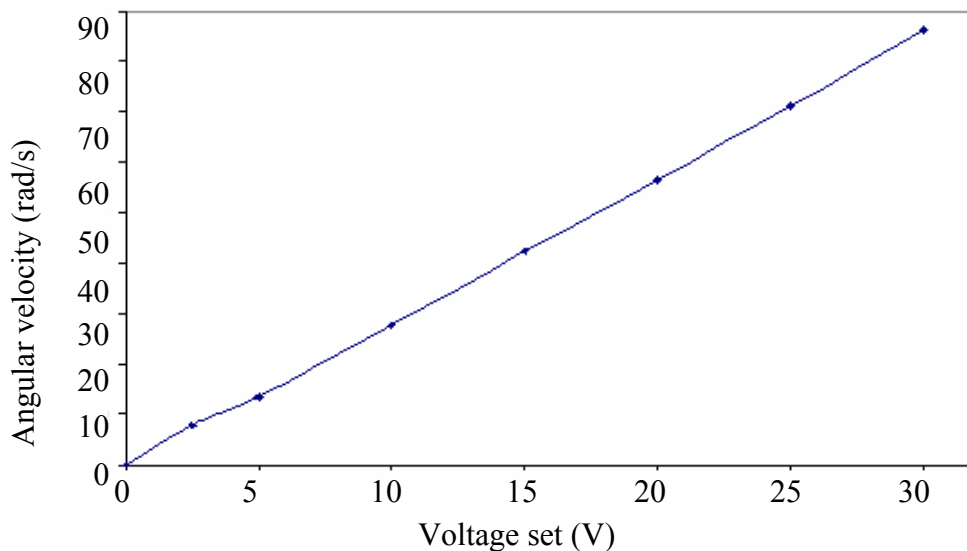

Figure 1: Radial velocity of the rotating inner 5mm tube of the couette cell (results adapted from previous work[1]).

Tests have been performed for the 0, 3 and 5 wt% TSC samples. The results are tabulated in Table 1.

Composition and age of samples	Power law index, (*n*)
0 wt% TSC, 10 days aged	0.215
0 wt% TSC, 7 months aged	0.179
3 wt% TSC, 10 days aged	0.338
5 wt% TSC, 10 days aged	0.359

Table 1: Determination of the power law index for use in the calculation of shear rate experienced by sample during flow in the couette cell.

The power law index is noted to be composition and age dependent. As mentioned above the power law index is used to determine the shear rate experienced by sample in the couette cell as shown in Equation 4.2.18. The results (motor voltage setting and shear rate) are tabulated in Table (6.3.1-3) (see Section 6.3.3) for each sample.

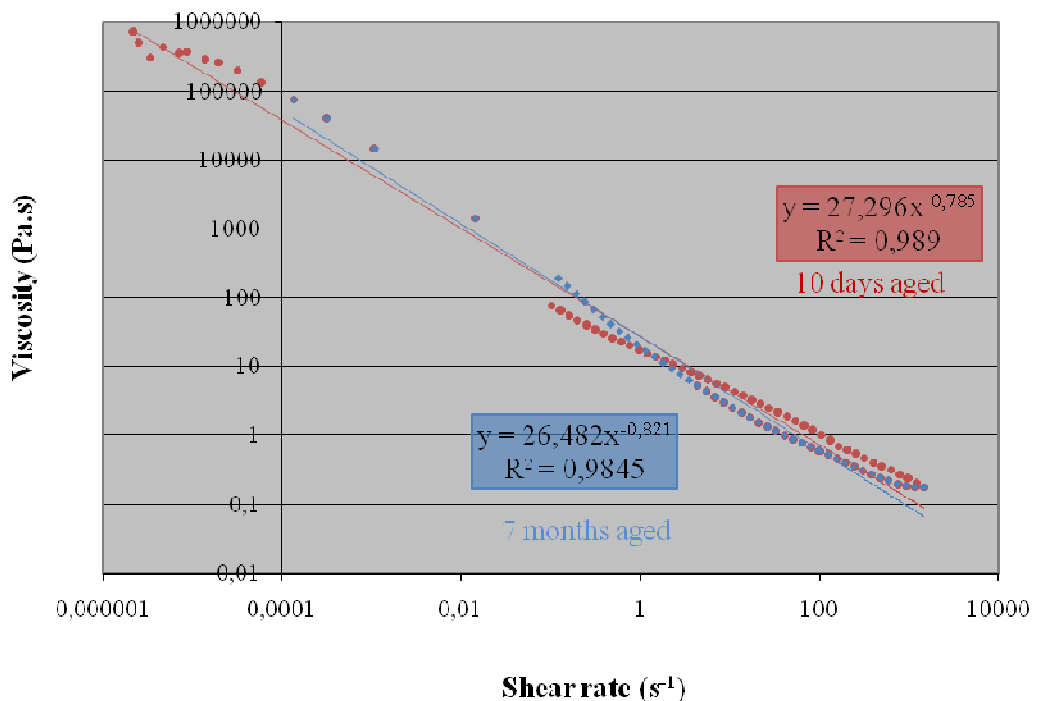Shown in Figure 2 are selected graphs obtained for the 0 wt% TSC sample (10 days and 7 months aged).

Figure 2: Determination of the power law index for the 0 wt% TSC sample (10 days and 7 months aged as indicated) at 25°C for varied shear rate ranges.

References

1.	Dutton, H. M. The behaviour of surfactant lamellar and gel phases under flow. The University of Manchester, Manchester, 2007.